INVESTIGATING PHYSIOLOGICAL VARIABILITY ACROSS DIFFERENT ALGAL AND CNIDARIAN SYMBIOSES: POSSIBLE IMPLICATIONS FOR CLIMATE CHANGE

by

Kenneth D. Hoadley

A dissertation submitted to the Faculty of the University of Delaware in partial fulfillment of the requirements for the degree of Doctor of Philosophy in Marine Studies

Summer 2016

INVESTIGATING PHYSIOLOGICAL VARIABILITY ACROSS DIFFERENT ALGAL AND CNIDARIAN SYMBIOSES: POSSIBLE IMPLICATIONS FOR CLIMATE CHANGE

by

Kenneth D. Hoadley

Approved: _____
Mark A. Moline, Ph.D.
Director of the School of Marine Science and Policy

Approved: _____
Mohsen Badiey, Ph.D.
Acting Dean of the College of Earth, Ocean, and Environment

Approved: _____
Ann L. Ardis, Ph.D.
Senior Vice Provost for Graduate and Professional Education

I certify that I have read this dissertation and that in my opinion it meets the academic and professional standard required by the University as a dissertation for the degree of Doctor of Philosophy.

Signed: _____

Mark E. Warner, Ph.D.
Professor in charge of dissertation

I certify that I have read this dissertation and that in my opinion it meets the academic and professional standard required by the University as a dissertation for the degree of Doctor of Philosophy.

Signed: _____

Adam G. Marsh, Ph.D.
Member of dissertation committee

I certify that I have read this dissertation and that in my opinion it meets the academic and professional standard required by the University as a dissertation for the degree of Doctor of Philosophy.

Signed: _____

Kathryn J. Coyne, Ph.D.
Member of dissertation committee

I certify that I have read this dissertation and that in my opinion it meets the academic and professional standard required by the University as a dissertation for the degree of Doctor of Philosophy.

Signed: _____

David J. Suggett, Ph.D.
Member of dissertation committee

ACKNOWLEDGMENTS

There are numerous individuals that I would like to thank for their help and efforts during my time at the University of Delaware. I am most indebted to my advisor Mark E Warner whom over the past five years has provided me with solid guidance and countless opportunities for additional professional development. I would also like to acknolwdge members of my committee, Kathryn Coyne, Dave Suggett and especially Adam G. Marsh for their help and insight during my dissertation. I would also like to thank Tye Pettay and Tom Hawkins along with numerous other collegues with whom I have had the opportunity to work with over the past few years. Much of the work we do is only successful through collaborations with multiple collegues and their help and efforts have contributed to the work presented here.

During my time in Delaware I have had the good fortune to meet my wife Elizabeth Baker and I thank her along with her family for the support they have provided me over the past few years. Lastly I would like to thank my two sisters and my parents for all that they have done for me over the years. I thank my mother, who pushed me to always do the best I could, leading by example and never allowing me to settle for less than perfection. I thank my father for continually being a role model and providing me with the support and means to pursue my interests. I could not have asked for a better set of parents. To them I dedicate my dissertation.

TABLE OF CONTENTS

LIST OF TABLES

.

LIST OF FIGURES

ABSTRACT

The unique and mutualistic symbioses between scleractinian corals and the dinoflagellate algae *Symbiodinium* spp. is critical to the overall success and continual growth of many reef corals worldwide. Unfortunately, these symbioses are susceptible to rising oceanic temperature and changes in carbonate chemistry. However, high genetic diversity within the host and symbiont suggests their responses may vary in a species-specific manner, potentially forming coral climate change 'winners' and 'losers'. Here I initially identified potential interactive effects between elevated temperature and pCO_2 concentration on the biochemical composition (protein, carbohydrate and lipid content) of the host and symbiont portions within four Pacific coral species and their respective symbionts. Temperature was the principle driver of physiological change and each host + symbiont combination responded to the stress differently, as greater change in biochemical composition was noted within the more thermally tolerant symbioses (*M. monastrea* and *T. reniformis*). I extended the question of interactive effects between independent variables by including nutrient concentration as a factor, along with temperature and pCO_2, focusing only on the coral *T. reniformis* with its symbiont *S. trenchii.* Temperature remained the leading factor in driving physiological change as net photosynthesis and cellular chlorophyll a

increased with temperature under ambient pCO_2, whereas temperature related differences in cellular volume were more pronounced under elevated pCO_2. Additionally, increased nutrient concentrations mitigated thermal affects under all pCO_2 conditions and suggest significant interactive effects between temperature, pCO_2 and nutrient concentrations.

Given the variability in physiological response to both temperature and pCO_2 previously observed, I next focused on a better characterization of the unique symbioses established within each host and symbiont combination, including two non-calcifying and symbiotic species. Specifically, I utilized multiple cnidarian symbioses to ask if symbiont type affects translocation of energy rich photosynthate to the host and if this varies with changes in pCO_2 and temperature. Two calcifying scleractinian corals (*Montipora hirsuta* and *Pocillopora damicornis*) and one non-calcifying coral (*Discosoma nummiforme*) were exposed to the individual and combined effects of elevated temperature and pCO_2 in order to induce a range of physiological states within each symbioses. An inverse relationship between cellular density and net photosynthesis is observed, as were differences in the ratio of photosynthesis $cell^{-1}$ to carbon translocation $cell^{-1}$, which appeared to be dependent on the host+symbiont combination. Because anemones represent one of the few cnidarian species where positive effects of elevated pCO_2 have been consistently documented, I also measured carbon uptake and translocation along with asexual reproduction within the anemone *Exaiptasia pallida* under ambient and elevated pCO_2 conditions. Additionally we asked whether physiological differences could be detected at the symbiont sub species

level, by infecting the host anemones with different *S. minutum* genotypes. Elevated pCO_2 conditions did increase net photosynthesis, carbon incorporation and asexual budding. Subtle differences were also observed across host/symbiont genotypes, placing functional significance on genotypic variance below the species level. I also had the opportunity to extend our comparison of host + symbiont diversity through field studies conducted in Palau. There I investigated the diversity of response strategies to elevated temperature for six congeneric coral species collected from an inshore rock island habitat and an offshore reef-system. Inshore reef corals harbored different symbiont species than their offshore counterparts and likely played a major role in establishing the greater thermal tolerance observed for colonies collected from the warmer inshore reefs. Host dependent differences in symbiont physiology were also observed and affected the overall response to high temperature.

Although symbiont phenotype can certainly provide a major source of adaptive potential for corals as they combat future climate change scenarios, host physiology also remains an important factor in establishing thermal resistance. As a proxy for phenotypic plasticity within the host coral, I quantified epigenetic modification of cytosine residues within the *E. pallida* genome in response to elevated temperature and across anemones housing *B1* vs. *D4-5* symbionts. Clear structure in CpG density across functional gene categories was apparent in both the promoter and gene body regions for *E. pallida* and changes in methylation status occurred in response to both temperature and symbiont species. Interestingly, the average net increase in methylation status observed between low and high temperature and between B1 and

D4-5 symbionts are significantly higher within the promoter region as compared to gene introns and exons and may point to the promoter regions as an important target for epigenetic control through DNA methylation.

Chapter 1

INTRODUCTION

The purpose of this introduction is to provide a brief summary of the relevant literature surrounding my dissertation topic. This is not an exhaustive summary, rather my goal is to simply introduce relevant concepts and ideas, with more specialized summaries for each specific topic available within their respective chapters.

1.1 Climate Impacts on Coral Reefs:

Photosynthetic dinoflagellates in the genus *Symbiodinium* reside in the gastrodermal cells of many cnidarians and represent a well-known and ecologically diverse symbiotic relationship, perhaps best known for its importance in reef-building scleractinian corals. Calcification by these corals is the biogeochemical process responsible for reef formation and is enhanced by the translocation of energy from *Symbiodinium* populations within the host tissue (Goreau 1959). Enhanced atmospheric pCO_2 and its role in increased sea–surface temperature and altered oceanic carbonate chemistry (referred to as ocean acidification) are now well-studied phenomena affecting coral reefs worldwide (Hoegh-Guldberg et al. 2007). In addition, localized problems such as anthropogenic eutrophication, especially within coastal regions where scleractinian corals are typically found, can also alter coral physiology and ecology. Because of the importance many of these species have to coastal ecology and in particular coral reef ecosystems, there is a high priority for better understanding how scleractinian corals

respond both physiologically and ecologically to the individual and combined effects of elevated temperature, ocean acidification (OA) and high nutrient levels. However, the high level of diversity found within the the broad genus of *Symbiodinium*, along with the unique physiologies of some host/symbiont combinations adds a level of complexity to coral biology that is only beginning to be understood and likely plays a major role in their ecological response to climate change.

Sea-surface temperatures of just a few degrees over the summer seasonal average have been linked to large-scale coral bleaching events worldwide (Hoegh-Guldberg and Bruno 2010). These bleaching events, characterized by a massive expulsion of the symbiotic dinoflagellates from the host coral, often result in high mortality rates which are already responsible for a 20% loss in global coral reefs (Hoegh-Guldberg 1999). Physiological changes in both the host coral species, and symbiont type are important for determining coral susceptibility and recovery from such high temperature events (LaJeunesse et al. 2007b, 2010; Levas et al. 2013; Grottoli et al. 2014; Silverstein et al. 2015). Phenotypic differences across symbiont types play a major role in establishing thermal tolerance (Grottoli et al. 2014), as can variation in host genetics (Kenkel et al. 2013; Parkinson et al. 2015). Assessing the role of physiological plasticity and genetic variability through comparative studies of different cnidarian symbioses will be critical as we move forward in our understanding of coral bleaching.

Although less of an immediate threat to coral reefs, changes to ocean carbonate chemistry and declines in pH associated with OA suggests that many different aspects of holobiont physiology may be affected. Because of the increase in pCO_2, it is thought that OA could affect symbiont productivity by providing a greater source of carbon for

photosynthesis (Langdon and Atkinson 2005; Cohen and Holcomb 2009). Symbionts living *in hospite* (i.e. within the host) are carbon limited (Weis et al. 1989; Weis 1993) and variation in carbon uptake under elevated pCO_2 has been noted for some cultured *Symbiodinium* isolates (Brading et al. 2011, 2013). However, the reduced aragonite saturation state of the water column may reduce overall calcification rates for scleractinian corals (Cohen and Holcomb 2009). This potential reduction in calcification may influence reef accretion rates, as deposition of calcium carbonate no longer outpaces bioerosion and dissolution. To date, the effect of elevated pCO_2 appears to be highly species specific and reductions in calcification rates are only recorded for some, but not all coral species studied thus far (Comeau et al. 2013; Edmunds et al. 2013; Schoepf et al. 2013). Effects of elevated pCO_2 are even more variable when also considering non-calcifying cnidarians, such as anemones, where positive affects including increased net photosynthesis and growth rate are observed (Suggett et al. 2012a; Towanda and Thuesen 2012b; Gibbin and Davy 2014). Different responses of the host and symbiont make ocean acidification a unique problem for the host/algal symbioses and future studies are required to better understand how effects vary between scleractinian coral species, as well as across the entire anthozoan lineage.

Depending on the host/symbiont combination, elevated nutrient concentrations can have varying effects on photophysiology and growth rates (Tomascik and Sander 1987). Marumbini and Davies (1996) showed differing responses to elevated NO_3 in the two coral species, *Porites porites* and *Orbicella annularis* (formerly *Montastraea*) (Marubini and Davies 1996). In both corals algal cell density, volume and chlorophyll a $cell^{-1}$ increased with elevated NO_3 concentrations, yet only increased maxium

photosynthesis and photosynthetic efficiency in *O. annularis,* suggesting a difference in photophysiology and nutrient demand between the two species. Phosphorous addition in the form of PO_4 increased the maximum photosynthetic efficiency within the host coral *Stylophora pistillata* (Ferrier-Pages et al. 2000) and was generally greater than when measured under nitrogen addition alone. Increases in maximum photosynthetic efficiency due to phosphorous addition were similar to increases under simultaneous nitrogen and phosphorous additions and suggests that, under normal conditions, phosphate is likely a limiting nutrient.

Like many marine and terrestrial ecosystems today, coral reefs face environmental threats from both global (e.g. elevated pCO_2 and temperature) and local (e.g. anthropogenic eutrophication) sources. With an increasing frequency, coral reefs will need to deal with multiple environmental threats and their combined effects on coral-algal physiology (Hughes and Connell 1999; Hughes et al. 2003; Hoegh-Guldberg et al. 2007). For example, increases in cellular density due to high nutrient concentration may lead to corals that are more susceptible to bleaching under high temperature conditions (Cunning and Baker 2013; Cunning et al. 2015) and represents a potentially important interactive effect to consider as reefs acclimate to multiple environmental stressors under future climate change scenarios.

1.2 Symbiodinium Genetic and Physiological Diversity:

The genus *Symbiodinium* is organized into nine genetically defined clades (A-I) and contains hundreds of distinct species, as delineated through analyses of the internal transcribed spacer 2 (ITS2) region of the ribosomal array (LaJeunesse 2001), SSU rDNA

and cp23 (Santos et al. 2002, 2003). While multiple *Symbiodinium* species may exist within a single host colony, most endosymbiont populations are typically dominated by a single species with potentially small background populations of types of *Symbiodinium* (Coffroth and Santos 2005). The genetic and phenotypic variability within *Symbiodinium* has significant influence on the host's response to changes in the environment (Baker 2003; Fabricius et al. 2004; LaJeunesse et al. 2007a; Grottoli et al. 2014; LaJeunesse et al. 2014). However, exactly how genetic diversity corresponds with physiological plasticity is not well understood. Better methods are needed to characterize and compare endosymbiont physiology in order to understand symbiont diversity in the context of coral acclimation to environmental stress.

As previously mentioned, some symbiont species appear more thermally tolerant than others, the most notorious of which is *Symbiodinium trenchii*. This symbiont has a proven thermal-tolerance and a global distribution, making it highly relevant to investigating acclimatization of cnidarian/*Symbiodinium* symbioses to climate change (Kemp et al. 2006; LaJeunesse et al. 2009a; Pettay et al. 2015). During a 2005 Caribbean bleaching event, the prevalence of *S. trenchii* increased in several scleractinian coral species prior to and during a high temperature period in the Caribbean (LaJeunesse et al. 2009a). This higher prevalence was also correlated with greater resilience from bleaching mortality as compared to coral colonies without *S. trenchii*. Within the Caribbean coral *O. faveolata,* a similar increase in *S. trenchii* after an initial bleaching episode, enabling greater tolerance during a repeat high temperature exposure the following year (Grottoli et al. 2014). Despite its high thermal tolerance, *S. trenchii* contribution to host energetics is thought to be significantly lower than that of other symbionts, calling into question its

desirability as an endosymbiont (Pettay et al. 2015). After an experimental thermal bleaching event, one Pacific coral, *A. millepora* hosting closely related clade D symbionts grew almost 30% slower than those hosting symbiont type C2. This reduction in growth was even greater in colonies collected from the field, showing a 38% reduction in colonies with cade D as compared to colonies hosting C2 (Jones and Berkelmans 2010a). Additionally, reversion back to the dominant symbiont type under normal conditions also suggest that *S. trenchii* may not be as desirable in many host species (Thornhill et al. 2006; LaJeunesse et al. 2009a). However, *S. trenchii* genetic variability is highly limited in the Caribbean whereas many clonal variants can be found in close proximity in the Pacific (Pettay et al. 2015). Along with the genetic variability observed for *S. trenchii,* physiological differences across clonal variants may also exist and further complicate what is known about coral symbioses with *S. trenchii.*

For some coral species, light intensity and depth can also play a role in *S. trenchii* prevalence. For the coral *Seriatopora hystrix* only colonies near the surfaced hosted *S. trenchii* whereas colonies collected at deeper sites hosted type C symbionts (Cooper et al. 2011). A similar trend was found around Palau where greater *S. trenchii* prevalence is observed in corals near rock island habitats characterized by greater shading and light attenuations as compared to offshore barrier reef habitats (Iwase et al. 2008). Interestingly many of these *S. trenchii* associations do not seem as detrimental towards host growth and energetics as they do in other areas, particularly in the Caribbean. *S. trenchii* diversity differs significantly between Caribbean and Pacific reefs as only one *S. trenchii* clone has ever been reported within the Caribbean (Pettay and Lajeunesse 2009). Using the same eight microsatellite loci to distinguish multi-locus genotypes, samples

collected on Indian and Pacific reefs revealed multiple *S. trenchii* types within a single reef (Pettay 2011; Wham et al. 2011). Whether these different *S. trenchii* subspecies are physiologically different, or how these differences in *S. trenchii* diversity affect overall host physiology remains unknown. Even less is known about the tolerance of *S. trenchii* to changes in pCO_2 concentrations or nutrient conditions.

1.3 Host Influence on Symbiont Physiology:

Along with symbiont phenotype, host physiology also plays a major role in dictating the holobiont's response to changes in the environment. High lipid reserves in the host can mitigate thermal stress in *Acropora intermedia* and *Montipora monasteriata* (Anthony et al. 2009) by serving as a source of easily accessible energy (Grottoli et al. 2004; Grottoli and Rodrigues 2011). Catabolization of host lipid reserves provides the animal with additional energy during high temperature stress (Grottoli et al. 2004) Similarly, differences in feeding rates across species may also influence bleaching susceptibility as species able to increase ingestion rates may better withstand thermal stress (Grottoli et al. 2006). These additional host derived sources of energy may also help initiate additional animal defenses such as elevated production of heat shock proteins and superoxide dismutase (Fitt et al. 2009). Increases in expression of heat shock proteins are observed in response to high temperature stress and may help stabilize otherwise thermally sensitive proteins within the host, allowing the organism to continue normal cellular functioning (Black et al. 1995; Ogawa et al. 2013). Differences in the rate of production of ROS scavenging molecules across coral colonies and/or species may also influence bleaching susceptibility by removing reactive oxygen species from the host

tissue (Lesser 2006; Krueger et al. 2015). Host morphology can also indirectly influence bleaching susceptibility through its influence on the symbiont's realized light field. Differences in host pigmentation, tissue thickness, skeletal light scattering and polyp extension can all directly change internal light fields for *in hospite* symbionts (Enríquez et al. 2005; Ulstrup et al. 2006b; Kaniewska et al. 2011; Wangpraseurt et al. 2012). Because excess excitation energy from high light can exacerbate thermal stress for certain *Symbiodinium*, changes in the light environment due to host dependent physiology should be considered in order to understand why some corals bleach and others do not. Regardless of what host specific physiological variables are responsible for influencing thermal bleaching tolerance, it is clear that such differences vary both across species (Fitt et al. 2009) and genotypes (Kenkel et al. 2013; Parkinson et al. 2015). Variability at the genotypic level allows for important variability on which natural selection can drive acclimation within a species (Kenkel et al. 2013; Parkinson et al. 2015). At the species level, variability in physiology can help predict 'winners and losers' of climate change.

1.4 Epigenetic Approaches to Coral Research:

As we gain a better understanding of coral acclimation and adaptive potential towards warming temperatures, the inherent phenotypic plasticity within a coral colony becomes an important point of interest. Phenotypic plasticity within the context of coral species has been previously discussed in terms of morphology and reef location as certain corals take on different morphologies (plating vs. branching) designed to optimize light capture on the reef and allow for an increase in niche width (Brown et al. 1985; Smith et al. 2007; Kaniewska et al. 2008). Similarly, plasticity in a colony's ability to mitigate

high temperature stress may play a critical role in understanding what species may be more or less capable of adapting to future climate change conditions (Parkinson et al. 2015). Adaptation to a new environment is typically thought of as the end result of natural selection towards the more fit genotypes within a population. However, the relatively slow nature of this process may not occur quick enough for many species to adapt to future climate change conditions. Phenotypic plasticity on the other hand, describes the inherent flexibility of a species or even an individual colony of coral to acclimate to different conditions, despite having the same genetic makeup. Because acclimation can occur on a much quicker timeline, understanding the role of phenotypic plasticity within a coral may be crucial towards predicting which species can and cannot acclimate to future climate scenarios.

In humans, epigenetic modification of the genome through cytosine methylation is an important regulatory method for gene expression (Majewski and Ott 2002). Changes in DNA methylation at specific CpG motifs (a C followed by a G nucleotide, 'CG') may provide a mechanism on which phenotypic plasticity functions, and the epigenetic potential of a genome may provide insights into an organism's ability to adapt to changes in the environment. Gene expression profiles for several coral species were compared to underlying CpG frequency within the mRNA transcripts (Dixon et al. 2014; Dimond and Roberts 2015). Interestingly greater changes in gene expression tended to occur within mRNA transcripts that had low CpG frequencies (Dixon et al. 2014). The two studies suggest a strong link between potential for change in gene expression and the underlying methylation potential of the genome. However, methylation of the CpG motifs needs to be established in order to understand the correlation between methylation and gene

expression values. Within vertebrate model systems, regulation of gene expression through epigenetic modification is typically observed as changes in methylation within the promoter region and CpG frequency tends to increase towards the transcriptional start site (Carninci et al. 2006; Saxonov et al. 2006; Elango and Soojin 2008a). Similar patterns are observed within the promoter regions of the cnidarians *A. digitifera* and *N. vectensis* (Marsh et al. 2016). Differences in CpG frequency also differ across functional gene categories within both the promoter (Marsh et al. 2016) and gene bodies (Dixon et al. 2014; Dimond and Roberts 2015) and suggests that methylation patterns within these basal group of metazoans may play an important role in transcriptional regulation. Analysis of cnidarian methylomes, along with changes in methylation patterns may provide a potentially useful metric for assessing phenotypic plasticity within corals.

1.5 Research Chapters:

I proposed a series of laboratory and field based experiments designed to pinpoint physiological changes in the coral-algal complex resulting from individual and combined effects of increased temperature, nutrient level and pCO_2 concentrations. My research aims to better understand photosynthetic efficiency, carbon uptake and stress response pathways as they relate to alterations in temperature, pCO_2 and nutrient inputs.

Chapter 2 examines the possible interactive effects between elevated temperature and pCO_2 concentration on the biochemical composition (protein, carbohydrate and lipid content) of the host and symbiont portions within the Pacific coral species *Acropora millepora* (*Symbiodinium C21a*), *Pocillopora damicornis* (*Symbiodinium C1c-d-t*), *Montipora monastrea* (*Symbiodinium C15*) and *Turbinaria reniformis* (*Symbiodinium*

trenchii). Focusing on just the coral *T. reniformis* and its symbiont *S. trenchii,* chapter 3 builds on the work of chapter 2 by adding the additional environmental factor of nutrient concentration. Multivariate analysis revealed strong interactive effects between all three factors within the symbiont in this coral.

In chapter 4, I characterize the inherent plasticity within each host+symbiont symbioses by utilizing temperature and pCO_2 to induce a range of physiological states within two calcifying scleractinian corals (*Montipora hirsuta* and *Pocillopora damicornis*) and one non-calcifying corallimorph (*Discosoma nummiforme*). Overall differences in host morphology and their role in establishing differences in symbiont bioptical and biophysical properties are considered. In addition, I traced carbon incorporation by symbiotic algae and translocation of photosynthate to the host and reveal an inverse relationship between cellular density and net photosynthesis, along with host+symbiont dependent differences in the ratio of photosynthesis $cell^{-1}$ to translocation $cell^{-1}$. Chapter 5 investigated the response of the anemone, *Exaiptasia pallida* to elevated pCO_2 conditions by measuring carbon uptake and translocation, as well as asexual reproduction in three separate *E. pallida,* hosting different strains of *Symbiodinium minutum*. My results show significant increases in carbon uptake and translocation along with asexual reproduction as pCO_2 conditions rise.

Chapter 6 looks at the diversity of the physiological thermal response strategies within six congeneric coral species (*Acropora muricata, Goniastrea aspera, Porities rus, Cyphastrea chalcidicum, Porites cylindrica* and *Pachyseris rugosa*) collected from an inshore and an offshore Palauan reef-system. I tracked photophysiological and biochemical parameters within the symbionts over a 14-day exposure to elevated

temperature and showed that differences in symbiont phenotype within inshore vs. offshore coral species resulted in greater thermal tolerance for inshore coral colonies as opposed to their offshore counterparts. However, host dependent differences also play a role in establishing the thermally tolerant phenotype and bleaching can still occur within colonies housing thermally tolerant symbionts.

Lastly, chapter 7 investigates the possibility of epigenetic modification of cytosine residues within the *E. pallida* genome in response to elevated temperature and differences in symbiont phenotype (*B1* vs. *D5b*). Aposymbiotic *E. pallida* were infected with either *Symbiodinium B1* or *Symbiodinium D4-5* and maintained in stable symbioses with their respective symbiont types for over 4 months, prior to increasing water temperature to 32 °C for one month in order to induce thermal stress. Clear structure between CpG density and functional gene categories was observed within the promoter region as well as within the gene body, similar to what has been previously documented for other cnidarian species. Changes in methylation status in response to temperature and symbiont species were also evident as overall methylation increased in response to high temperature. Methylation status along with the underlying CpG frequency increased with proximity to the transcriptional start site and changes in methylation were greatest within the promoter regions as opposed to the gene-body. Lastly, in response to temperature and symbiont type, the majority of changes in methylation occurred in genes involved with environmental information processing.

Chapter 2

PHYSIOLOGICAL RESPONSE TO ELEVATED TEMPERATURE AND pCO_2 VARIES ACROSS FOUR PACIFIC CORAL SPECIES: UNDERSTANDING THE UNIQUE HOST+SYMBIONT RESPONSE.

2.1 Abstract:

The physiological response to individual and combined stressors of elevated temperature and pCO_2 were measured over a 24-day period in four Pacific corals and their respective symbionts *(Acropora millepora / Symbiodinium C21a, Pocillopora damicornis / Symbiodinium C1c-d-t, Montipora monasteriata / Symbiodinium C15*, and *Turbinaria reniformis / Symbiodinium trenchii*). Multivariate analyses indicated that elevated temperature played a greater role in altering physiological response, with the greatest degree of change occurring within *M. monasteriata* and *T. reniformis.* Algal cellular volume, protein, and lipid content all increased for *M. monasteriata*. Likewise, *S. trenchii* volume and protein content in *T. reniformis* also increased with temperature. Despite decreases in maximal photochemical efficiency, few changes in biochemical composition (i.e. lipids, proteins, and carbohydrates) or cellular volume occurred at high temperature in the two thermally sensitive symbionts *C21a* and *C1c-d-t*. Intracellular carbonic anhydrase transcript abundance increased with temperature in *A. millepora* but not in *P. damicornis*, possibly reflecting differences in host mitigated carbon supply during thermal stress. Importantly, our results show that the host and symbiont response to climate change differs considerably across species and that greater physiological

plasticity in response to elevated temperature may be an important strategy distinguishing thermally tolerant vs. thermally sensitive species.

2.2 Introduction:

Coral reefs represent one of the most biologically rich ecosystems on the planet. The importance of scleractinian corals to continual reef accretion has placed much attention on understanding how they will respond to future climate conditions, including elevated seawater temperature and ocean acidification. Water temperatures of just a few degrees above the summer maximum average can lead to large-scale coral bleaching events (Hoegh-Guldberg and Bruno 2010), which are often characterized by the expulsion of symbiotic dinoflagellates (*Symbiodinium* spp.). Such bleaching events can result in high coral mortality and a significant loss in coral cover (Hoegh-Guldberg and Bruno 2010).

Photoinactivation and damage to the photosystem II (PSII) reaction center is often a first sign of temperature stress within thermally susceptible *Symbiodinium* (Warner et al. 1999; Fitt et al. 2001). Photoinactivation can result in reduced photosynthetic rates and elevated reactive oxygen species, further damaging the symbiont and coral (Nishiyama et al. 2001; Takahashi and Murata 2008; Baird et al. 2009). This stress can change the energetic/metabolic demands of the symbiont, reducing the amount of photosynthate translocated to the host. In turn, host catabolic pathways are utilized to supply additional energy to compensate for the loss of translocated carbon and/or to keep pace with greater metabolic demand from high temperature stress, leading to a decline in one or more of the host's energy reserves of proteins, carbohydrates and lipids (defined hereafter as the

biochemical composition) (Grottoli et al. 2006; Anthony et al. 2009; Grottoli et al. 2014). However, other mechanisms such as enhanced heterotrophy can compensate for reduced photosynthate translocation, and maintain biochemical composition (Grottoli et al. 2006; Levas et al. 2013; Schoepf et al. 2013). Similar to other marine phytoplankton, symbiont biochemical composition may also change in response to temperature stress (Carvalho et al. 2009; Gigova et al. 2012). Thus, due to variation in host and symbiont thermal tolerance, the overall thermal response of the holobiont (i.e. the host + the symbiont) can vary widely across different corals.

Ocean acidification (abbreviated OA hereafter), which describes the decrease in seawater pH resulting from increasing atmospheric CO_2 partial pressure (pCO_2) levels and subsequent dissolution and acid production, has the potential to affect many aspects of coral physiology. Several studies have noted reduced coral calcification at high pCO_2 (e.g.,Anthony et al. 2008; Comeau et al. 2013; Schoepf et al. 2013). However, some corals show no decline or a delayed decline in calcification well below the current aragonite saturation state, suggesting the response to high pCO_2 is highly species specific (e.g., Comeau et al. 2013; Edmunds et al. 2013; Schoepf et al. 2013). Compared to calcification studies, less attention has been placed on other aspects of holobiont physiology, including primary productivity and biochemical composition. As $CO_{2(aq)}$ concentrations increase with OA, symbiont productivity could increase due to a release from carbon limitation (Cohen and Holcomb 2009). Greater net productivity with elevated CO_2 was reported for symbiotic sea anemones in laboratory experiments and near natural CO_2 seeps (Suggett et al. 2012a; Towanda and Thuesen 2012b). Highly variable, CO_2 driven changes in respiration and productivity may result in significant

changes to host and symbiont metabolism, and are likely to affect the overall health and resilience of the coral as these organisms cope with additional environmental stressors.

High CO_2 conditions enhanced productivity for some cultured *Symbiodinium*, but not others (Brading et al. 2011), and this variability may be linked with differences in carbon acquisition as well as the preference in dissolved inorganic carbon (CO_2 vs. HCO_3^-) among algal species (Brading et al. 2013). In addition, increased respiration rates, along with changes in the transcriptional response of genes involved with metabolic pathways and cellular structure, were noted in scleractinians in response to OA (Kaniewska et al. 2012; Moya et al. 2012). Specifically, genes associated with energy production and ion transport were up-regulated under acidification conditions (Vidal-Dupiol et al. 2013), suggesting changes in the biochemical composition of the symbiosis.

Research to date has largely focused on the physiological changes and metabolic pathways most important towards understanding the coral response to climate change. However, because most studies have focused on just a few model scleractinian species (Muller-Parker et al. 1994; Hoegh-Guldberg and Williamson 1999; Grover et al. 2003; Moya et al. 2008; Miller et al. 2011), less is known about the potential for physiological diversity within each unique host/symbiont combination. Whether or not the physiological responses to both elevated temperature and pCO_2 that have been described (Reynaud et al. 2003; Rodolfo-Metalpa et al. 2010; Schoepf et al. 2013) accurately depict the range of coral responses within the entire Scleractinian taxa remains to be seen.

Here, we utilized a combination of physiological, and transcriptional approaches to characterize both the host and symbiont response to elevated temperature and pCO_2. Through the comparative analysis of multiple physiological variables within the host and

symbiont, the unique response to temperature and pCO_2 within each species was characterized. This approach highlights the diversity of physiological responses within scleractinian corals and how each host/symbiont system responds uniquely to a changing environment anticipated under future climate change conditions.

2.3 Materials and Methods:

2.3.1 Experimental Design:

A detailed description of the experimental design is found in (Schoepf et al. 2013). Briefly, six colonies of *Acropora millepora, Pocillopora damicornis*, *Montipora monasteriata,* and *Turbinaria reniformis* were collected in northwest Fiji at a depth between 3-10 m, transported to a coral mariculture facility (Reef Systems Coral Farm, Ohio), and allowed to acclimate for two months prior to experimentation. Six fragments were removed from each parent colony species^{-1} and allowed to recover. Coral fragments were slowly acclimated (over a three weeks) to custom-made synthetic seawater closely resembling natural seawater chemistry (ESV Aquarium Products Inc.). There were 6 treatment systems, each consisting of six, 57 L aquaria connected to a central 905 L sump. One colony fragment species^{-1} was placed into each of the six replicate tanks in each system, with a separate colony fragment from each species in each replicate tank (i.e., four fragments per tank). Because replicate tanks were connected via a central sump per treatment, our design is technically a pseudo-replicate design (Cornwall and Hurd 2015). However, controlling temperature, CO_2, salinity and light intensity within individual replicate tanks is technically difficult and impractical for this type of study. Corals were maintained under a 9:15 hour light:dark cycle, providing light at 275 μmol

quanta m^{-2} s^{-1} at the base of the filled aquaria. Each treatment ran for 24 days, with a 25% water change every three days. Salinity was maintained at 35 ppt through daily top-offs with RO filtered fresh water. Corals were fed *Artemia nauplii* every three days.

Treatments consisted of an ambient and high temperature treatment at three pCO_2 conditions set to ambient (382 µatm), medium (607 µatm) and high CO_2 (741 µatm). The pCO_2 conditions reflect current (382 µatm) and elevated conditions expected by the mid (607 µatm) and late (741 µatm) 21st century (IPCC 2013). Temperature within the high temperature treatments was slowly increased with titanium heaters from the ambient temperature of 26.5°C to a maximum of 31.5°C over the course of the experiment (see supplemental figure 1 for temperature ramping profiles).

pH measurements were taken every 30 seconds (Thermos Scientific Orion Ross Ultra pH glass electrode) and were integrated into a pH stat system for precise control of air and CO_2 gas input into each sump (KSgrowstat, University of Essex). For elevated pCO_2 treatments, CO_2 was increased by 100 µatm day^{-1} until the desired pCO_2 was met. All pH electrodes were calibrated daily using three NBS standards (4.00, 7.00, 10.00), and independent measurements of pH with a dedicated Ross pH electrode and alkalinity with Gran titration were made using published protocols (Cai et al. 2010). Total alkalinity, pH, salinity, and temperature over the 24-day experiment were used to calculate carbonate system speciation using the CO2SYS program (Lewis & Wallace, 1998). The results are shown in supplementary table 1.

2.3.2 Symbiont Photophysiology:

Daily dark acclimated maximum quantum yield of photosystem II (F_v/F_m) was measured one hour after the light period by pulse amplitude modulation fluorometry (Diving PAM, Waltz, Germany), by supplying a 600 ms pulse of saturating light to the surface of each coral fragment. On day 23, maximal photosynthetic rates and light acclimated dark respiration (R_L) were measured for 6 fragments species^{-1} treatment^{-1} via respirometry with galvanic oxygen electrodes (Qubit systems) housed in clear acrylic chambers (350 mL). Chambers were temperature controlled to match experimental conditions and constantly stirred. Maximal photosynthesis was measured by providing illumination from a 24 LED array (Cree Cool White XP-G R5) set to 600 μmol quanta m^{-2} s^{-1}. Pilot experiments at this light intensity showed no decrease in oxygen evolution (data not shown). Net maximal photosynthesis ($Pmax_{net}$) was recorded for 15-20 minutes, followed by a 10-minute dark incubation to record the light enhanced dark respiration (R_L) also known as the post-illumination respiration (referred to hereafter as the LEDR). The photosynthesis to respiration ratio was calculated as $Pmax_{gross}/R_L$ where $Pmax_{gross}$ = (net photosynthesis + light enhanced dark respiration). Net photosynthesis (data not shown) and light enhanced dark respiration (R_L) were normalized to total fragment surface area (cm^2) (described below).

2.3.3 Host and Symbiont Physiology:

At the end of the 24-day treatment, samples were frozen in liquid N_2 and stored at -80°C until further processing. All coral tissue was removed from each fragment using a water pick (Johannes and Wiebe 1970). This is fundamentally different from our

companion paper (Schoepf et al. 2013) based on the same experiment, where only tissue from the branch tips or the leading edge of plating corals were analyzed (with the exception of cell density and chlorophyll content which were both integrated from the whole fragment). In contrast, this paper focuses on the physiological responses integrated over the entire fragment area. The resulting slurry was homogenized with a tissue tearer (Biospec products, Inc), and then centrifuged for 5 minutes (5,000 g) to separate the algal and coral fractions. Pelleted symbionts were resuspended in synthetic seawater and divided into 1mL aliquots. One algal aliquot was preserved with 10 μL of 1% glutaraldehyde for cell enumeration, and cell density and volume were recorded by light and fluorescence microscopy. Six independent replicate counts were performed for each algal sample on a hemocytometer. Samples were photographed using a Nikon microphot-FXA epifluorescent microscope (100x magnification) and analyzed using the software Image J (NIH) with the Analyze Particles function. Pixel size of each cell was converted to μm^2 using a calibrated scale micrometer and then used to calculate cell diameter and volume based on calculations for a sphere. Surface area of *T. reniformis* and *M. monasteriata* was determined by the foil method (Marsh 1970), while area for the branching *A. millepora* and *P. damicornis* was determined by the wax method (Stimson and Kinzie 1991).

For soluble protein concentration of the host and symbiont, 1 mL samples were homogenized with a bead-beater (BioSpec) for 2 minutes and then analyzed using the BCA protein method (Thermo Scientific Pierce), with a bovine serum albumin standard (Smith et al. 1985). For lipid extraction, host and symbiont portions were freeze-dried overnight and then extracted using a 2:1:0.8 chloroform:methanol:sodium chloride ratio

(Folch et al. 1957). Lipid quantification was carried out by a vanillin colorimetric assay using corn oil as standards (Cheng et al. 2011). For carbohydrate quantification, host and symbiont aliquots were homogenized with a bead-beater for 1.5 minutes and then extracted using a sulfuric acid/phenol, using glucose as standard (Dubois et al. 1956). Absorbance measurements for lipid, carbohydrate and protein assays were made at 540, 485 and 595 nm respectively using a FLUOstar Omega plate reader (BMG Labtech, Germany). Biochemical composition was normalized to coral surface area and algal cell number.

The genetic identity of the dominant algal symbiont of each coral fragment was determined through amplification of the internal transcribed spacer 2 region (ITS2) of the ribosomal array, and subsequently analyzed by previously published protocols for denaturing gradient gel electrophoresis (DGGE) fingerprinting and cycle sequencing (LaJeunesse et al. 2003). This method identifies the dominant (or co-dominant) sequence variants for the ribosomal genome of a particular symbiont lineage.

2.3.4 Targeted Host and Symbiont Gene Expression:

Due to the greater availability of genomic data for the coral *A. millepora* and *P. damicornis* and their respective *Symbiodinium*, gene expression was examined only in these two species and their respective symbionts. Transcript abundance for host genes involved in several metabolic roles was investigated, including carbon acquisition (intra and extracellular carbonic anhydrase), calcium and ATP exchange (CA-ATPase), carbon metabolism (Glyceraldehyde 3-phophate dehydrogenase (GAPDH)) and thermal response (Heat Shock Protein 90 (HSP90)). For algal gene expression, transcript

abundance was monitored in pathways related to carbon metabolism (α-ketoglutarate dehydrogenase), nitrogen metabolism (glutamine synthetase), and fatty acid synthesis (malonyl Co-A acyl transferase) (Leggat et al. 2011).

For intra and extracellular carbonic anhydrases and Ca-ATPase*, A. millepora* and *P. damicornis* expressed sequence tags were searched using a conventional BLAST search within the National Center for Bioinformatics (NCBI) and PocilloporaBase (cnidarians.bu.edu/PocilloporaBase/cgi-bin/index.cgi) databases respectively. Databases were queried with well-characterized gene transcripts from *Stylophora pistillata,* intra and extracellular carbonic anhydrase (STPCA-2, EU532164.1 and STPCA EU159467.1 respectively) and CA-ATPase (AY360080.1) (Zoccola et al. 2004; Moya et al. 2008; Bertucci et al. 2011). Databases were also searched using the sequences for GAPDH (EZ026309.1) and HSP90 (DY584045.1) from *Acropora aspera* (Leggat et al. 2011). The top blast hits were confirmed as homologous genes through phylogenetic analysis (Geneious, Biomaters Ltd). All coral genes were normalized to transcripts encoding ribosomal subunit protein 7 (rsp7) and Elongation factor 1 α (EF1α) (Seneca et al. 2010). Algal transcripts were normalized to the housekeeping genes encoding S-adenosyl methionine synthetase (SAM) (Rosic et al. 2011a) and the proliferating cell nuclear antigen (PCNA) (Leggat et al. 2011). Primers for qPCR were designed with Primer-Quest software (Integrated DNA Technologies) or from published studies (Seneca et al. 2010; Leggat et al. 2011). Primer sets and efficiency scores for each gene are listed in Appendix A, table 2.

Frozen coral samples were ground into a powder using a mortar and pestle chilled on a bed of dry ice. Total RNA was extracted and purified from each sample using

TRIzol Reagent (Invitrogen) and an Aurum Total RNA Mini kit (Bio-Rad). Purified RNA samples were quantified by spectrophotometry (NanoDrop 2000, ThermoScientific). Only samples with concentrations greater than 50 ng μL^{-1} were used for subsequent analyses, and samples typically had 260 nm:280 nm and 260 nm:230 nm ratios greater than 2.0 and 1.9 respectively. RNA samples were diluted to 20 ng μL^{-1} prior to cDNA synthesis. Reverse transcription PCR reactions were performed using the high capacity cDNA Reverse Transcription Kit (Applied Biosystems). For each sample, a total of 120 ng of total RNA was added to a single 10 µl cDNA reaction.

Quantitative PCR reactions were performed on 96 well plates with optical film, using a SensiMix real time detection system with 2X SYBR Hi-ROX Mastermix (BIOLINE) and an ABI Prism 7500 Sequence Detection System (Applied Biosystems). Each 10 µL reaction contained 5 µL of SYBR Hi-ROX, 0.2 µL each of 10 mM forward and reverse primer, 2.6 µL nuclease-free water and 2 µL of 1:5 diluted cDNA. All qPCR reactions were performed with the following thermal profile: 50°C for 2 min, 95°C for 10 min, followed by 40 cycles of 95°C for 15s, 61°C for 15s and 72 °C for 45s. Standards were constructed from pooled total RNA samples from multiple treatments and diluted in a 4-fold dilutions series. For each plate, standards were run in triplicate and samples run in duplicate. A dissociation curve between 61°C and 95°C (0.5°C intervals) was performed immediately after each PCR reaction to ensure the absence of any non-specific, multi-product amplification. Negative control reactions were carried out on a subset of samples and pooled standards (not shown).

Standards were constructed from pooled total RNA samples from multiple time points and diluted in a 4-fold dilutions series prior to cDNA synthesis.

Standards were run in triplicate and samples run in duplicate. Efficiency values for each gene were calculated using the formula $E = 10^{(-1/\text{slope})}$ and are available in supplementary table S3. GeneEx expression software was used to normalize all data to total RNA and to the multiple house-keeping genes listed above and to account for differences in amplification efficiency. As the goal of this work was to compare gene expression across multiple variables and treatments rather than to a single control treatment, relative expression values for each gene of interest were calculated by dividing each value by the highest value within each gene assay (Levy et al. 2007) (Hoadley et al. 2011).

2.3.5 Statistical Analysis:

For each species, the overall importance of elevated temperature and pCO_2, were analyzed for their significance in separating samples using an ANalyses Of SIMilarities (ANOSIM) with 9,999 permutations. If resulting correlation from the ANOSIM was above 0.2, a subsequent SIMPER analysis was used to determine which variables contributed the greatest towards dissimilarity between treatment factor levels (2 temperature and 3 pCO_2 levels) within each species. Lastly, physiological variables across all four coral species were analyzed using non-metric multidimensional scaling (nMDS) on Euclidean distances after log(x+1) transformation (Ziegler et al. 2014).

In order to better understand possible nuanced physiological changes within each species, individual variables were also analyzed. For each species, individual variables were tested for homogeneity of variance and normality of distribution using the Levene and Shapiro-Wilks tests, respectively. If either test was significant ($p < 0.05$), the data

was log transformed. A two-way analysis of variance (ANOVA) was utilized to test for significant main and interactive effects of pCO_2 and temperature. As our focus was primarily on the main effects, and because only two temperatures were utilized, significant temperature effects were not followed up with post-hoc analyses. Significant differences for pCO_2, were followed by Tukey post-hoc testing to distinguish between the three pCO_2 treatments. Significant interactive effects were followed up by a pairwise comparison among all 6 treatments (Tukey post-hoc). Alternatively, if data failed to meet assumptions of normality even after log-transformation, a Kruskal-Wallis test with multiple comparisons was used. All statistical analyses were performed using R software with the 'vegan', 'car' and 'pgirmess' packages installed. Resulting output from SIMPER, ANOVA and Kruskal-Wallis tests are provided as supplemental information.

2.4 Results:

2.4.1 Symbiont Identification:

Continual specificity between hosts and symbionts was noted for the duration of the experiment, with *Symbiodinium C21a* in *A. millepora, C1c-d-t* in *P. damicornis, C15* in *M. monasteriata,* and *S. trenchii* (formerly called *D1a*) in *T. reniformis.* No other symbiont fingerprints were detected.

2.4.2 Multivariate Analyses (ANOSIM and SIMPER):

The greatest separation between low and high temperature treatments was found within *M. monasteriata,* followed by *T. reniformis* and then *A. millepora* (Table. 1). Although separation between temperature treatments was also significant for *P.*

damicornis, the correlation was very low ($r < 0.2$), suggesting only a minimal thermal effect within this species. The relative contribution of the measured variables to the overall dissimilarity between low and high temperature differed among species, with host lipid and protein and LEDR contributing 36% in *A. millepora* whereas symbiont lipids and LEDR contributed the most (30%) in *M. monasteriata.* Lastly, temperature induced changes in *T. reniformis* were mostly explained through changes in symbiont protein and lipid content, as well as LEDR, accounting for 43% of the dissimilarity (Appendix A; S9). Significant CO_2 effects were only observed for *A. millepora* and *T. reniformis* (Table 1). However, correlation values for CO_2 in both *A. millepora* and *T. reniformis* were very low and therefore were not followed by SIMPER analysis. Figure 1 provides an overview of the above trends. (Fig. 1).

2.4.3 Photosynthesis and Respiration:

Elevated temperature significantly reduced maximum PSII photosynthetic efficiency (F_v/F_m) in both *C21a* in *A. millepora* and *C1c-d-t in P. damicornis* (Fig. 2a-b) (Appendix A; Section S3). Significant interactive effects were observed for *C15* in *M. monasteriata*, as F_v/F_m decreased with temperature only within the ambient pCO_2 treatment (Fig. 2c) (Table S3). The control treatment was also significantly higher than medium pCO_2 treatments and the high temperature, high pCO_2 treatment as well. F_v/F_m did not change for *S. trenchii* in *T. reniformis* (Fig. 2d). There was no change in the photosynthesis to respiration ratios (P:R) across treatments for any coral species (Fig. 3a-d) (Appendix A; Section S4). For *A. millepora, a* significant interactive effect was observed for light enhanced dark respiration (LEDR). However, pair-wise comparisons

revealed significant differences only between the high temperature, medium pCO_2 treatment and the ambient temperature, high pCO_2 treatment (Fig. 3e). For *P. damicornis*, significant interactive effects were also observed, as LEDR increased with temperature but was significant only within the low and high pCO_2 treatments (Fig. 3f). Elevated temperature also significantly increased LEDR in *M. monasteriata*, and *T. reniformis* (Fig. 3g,h).

2.4.4 Symbiont Soluble Protein, Carbohydrate, Lipid, and Cell Volume:

Symbiont protein concentration differed with CO_2 for all three clade C symbionts (Fig. 4a-c), significantly increasing between ambient and medium pCO_2 treatments in *C15* and decreasing between medium and high pCO_2 treatments in *C21a* (Appendix A; Section S5). An interactive effect was noted for *C1c-d-t*, as protein content was significantly elevated within the high temperature, medium CO_2 treatment as compared to the ambient temperature, low CO_2 treatment. Notably, protein concentration increased significantly in *S. trenchii* under elevated temperature by an average of 297% (Fig. 4d) whereas a smaller (25%) increase was noted for *Symbiodinium C15* (Appendix A; Section S5).

While there were no changes in carbohydrates for *C1c-d-t* and *C15* symbionts, an interactive effect was observed for *C21a*, as carbohydrates decreased between ambient and medium pCO_2 only within the ambient temperature treatments (Fig. 4e-g). Overall carbohydrates in *S. trenchii* dropped significantly with elevated temperature (Fig. 4d) (Appendix A; Section S5).

Lipid concentrations did not change significantly in *Symbiodinium C21a* or *C1c-d-t* (Fig. 4i-j). However, an interactive effect was observed for symbiont *C15* (), as lipid concentrations increased with temperature but only within the low and high pCO_2 treatments (Fig. 4k). For *S. trenchii*, lipid concentration declined with both temperature and pCO_2 with the high pCO_2 treatments significantly lower than the low and medium pCO_2 treatments (Fig. 4l).

Cell volume of the *C21a* symbiont within the medium pCO_2 treatments was significantly elevated over both ambient and high pCO_2 treatments (Fig. 4m). No significant changes in volume were detected for the *C1c-d-t* symbiont (Fig. 4n). Cell volume increased significantly with temperature for both *C15* (and *S. trenchii* (Fig. 4o,p). For *S. trenchii,* cell volume also varied with pCO_2, as cells within the medium pCO_2 treatment were significantly smaller than those within the low and high pCO_2 treatments (Appendix A; Section S5).

2.4.5 Host Soluble Protein, Carbohydrate and Lipid Content:

Host protein concentrations declined with temperature in *A. millepora* and *M. monasteriata*. In contrast, host protein generally increased with temperature in *T. reniformis* (Fig 5a, c, d; Appendix A section S6). In addition, *A. millepora* protein content was significantly lower within the medium pCO_2 treatments as compared to both low and high pCO_2 treatments. Host protein content decreased with increasing pCO_2 for *P. damicornis* and medium and high pCO_2 treatments were significantly lower than ambient pCO_2 (Fig. 5b).

A. millepora carbohydrates did not change (Fig. 5e). However, *P. damicornis* carbohydrates decreased with elevated pCO_2 (Fig. 5f), while carbohydrates decreased with temperature in *M. monasteriata* (Fig. 5g). A significant interactive effect was observed for *T. reniformis*, however post hoc analyses found no significant differences among any of the pCO_2 treatments (Fig. 5e) (Appendix A; Section S6).

A. millepora lipids decreased significantly as temperature and pCO_2 increased (Fig. 5i). Lipid content did not change significantly in *P. damicornis* (Fig. 5j). Significant interactive effects were observed for *M. monasteriata*, as lipid content was significantly higher within the control temperature and CO_2 treatment as compared to all other treatments (Fig. 5k). For *T. reniformis*, lipid content was significantly higher in the high pCO_2 treatments as compared to the medium and low pCO_2 treatments (Fig. 5l) (Appendix A; Section S6).

2.4.6 Gene Expression Patterns in Hosts and Symbionts:

Intracellular carbonic anhydrase transcript abundance was significantly up-regulated at high temperature in *A. millepora* (Fig 6a; Appendix A section S7). In contrast, no significant differences were observed for *P. damicornis* (Fig 6b) or for *extracellular carbonic anhydrase* and *Calcium-ATPase* in either species (Fig. 6c-f) (Appendix A section S7). There was a significant interaction for *GAPDH* in *A. millepora* and transcript abundance was significantly higher within both the low and high pCO_2 treatments when compared to the medium pCO_2 treatment, but only within the ambient temperature treatments (Fig. 6g). An interactive effect was also observed for *HSP90* where transcript abundance was significantly higher within the high pCO_2 treatment

compared to the medium pCO_2, but only within the ambient temperature treatments (Fig. 6i) (Appendix A; section S7). There was no change in the GAPDH transcript abundance for *P. damicornis* (Fig. 6h). However there was a significant increase in *HSP90* transcript abundance with temperature (Fig. 6j).

There was no significant difference in *glutamine synthetase* gene expression for the *C21a* symbiont, whereas transcript abundance decreased with elevated temperature for *C1c-d-t* (Fig. 7a-b). High pCO_2 exposure led to a significant up-regulation in symbiont *C21a* α-*ketoglutarate dehydrogenase* transcript abundance (Fig. 7c). Elevated temperature also increased *C21a α-ketoglutarate dehydrogenase* transcript abundance. However this thermal increase was principally driven by the increase observed under medium pCO_2 (Fig. 7c). There was a significant interactive effect for α-*ketoglutarate dehydrogenase* (Appendix A; section S8) in *Symbiodinium C1c-d-t* in *P. damicornis*, as transcript abundance increased significantly with temperature but only within the high pCO_2 treatment (Fig. 7d). For the *C21a* symbiont, *malonyl Co-A acyl transferase* increased with pCO_2 and both medium and high pCO_2 treatments were significantly elevated over low pCO_2 (Fig. 7e). Elevated temperature also significantly increased *malonyl Co-A acyl transferase* in this symbiont, yet again, this was principally driven by the increase observed under medium pCO_2 (Fig. 7e). M*alonyl Co-A acyl transferase* expression did not change in the *C1* symbiont (Fig. 7f, Appendix A section S8).

2.5 Discussion:

The consequence of both host and alga in forming a physiologically unique symbiosis is becoming increasingly clear as we gain a better understanding of the

extensive genetic and physiological diversity that exists for both partners. Multivariate analyses utilized here show clear separation among coral species and a more definitive thermal response as compared with pCO_2. Importantly, the largest thermal separation occurred within species hosting the more historically thermally tolerant symbiont types: *Symbiodinium C15* (*M. monasteriata*) and *S. trenchii* (*T. reniformis*) (LaJeunesse et al. 2009b; Grottoli et al. 2014) indicating larger physiological changes in response to elevated temperature. Assessing thermal sensitivity in corals has largely relied on stability of physiological measurements such as cellular density, chlorophyll and Fv/Fm at elevated temperatures to define thermal tolerance (Fitt et al. 2001). However, by incorporating a broad range of both host and symbiont physiological variables into our analyses, we show that physiological plasticity may be an important thermal stress mechanism, enabling high temperature tolerance in certain host-symbiont combinations. Additionally, because the direction of thermal separation within *M. monasteriata* and *T. reniformis* differed (Fig 1), the specific holobiont response to high temperature also differed between species. By comparing changes observed in the physiological variables measured, we can better understand the unique physiological responses to both temperature and pCO_2 found within each species.

With respect to elevated temperature, there were significant changes in cell volume and biochemical composition in *Symbiodinium C15* and *S. trenchii* (Figs. 3), whereas there were no changes for the more thermally sensitive symbionts *C21a* and *C1c-d-t*. In agreement, heat-induced reductions in PSII efficiency were more pronounced in symbionts *C21a* and *C1c-d-t* as compared to *C15* and *S. trenchii*, and are likely due to an initial increase in photo-stress within the photosynthetic apparatus. While the

photochemical response of *S. trenchii* noted here is consistent with thermal tolerance, there was a significant reduction in F_v/F_m under elevated temperature and ambient pCO_2 in the *C15* symbiont. Additionally, reductions in Fv/Fm in the *C15* symbiont were also observed with increasing pCO_2. This contrasts with Wall et al. (2013) where there was no change in maximal PSII efficiency in *Seriatopora caliendrum* due to elevated pCO_2 exposure (Wall et al. 2014). It is also likely that the photochemical responses noted here were influenced by relatively low light levels (275 μmol quanta m^{-2} s^{-1}), as previous work has highlighted the importance of light intensity in the physiological response to elevated temperature (Mumby et al. 2001) and pCO_2 (Suggett et al. 2012b).

The contrasting trends in PSII photosynthetic efficiency, along with changes in algal density and size may point to important differences in response to high temperature between thermally tolerant vs. sensitive symbionts. We have previously shown that there was a significant drop in *C15* density with elevated temperature (described in Schoepf et al. 2013) which may have increased the internal light field for the remaining symbionts (Enriquez et al. 2005), resulting in a high-light acclimation phenotype. Previous studies have provided a clear link to internal light fields playing a substantial role to the bleaching response (Rodriguez-Román et al. 2006) with high light intensity exacerbating thermal stress. It is interesting to note that increased cell volume is a common strategy for high light acclimation within many phytoplankton species (Thompson et al. 1991), and may also have played a similar function for the *C15* symbiont. Despite thermal reductions in algal density only occurring under high pCO_2 in *T. reniformis*, an increase in cell volume could still play a similar role in changing light fields for *S. trenchii*. While not reported here, pigment analysis from this study did result in a slight yet significant

thermal rise in chlorophyll *a* cell^{-1} in *T. reniformis* (Pettay et al. in prep). An increase in cell volume would help offset potential increases in optical absorption cross section due to increases in chlorophyll density (Finkel 2001). In addition, although thermally-induced changes in biochemical composition were observed for *S. trenchii* and *C15*, they differed with respect to which component (i.e., proteins or lipids) changed significantly (Fig 4), likely also influencing the direction of thermal change between the two species as observed in figure 1. This may indicate differences in the biochemical pathways that correlate to specific changes in light absorption and thermal tolerance. Indeed, recent large-scale metatranscriptome analyses of phytoplankton across different ocean provinces have noted the incredible influence that temperature has over metabolic variability (Toseland et al. 2013). While protein cell^{-1} often rises with temperature in other phytoplankton (Berges et al. 2002), shifting lipid composition has also been noted (Renaud et al. 1995).

Thicker coral tissue could provide greater symbiont photoprotection by changing the intensity and spectral properties of the internal light field (Loya et al. 2001; Dimond et al. 2012) and higher levels of energy reserves (the sum total of lipid, protein and carbohydrate) have been implicated in facilitating bleaching resistance in some Caribbean corals (Grottoli et al. 2014), Hawaiian (Grottoli et al. 2006), and Australian (Anthony et al. 2009) corals. Notably, coral tissue biomass was roughly 25% higher in *T. reniformis* as compared to the other three species (Schoepf et al. 2013). In addition, host protein concentrations in *T. reniformis* were almost twice as high as *A. millepora* and *P. damicornis* (Fig 5). At the same time, carbohydrate concentration in both *M. monasteriata* and *T. reniformis* were roughly 5-10 fold greater than either *A. millepora* or

P. damicornis (Fig 5). This higher biomass may have contributed to providing the symbionts with additional photoprotection and a significant advantage within a high temperature and/or high CO_2 environment.

Interestingly, host protein, lipid and carbohydrate concentrations within this study differ from Schoepf et al., (2013) where whole coral lipid concentrations for *A. millepora* declined at elevated temperature but only at the highest pCO_2 level, whereas few physiological changes were observed within the other three species (Schoepf et al. 2013). However, coral samples were sampled only from the growth tip of each coral species (Schoepf et al. 2013). As skeletal porosity and thickness, along with symbiont cell density, photopigment concentrations, and lipid concentrations may increase with distance from the growth tip (Stimson 1987; Helmuth et al. 1997; Roche et al. 2011), it is likely that the biochemical composition of the symbiosis does as well. Therefore our approach here was to integrate these metrics over the whole coral fragment and quantify host and symbiont biochemical composition separately. As a result, the different trends in host soluble protein and carbohydrates between this study and Schoepf et al (2013) likely reflect spatial differences in physiological function and biochemical makeup between the growing tip (or edge) and the rest of the coral colony as a whole. Such spatial differences may be important in differentiating effects on short-term colony growth versus long-term colony maintenance, and understanding if environmental stress differentially affects small coral recruits (which are likely most similar to coral tips) as compared to larger adult colonies.

The animal host fraction of *A. millepora* and *M. monasteriata* biochemical composition declined the most in response to elevated temperature (Fig 5), yet no

thermally-induced differences were observed for *Symbiodinium C21a*, while *C15* in *M. monasteriata* increased soluble protein and lipid concentrations with temperature (Fig 4). Increased symbiont lipid production, along with reductions in host energetic reserves in *M. monasteriata*, likely imposed substantial metabolic demand on the holobiont and may have contributed to the greater LEDR at high temperature. In contrast, few physiological changes were observed for *P. damicornis,* yet equally large increases in LEDR were noted, suggesting different oxygen consuming pathways are responsible for increased respiration in each species. In addition to thermal enhancement of respiration, divergent use of oxygen consuming pathways within the symbiont may play a role. Photorespiration, alternative oxidase, and especially the Mehler ascorbate peroxidase cycle are all mechanisms possibly used for energy regulation in different phytoplankton, including *Symbiodinium* (Oakley et al. 2014a; Roberty et al. 2014). Likewise, several of these pathways have been implicated in different *Symbiodinium* subjected to high temperature (Warner et al. 1999; Hennige et al. 2011).

Previous studies have reported a significant drop in coral carbonic anhydrase (CA) expression during acute heat (Edge et al. 2005; Leggat et al. 2011) and combined high temperature and pCO_2 exposure (Ogawa et al. 2013). In contrast, we note a temperature-driven increase for intracellular CA in *A. millepora* (Fig. 5a). If the intracellular carbonic anhydrase in *A. millepora* is heavily localized within the gastrodermal tissue layer, as in the coral *Stylophora pistillata* (Bertucci et al. 2011), thermal up-regulation of this CA isoform could indicate enhanced host delivery of carbon to the symbiont. *A. millepora* also displayed a significant increase in net photosynthesis under high temperature (Pettay at al. in prep, data not shown) indicating a potential link

between enhanced carbon delivery by the host and symbiont productivity. However, thermal reductions in Fv/Fm were also noted for *A. millepora* and further complicate the issue. The lack of change in CA expression in *A. millepora* with respect to pCO_2 concentration is consistent with previous OA experiments with adult *A. millepora* colonies (Kaniewska et al. 2012).

Because both extracellular CA and CA-ATPase genes are thought to be involved in calcification (Moya et al. 2008), it is of interest that no change in expression was noted for *A. millepora* despite pCO_2 induced reductions in calcification (Schoepf et al. 2013). In contrast, CA expression drops significantly under elevated CO_2 in *A. millepora* planulae larvae undergoing initial stages of settlement and skeletal formation (Moya et al. 2012), showing that the discrepancies between studies may be driven in part by different life stages tested. The complete lack of changes in either of the carbonic anhydrase or CA-ATPase genes tested within *P. damicornis* may indicate that carbon concentrating mechanisms may differ among species.

The increase in transcripts for heat shock protein 90 (HSP90) in *A. millepora* under high temperature and medium pCO_2 agrees with previous studies, which documented up-regulation of heat-shock proteins as an important component of the thermal stress response (Osovitz and Hofmann 2005; Rosic et al. 2011b). However, for *A. millepora,* this increase in HSP90 transcript was not observed in the highest or lowest pCO_2 treatment and may indicate a sensitivity in the host thermal response to pCO_2. Significant thermal up-regulation of HSP90 transcripts were observed for *P. damicornis,* with the most pronounced increase occurring within the low pCO_2 treatments (Fig 5j), again suggesting that the thermally induced increase in HSP90 may change with pCO_2.

As some heat shock proteins play a fundamental role in protein stabilization, the low pH associated with OA may also affect protein conformation, further complicating the HSP90 response under elevated temperature and high CO_2 (Seveso et al. 2013). Lack of change in expression of GAPDH within either species is not surprising, as previous studies have suggested its relatively stable transcription rate can be utilized as a housekeeping gene for normalization of qPCR data (Seneca et al. 2010).

Studies of nuclear encoded gene expression in *Symbiodinium* typically note small to minimal changes, even when significant thermal and or light stress is applied (Boldt et al. 2009; Rosic et al. 2011a). This is likely a consequence of greater dependency on post-transcriptional regulation within dinoflagellates in general (Okamoto et al. 2001; Bachvaroff and Place 2008). Nevertheless, our results demonstrate distinct expression patterns for two clade C symbionts in two different host species, thus illustrating the physiological diversity contained among different host/symbiont combinations. The symbiont genes studied here represent various metabolic pathways, including nitrogen metabolism (glutamine synthetase), the citric acid cycle (α-ketoglutarate dehydrogenase) and fatty acid synthesis (malonyl Co-A acyl transferase). Interestingly, high temperature-induced down-regulation of glutamine synthetase (*GSII*) in *Symbiodinium C1c-d-t* is similar to the reduction in *GSII* transcripts within the diatom *Thalassiosira pseudonana* and may indicate a reduction in nitrogen metabolism from nitrate (Parker and Armbrust 2005). Although minimal, the increase in α-ketoglutarate dehydrogenase gene expression with increasing pCO_2 in *C21a* correlated with the decline in carbohydrates, possibly indicating an increase in the citric acid cycle, which links amino acid synthesis and breakdown with sugar metabolism. While expression of malonly Co-A acyl transferase in

Symbiodinium C21a increased, this may not suggest enhanced lipid synthesis at high pCO_2, as there was little evidence for this based on cellular lipid content (figure 4i). However, it is possible that additional lipids synthesized by the symbiont were translocated to the host, where evidence of significant lipid catabolism in response to both temperature and pCO_2 was noted.

Similarity analyses indicate that the physiological variables that explain the largest change in one species may be less important in explaining physiological change in another. For example, with respect to temperature, host parameters contributed the most to the physiological response of *A. millepora,* whereas symbiont metrics changed to a greater extent in *T. reniformis*. This highlights the uniqueness of each holobiont as host and symbiont tolerances to environmental stress may differ and greatly influence the resulting physiological responses. In addition, our results indicate that focusing on just a few key variables may not capture the full breadth of physiological change that may occur in response to thermal stress.

When directly comparing trends in each variable, substantial shifts in cell volume and biochemical composition within *Symbiodinium C15* and *S. trenchii* point to potential strategies in thermal tolerance and acclimation not observed within *C21a* and *C1c-d-t*. With respect to elevated pCO_2, increased expression of α-ketoglutarate dehydrogenase correlated with declines in carbohydrate concentration for *C21a* and may reflect an increase in the citric acid cycle. In contrast, protein concentrations within the other two clade-C symbionts increased with pCO_2 and reflect the physiological differences amongst symbiont types at the intra-cladal scale. Furthermore, differing thermal responses in biochemical composition within *A. millepora* and *M. monasteriata* belie similarities in

respiration rates, and suggest that reliance on a few physiological metrics may not fully characterize nuanced physiological differences in response to environmental change. Our results suggest that conclusions based on experimental work may only be applicable to the host/symbiont combination in question and care should be taken in attempting to apply "species-specific" responses towards a more general understanding of coral reef system-wide effects from climate change. Overall, elevated pCO_2 induced very little change across all species, as compared to elevated temperature. However, these results are based on a relatively short-term exposure to OA as compared to what future reefs will endure. Therefore, further studies are required to better understand the extent of physiological change under long-term elevated pCO_2.

Table 2.1: Contribution of temperature and CO_2 to changes in 11 different variables within the four coral species. *A. millepora, P. damicornis, M. monasteriata, T. reniformis.* ANalysis Of SIMilarity (ANOSIM with 9,999 permutations).

	Source of variation	r	*p* value
A. millepora	Temperature	**0.2121**	**1.00E-04**
	CO_2	**0.1218**	**0.0051**
P. damicornis	Temperature	**0.1787**	**4.00E-04**
	CO_2	0.05743	0.1293
M. monasteriata	Temperature	**0.4117**	**1.00E-04**
	CO_2	0.03002	0.2199
T. reniformis	Temperature	**0.3437**	**1.00E-04**
	CO_2	**0.1034**	**0.0234**

Figure 2.1: Non-metric multidimensional scaling (nMDS) plot. Displays similarities within temperature treatments for the four coral species. Black = *A. millepora,* green = *P. damicornis,* red = *M. monsateriata* and blue = *T. reniformis*. Closed circles represent low temperature treatments and open circles represent high temperature treatments. Ellipses represent a 99% confidence bubble around the mean for low temperature (closed ellipse) and high temperature (open ellipse) treatments. Because the ANOSIM analysis found CO_2 to be insignificant or explain only minimal separation across fragments, only temperature differences are depicted in this figure.

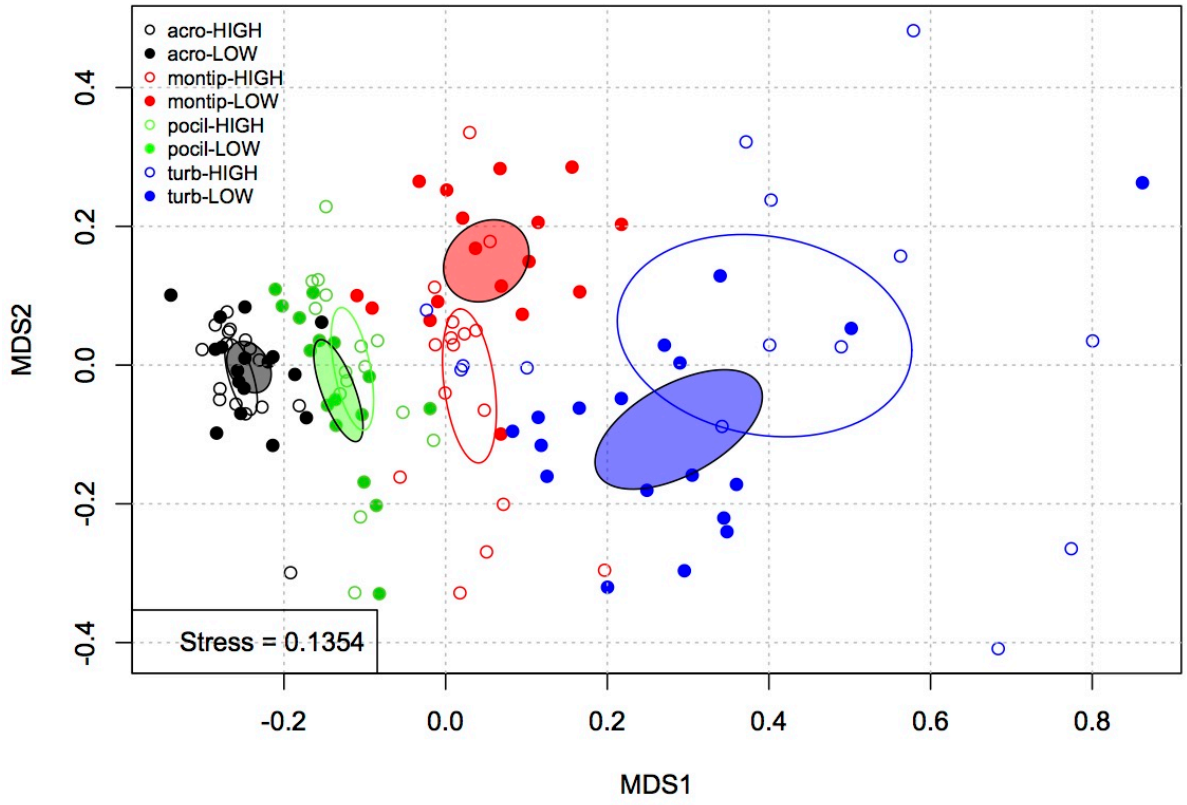

Figure 2.2: Average (± 1SE) maximum photosynthetic efficiency of PSII (F_v/F_m). *Acropora millepora* (a), *Pocillopora damicornis* (b), *Montipora monasteriata* (c), and *Turbinaria reniformis* (d) at three pCO_2 levels and 26.5°C (light bars) or 31.5°C (dark bars). For each pane, the designations 'temp', 'pCO_2' and 'int' indicate significant temperature, pCO_2 or interactive effects (two-way ANOVA). If a pCO_2 effect was observed, the letters indicate significant differences between pCO_2 groups (n = 6). If an interactive effect was observed, the letters above each bar indicate significant differences among the 6 treatments.

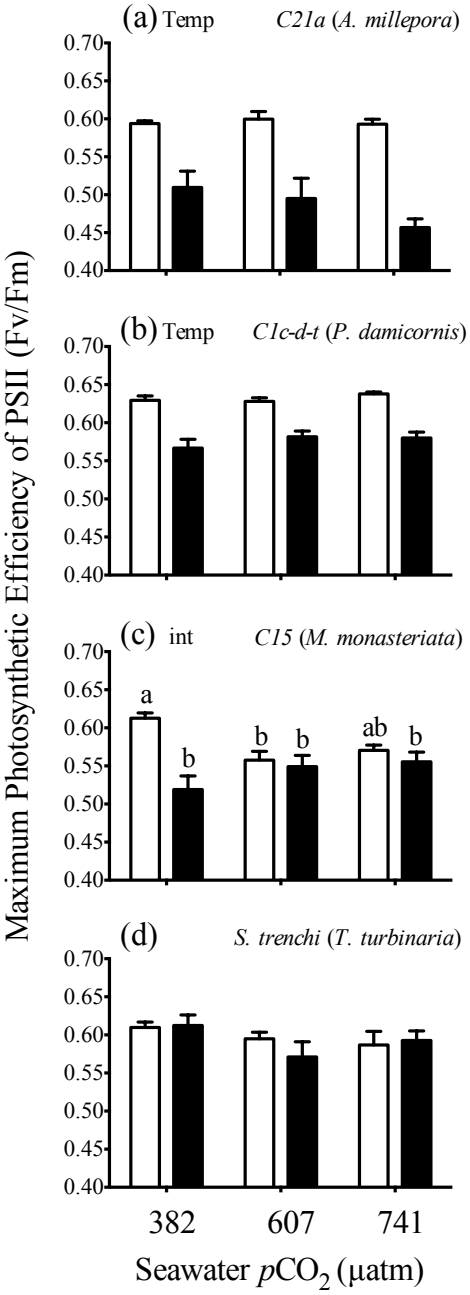

Figure 2.3: Average (± 1SE) photosynthesis to respiration (P:R) and light enhanced dark respiration (LEDR). *Acropora millepora* (a, e), *Pocillopora damicornis* (b, f), *Montipora monasteriata* (c, g), and *Turbinaria reniformis* (d, h) at three pCO_2 levels and 26.5°C (light bars) or 31.5°C (dark bars). For each pane, the designations 'temp', 'pCO_2' and 'int' indicate significant temperature, pCO_2 or interactive effects (two-way ANOVA). If a pCO_2 effect was observed, the letters indicate significant differences between pCO_2 groups (n = 6). If an interactive effect was observed, the letters above each bar indicate significant differences among the 6 treatments.

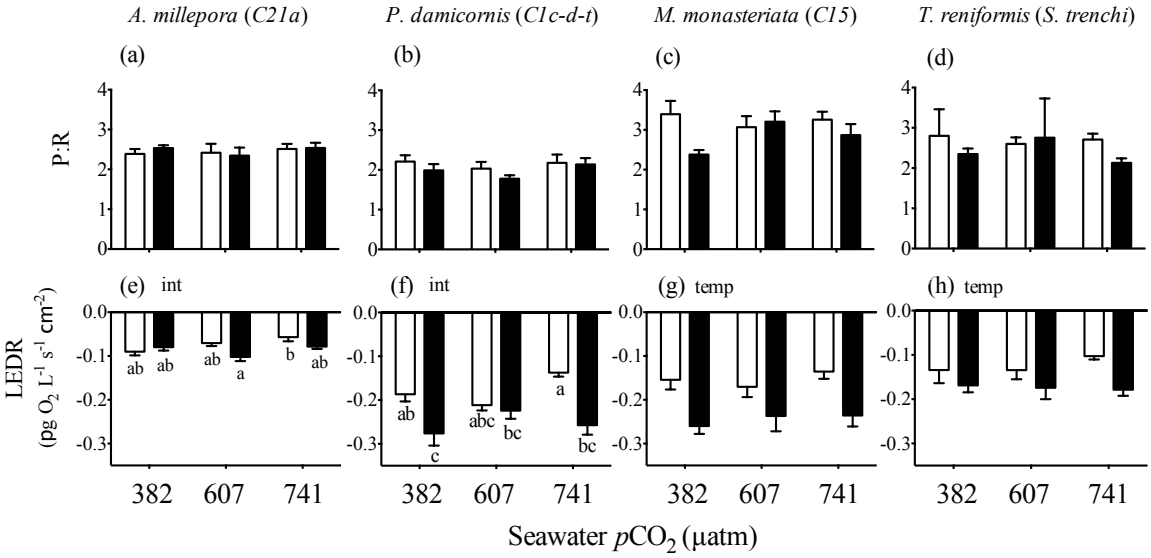

Figure 2.4: Average (± 1SE) total (µg cell^{-1}) protein, carbohydrates and lipid content and cell volume for symbiont type *C21a-A. millepora* (a, e, i, m), *C1-P. damicornis* (b, f, j, n), *C15-M. monasteriata* (c, g, k, o), and *S. trenchii-T. reniformis* (d, h, l, p) at three pCO_2 levels and 26.5°C (light bars) or 31.5°C (dark bars). For each pane, the designations 'temp', 'pCO_2' and 'int' indicate significant temperature, pCO_2 or interactive effects (two-way ANOVA). If a pCO_2 effect was observed, the letters indicate significant differences between pCO_2 groups (n = 6). If an interactive effect was observed, the letters above each bar indicate significant differences among the 6 treatments.

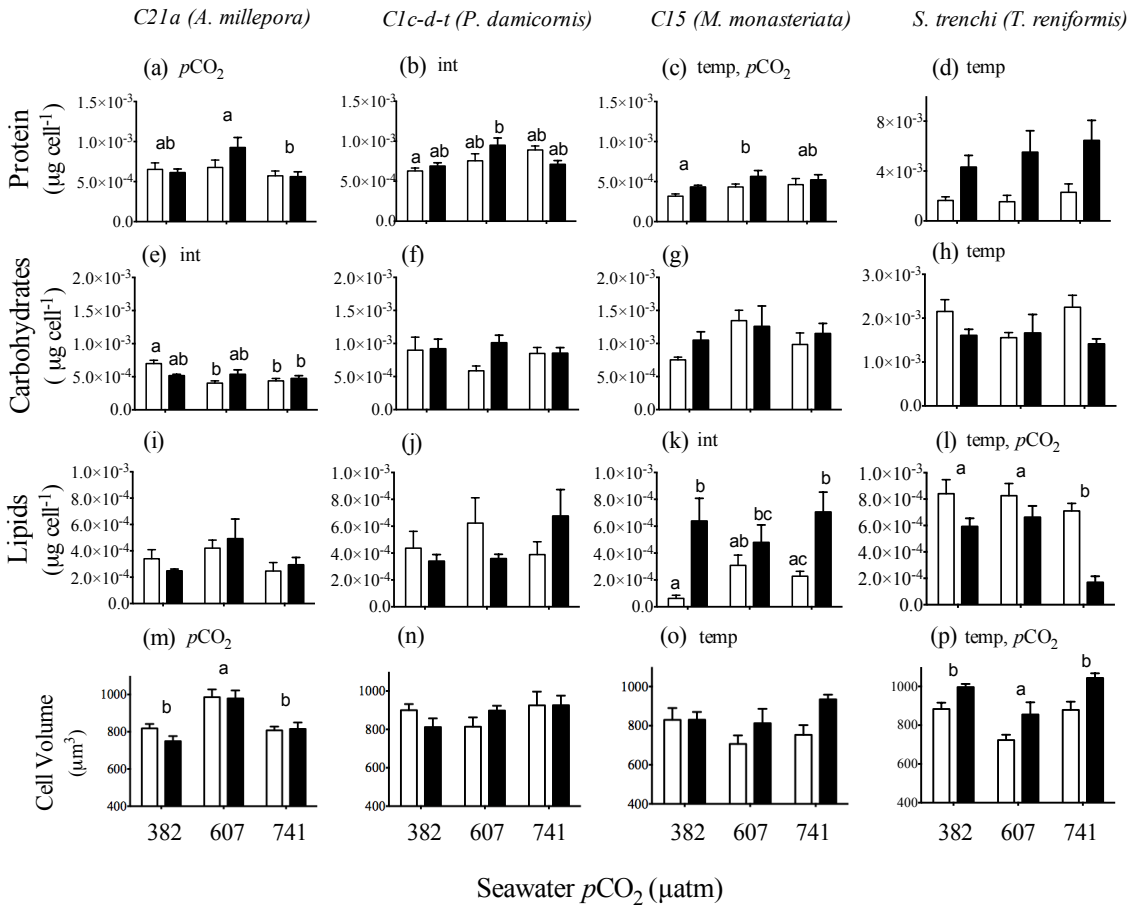

Figure 2.5: Average (± 1SE) total (μg cm^2) animal protein, carbohydrates and lipid from the host corals *Acropora millepora* (a, e, i), *Pocillopora damicornis* (b, f, j), *Montipora monasteriata* (c, g, k), and *Turbinaria reniformis* (d, h, l) at three pCO_2 levels and 26.5°C (light bars) or 31.5°C (dark bars). For each pane, the designations 'temp', 'pCO_2' and 'int' indicate significant temperature, pCO_2 or interactive effects (two-way ANOVA). If a pCO_2 effect was observed, the letters indicate significant differences between pCO_2 groups (n = 6). If an interactive effect was observed, the letters above each bar indicate significant differences among the 6 treatments.

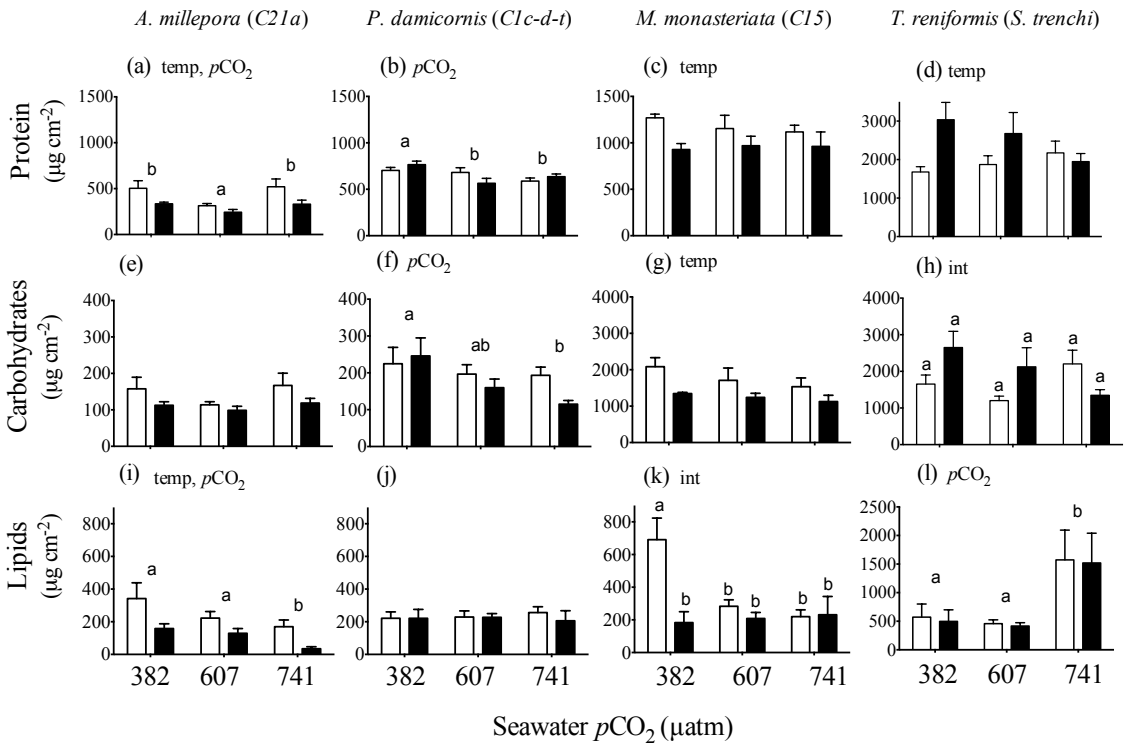

Figure 2.6: Average (± 1SE) relative expression of genes in *A. millepora* and *P. damincornis* encoding intercellular carbonic anhydrase (a, b), extracellular carbonic anhydrase (c, d), calcium ATP ion channel (e, f), glyceraldehyde 3-phosphate dehydrogenase (g, h), and heat shock protein 90 (i, j) at three pCO_2 levels and 26.5°C (light bars) or 31.5°C (dark bars). For each pane, the designations 'temp', 'pCO_2' and 'int' indicate significant temperature, pCO_2 or interactive effects (two-way ANOVA). If a pCO_2 effect was observed, the letters indicate significant differences between pCO_2 groups (n = 6). If an interactive effect was observed, the letters above each bar indicate significant differences among the 6 treatments.

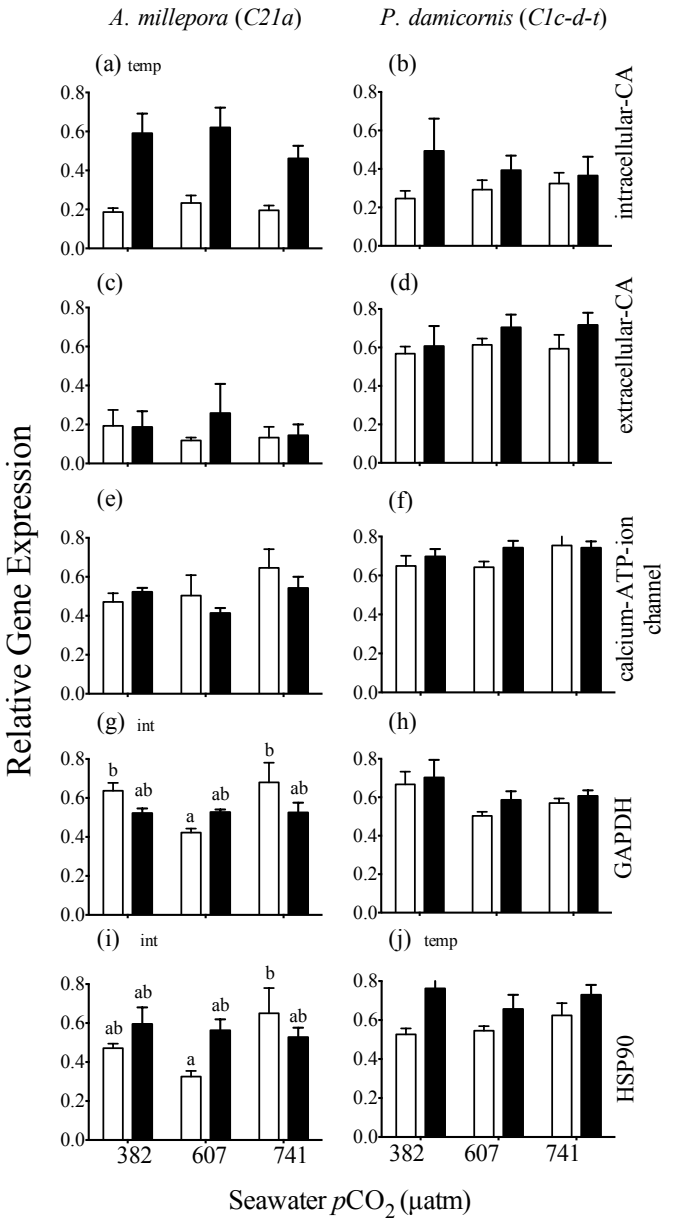

Figure 2.7: Average (± 1SE) relative expression of genes within *Symbiodinium C21a* and *C1c-d-t* encoding glutamine synthetase (a, b), α-ketoglutarate dehydrogenase (c, d), malonyl Co-A acyl transferase (e, f) at three pCO_2 levels and 26.5°C (light bars) or 31.5°C (dark bars). For each pane, the designations 'temp', 'pCO_2' and 'int' indicate significant temperature, pCO_2 or interactive effects (two-way ANOVA). If a pCO_2 effect was observed, the letters indicate significant differences between pCO_2 groups (n = 6). If an interactive effect was observed, the letters above each bar indicate significant differences among the 6 treatments.

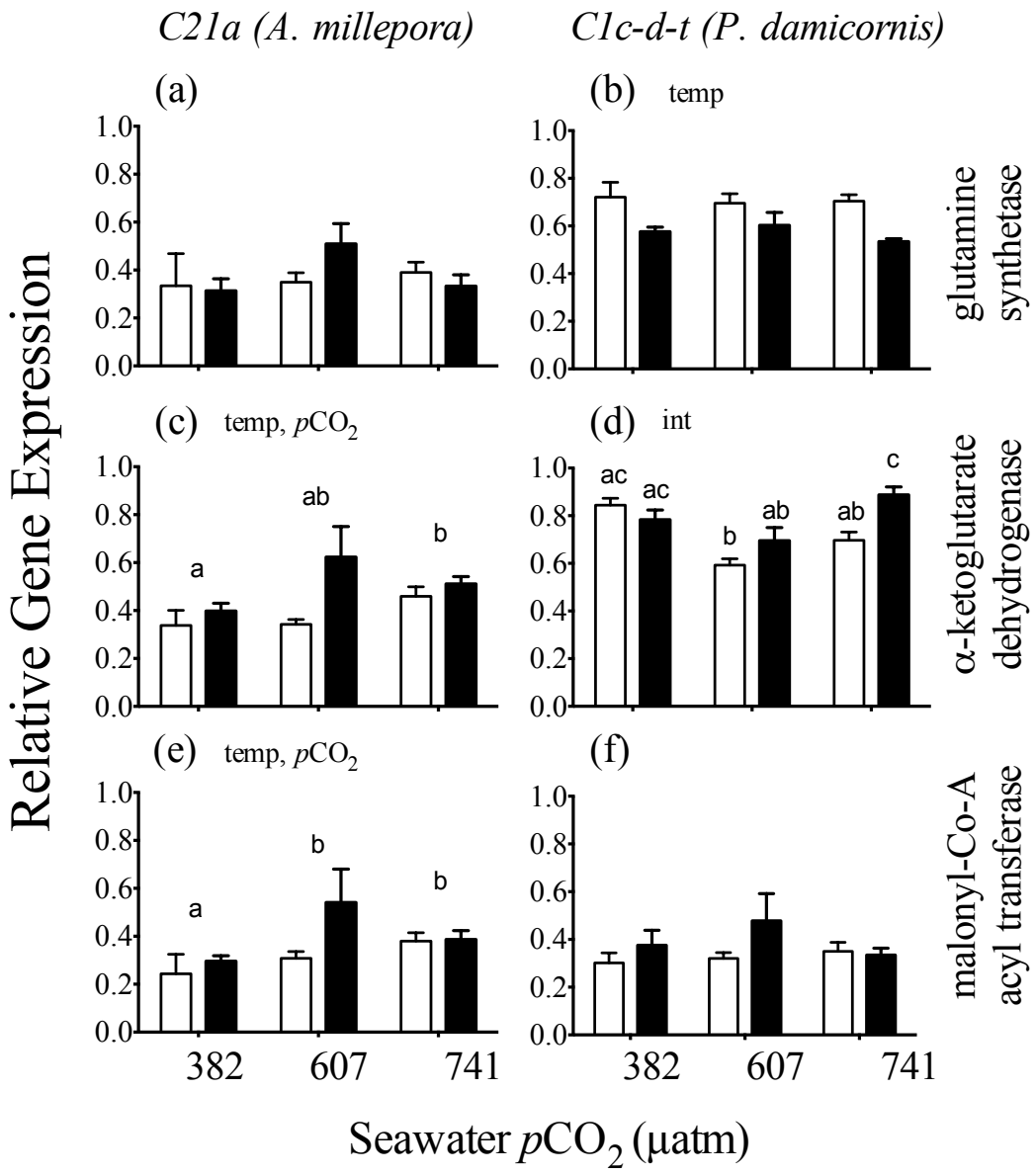

Chapter 3

HIGH TEMPERATURE ACCLIMATION STRATEGIES WITHIN THE THERMALLY TOLERANT ENDOSYMBIONT *SYMBIODINIUM TRENCHII* AND ITS CORAL HOST, *TURBINARIA RENIFORMIS*, DIFFER WITH CHANGING pCO_2 AND NUTRIENTS

3.1 Abstract:

The dinoflagellate *Symbiodinium trenchii* associates with a wide array of host corals throughout the world, and its thermal tolerance has made it of particular interest within the context of reef coral resilience to a warming climate. However, future reefs are increasingly likely to face combined environmental stressors, further complicating our understanding of how *S. trenchii* will possibly acclimatize to future climate scenarios. Over a 33-day period, we characterized the individual and combined affects of high temperature (26.5 vs. 31.5^{o}C), pCO_2 (400 vs. 760 µatm), and elevated nutrients (0.4 and 0.2 vs. 3.5 and 0.3 µmol of NO_3/NO_2 and PO_4^{-3} respectively) on *S. trenchii* within the host coral species *Turbinaria reniformis*. Global analysis across all treatments found temperature to be the largest driver of physiological change. However, exposure to elevated temperature led to changes in symbiont physiology that differed across pCO_2 concentrations. Net photosynthesis and cellular chlorophyll a increased with temperature under ambient pCO_2, whereas temperature related differences in cellular volume and its affect on pigment packaging were more pronounced under elevated pCO_2. Furthermore, increased nutrients mitigated the physiological response to high temperature under both ambient and elevated pCO_2 conditions and represented a significant interaction between all three physical parameters. Individual responses to temperature and pCO_2 were also

observed as cellular density declined with elevated temperature and calcification along with respiration rates declined with increased pCO_2. *S. trenchii* remained the dominant symbiont population within the host across all treatment combinations. Our results reveal distinct physiological changes in response to high temperature within the *S. trenchii/T. reniformis* symbioses that are dependent on pCO_2 and nutrient concentration, and represent important interactive effects to consider as we consider how corals will respond under future climate change scenarios.

3.2 Introduction:

For scleractinian corals, tolerance to high temperature stress is influenced in part by the type of dinoflagellate algal symbiont (*Symbiodinium* .spp) living within the hosts' gastrodermal cells (e.g., (Fitt et al. 2001; Hennige et al. 2011). Association with thermally tolerant symbionts is relevant, as corals face an ever-greater frequency of high temperature events (Hoegh-Guldberg and Bruno 2010; Anthony et al. 2011; Manzello 2015). Although several *Symbiodinium* species have been described as thermally tolerant, *Symbiodinium trenchii* is perhaps best known, with both global distribution and multiple host associations (LaJeunesse et al. 2009b; Hennige et al. 2011; LaJeunesse et al. 2014). However, future climate projections suggest coral reefs will face the combined stress of increased temperature, high pCO_2 and nutrient levels (Hughes and Connell 1999; Hughes et al. 2003; Hoegh-Guldberg et al. 2007). Whether or not different genotypes of *S. trenchii* and their respective hosts are robust, stress tolerant species under a combination of environmental stressors requires further investigation.

Previous studies report both positive and negative interactions between elevated temperature and pCO_2, which are likely dependent on the specific host/symbiont combination in question (Reynaud et al. 2003; Anthony et al. 2008; Rodolfo-Metalpa et al. 2010; Schoepf et al. 2013; Wall et al. 2014; Kwiatkowski et al. 2015). Enhanced carbon availability due to high pCO_2 can stimulate greater carbon fixation rates, thereby altering electron transport through the photosynthetic apparatus (Suggett et al. 2012a; Brading et al. 2013), a common site for thermal damage (Warner et al. 1999). Additionally, higher carbon fixation may also provide greater photosynthate to the host (Hoadley et al. 2015b), which may be advantageous during high temperature stress as an additional source of carbon. However, most beneficial effects of elevated pCO_2 such as increased photosynthetic rates, carbon uptake, growth rates and asexual reproduction have only been observed within symbiotic anemones (Suggett et al. 2012a; Towanda and Thuesen 2012b; Gibbin and Davy 2014; Hoadley et al. 2015b). Effects of elevated pCO_2 appear more varied within scleractinian coral species (Comeau et al. 2009, 2013; Edmunds et al. 2013; Schoepf et al. 2013), with both reductions, no change and increases in calcification rates observed across various coral species.

High rates of PSII reaction center repair are critical for maintaining PSII maximum quantum yields during thermal stress (Takahashi et al. 2004; Smith et al. 2005; Takahashi et al. 2009). However, Symbiodinium living *in hospite* are thought to be nitrogen and phosphorus limited (Cook et al. 1994). Increased nutrient concentrations may mitigate thermal stress by improving rates of repair to the photosynthetic apparatus. Similarly, for certain host/symbiont combinations, increased heterotrophy, and hence nutrient delivery, during thermal stress can minimize reductions in PSII maximum

quantum yields by improving nitrogen availability (Borell and Bischof 2008; Borell et al. 2008). Improved nutrient availability may also be beneficial under high pCO_2 conditions as elevated nitrate and phosphate concentrations ameliorated CO_2 induced reductions in calcification within the temperate coral species *Astrangia poculata* (Holcomb et al. 2010). Similarly, increased heterotrophy enabled the massive *Porites* spp to resist CO_2 induced reductions in calcification (Edmunds 2011). Despite these examples of positive impacts of increased nutrient availability on coral physiology, negative effects from elevated nutrient concentrations may also be present. For symbionts *in hospite,* nutrient availability is largely influenced by the host (Rands et al. 1993; Yellowlees et al. 2008). Therefore, increased environmental nutrient concentrations may disrupt the carefully balanced host/algal symbioses (Cook et al. 1994), potentially leading to a loss in coral growth and/or resilience (Marubini and Atkinson 1999). Increased dissolved inorganic nutrients have been linked to increased disease prevalence (Vega Thurber et al. 2014) and reductions in the bleaching threshold for certain coral species (Wooldridge 2009a; Wiedenmann et al. 2013). Increased nutrient concentrations may also lead to greater symbiont cell density within certain coral species (D'Angelo and Wiedenmann 2014). On an ecosystem level, increased nitrogen concentrations can benefit spatially competitive macroalgal species, impeding recovery of corals during and after bleaching events through physical contact and encroachment onto damaged tissue (Aronson and Precht 2000; Furman and Heck 2008; Smith et al. 2010).

Previous studies characterized the coral *Turbinaria reniformis* as having relatively high biomass and total energy reserves as compared to other Pacific coral species (Schoepf et al. 2013). Energy stores in the form of lipids, carbohydrates and protein

content form the majority of a coral's tissue biomass and species with greater energetic reserves are more likely to recover from thermal bleaching events, when energy-rich symbiont photosynthate is reduced (Grottoli et al. 2004, 2014; Schoepf et al. 2015). Additionally, greater tissue biomass may also be advantageous during thermal stress as thicker tissue provides better photoprotection to the symbionts (Loya et al. 2001; Dimond et al. 2012).

This study tests for the presence of interactive effects between elevated temperature, pCO_2 and nutrients on the photobiology and physiology of *S. trenchii* and its host coral species *Turbinaria reniformis* over a 33-day period. Specifically, we were interested in whether the physiological response to elevated temperature differs when combined with either elevated pCO_2 and/or nutrient concentrations. Overall, physiological changes in response to elevated temperature were observed primarily within the symbiont. However, temperature-induced changes in symbiont physiology differed across pCO_2 concentrations and were mitigated under elevated nutrient conditions. We confirm the presence of interactive effects across all three parameters (temperature, pCO_2 and nutrients) within this host/symbiont combination and discuss potential implications of these results in the context of future climate change scenarios.

3.3 Materials and Methods:

3.3.1 Experimental Design:

The experimental systems, along with many of the methodologies used in this current study are the same as those utilized in an earlier companion study which are

described in greater detail within (Schoepf et al. 2013; Hoadley et al. 2015a). In brief, six colonies of *T. reniformis* were collected at a depth of between 3-10 meters in northwest Fiji, and transported to a coral aquaculture facility in New Albany, Ohio (Reef Systems Coral Farm). Coral colonies were maintained within the aquaculture facility for over 16-months prior to the start of this experiment in October, 2012. Eight fragments from each colony were removed and mounted on 2-inch plastic tiles using coral glue (Eco Tech). After 1-month of recovery, coral fragments were transferred into the experimental systems and slowly acclimated over 10-days to synthetic-seawater closely resembling natural seawater chemistry with regards to dissolved inorganic carbon and total alkalinity (ESV Aquarium Products Inc.). Corals were further acclimated to the experimental systems for an additional month prior to the start of the experiment. The experimental system was comprised of eight separate seawater treatment systems, each consisting of six, 57-L aquaria connected to a central 905-L sump. For each of the 8 treatment systems, one fragment from each of the 6 colonies was placed into each treatment system, with a separate colony fragment in each replicate tank for a sample size of 6 per experimental system. Corals were maintained under a 12:12 hour light:dark cycle with fluorescent lights (Tek Light T5), providing 275-µmol quanta m^{-2} s^{-1} at the base of the filled aquaria. After initial acclimation to the experimental systems, each treatment ran for 33-days. A 25% volume water change was completed every three days on each system, and aquaria were kept free of any bio fouling by periodic cleaning. Salinity was maintained at 35-ppt through daily top-offs with reverse osmosis filtered fresh water. Corals were fed freshly hatched *Artemia nauplii* twice a week.

The experimental treatments consisted of all combinations of ambient (26.5°C) and high (31.5°C) temperature, ambient (400-µatm) and high pCO_2 (760-µatm), and ambient (0.4-µmol NO_3/NO_2 and 0.2-µmol PO_4^{-3}) and high (3.5-µmol NO_3 and 0.3-µmol PO_4^{-3}) nutrient concentrations, for a total of eight separate treatment conditions. Temperature and pCO_2 levels were selected as described in Schoepf at al., 2013. Briefly, ambient temperatures represent average annual temperatures for Fiji and elevated temperatures reflect the bleaching threshold for the area (www.ospo.noaa.gov/Products/ocean/index.html). CO_2 conditions reflect the current global average whereas the elevated CO_2 conditions reflect conditions predicted by the end of this century (IPCC 2013). Nutrient concentrations were deliberately chosen to only be slightly higher than ambient conditions. Temperature within the high temperature treatment tanks was slowly increased (0.5°C day^{-1}) to a maximum of 31.5°C. Temperature was maintained using titanium heaters housed in each sump and regulated with a digital controller (Apex AquaController, Neptune Sys).

pCO_2 within each sump was controlled by a pH stat system for precise control of air and CO_2 gas input into each sump (KSgrowstat, University of Essex). For elevated pCO_2 treatments, CO_2 was increased 100-µatm day^{-1} until the desired pCO_2 concentration was met. Within each treatment, pH measurements were taken every 30-seconds with a glass microelectrode (Thermos Scientific Orion Ross Ultra pH glass electrode) which then controlled a series of solenoids for delivery of CO_2 gas, air, or CO_2-free air (provided by a soda lime scrubber). All pH electrodes were recalibrated daily to NBS standards and independent measurements of pH and alkalinity were made using an AS-ALK2 (Apollo SciTech Inc) titrator according to published protocols (Cai et al. 2010).

Seawater carbonate chemistry based on pH and alkalinity measurements was calculated using the CO2SYS program (Lewis & Wallace, 1998) and is reported in Table 1. TA values were compared against known seawater standards provided by the laboratory of Dr. A Dickson (San Diego, CA, USA).

During the experiment, daily concentrations of NO_3 and PO_4 in each treatment were measured spectrophotometrically using the Hach Nitrate (Method 8192) and Phosphate (Method 8084) assay kits. Based on these measurements, appropriate additions of KNO_3 and KH_2PO_4 from 1M stock solutions, were added in order to bring nutrient treatment concentrations back up to 3.5-µmol NO_3 and 0.3-µmol PO_4, respectively. One hour after the addition of nutrients, concentrations of NO_3 and PO_4 were again spectrophotometrically measured in order to verify the correct amount of nutrients was added. Because nutrient levels would decrease throughout the following 24-hours, these nutrient additions can be described as pulses as opposed to a stable nutrient concentration. In addition to the spectrophotometric measurements mentioned above, water samples were collected into a 10% acid-cleaned 50ml syringe approximately one hour after each nutrient addition and filtered through a GF/F filter (0.7-µm nominal pore size) into 10% acid-cleaned 30ml polycarbonate bottles. These samples were immediately frozen until nutrient concentration measurements were made on a 3-channel Lachat QuikChem 8500 in order to quantify total nitrogen (TN), nitrate/nitrite (NO_3/NO_2), ammonia (NH_3), total phosphorus (TP) and orthophosphate (PO_4) (Table 2). Inorganic nutrient fractions were analyzed simultaneously using the following chemical methods from Lachat instruments: 10-107-06-1-M (NH_3); 10-107-04-1-C/J (NO_3/NO_2); 10-115-01- 1-M (PO_4). TN and TP methods were performed using in-line digestions

(K2S2O8 oxidation): 10-107-04-3-A (TN); 10-115-01-3-F (TP). The sample loops used with this instrument offered sensitivity to 0.002 mg L^{-1} PO_4, 0.005 mg L^{-1} NO_2, 0.01 mg L^{-1} NH_3, 0.002 mg L^{-1} TP and 0.01 mg L^{-1} TN.

3.3.2 Symbiont Identification:

Symbionts were identified through amplification of the internal transcribed spacer 2 region (ITS2) of the ribosomal array, and analysis by previously published protocols for denaturing gradient gel electrophoresis (DGGE) and cycle sequencing (LaJeunesse et al. 2003).

3.3.3 Symbiont Photophysiology:

Dark acclimated maximum quantum yield of photosystem II (Fv/Fm^{MT}) was measured every other day, one hour after the end of the light period by pulse amplitude modulation fluorometry (Diving PAM, Waltz, Germany). Fragments were probed in three separate locations using a 0.6-second saturation pulse (saturation intensity > 8000-μmol quanta m^{-2} s^{-1}) and then averaged together in order to calculate a colony mean maximum quantum yield of PSII. In addition, the single turnover maximum quantum yield of PSII (Fv/Fm^{ST}), functional absorption cross section of PSII (σ_{PSII}) and the maximum electron transport rate between Q_A and Q_B on the acceptor side of the PSII reaction center were collected with a Fluorescence Induction and Relaxation (FIRe) fluorometer (Satlantic Inc., Halifax) (Gorbunov and Falkowski) on the final night of the experiment. Measurements were taken one hour after the start of the dark period and consisted of five iterations of a 120-μs single turnover flash followed by a 2000-μs

relaxation phase consisting of 1-*μs* flashes of a weaker light spaced 59-*μs* apart. Each of the five iterations was spaced 5-seconds apart and provided by an external blue (455nm) LED light source (Satlantic Inc, Halifax). All photochemical parameters listed above were calculated by fitting each fluorescence transient curve using the *FIREPRO* software (Kolber and Falkowski 1998). Excitation via a single turnover fluorometer (such as the FIRe flurometer) only reduces the primary electron acceptor (Q_A) within the PSII reaction center whereas the longer saturation flash of PAM fluorometer reduces both primary and secondary acceptors within the PSII reaction center and the plastoquinone pool (Suggett et al. 2003).

On the final day, Maximal photosynthetic rates and light acclimated dark respiration (R_L) were measured via oxygen evolution and consumption with galvanic electrodes (Qubit systems) housed in clear acrylic chambers (350-mL). Chambers were surrounded by a water bath to maintain the control and experimental temperatures. Constant circulation was provided by a stirbar in each chamber. Illumination was supplied by a customized 24 LED array (Cree Cool White XP-G R5). In order to ensure maximal photosynthetic rates, light intensity was set to 600-μmol quanta m^{-2} s^{-1}, and pilot experiments at this light intensity showed no signs of photoinhibition (not shown). Maximal net photosynthesis ($Pmax_{net}$) was recorded for 15-20 minutes, followed by a 10-minute dark incubation after the lights were switched off to record the light acclimated dark respiration (R_L). After incubation, coral fragments were returned to their respective treatments tanks. The photosynthesis to respiration ratio was calculated as $(Pmax_{gross})/(R_L)$ where $Pmax_{gross} = (Pmax_{net} + R_L)$. Gross photosynthesis and light acclimated dark respiration (R_L) were normalized to total surface area (cm^2) for each

coral fragment (described below) and net photosynthesis was normalized to algal cell number.

3.3.4 Host and Symbiont Physiology:

At the end of the 33-day treatment, samples were frozen in liquid N_2 and stored at -80°C until further processing. Coral tissue was removed with a water pick (Johannes and Wiebe 1970) in 40mL of recirculating synthetic seawater. The resulting slurry was homogenized with a Tissue-Tearor ™ (BioSpec products, Inc), and then centrifuged for 5 minutes (5,000-g) to separate the algal symbiont and coral fractions. Pelleted symbionts were resuspended in synthetic seawater and divided into 1mL aliquots. For algal cell density and volume calculations, an aliquot was preserved with 10-μL of 1% glutaraldehyde. Six independent replicate counts were performed for each algal sample on a hemocytometer. Samples were photographed using a Nikon microphot-FXA epifluorescent microscope (100x magnification). Photographs were then analyzed by computer using Image J (NIH) with the analyze particles function. Pixel size of each cell was converted to μm^2 using a calibrated scale micrometer and then used to calculate cell diameter and volume based on calculations for a sphere.

For symbiont cell protein concentration, 1-mL samples were homogenized with a bead-beater (BioSpec) for 2-minutes and then analyzed using the BCA method by absorbance at 595-nm (Smith et al. 1985) (Thermo Scientific Pierce), with bovine serum albumin standards. For determination of chlorophyll *a*, a second 1-mL aliquot of pelleted symbionts was resuspended in 90% methanol and then homogenized via bead beating for two minutes. Samples were then incubated at -20°C for two hours, and then centrifuged

at 2300-g for five minutes. Absorbance of the resulting supernatant was measured at 665, 652 and 750-nm and chlorophyll *a* calculated by published equations (Porra et al. 1989). All absorbance measurements were recorded by a FLUOstar Omega plate reader (BMG labtech). Coral skeletal surface area was determined by the foil method (Marsh 1970).

3.3.5 Calcification Rates:

Net calcification was determined using the buoyant weight technique (Jokiel et al. 1978) and then converted to dry weight. Each coral fragment was buoyantly weighed at the beginning and end of the experiment. Daily calcification rates were calculated as the difference between initial and final weights, divided by number of experimental days, and standardized to coral surface area.

3.3.6 Statistical Analysis:

Physiological variables were split into symbiont specific ($FvFm^{ST}$, $\sigma_{PSII,}$ Chlorophyll a $cell^{-1}$, Symbiont cellular volume, Photosynthesis $cell^{-1}$ and symbiont protein $cell^{-1}$) and holobiont (Cellular density, PR ratio, LEDR and Calcification) physiological parameters. Symbiont specific and holobiont physiological parameters were analyzed using an ANalyses Of SIMilarities test (ANOSIM) with 9,999 permutations to test for significant separation between Temperature, CO_2 and Nutrient treatments. Because only temperature revealed any significant separation, ANOSIM was again utilized to test for significant temperature affects within each CO_2 and Nutrient combination. Non-metric multidimensional scaling (nMDS) on Euclidean distances after log(x+1) transformation (Ziegler et al. 2014) for each set of physiological variables was

also utilized to visualize separation across treatment groups. Multivariate analysis was followed up with univariate analysis in order to better elucidate small-scale differences observed among individual variables. A three-factor analysis of variance (ANOVA) was utilized to test for significant effects and any possible interactive effects between pCO_2, temperature and nutrients. When significant differences were observed, a Tukey post-hoc test was performed for analysis between different factor combinations. If there was a significant interaction between all three factors, a pairwise analysis between all 8 treatments was performed, and the main effects were ignored if interactive effects were observed. All data sets were tested for homogeneity of variance and normality of distribution using the Levene and Shapiro-Wilks tests respectively. If either test was significant ($P < 0.05$), the data was log transformed and retested prior to further analysis. For PAM based measurement of the maximum quantum yield of PSII (Fm/Fm^{MT}), a generalized linear mixed model (GLMM) was used to test for the effects of time, temperature, pCO_2 and nutrients (Appendix B; supplementary table 3). All statistical analyses were performed using R software with 'ez', 'car' and 'pgirmess' packages installed. Resulting statistical tables can be found within the supplementary materials (Appendix B; table S1-5).

3.4 Results:

3.4.1 Symbiont Identification:

S. trenchii (ITS2-type *D1a*) was the only symbiont detected within all fragments of *T. reniformis* throughout the duration of the experiment.

3.4.2 Multivariate Analysis:

Global analysis across all treatments found only temperature induced significant separation (ANOSIM: R=0.220, *P*=1e-04), and only with respect to symbiont specific physiology (Fig. 1). However, dissimilarity between ambient and elevated temperature treatments was only significant under low nutrient conditions as elevated nutrient concentrations mitigated the thermal response for both ambient and elevated pCO_2 treatments. In addition, the nMDS analysis shows the direction of thermal separation within the low nutrient treatments differs between ambient and elevated pCO_2 conditions, suggesting that the physiological changes in response to temperature also differ (Fig 1).

3.4.3 Symbiont Physiology:

Net photosynthesis $cell^{-1}$ increased with temperature by an average of 47% but only at low pCO_2 levels ($P = 0.03839$) (Fig. 2a, Appendix B table S1). Cellular volume increased with temperature ($P < 0.0001$) and decreased with pCO_2 ($P = 0.0138$) (Fig. 2b, Appendix B table S1). Chlorophyll *a* $cell^{-1}$ significantly increased (av. 38%) with temperature but only within the ambient pCO_2 treatments ($P= 0.0109$) (Fig. 2c, Appendix B table S1). Cell protein concentration increased significantly with temperature *(*$P = 0.0087$) on average by 21% (Fig. 2d, Appendix B table S1).

3.4.4 Holobiont Physiology:

Cell density declined by an average of 34% with increasing temperature ($P = 0.00857$), irrespective of pCO_2 (Fig. 3a, Appendix B table S2). Likewise, calcification rates decreased significantly by 35% with elevated pCO_2 ($P = 0.01$) (Fig. 3b, Appendix B

table S2). Light enhanced dark respiration decreased significantly by 37% ($P = 0.0189$) with elevated pCO_2 (Fig. 3c, Appendix B table S2). The ratio of photosynthesis to respiration (P:R) increased 37% with elevated pCO_2 but only under low nutrient concentrations ($P = 0.0210$) (Fig. 3d, Appendix B table S2).

3.4.5 Photochemistry:

On the final day of the experiment, Fv/Fm^{ST}, as measured by single turnover chlorophyll fluorometry, was significantly reduced by 20% with elevated temperature and nutrients but only within the high pCO_2 treatments ($P = 0.015$) (Fig 4a, Appendix B table S4). A significant interactive effect among all three factors ($P = 0.0129$) was observed for the functional absorption cross section of PSII (σ_{PSII}), which was 40% higher in the high pCO_2 treatment compared to the ambient pCO_2 treatment but only under ambient temperature and nutrient conditions (Fig. 4b, Appendix B table S4).

Although no significant four-way interaction between time, temperature, pCO_2 and nutrient concentration was noted for Fv/Fm^{MT}, minimal yet significant interactions ($P < 0.0001$) between temperature, pCO_2 and nutrient concentrations were noted (Appendix B table S3). Under elevated nutrient conditions, Fv/Fm^{MT} declined due to either increased pCO_2 and/or elevated temperature, whereas under low nutrients, Fv/Fm^{MT} declined only when both pCO_2 and temperature were elevated (Fig 5). Elevated pCO_2 also decreased Fv/Fm^{MT} but only under elevated nutrient conditions (Fig 5).

3.5 Discussion:

3.5.1 Symbiont Physiology:

Although previous studies have observed interactive effects between elevated temperature and pCO_2 or nutrient concentrations on coral physiology (Holcomb et al. 2010; Edmunds 2011; Schoepf et al. 2013; Wall et al. 2014; Kwiatkowski et al. 2015), few studies have tested interactive effects between all three factors. In this study, temperature was the main factor driving physiological change. However, there was a clear difference in how *S. trenchii* responded to elevated temperature while under ambient or elevated pCO_2 treatments. Under ambient pCO_2, elevated temperature led to an increase in net photosynthesis (normalized to algal number) and chlorophyll content despite a loss in algal density (Figs 2a,c and 3a). Symbiont loss may increase the availability of dissolved inorganic carbon (DIC) for remaining symbionts (Wooldridge 2009a), potentially explaining the increase in productivity (Weis et al. 1989; Weis 1993; Weis and Reynolds 1999). In addition, there was no temperature-induced change in Fv/Fm or functional absorption cross section of PSII under ambient pCO_2 and nutrient conditions, suggesting that physiological changes observed in *S. trenchii* indicate minimal, if any, thermal stress. In contrast, under high pCO_2 conditions, the drop in cell density with high temperature was not accompanied by increased chlorophyll a or net photosynthesis (Fig 2a, c and 3c). Interestingly, while cell density decreased with elevated temperature, cellular volume of the remaining *Symbiodinium* increased (Fig. 2c and 3a). Increased cell volume in free-living phytoplankton is typically associated with a higher 'package effect' where greater chlorophyll concentrations within larger cells

increase self-shading and thereby attenuate the light intensity within the cell (Finkel 2001; Key et al. 2010). Increased chlorophyll concentration with temperature may have increased the package effect under ambient pCO_2, however no increase was observed within the elevated pCO_2 treatments. Static chlorophyll content, combined with increased cellular volume, would decrease pigment packaging and enhance light intensity within the cell. This in turn may have increased the excess excitation energy within the symbionts subjected to high temperature, thus leading to the decline in PSII maximum quantum yield (for both Fv/Fm^{MT} and Fv/Fm^{ST}) observed under elevated pCO_2 and ambient nutrient levels.

Similar to that observed in another study that examined the physiological impacts of ocean acidification and temperature in four Pacific coral species (Hoadley et al., 2015a), algal cellular protein levels increased with temperature and were unaffected by pCO_2 in this study (Fig 2d). However, increased symbiont protein content at low pCO_2 was most likely due to the coinciding increase in chlorophyll *a*, whereas chlorophyll *a* did not change in the high pCO_2 treatments. Although algal proteins increased with temperature at both pCO_2 concentrations, the type of proteins synthesized may have differed. Host and symbiont heat-shock protein expression are commonly unregulated in response to thermal stress (Leggat et al. 2011; Rosic et al. 2011b), and under high pCO_2 and temperature, heat shock protein synthesis may have been higher relative to ambient conditions. Additionally, elevated Rubisco content may have also accounted to the increased protein content at high temperature. Greater photosynthetic carbon acquisition has been observed in response to elevated temperature within certain *Symbiodinium* strains (Oakley et al. 2014b). Similarly, Rubisco activity and gene expression were both

elevated with temperature in the marine Diatom *Thalassiosira weissflogii* (Helbling et al. 2011). Such different patterns in cellular protein content highlights another important interactive effect between environmental stressors that warrants further investigation.

Despite the differences observed in response to elevated temperature between ambient and elevated pCO_2 conditions, the multivariate analysis showed dissimilarity between ambient and elevated temperature groups is minimized under elevated nutrient conditions (Fig 1). Additional nutrients to the host and symbiont provided through increased feeding rates or food availability can lead to lower rates of both bleaching and photosynthetic damage during high temperature events (Grottoli et al. 2006; Ferrier-Pagès et al. 2010; Tolosa et al. 2011; Béraud et al. 2013). For cultured *Symbiodinium* grown under nutrient replete conditions, enhanced nitrate reductase activity can provide an important electron sink within the photosynthetic apparatus, thereby helping to reduce partial pressure over the PSII reaction center (Lomas and Glibert 1999; Rodríguez-Román and Iglesias-Prieto 2005). In addition, greater nutrient availability within the alga can also increase repair rates of the D1 protein in PSII, as nitrogen is no longer a limiting factor in protein synthesis (Steglich et al. 2001). This is of particular interest under elevated temperature conditions since the D1 protein is especially susceptible to thermal damage within certain symbionts (Warner et al. 1999). High nutrient conditions may increase cellular densities within certain scleractinian coral species (Falkowski et al. 1993; Fabricius 2005) and recent work has suggested that environmental stressors which increase cellular densities may increase susceptibility to thermal bleaching (Cunning and Baker 2013). For *T. reniformis* housing *S. trenchii,* no difference in cellular density due

to elevated nutrient concentrations is observed and may suggest that nutrient dependent changes in cellular density may be species specific.

3.5.2 Holobiont Physiology:

Although the interactive effects observed within this experiment were predominantly symbiont driven, holobiont physiology also changed in response to temperature and pCO_2. Symbiont cellular density can be highly dynamic and seasonal and environmental differences in algal density have been noted across many species (Fitt et al. 2000; Cunning et al. 2015). Many corals lose *Symbiodinium* during high temperature stress, and while the precise cellular triggers for expulsion are still unknown, one predominant hypothesis is that cell loss is due to a host response to increased reactive oxygen species produced by photodamaged algal symbionts (Lesser 1997; Fitt et al. 2001; Smith et al. 2005). However, for certain thermally tolerant host/symbiont combinations, a loss of symbionts during high temperature exposure may also reflect acclimation (Jones and Berkelmans 2010b; Takahashi et al. 2013) or be driven by a host derived stress response alone. Ulstrup et al., (2006) demonstrated symbiont loss with elevated temperature in *T. reniformis* harboring thermally sensitive *Symbiodinium C1* as well as colonies harboring more thermally tolerant clade D symbionts. Since *S. trenchii* is often considered a thermally tolerant symbiont (Grottoli et al. 2014; Silverstein et al. 2015) and Fv/Fm did not decline under elevated temperature alone (Fig 4), symbiont loss with high temperature (Fig 1a) may indicate a host response independent of symbiont stress level. Because symbiont loss with elevated temperature may occur independently of major reductions in PSII photochemistry (Ulstrup et al. 2006a; Tolosa et al. 2011), it is

likely that reduced cell density is a host response of *T. reniformis* to high temperature and not necessarily in response to thermal damage within the symbionts.

Although minimal, the lower rates of LEDR noted at higher pCO_2 likely reflected a lower metabolic demand in *T. reniformis* (Fig. 2d). However, as respiration rates incorporate simultaneous host and symbiont O_2 consumption and the relative proportion from each can vary (Hawkins et al. 2016), we are unable to pinpoint how this decline is partitioned between the symbiont and host. Reduced respiration was also observed for *A. millepora* under elevated pCO_2, and corresponded with transcriptional down regulation of metabolic activity within the host (Kaniewska et al. 2012). It is possible that lower calcification rates in corals under elevated pCO_2 reduces metabolic demand thereby driving down respiration further. However, lower respiration and calcification rates with elevated pCO_2 were not observed for *T. reniformis* in previous work by Hoadley et al. (2015a) and Schoepf et al. (2013) and this difference may have resulted from the longer duration of the current experiment. From this study and others, it is clear that the metabolic demand of the symbioses can be significantly influenced by changing pCO_2 (Kaniewska et al. 2012, 2015). Interestingly, respiration rates increased with high pCO_2 for the anemones *E. pallida* and *Anemonia viridis*, possibly reflecting fundamental differences in how ocean acidification impacts calcifying vs. non-calcifying cnidarian/alga symbioses (Suggett et al. 2012a; Gibbin and Davy 2014).

3.5.3 Symbiont Photophysiology:

Although minimal, Fv/Fm^{MT} declined with high temperature within both the 'ambient pCO_2 and high nutrient' treatment as well as within the 'elevated pCO_2 and

ambient nutrient' treatments (Fig 5). However, when active chlorophyll a fluorescence was measured with the FIRe fluorometer, significant declines in Fv/Fm^{ST} due to high temperature were only observed within the elevated pCO_2 and ambient nutrient treatment (Fig 5a). Because Fv/Fm^{ST} is insensitive to changes occurring downstream of the Q_A^- site in the PSII reaction center, it is likely that the site of thermal stress within the high pCO_2 and low nutrient treatment resided within the PSII reaction center. In contrast, the absence of a significant decline in Fv/Fm^{ST} while Fv/Fm^{MT} was reduced within the ambient pCO_2 and high nutrient treatment likely reflected changes occurring within the plastoquinone pool or even further downstream in the electron transport chain or other locations within the chloroplast (Buxton et al. 2012). These differences provide an additional example of how the *S. trenchii* response to high temperature differs with respect to pCO_2 and nutrient concentrations and suggests that the mechanism responsible for high temperature induced reductions in Fv/Fm likely differ between the two groups

Enhanced PSII repair with high N availability is of particular importance, as high temperature or high pCO_2 may increase rates of D1 protein degradation (Warner et al. 1999; Gao et al. 2012). For these reasons, high-temperature induced declines in Fv/Fm^{MT} are contrary to that expected for symbionts under high temperature and elevated nutrient conditions. However, for the high nutrients and ambient pCO_2 treatment, the decline in Fv/Fm^{MT} observed under high temperature occurred early in the experiment and was then maintained throughout the remainder of the experiment, likely reflecting a different acclimation state and not thermal stress and photoinactivation per se (Rodríguez-Román and Iglesias-Prieto 2005). In contrast, small yet significant high temperature induced reductions in Fv/Fm^{MT} were observed only within the last days of the elevated pCO_2 and

low nutrient treatment. It is unclear if these represent a threshold where PSII protein repair rates could no longer keep up with damage caused by compounding temperature and/or pCO_2 stress, or a change in acclimation state similar to that observed early on in the experiment within the low pCO_2 and high nutrients treatment.

3.5.4 Conclusion:

Although previous studies found few interactive effects between temperature and pCO_2 within the *T. reniformis / S. trenchii* symbiosis (Schoepf et al. 2013; Hoadley et al. 2015a; Levas et al. 2015), the longer experimental duration of this study (24-days in Schoepf at al., 2013, Levas et al., 2015 and Hoadley et al. 2015a vs. 33-days in this study) may account for the greater number of interactive effects observed here. Overall, temperature was the largest factor in driving physiological change. However, interactive effects are also present as under ambient pCO_2, cellular density declined with elevated temperature, allowing remaining symbionts to possibly take advantage of an increase in DIC availability, resulting in increased photosynthetic productivity on a per cell basis and increases in chlorophyll a. Under elevated pCO_2 conditions, reduced cell density due to high temperature was not accompanied by increases in chlorophyll a or net photosynthesis. Instead a larger difference in cellular volume between ambient and elevated temperature was observed, potentially altering the package effect and increasing light intensity within the cell. Differences in the ratio of chlorophyll *a* to protein also suggest that symbiont protein expression during thermal stress is also pCO_2 dependent. Decreased holobiont respiration and coral calcification rates confirm previously reported changes in metabolism and growth rates that are dependent on pCO_2 concentration

(Kaniewska et al. 2012; Comeau et al. 2013). Despite pCO_2 based differences in the physiological response to high temperature, our multivariate analysis shows that elevated nutrient concentrations minimize the thermal response under both ambient and elevated pCO_2 conditions. This is of particular importance given the global distribution of *S. trenchii* and its association with multiple host species. However, our study utilized only minor nutrient pulses and results may differ under higher nutrient loads. Additionally, such interactive effects will almost certainly vary across host/symbiont combinations and future research is needed to incorporate additional species responses from both Pacific and Caribbean coral reefs.

Table 3.1: Mean (± 1 SE) carbonate chemistry parameters for the eight treatments representing two pCO_2 levels (400 vs 760 µatm), nutrient concentrations (low vs. high) and two temperatures (26.5 vs 31C) (n = 20-26). HT = high temperature, LT = low temperature, HC = high pCO_2, LC = low pCO_2, HN = high nutrients and LN = low nutrients.

	Temp (°C)	**pH (NBS scale)**	**TA (µmol kg^{-1})**	**pCO_2 (µatm)**	**xCO_2 (ppm)**	**Ω_{arag}**
LT+LC+LN	26.06 ± 0.05	8.19 ± 0.01	2350.87 ± 18.12	410.63 ± 17.42	424.50 ± 18.01	3.59 ± 0.09
HT+LC+LN	29.34 ± 0.41	8.18 ± 0.01	2302.01 ± 16.34	414.56 ± 10.34	432.27 ± 10.90	3.81 ± 0.08
LT+HC+LN	26.60 ± 0.16	7.97 ± 0.02	2333.18 ± 11.15	752.82 ± 30.49	778.95 ± 31.50	2.41 ± 0.09
HT+HC+LN	30.13 ± 0.30	7.98 ± 0.01	2338.55 ± 12.31	741.93 ± 25.56	774.34 ± 26.90	2.74 ± 0.07
LT+LC+HN	26.51 ± 0.03	8.22 ± 0.01	2293.55 ± 14.16	358.34 ± 6.50	370.76 ± 6.71	3.74 ± 0.06
HT+LC+HN	30.01 ± 0.30	8.17 ± 0.01	2319.94 ± 12.85	423.89 ± 10.38	442.26 ± 10.95	3.84 ± 0.06
LT+HC+HN	26.33 ± 0.04	7.97 ± 0.01	2377.92 ± 8.78	752.10 ± 28.14	777.88 ± 29.10	2.45 ± 0.07
HT+HC+HN	29.59 ± 0.33	7.96 ± 0.02	2365.49 ± 11.51	794.31 ± 32.51	828.10 ± 34.20	2.64 ± 0.08

Table 3.2: Mean (± 1 SE) nutrient concentrations for the eight treatments representing two pCO_2 levels (400 vs 760 µatm), nutrient concentrations (low vs. high) and two temperatures (26.5 vs 31C) (n = 20-26). HT = high temperature, LT = low temperature, HC = high pCO_2, LC = low pCO_2, HN = high nutrients and LN = low nutrients.

	TN (µmol N/L)	**NO_3/NO_2 (µmol N/L)**	**NH_3 (µmol N/L)**	**TP (µmol P/L)**	**Ortho PO_4 (µg P/L)**
LT+LC+LN	3.81 ± 1	0.39 ± 0.08	0.26 ± 0.19	0.24 ± 0.02	6.54 ± 0.29
HT+LC+LN	3.97 ± 1.45	0.35 ± 0.05	0.49 ± 0.65	0.27 ± 0.02	6.57 ± 0.35
LT+HC+LN	5.67 ± 2.24	0.49 ± 0.19	0.22 ± 0.09	0.25 ± 0.02	6.84 ± 0.28
HT+HC+LN	3.88 ± 0.79	0.41 ± 0.22	0.24 ± 0.11	0.25 ± 0.03	7.41 ± 1.33
LT+LC+HN	7.40 ± 1.58	3.48 ± 0.64	0.55 ± 0.67	0.32 ± 0.02	9.97 ± 1.85
HT+LC+HN	7.10 ± 1.55	3.52 ± 1.21	0.32 ± 0.47	0.32 ± 0.09	9.81 ± 1.85
LT+HC+HN	7.62 ± 2.67	3.68 ± 1.60	0.16 ± 0.17	0.29 ± 0.04	9.04 ± 1.89
HT+HC+HN	7.19 ± 0.88	3.56 ± 0.96	0.19 ± 0.09	0.32 ± 0.07	9.23 ± 2.35

Figure 3.1: Non-metric multidimensional scaling (nMDS) plot. **Top:** Symbiont physiology and photobiology and **Bottom:** Holobiont physiology. Colors depict each of the four pCO_2 and nutrient treatments. Closed circles represent low temperature treatments and open circles represent high temperature treatments. Because global analysis via ANOSIM only found significant separation with respect to temperature, subsequent multivariate analysis test for temperature effects within each pCO_2 and nutrient treatment and are included within the figure (**Table**). Ellipses represent a 95% confidence bubble around the mean for low temperature (open ellipse) and high temperature (closed ellipse) treatments and are displayed only for groups with significant separation as observed using ANOSIM.

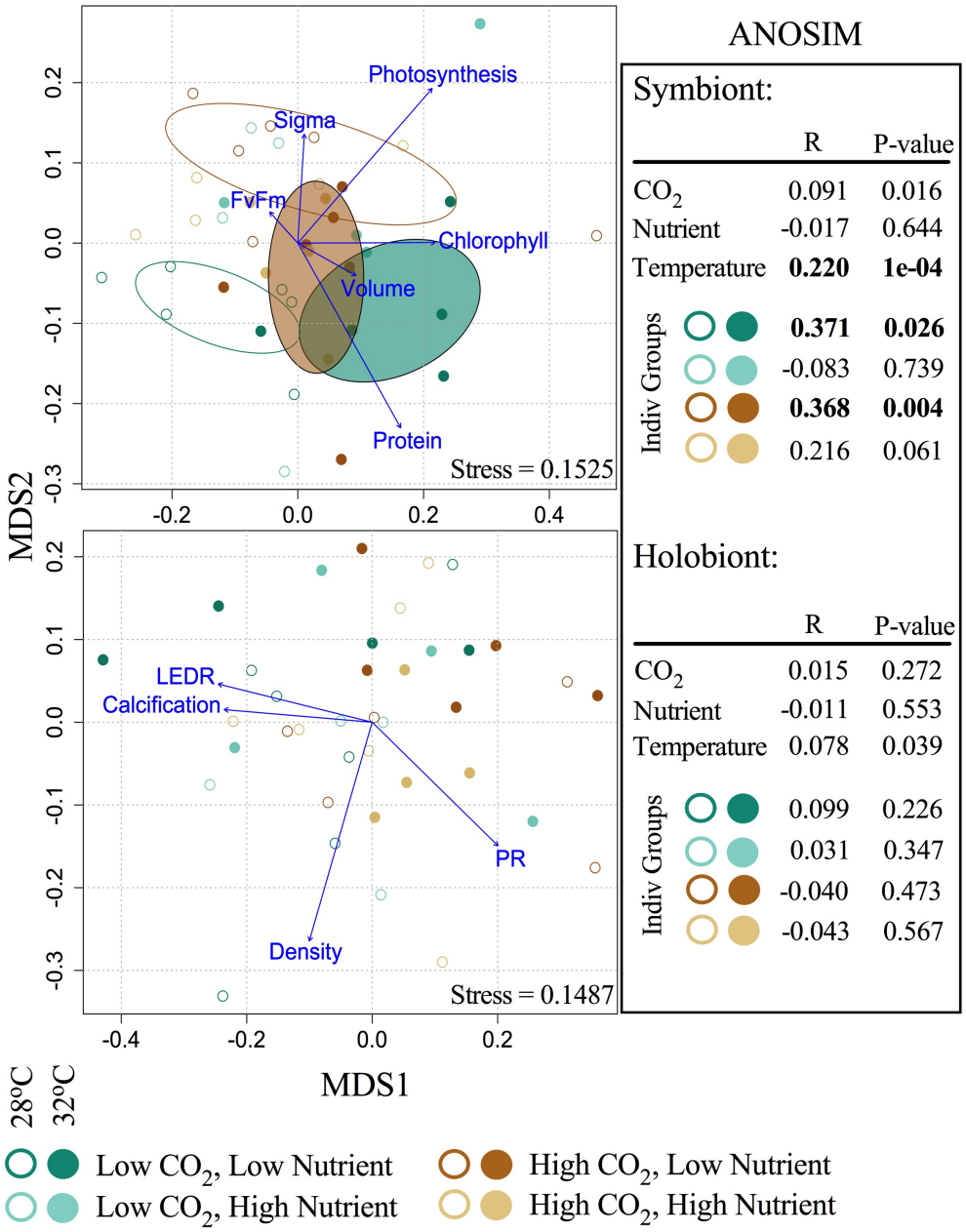

Figure 3.2: *S. trenchii* cell physiology. Average (± 1 SE) net photosynthesis cell^{-1} (a), cell volume (b), chlorophyll *a* cell^{-1} (c), protein cell^{-1} (d) at two pCO_2 levels, nutrient concentrations (LN = low nutrients, HN = high nutrients) and 26.5°C (light bars) or 31.5°C (dark bars). For each panel, the designations 'temp', 'pCO_2' and 'nutr' indicate significant temperature, pCO_2, nutrient concentration, or their interactive effects (multifactorial ANOVA results in Table S1). n = 5-6 per average.

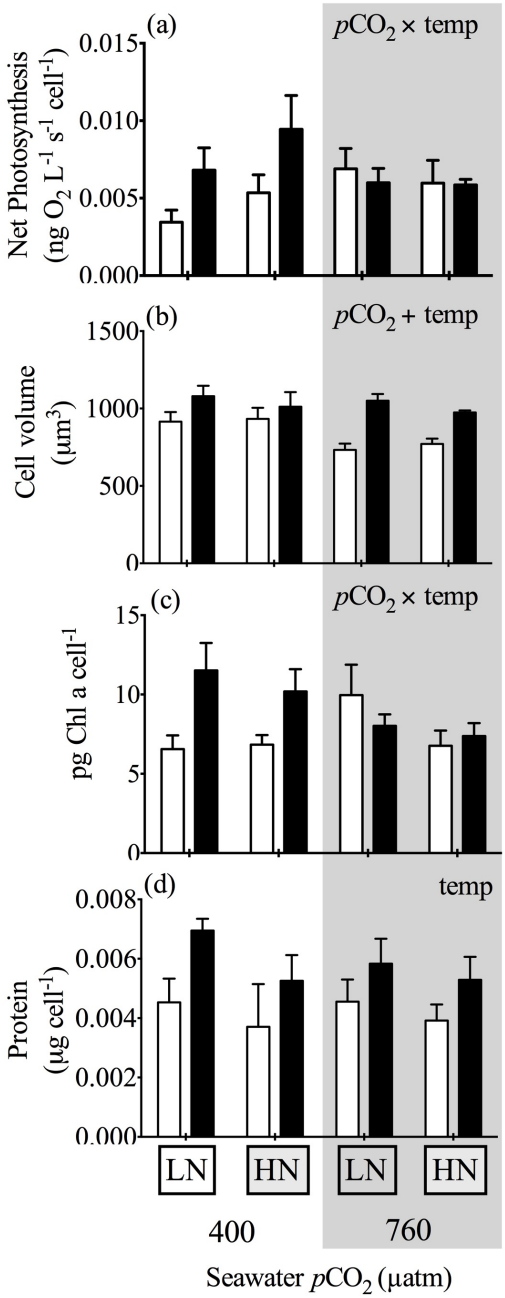

Figure 3.3: *T. reniformis* host physiology. Average (± 1 SE) cell density (a), calcification rates (b), light enhanced dark respiration cm^{-2} (LEDR) (c), photosynthesis to respiration (P:R) (d) at two pCO_2 levels, nutrient concentrations (LN = low nutrients, HN = high nutrients) and 26.5°C (light bars) or 31.5°C (dark bars). For each panel, the designations 'temp', 'pCO_2' and 'nutr' indicate significant temperature, pCO_2, nutrient concentration, or their interactive effects (multifactorial ANOVA results in Table S2). n = 5-6 per average.

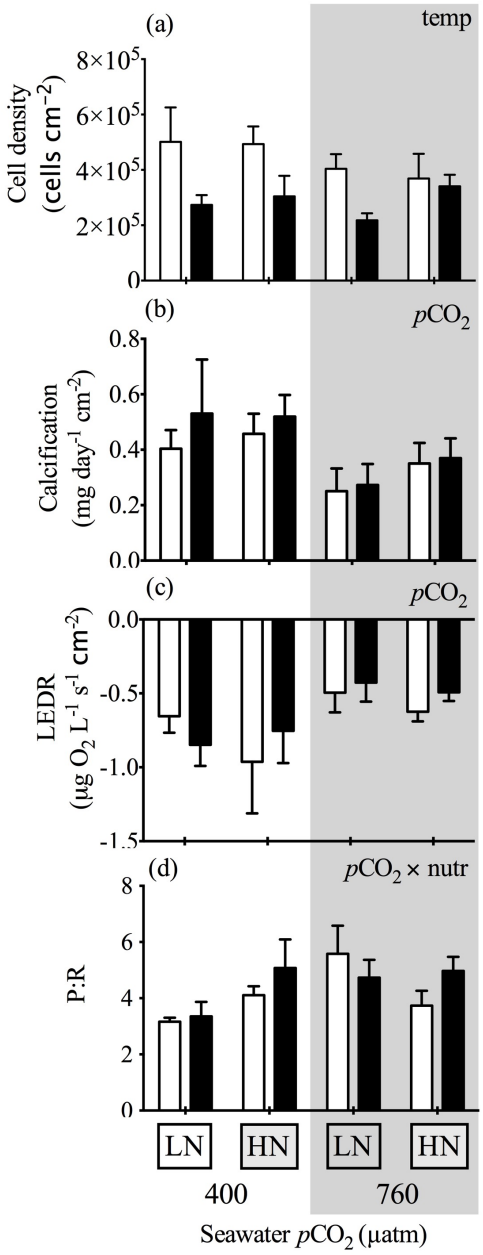

Figure 3.4: *S. trenchii* cell photobiology. Average (± 1 SE). Fv/Fm^{ST} (a), Functional absorption cross-section of PSII (b) at two pCO_2 levels, nutrient concentrations (LN = low nutrients, HN = high nutrients) and 26.5°C (light bars) or 31.5°C (dark bars). For each panel, the designations 'temp', 'pCO_2' and 'nutr' indicate significant temperature, pCO_2, nutrient concentration, or their interactive effects (multifactorial ANOVA results in Table S4). If an interactive effect between all three factors was observed, letters above each bar indicate significant differences among the 8 treatments. n = 5-6 per average.

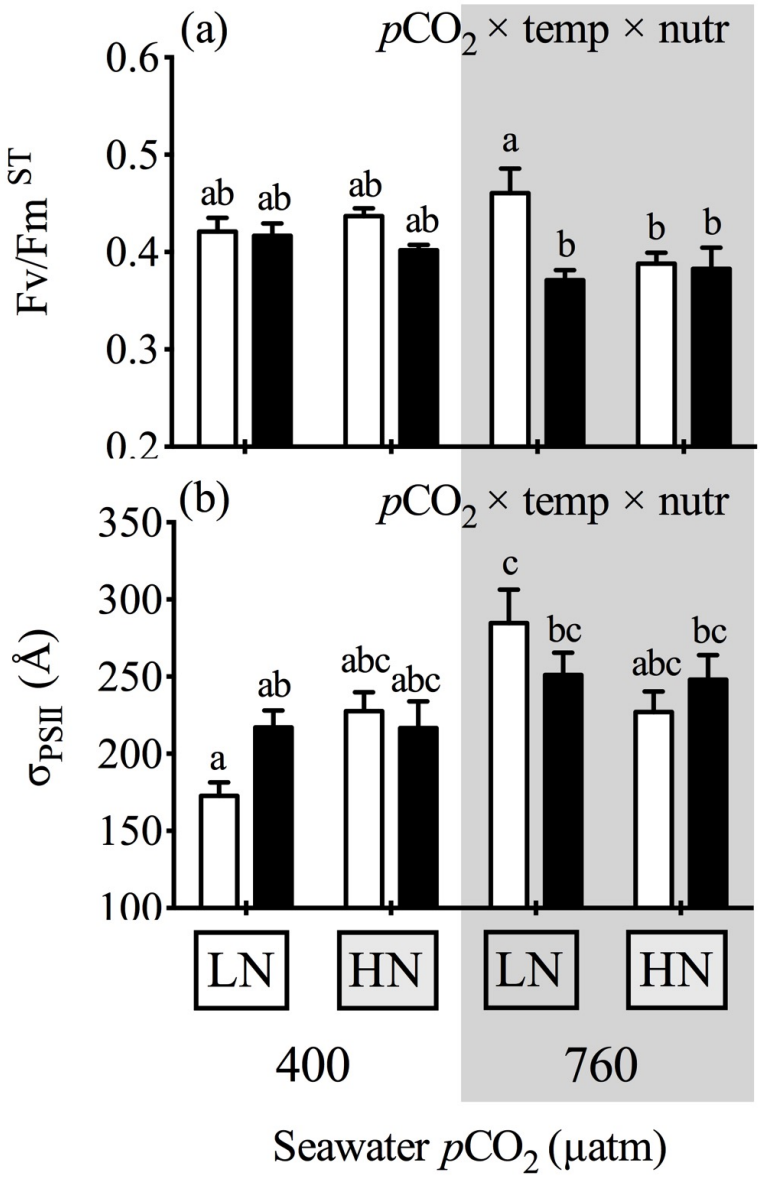

Figure 3.5: Maximum photosynthetic efficiency of PSII (Fv/Fm^{MT}): Average (± 1 SE) in *S. trenchii* (*T. reniformis*) at low nutrients (top panel) and high nutrients (bottom panel). Treatment abbreviations are LT = low temperature, HT = high temperature, LN = low nutrients, HN = high nutrients, LC = low CO_2 and HC = high CO_2. Letters next to treatment abbreviations indicate significant differences among the 8 treatments (Tukey post-hoc). n = 5 - 6 per average.

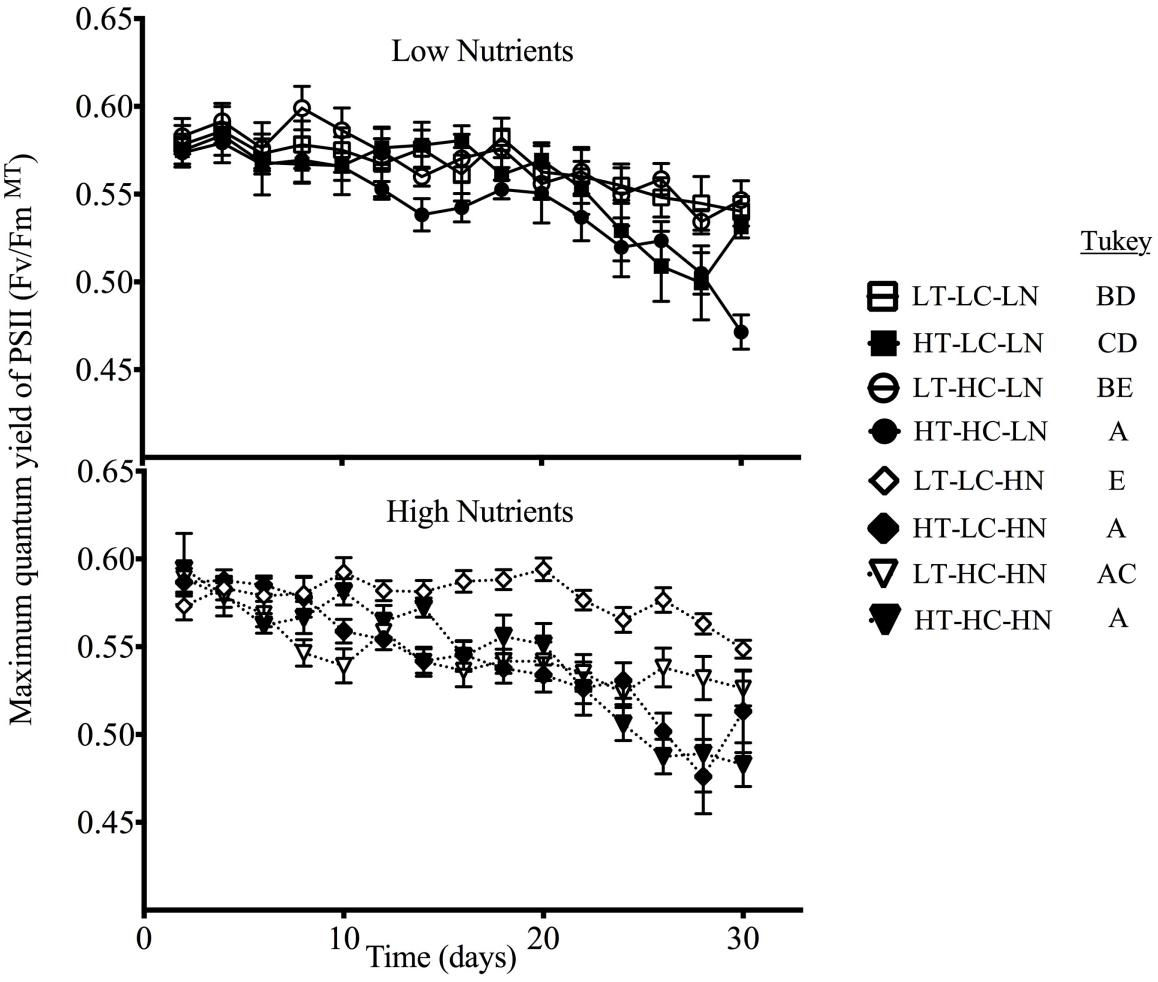

Chapter 4

CONTRASTING PHYSIOLOGICAL PLASTICITY IN RESPONSE TO ENVIRONMENTAL STRESS WITHIN DIFFERENT CNIDARIANS AND THEIR RESPECTIVE SYMBIONTS

4.1 Abstract:

Given concerns surrounding coral bleaching and ocean acidification, there is renewed interest in characterizing the physiological differences across the multiple host-algal symbiont combinations commonly found on coral reefs. Elevated temperature and CO_2 were used to compare physiological responses within the scleractinian corals *Montipora hirsute* (*Symbiodinium C15*) and *Pocillopora damicornis* (*Symbiodinium D1*), as well as the corallimorph (a non-calcifying anthozoan closely related to Scleractinians) *Discosoma nummiforme* (*Symbiodinium C3*). Several physiological proxies were affected more by temperature than CO_2, including photochemistry, algal number and cellular chlorophyll *a*. Marked differences in symbiont number, chlorophyll and volume contributed to distinctive patterns of chlorophyll absorption between these animals. In contrast, carbon fixation either did not change or increased under elevated temperature. Also, the rate of photosynthetically fixed carbon translocated to each host did not change, and the percent of carbon translocated to the host increased in the corallimorph. Comparing all data revealed a significant negative correlation between photosynthetic rate and symbiont density that corroborates previous hypotheses about carbon limitation in these symbioses. The ratio of symbiont normalized photosynthetic rate relative to the rate of symbiont normalized carbon translocation (P:T) was compared in these organisms

as well as the anemone, *Exaiptasia pallida* hosting *Symbiodinium minutum*, and revealed a P:T close to unity (*D. nummiforme*) to a range of 2.0–4.5, with the lowest carbon translocation in the sea anemone. Major differences in the thermal responses across these organisms provide further evidence of a range of acclimation potential and physiological plasticity that highlights the need for continued study of these symbioses across a larger group of host taxa.

4.2 Introduction:

The genus *Symbiodinium* represents a highly diverse group of dinoflagellates well known for forming unique symbioses with several marine invertebrate taxa, including cnidarians, mollusks, and sponges (Fitt 1985; Hoegh-Guldberg and Bruno 2010; Weisz et al. 2010). Through phylogenetic analysis of several genes, *Symbiodinium* are commonly divided into 9 major clades (LaJeunesse 2001; Coffroth and Santos 2005). Recent attention has been placed on comparing this genetic diversity with physiological differences and tolerance to environmental stress. Coral bleaching, which describes the expulsion of symbionts from the host tissue, is a frequent and often fatal, phenomena most commonly associated with high temperature stress (Brown 1997). In addition, stress brought on by changes in pH and carbonate chemistry due to ocean acidification (OA) is also of concern with respect to coral reef health (Brading et al. 2011; Comeau et al. 2013). With major increases in sea surface temperature and pCO_2 predicted by the end of this century (IPCC 2013), understanding the physiological differences among host/*Symbiodinium* combinations and how they possibly mitigate stress related to climate

change will become increasingly important in predicting the success of these organisms (Baker 2003).

Much *Symbiodinium* research has focused on scleractinian coral species due to their importance in calcium carbonate deposition and reef growth. However, non-calcifying symbiotic cnidarians also provide critical ecological functions, making their response to environmental change also of importance (Tkachenko et al. 2007). Recent, disturbance-induced phase shifts from calcifying scleractinians, to non-calcifying anthozoans are one example (Tkachenko et al. 2007; Norström et al. 2009; Dudgeon et al. 2010), and highlight this possibility in response to high temperature and or elevated pCO_2. The growth rates and productivity of the anemone, *Anemonia viridis* increased with proximity to naturally occurring CO_2 seeps off the coast of Italy (Suggett et al. 2012a) and numerous laboratory experiments have now documented the benefits of elevated pCO_2 on different anemone species (Towanda and Thuesen 2012a; Gibbin and Davy 2014). In contrast, scleractinian studies have documented a much broader range of effects in both calcification, respiration and photosynthesis (Kaniewska et al. 2012; Comeau et al. 2013; Edmunds et al. 2013; Schoepf et al. 2013). Reductions in scleractinian coral coverage due to thermal bleaching and ocean acidification, along with documented pCO_2 benefits to anemones suggests that future corals reefs could be dominated by non-calcifying species. Nevertheless, additional research on other non-calcifying anthozoans is needed. For example, taxonomically, corallimorphs are rooted within the scleractinian lineage, making them an ideal (yet understudied) group of cnidarians for comparison with calcifying coral species (Medina et al. 2006; Kitahara et al. 2014). Understanding how different cnidarian symbioses respond to environmental

stressors, including increased temperature and elevated pCO_2 may be a critical factor in predicting what cnidarian species dominate future coral reefs. Importantly, given that future reefs will likely encounter both elevated temperature and pCO_2 (Hughes and Connell 1999; Hughes et al. 2003; Hoegh-Guldberg et al. 2007), understanding their possible antagonistic or synergistic effects, and if this varies across anthozoans, is of high importance.

For Scleractinian corals, the efficiency for capturing solar radiation for photosynthesis is increased through light scattering by the skeleton (Enriquez et al. 2005; Wangpraseurt et al. 2012). Although these bio-optical properties result in highly efficient light capture, drawbacks exist. Reductions in symbiont densities from thermal bleaching dramatically increase the internal light field for remaining symbionts, potentially increasing the possible damage to the photosynthetic apparatus, resulting in a negative feed-back for light capture efficiency (Rodriguez-Román et al. 2006; Wangpraseurt et al. 2012). In contrast, the bio-optical properties of symbionts in non-calcifying symbiotic anthozoans likely differs and may significantly alter their photophysiological response to thermal stress and the light environment (Kuguru et al. 2010).

Changes in algal cell size and chlorophyll concentration can also be critical in managing environmental stressors such as high solar irradiance, allowing the symbiont to acclimatize to varying conditions so as to optimize productivity (Warner et al. 1996; Fitt et al. 2001; Key et al. 2010). However, the degree of plasticity can vary widely among different symbiont types, and within different host species and taxa (Leal et al. 2015). The potential for physiological variability both among and within specific groups of *Symbiodinium*, along with differences in cnidarian host morphologies significantly

expands the array of possible acclimation and stress mitigation strategies for coping with climate change (Cooper et al. 2011; Leal et al. 2015).

Variable rates of autotrophic carbon uptake and translocation have been observed, suggesting that the specific host-symbiont combinations play an important role in establishing rates of carbon incorporation in these symbioses (Davy et al. 1996; Engebretson and Muller-Parker 1999; Davy and Cook 2001; Leal et al. 2015). Understanding differences in carbon incorporation among anthozoan species, and how environmental stress affects them may be critical towards our understanding of future reefs and their symbiotic constituents. However, characterizing symbiont productivity across coral species can be somewhat complex due to species-specific differences among host organisms. Better comparative metrics are needed in order to understand differences across host taxa.

The goal of this study was to utilize high temperature and elevated CO_2 conditions to characterize physiological plasticity across three different host symbiont combinations representing two different host taxa (scleractinia and corallimorpharia) in order to highlight physical features that are most important in responding to environmental stress within each holobiont. Bio-optical and biophysical differences among symbiont types were considered, and how holobiont physiology may influence the symbionts response/acclimation to environmental stress. When compared across species, our data set highlights a distinct inverse relationship between productivity and cell density, in agreement with previously established hypothesis regarding carbon limitation within the host. Rates of photosynthesis $cell^{-1}$ to translocation $cell^{-1}$ (P:T) are compared across species and discussed in reference to environmental stress.

4.3 Materials and Methods:

4.3.1 Experimental Setup:

Two scleractinian species, *Montipora hirsuta* and *Pocillopora damicornis* were obtained from a commercial coral mariculture facility in New Albany, Ohio (Reef Systems Coral Farm), where the corals were held for over 10 years. Individual nubbins were originally harvested from a single adult colony between 1-2 years prior to transportation to Lewes, Delaware. Once in Delaware, coral nubbins were allowed to acclimate for an additional 10 months prior to experimentation. Several individuals of the corallimorph, *Discosoma nummiforme* were purchased from a local aquarium shop and maintained under laboratory conditions for over three years prior to experimentation such that the samples used in this study were second or third generation specimens. As the organisms utilized in this experiment represent clonal copies or fragments originally isolated from a single colony, our results cannot be utilized to infer population-wide trends. Rather, similar to other published physiological comparisons (Shick and Dowse 1985; Shick et al. 2011), our design appropriately highlights the degree of variation and acclimation within an individual colony as it pertains to changes in temperature and pCO_2, while minimizing experimental variability.

All samples were maintained in seawater collected from the Indian River Inlet, DE, during incoming tides. Seawater was filtered down to 1 micron and UV sterilized prior to use. Typical seawater parameters after filtration were; temperature = 27±0.5°C, salinity = 33±0.58, pH = 8.17±0.05, total alkalinity = 2072 ± 47 ($\mu mol\ kg^{-1}$**)**. All coral specimens were illuminated by a customized LED array (Cree XPG-R5, cool white;

5000–8300 K). To better simulate a natural diel light cycle, lights were ramped up from a minimum of 10 μmol quanta m^{-2} s^{-1} to a maximum of 400 μmol quanta m^{-2} s^{-1} over a three hour period, then remained at 400 μmol quanta m^{-2} s^{-1} for six hours, prior to ramping back down over the last three hours within the 12:12 light dark cycle.

Treatments consisted of two temperatures (26.5°C and 31.5°C) and two pCO_2 conditions (400 μatm and 800 μatm) for a total of four separate treatment conditions. Corals were exposed to treatment conditions for a total of 18 days. Ambient and elevated pCO_2 conditions were maintained via a pH stat system, which controlled the bubbling of air, CO_2 free air and/or CO_2 into each treatment system based on the pH of the seawater. Temperature was maintained using electronically controlled titanium heaters housed in each sump (Neptune Systems). Within the high temperature treatments, temperature was ramped 0.5°C day^{-1} from a starting temperature of 26.5°C, until reaching the target of 31.5°C. Each treatment system consisted of 5, 15L aquaria connected to a central 416L-recirculating sump. Flow rates within each aquarium were held at 567L hr^{-1}. A 40% water change was preformed on each system every other day. Salinity was maintained at 32ppt through daily top-offs with reverse osmosis and deionized (RO/DI) filtered water.

The pH stat microelectrodes (Ross Ultra Semi-Micro pH Electrode) were recalibrated every other day with NBS buffer standards and confirmed through independent measurements of pH (Fischer Scientific A815 Plus pH meter). Temperature was monitored electronically every five minutes (Neptune Systems inc.) and salinity monitored every other day with a refractometer. Alkalinity within each system was measured every six days using a bromocresol blue based colorimetric assay with a fiber optic spectrometer (USB4000, Ocean Optics) and titrator (876 Dosimat plus) (Yao and

Byrne 1998). Accuracy of TA measurements was checked against a seawater standard (Scripps) and typically deviated by less than 5%. Seawater chemistry and average temperatures for each treatment system are shown in Table 1 and Appendix C figure 1.

4.3.2 Symbiodinium Identity:

Symbiont genotypes were identified for each nubbin at the end of the experiment through amplification of the internal transcribed spacer 2 region (ITS2) of the ribosomal array, and subsequently analyzed by previously published protocols for denaturing gradient gel electrophoresis (DGGE) and cycle sequencing (LaJeunesse et al. 2003).

4.3.3 Symbiont Photochemistry and Spectral Absorbance:

Maximum quantum yield of PSII (Fv/Fm) and the functional absorption cross section of PSII (σ_{PSII}) were measured using a Fluorescence Induction and Relaxation (FIRe) fluorometer (Satlantic Inc., Halifax) on the final night of the experiment. Measurements were taken one hour after the start of the dark period and consisted of five iterations of a 120μs single turnover flash, and analyzed by fitting each fluorescence transient curve using the *FIREPRO* software (Kolber and Falkowski 1998; Hennige et al. 2011).

PSII electron transport rates (ETR) were also measured on the last day. All measurements were first dark acclimated for 30 minutes and then exposed to an actinic light source (Cree XPG-R5, cool white; 5000–8300 K, 354 μmol quanta m^{-2} s^{-1}) for four minutes. Electron transport rates were calculated as $ETR = \sigma_{PSII}' \times F_q'/F_m' \times PFD \times 21.683$, where σ_{PSII}'= is the functional cross section of PSII measured under actinic light,

F_q'/F_m' = effective quantum yield, PFD = photon flux density (354 μmol quanta m^{-2} s^{-1}) and 21.683 converts seconds to hours, μmol e^- to mol e^- and $Å^2$ $quanta^{-1}$ to m^2 mol PSII reaction $center^{-1}$ (RCII) (Suggett et al. 2003).

Spectral absorbance measurements were performed as described in (Enriquez et al. 2005) with reflectance (*R*) measured using a spectrometer (USB2000 Ocean Optics) and absorbance (*A*) calculated as $A = \log[1/R]$. Bleached skeletons were utilized as blanks for 100% reflectance for the scleractinian corals, whereas a spectralon reflectance standard functioned as the blank for the corallimorphs. Irradiance was provided by a full spectrum halogen light source (KL2500 LCD Schott). A running average was utilized to smooth data. Because we were only interested in chl a absorption, only the chlorophyll peak (675 nm) was tested for significant differences across treatments.

4.3.4 Photosynthetic Carbon Assimilation and Translocation:

Coral nubbins were placed in separate 7 mL scintillation vials containing 4 mL of seawater spiked with 15 μL of ^{14}C-labeled bicarbonate (specific activity 17 μCi μmol^{-1}). Six nubbins per treatment were used for each coral species. Due to their size, *D. nummiforme* were placed in 20mL vials containing 10 mL of spiked seawater with the same concentration of ^{14}C-labeled bicarbonate. Vials were placed on a LED light-table (Cool White Cree XPG-R5; 600 μmol photons m^{-2} s^{-1}; 28 °C) for 90 min. A higher light intensity was utilized during the incubation to ensure all samples were at maximum photosynthesis, and preliminary tests ensured that no signs of photoinhibition were evident (data not shown). An additional 6 nubbins from each species and treatment were placed in vials with ^{14}C-spiked seawater and held in the dark for 90 minutes to account

for carbon uptake in the dark. Three additional vials containing only the spiked seawater were also included for measurement of total activity.

After ^{14}C incubations, a 400 μL sample of seawater was removed from each vial for calculation of total labeled organic carbon (TOC) released by the holobiont. For *P. damicornis* and *M. hirsuta,* nubbins were then removed from the spiked seawater and placed into a 1 mol L^{-1} HCl in seawater solution for less than 2 hours in order to dissolve the skeleton. The remaining tissue was then homogenized in 1 mL of seawater using a tissue homogenizer (Tissue tearor, Biospec). For *D. nummiforme*, each specimen was removed from the spiked seawater and ground in 6 mL of seawater. The resulting homogenate was centrifuged (5000 × g) for 5 minutes to separate the host and symbiont portions. A 500 μL (1 mL for *D. nummiforme*) subsample was removed and used to measure carbon translocated to the host (H_s), while 100 μL of the remaining supernatant was used for calculating host protein content. The remaining algal cell pellet was re-suspended in 500 μL of FSW (1 mL for *D. nummiforme*), vortexed and then centrifuged again to extract any remaining host supernatant (RH_s) from the algal pellet. The resulting algal pellet (S) was then resuspended a final time in 400μL of FSW. All samples measured for radioactivity were acidified with an equal volume of 0.1 mol L^{-1} HCl, placed in 7 mL scintillation vials for 24 hours and then combined with 5 mL of scintillation cocktail (Ultima Gold, Perkin Elmer) prior to reading with a liquid scintillation counter (Beckman LS-6500). All measurements and calculations follow established methods for *E. pallida* (Davy & Cook, 2001). Translocation (T_L) and photosynthesis (P_{net}) rates were determined by the average specific activity (grams C

dpm^{-1}) and the duration of the incubation. The fraction of carbon translocated (T_L) was calculated as,

$$T_L = TOC + H_s + RH_s$$

and then normalized to host protein. TOC is the total organic carbon while H_s and RH_s are the host supernatant and remaining host supernatant respectively.

Net photosynthesis (P_{net}) was normalized to total algal cells and calculated as,

$$P_{net} = TOC + H_s + RH_s + S$$

where S is the algal pellet described above. Using the ratio of the above equations, the fraction of photosynthate translocated to the host was calculated as,

$$T_L/P_{net} = (TOC + H_s + RH_s)/(TOC + H_s + RH_s + S)$$

Cell density and chlorophyll samples (200 μL each) were removed from the initial homogenized sample of the animal prior to centrifugation for ^{14}C analysis. Algal cell density and volume was assessed by replicate haemocytometer counts (n=6) under 100x magnification. Samples were photographed using a Nikon microphot-FXA epifluorescent microscope and then analyzed by computer using Image J software (NIH). For photopigment quantification, pelleted cells were lysed in 90% methanol with a bead beater (BioSpec) for 60s, incubated at -20°C for two hours and then centrifuged for 5min at 5000 rpm to remove remaining debris. Chlorophyll *a* concentration was then calculated utilizing established protocols (Porra et al. 1989). Host protein concentrations were measured by the BCA method (Thermo Scientific), with bovine serum albumin used for standards. All absorbance measurements (chlorophyll and protein) were performed with a plate reader (FLUOstar Omega BMG labtech).

4.3.5 Photosynthesis:Translocation Ratio:

Photosynthetic activity was compared directly to translocation by plotting symbiont normalized maximal photosynthetic rates against symbiont normalized translocation rates. This analysis also included data from an earlier study with an additional non-calcyifying symbiotic anthozoan, the anemone *Exaiptasia pallida*, which hosted three different genotypes of *S. minutum*. This additional data originated from a similar experiment, utilizing the same treatment system and methods herein, with anemones exposed to pCO_2 levels of 400 and 800 μatm for one month and at 26.5°C (Hoadley et al. 2015b).

4.3.6 Statistical Analysis:

Individual variables were tested for assumptions of homogeneity of variance and normality of distribution using the Levene and Shapiro-Wilk tests respectively. If either test invalidated these assumptions, the data was square root or log transformed prior to further analysis. A two-way analysis of variance (ANOVA) was used to test for significant main effects of pCO_2 and temperature and any potential interactive effects between the two (α=0.05). When interactive effects were found, a Tukey post-hoc test was performed in order to test for differences among the four treatments. If data failed to meet assumptions of normality, a Kruskal-Wallis test with multiple comparisons was used instead. Nonlinear (Fig. 6a) and linear (Fig. 6b) regression was utilized to fit lines to the data depicted in figure 6.

Associations among all of the physiological variables measured were examined by a principle components analysis (PCA). Variables were normalized to remove

potential error from differences in unit scale associated with the different physiological measurements included in the analysis. Only principle components (PC) with eigenvalues greater than 1 were retained in the analysis. Significant correlations with each principle component for the 11 variables are provided in Table 2. All statistical analyses were performed using the open source software R with 'car' and 'pgirmess' and 'FactoMineR' packages installed (http://www.R-project.org) or with Prizm 6 (GraphPad Software).

4.4 Results:

4.4.1 Symbiont Identification and Stability:

A subset of each species was genotyped prior to the start of the experiment. Only one dominant symbiont-type was detected in each sample, specifically, *Symbiodinium C3* was found in *D. nummiforme*, *C15* in *M. hirsuta* and *D1* in *P. damicornis*. In addition, each symbiosis remained stable throughout the experiment, with no additional algal types detected within the different treatments.

4.4.2 Photochemistry:

There was a significant interaction with temperature and pCO_2 for the *C3* symbiont ($P = 0.0016$) as Fv/Fm declined with increasing temperature. However, the decline was significantly less under high pCO_2 (Table 2). An interactive effect was also observed for the *D1* symbiont ($P = 0.0011$) as Fv/Fm significantly increased with temperature under both pCO_2 treatments. Fv/Fm yields also significantly increased with

CO_2 but only at ambient temperature (Table 2). No significant differences were observed within the *C15* symbiont.

The electron transport rate significantly declined with elevated temperature within the *C3* ($P = 0.0297$) and *D1* ($P = 0.0277$) symbionts, whereas no change occurred for the *C15* symbiont (Fig. 1). Likewise, the functional absorption cross-section (σ_{PSII}) did not change significantly for the *C15* symbiont, but σ_{PSII} significantly decreased with temperature ($P = 0.0040$) in *Symbiodinium D1* (Table 3). In addition, there was a significant interactive effect of temperature and CO_2 ($P = 0.0059$) within the *C3* symbiont as σ_{psII} increased with temperature within the low but not elevated pCO_2 treatments (Table 3).

4.4.3 Symbiodinium Physiology:

Chlorophyll concentration $cell^{-1}$ significantly declined with temperature for *Symbiodinium C3* ($P < 0.0001$) and *D1* ($P = 0.0140$) while it increased significantly ($P = 0.0150$) for *C15* (Fig. 2a-c). Although *C3* density did not change, a significant temperature induced decline occurred for the *C15* symbiont ($P = 0.0212$) (Fig. 2d, e). A significant interactive effect for temperature and pCO_2 was observed for *Symbiodinium D1* ($P = 0.0198$), as cell density significantly declined with temperature within the ambient treatment but not within the elevated pCO_2 treatments (Fig. 2f). Cell volume also did not change significantly within *Symbiodinium* C3 whereas cell volume increased with temperature for *C15* ($P = 0.0042$) (Fig. 2g, h). A significant interactive effect for the *D1* symbiont volume ($P = 0.0068$) was observed, as cell volume increased significantly with elevated temperature but only at ambient pCO_2 (Fig. 2i). Cellular chlorophyll density (pg

Chla μm^{-3}) decreased with temperature ($P < 0.0001$) in the *C3* symbiont (Fig. 2j). Although no significant changes were observed within *C15* cells, an interactive effect ($P = 0.0093$) was noted for *D1* symbionts with cellular chlorophyll density decreasing with temperature under ambient but not elevated pCO_2 conditions (Fig. 2k,l).

Although there was no significant difference in colony light absorption in the corallimorph, elevated temperature resulted in a significant increase in absorbance in *M. hirsuta* ($P = 0.0002$) (Fig. 3a,b). In contrast, an interactive effect was observed for *P. damicornis* ($P < 0.0001$) where absorbance decreased with temperature within the low, but not elevated pCO_2 treatment. In addition, absorbance in the elevated pCO_2 treatments was significantly lower than the ambient pCO_2 and ambient temperature treatment but significantly higher than the combined ambient pCO_2 and elevated temperature treatment (Fig. 3c).

4.4.4 Carbon Uptake and Translocation:

Although no significant difference in net photosynthesis were noted for *D. nummiforme,* net photosynthesis increased with elevated temperature in *M. hirsuta* ($P < 0.0001$) and *P. damicornis* ($P = 0.0104$) (Fig. 4a-c). When viewed from the host perspective (as g Carbon translocated g host protein^{-1}), there were no significant changes in translocation rates. (Fig. 4d-f). The fraction of photosynthate translocated to the host did not change significantly with treatment type for *M. hirsuta* or *P. damicornis* (Fig. 4h, i). However, the percent of photosynthate translocated to the host did increase with temperature for *D. nummiforme* ($P < 0.0001$) (Fig. 4g). When net photosynthesis was compared to symbiont density, a nonlinear trend was revealed with a noted exponential

increase in photosynthesis as cell density declined (Fig. 5). With respect to linear trends between net photosynthesis and total translocation, *A. pallida* had the highest ratio of net photosynthesis:total translocation (m = 4.52), followed by the two scleractinian corals *M. hirsuta* (m = 2.203) and *P. damicornis* (2.155) (Fig. 5). Interestingly, the corallimorph, *D. nummiforme* had the smallest ratio (m = 1.283) suggesting the largest amount of carbon assimilated within the host and not the symbiont.

4.4.5 Principle Components Analysis:

A total of three principle components with eigenvalues of greater than 1 were extracted from our analysis of physiological variables (Cellular density, chlorophyll, chlorophyll volume^{-1}, photosynthesis, translocation, % translocation, ETR, sigma, FvFm, absorbance) (Fig. 6). Physiological PC1 (eigenvalue = 4.95) explained 45% of the variance whereas PC2 (eigenvalue = 1.949) and PC3 (eigenvalue = 1.218) explained an additional 17.7% and 11% respectively. Host density, volume, percent translocation, sigma and absorbance all had their highest loadings on PC1 varied positively whereas photosynthesis and FvFm varied negatively (Table 4). Highest loadings for Chlorophyll, chloropyll volume^{-1} and ETR correlated positively with PC2.

4.5 Discussion:

Previous work has suggested carbon limitation in some symbiont species (Weis 1993; Brading et al. 2011). From a photochemical perspective, greater availability of DIC through ocean acidification may alleviate such limitation by providing a greater sink through the photosynthetic electron transport chain and maintain the plastoquinone pool

in a more oxidized state. This may reduce potential heat stress to the PSII reaction center, a common site of thermal damage in thermally sensitive symbionts (Warner et al. 1999; Hill et al. 2011). For *C3*, an increase in pCO_2 partially mitigated the thermal decline in Fv/Fm. Under ambient pCO_2 conditions, the functional absorption cross section ($\sigma_{\mathbf{psII}}$) increased with temperature, increasing the light energy captured for photochemistry, and thus increasing the partial pressure over PSII and the potential for PSII degradation. However, elevated pCO_2 mitigated the thermal increase in σ_{psII}, thereby reducing the potential for reaction center degradation and allowed for thermal mitigation of Fv/Fm. This contrasts with the *D1* symbiont, where reductions in ETR were also observed, despite both thermal and pCO_2 induced increases in maximum quantum yield. However, for the *D1* symbiont, σ_{psII} decreased with temperature, reducing the number of photons used for photosynthesis and decreasing ETR despite an increase in overall efficiency of PSII. Importantly, maximum quantum yields were relatively low within all species, consistent with yields observed in high-light acclimated symbionts (Hennige et al. 2009). Likewise, Fv/Fm did not decrease over time within the control treatments (data not shown) and further substantiates the interpretation that these values reflect light acclimation as opposed to photoinactivation.

It is interesting to note that the thermal increase in net photosynthesis in the *D1* symbiont contrasted with a reduction in ETR. Major differences in the thermal response for these two metrics of photosynthetic activity suggest some decoupling between linear electron flow and downstream carbon utilization. For many classes of phytoplankton, as much as 60% of gross photosynthesis can represent non-carbon assimilatory electron flow (Suggett et al. 2009; Halsey et al. 2013). In addition, a recent study showed

photoreduction of oxygen to be a major alternative electron sink for cultured *Symbiodinium* during photosynthesis (Roberty et al. 2014). Hence, the reduction of ETR in the *D1* symbiont may reflect an alleviation of alternative electron flow and a greater use of reductant for carbon fixation in the Calvin cycle. In addition, the mitochondrial alternative oxidase (AOX) pathway may also be an important factor in this reduction of ETR, as AOX can account for 25-50% of respiration in *Symbiodinium* and serve as a major electron sink (Oakley et al. 2014a). A reduction in any or all of these pathways due to elevated temperature could explain the dichotomy between the reduction in PSII ETR and increased carbon incorporation observed here.

Along with PSII photochemical efficiency, reductions in symbiont number and chlorophyll concentration can indicate thermal or pCO_2 stress and/or acclimation (Grottoli et al. 2006; Kaniewska et al. 2012; Takahashi et al. 2013). A loss of symbionts is often thought to result from an increase in reactive oxygen species produced by the symbionts under thermal stress (Suggett et al. 2008; Weis 2008; Baird et al. 2009). Although the photochemical evidence suggests that the *C3* symbiont was thermally sensitive while the *C15* and *D1* symbionts were more thermally tolerant, patterns in symbiont density did not match this trend. *D. nummiforme* maintained symbiont number, while both scleractinian species lost symbionts. As has been previously suggested (Hawkins et al. 2015; Krueger et al. 2015), increases in host reactive oxygen species (ROS) may have induced bleaching at high temperatures despite any evidence of thermal damage within the *D1* and *C15* symbionts. For *D. nummiforme,* greater host ROS scavenging and/or minimal increase in host ROS production may have allowed for stable symbiont cell numbers at high temperatures despite obvious signs of photo-stress in the

C3 symbiont. Nevertheless, reductions in cellular density and/or chlorophyll content are likely to impact the light environment for remaining cells.

For free-living phytoplankton, larger cell size tends to lead to smaller functional absorption cross sections, thereby reducing the susceptibility to photodamage from high light stress (Finkel 2001; Key et al. 2010). This is typically due to a greater package affect as self-shading among chlorophyll molecules within the cell becomes more pronounced as cell size increases (Kirk 1994). Thermal reduction in chlorophyll a in the *C3* symbiont likely reduced the package effect, allowing for greater light capture per chlorophyll molecule. However, as previously mentioned, an increase in the functional absorption cross-section (σ_{psII}) only occurred within the ambient pCO_2 treatment, indicating a greater target for light harvesting and photochemistry at PSII under ambient pCO_2 conditions. The functional absorption cross section of PSII has been noted to both increase or decrease in free-living phytoplankton under high CO_2 which may be due to a reconfiguration of the light-harvesting antenna (Jin et al. 2013; Trimborn et al. 2014).

Despite a ca. 50% reduction in cell density, absorbance within *M. hirsuta* increased with temperature. It's possible that this resulted from the slight increase in chlorophyll content and cellular volume, enabling better light capture within the symbiont. Alternatively, changes in the vertical distribution of remaining symbionts within the host tissue may also have influenced absorbance readings (Wangpraseurt et al. 2012). Changes in host fluorescent protein content may also have influenced the absorbance readings at elevated temperature. High light acclimation increased fluorescence within the Scleractinian coral *Galaxea fascicularis* (Ben-Zvi et al. 2014) and a similar increase in perceived light with a decrease in symbiont density within *M.*

hirsuta may have triggered an increase in host fluorescent protein content, thereby increasing the absorbance under high temperature. An equally large (ca. 50%) thermal reduction in cell density also occurred in *P. damicornis* in the ambient pCO_2 treatment. However, a loss in chlorophyll, along with an increase in cell size resulted in major differences in intracellular chlorophyll density, largely influencing the light capture properties and the absorption spectra of this coral (Fig 3, bottom panel). These changes in absorption contrast with that of *D. nummiforme* where despite a significant loss in cellular chlorophyll *a* with elevated temperature, the high symbiont density (normalized to animal protein) and absence of any change in cell volume lead to minimal differences in colony absorbance. In addition, the lack of a highly reflective calcium carbonate skeleton and the greater tissue thickness may have further influenced this trend in *D. nummiforme*. Although further studies are needed to fully understand these bio-optical properties, it is clear that differences in morphology and light absorbance among anthozoan body types and cell physiology can significantly influence the internal light field and productivity rates, and likely further influence downstream processes important to the host/algal symbioses.

Although major differences in net photosynthetic rates across symbiont types was apparent, no differences in translocation rate were observed across species or treatment conditions. Our results are similar to those observed for the coral *Stylophora pistillata*, where net photosynthesis and translocation rates were measured via ^{13}C isotopic analysis and did not change under high pCO_2 (Tremblay et al. 2013). However, Tremblay et al. (2013) noted that the percent of translocated photosynthate did increase with high pCO_2, whereas no change in percent translocation in *P. damicornis* or *M. hirsuta* in response to

pCO_2 or temperature was noted here. Methodological differences may play a role in this comparison since the ^{14}C method cannot account for autotrophically fixed carbon that is then respired which may cause an underestimation in photosynthetic rates and translocation (Tremblay et al. 2012). Likewise, the significantly higher pCO_2 concentration used by Tremblay et al (3898 μatm) may have played a role in this difference. Increased pCO_2 significantly increased productivity rates for several different anemone species (Suggett et al. 2012a; Towanda and Thuesen 2012a; Gibbin and Davy 2014), however no changes in the per-cent of photosynthate translocated to the host have been reported under elevated pCO_2.

Comparisons of productivity rates revealed a negative correlation between cell density and net photosynthesis (Fig. 5a). Additionally, increased photosynthesis with elevated temperature was only observed for the two scleractinians, where cell density also declined significantly, further strengthening the inverse relationship between productivity and cell density. A similar relationship was reported by (Middlebrook et al. 2010) for *Acropora formosa* under thermal stress, where photosynthetic rates were measured via O_2 evolution. As previously mentioned, symbionts living *in hospite* are thought to be DIC limited (Weis 1993; Davy and Cook 2001; Wooldridge 2009b). By reducing the cell density within the host, DIC availability may increase for the remaining symbionts, thus increasing the photosynthetic rate on a per cell basis. The two figures show that this inverse relationship between photosynthesis and cell density exists both within the physiological constraints of a single species (Middlebrook et al. 2010) and as a ubiquitous response across multiple symbioses (Figure 5a).

The physiological characteristics of each host/symbiont combination are critical for understanding the overall symbioses and its unique acclimation strategies in response to environmental stress. The comparison between net maximal photosynthesis algal cell^{-1} (P) and total carbon translocation algal cell^{-1} (T) (figure 5b) provides a simple yet useful ratio (P:T) comparison for assessing different symbionts *in hospite*. The slope and range of data provides a snapshot of one benefit of these symbioses, providing a useful cross taxa comparison as we attempt to better understand how climate change will influence different anthozoan/symbiont symbioses. Because the data reflect both controlled conditions as well as while under a range of physical stressors, the resulting slopes for each species are indicative of each symbioses across a physiological continuum. The greater slope within *E. pallida* is indicative of symbionts translocating far less photosynthate to their host relative to their rate of carbon production, whereas the P:T ratio in *D. nummiforme* is much closer to unity and suggests that the *C3* symbiont shares a much larger percentage of the autotrophically fixed carbon with their host, regardless of the condition or applied stressor.

Overall, *P. damicornis* and *D. nummiforme* show major changes in physiology in response to temperature, whereas little change is observed for *M. hirsuta* (Figure 6). Differences in the bio-physical and bio-optical properties along with carbon uptake and translocation form three clearly distinct host-symbiont combinations each with a notably different response to thermal stress. The cartesian distance between species within the PCA plot, along with the direction of change in response to elevated temperature indicates major physiological differences in thermal stress mitigation or acclimation. Importantly, because fragments for each species were initially collected from a single

colony, our results cannot be utilized to understand a coral population-wide response. Nevertheless, a large degree of physiological plasticity is still observed both within different fragments of the same colony and across the three coral species. Understanding how differences in physiological plasticity among coral species will influence the impact of future climate change on coral reef systems is an increasingly important topic. However, as discussed above, the unique acclimation strategies inherent to each host/symbiont combination require a broader spectrum of physiological variables be measured in order to accurately characterize plasticity in response to environmental stress.

As noted for the *C1* and *D1* symbionts, similar thermal reductions in ETR can be brought about via vastly different photophysiological responses to elevated temperature and pCO_2. Additionally, reductions in PSII activity were not reflected within the overall carbon fixation and suggest that care must be taken when interpreting chlorophyll a fluorescence data alone. The inverse relationship between cell density and net photosynthesis corroborates previous work on carbon limitation and how it may apply during thermal bleaching events. Lastly, differences in the P:T ratio provide a unique metric with which to compare symbionts across different host/symbiont combinations. Future work will need to better focus on host/symbiont physiological diversity in order to better understand which cnidarian symbioses are more or less well poised to survive future climate change conditions.

Table 4.1: Average conditions (mean ± SE) for each of the treatments. All seawater carbonate chemistry based on pH (NBS) and total alkalinity (TA) measurements were calculated using the CO2SYS program (Lewis and Wallace 1998).

	Ambient CO_2		**High CO_2**	
Temperature (°C)	Ambient	Elevated	Ambient	Elevated
pH	8.15 ± 0.027	8.16 ± 0.034	7.91 ± 0.101	7.86 ± 0.062
***p*CO_2 (µatm)**	376 ± 11.23	381 ± 2.48	850 ± 27.19	812 ± 22.98
TA (µmol kg^{-1})	2074 ± 69.67	2070 ± 113.17	2158 ± 13.62	2107 ± 16.13
Aragonite Saturation Ω_a	3.04 ± 0.12	2.99 ± 0.02	1.83 ± 0.04	1.82 ± 0.05
Salinity (ppt)	33.21 ± 0.81	32.93 ± 0.61	33.50 ± 0.50	33.07 ± 0.18

Table 4.2: Maximum quantum yield of PSII (Fv/Fm). Mean ± SE are shown for each species (N = 6). ANOVA column reflects statistical results from Two-Way ANOVA. Significant main effects are marked as temp for temperature and CO2 for pCO_2. Significant interactive effects are reflected by Temp*CO_2. The Post hoc column reflects Tukey post hoc analysis when a significant interactive effect was observed. LT = low temp; HT = high temp; HTHC = high temperature and high pCO_2 treatment, HTLC = High temperature and low pCO_2 treatment, LTHC = low temperature and high pCO_2 treatment and LTLC = low temperature and low pCO_2 treatment.

	Ambient CO_2		**High CO_2**			
Temperature (°C)	Ambient	Elevated	Ambient	Elevated	ANOVA	Post hoc
(*C3*) ***D. nummiforme***	0.338 ± 0.011	0.173 ± 0.011	0.323 ± 0.019	0.256 ± 0.012	temp*CO2, p = 0.002	LT > HT; HTLC < HTHC
(*C15*) ***M. hirsuta***	0.204 ± 0.005	0.211 ± 0.009	0.227 ± 0.009	0.218 ± 0.013	Not significant	
(*D1*) ***P. damicornis***	0.267 ± 0.002	0.348 ± 0.004	0.301 ± 0.007	0.336 ± 0.005	temp*CO2, p = 0.0001	LT < HT; LTLC < LTHC

Table 4.3: Functional absorption cross-section of PSII. Mean ± SE are shown for each species ($Å^2$ $quantum^{-1}$, N = 6). ANOVA column reflects statistical results from Two-Way ANOVA. Significant main effects are marked as temp for temperature and CO2 for pCO_2. Significant interactive effects are reflected by Temp*CO_2. The Post hoc column reflects Tukey post hoc analysis when a significant interactive effect was observed. LT = low temp; HT = high temp; HTHC = high temperature and high pCO_2 treatment, HTLC = High temperature and low pCO_2 treatment, LTHC = low temperature and high pCO_2 treatment and LTLC = low temperature and low pCO_2 treatment.

	Ambient CO_2		**High CO_2**			
Temp. (°C)	Ambient	Elevated	Ambient	Elevated	ANOVA	Post-hoc test
(*C3*) *D. nummiforme*	379 ± 13	726 ± 76	403 ± 16	480 ± 24	Temp*CO_2 *P* = 0.00594	HTLC > HTHC; LTLC < HTLC
(*C15*) *M. hirsuta*	477 ± 17	498 ± 23	472 ± 34	418 ± 28	Not significant	
(*D1*) *P. damicornis*	421 ± 21	351 ± 11	401 ± 10	371 ± 16	Temp *P* = 0.004	

Table 4.4: Factor loadings for each variable within the principal components (PC) analysis. Only significant ($p < 0.05$) correlations are included. Values in bold indicate the axis of strongest loading for each physiological variable.

Variable	PC 1	PC 2	PC 3
Symbiont Density	**0.8587**		
Symbiont Cellular Volume	**0.8508**		0.3485
Chl a per Cell	0.3342	**0.7581**	0.4413
Chl a per um^{-3}	-0.4171	**0.7911**	
Photosynthesis Cell^{-1}	**-0.8344**		
Total Translocation	**0.4939**	0.3886	-0.2563
Percent Carbon Incorporation	**0.8148**		
Electron Transport Rate	-0.3861	**0.5424**	-0.2758
Functional Absorption Cross Section of PSII	**0.6561**		-0.6226
Fv/Fm	**-0.7601**		0.5298
Absorbance at 675nm	**0.6608**	0.4210	

Figure 4.1: Electron transport rates for *Discosoma nummiforme* (a), *Montipora hirsuta* (b), *Pocillopora damicornis* (c). Averages plus standard error are shown for two pCO_2 levels and two temperatures (26.5°C = open bars, 32°C = dark bars). The designations 'temp', 'pCO_2' and 'temp x pCO_2' indicate significant temperature, pCO_2 or interactive effects (two-way ANOVA).

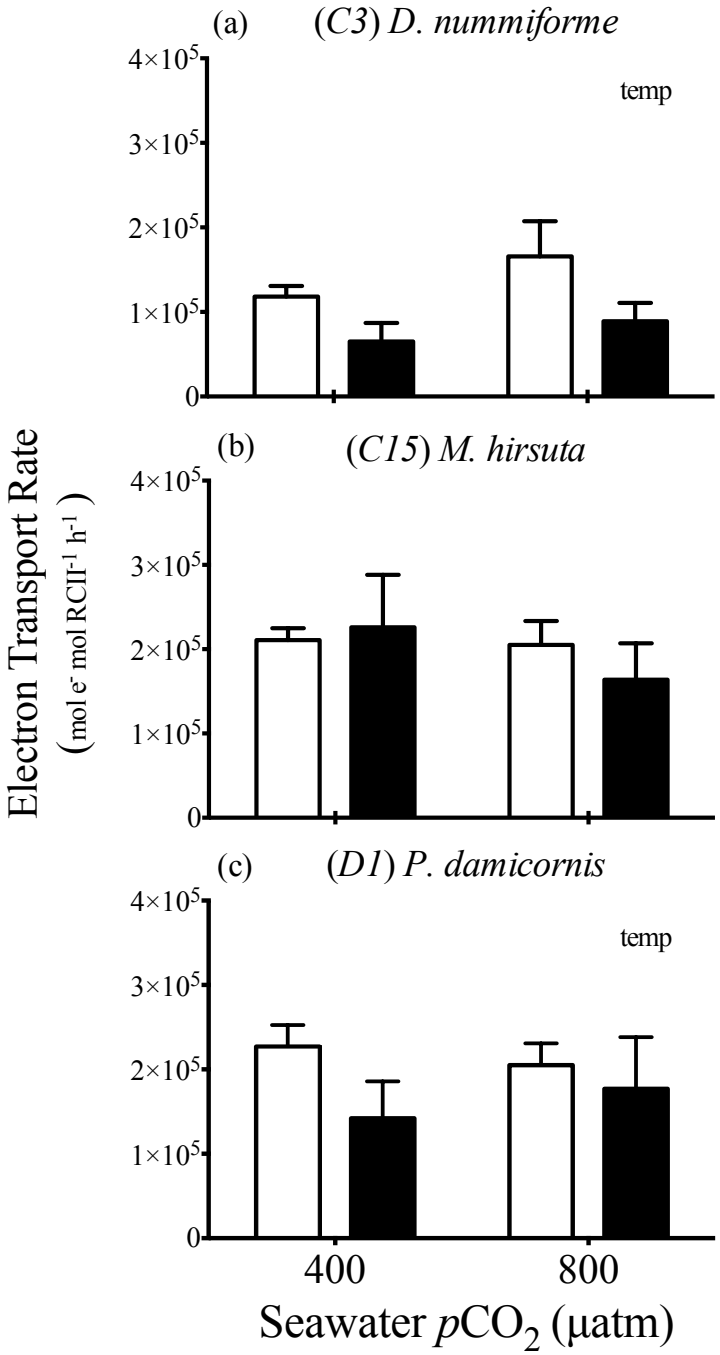

Figure 4.2: Chlorophyll a content per cell, cell density, cell volume and chlorophyll density for *Discosoma nummiforme* (a, d, g, j), *Montipora hirsuta* (b, e, h, k) and *Pocillopora damicornis* (c, f, i, l). Averages plus standard error are shown for two pCO_2 levels and two temperatures (26.5°C = open bars, 32°C = dark bars). For each pane, the designations 'temp', 'pCO_2' and 'temp x pCO_2' indicate significant temperature, pCO_2 or interactive effects (two-way ANOVA). The letters above each bar indicate the results of the tukey pairwise analysis when a significant interactive effect is observed (n = 6 ± SE).

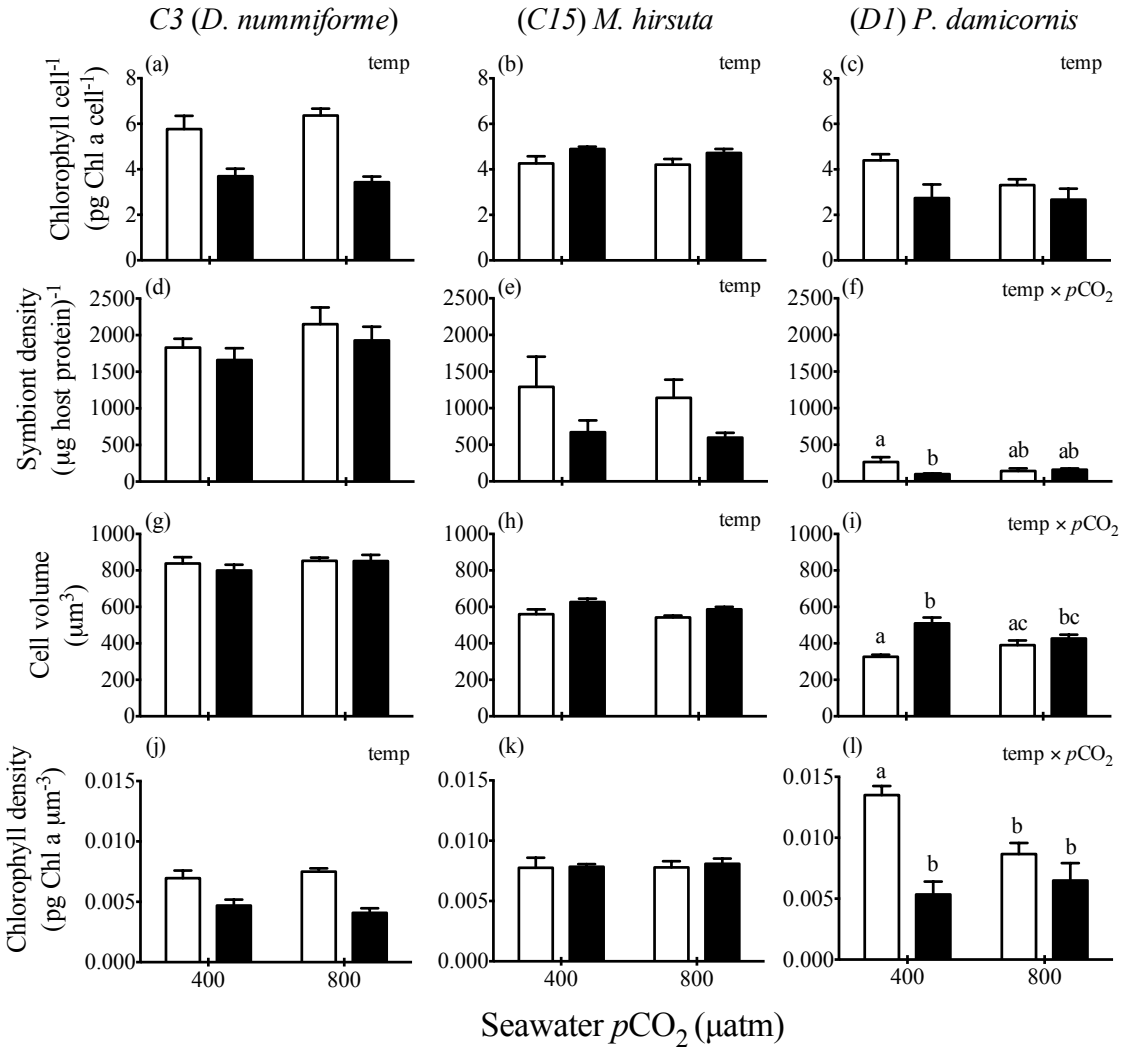

Figure 4.3: Spectral absorbance profiles for *Discosoma nummiforme* (a), *Montipora hirsuta* (b) and *Pocillopora damicornis* (c). Lines represent the mean ± standard error for each treatment. The black line signifies ambient temperature and CO_2. Grey is ambient temperature and elevated CO_2. Red is high temperature at ambient CO_2 and maroon is high temperature and high CO_2. The dotted line signifies peak absorbance for chlorophyll a (675nm).

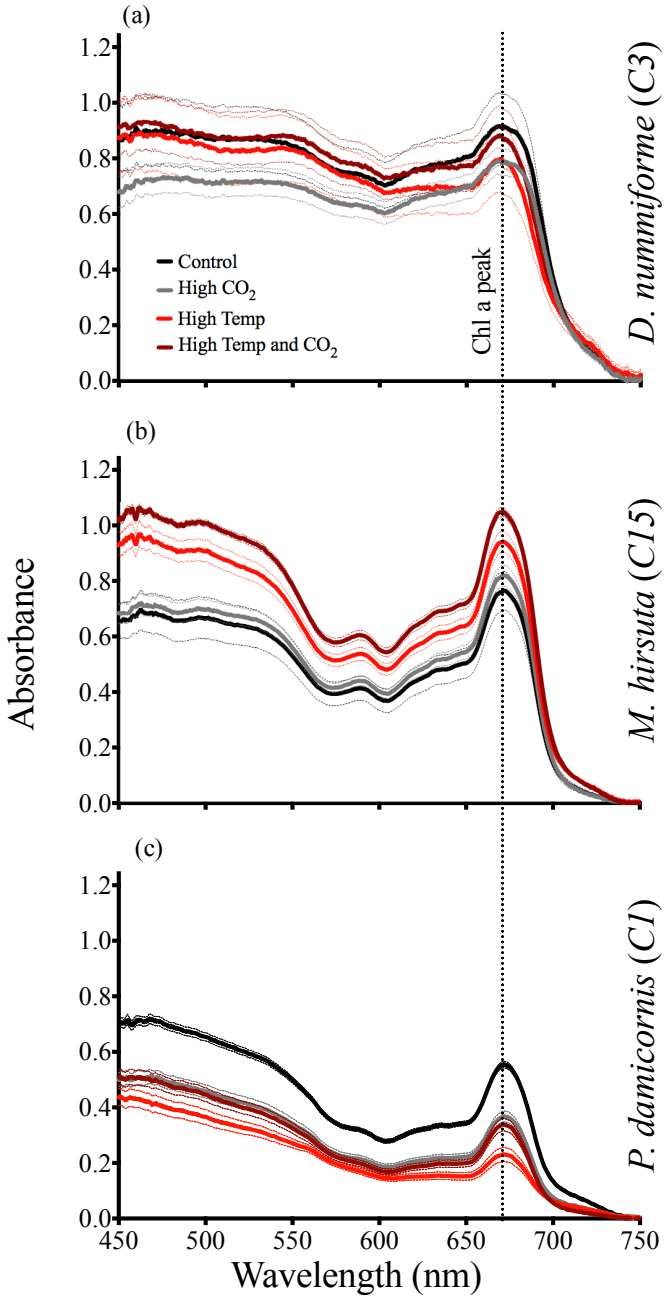

Figure 4.4: Net photosynthesis, translocation and percent translocation for *Discosoma nummiforme* (a, d, g), *Montipora hirsuta* (b, e, h) and *Pocillopora damicornis* (c, f, i). Averages plus standard error are shown for two pCO_2 levels and two temperatures (26.5°C = open bars, 32°C = dark bars). For each pane, the designations 'temp', 'pCO_2' and 'temp x pCO_2' indicate significant temperature, pCO_2 or interactive effects (two-way ANOVA). The letters above each bar indicate the results of the tukey pairwise analysis when a significant interactive effect is observed (n = 6 ± SE).

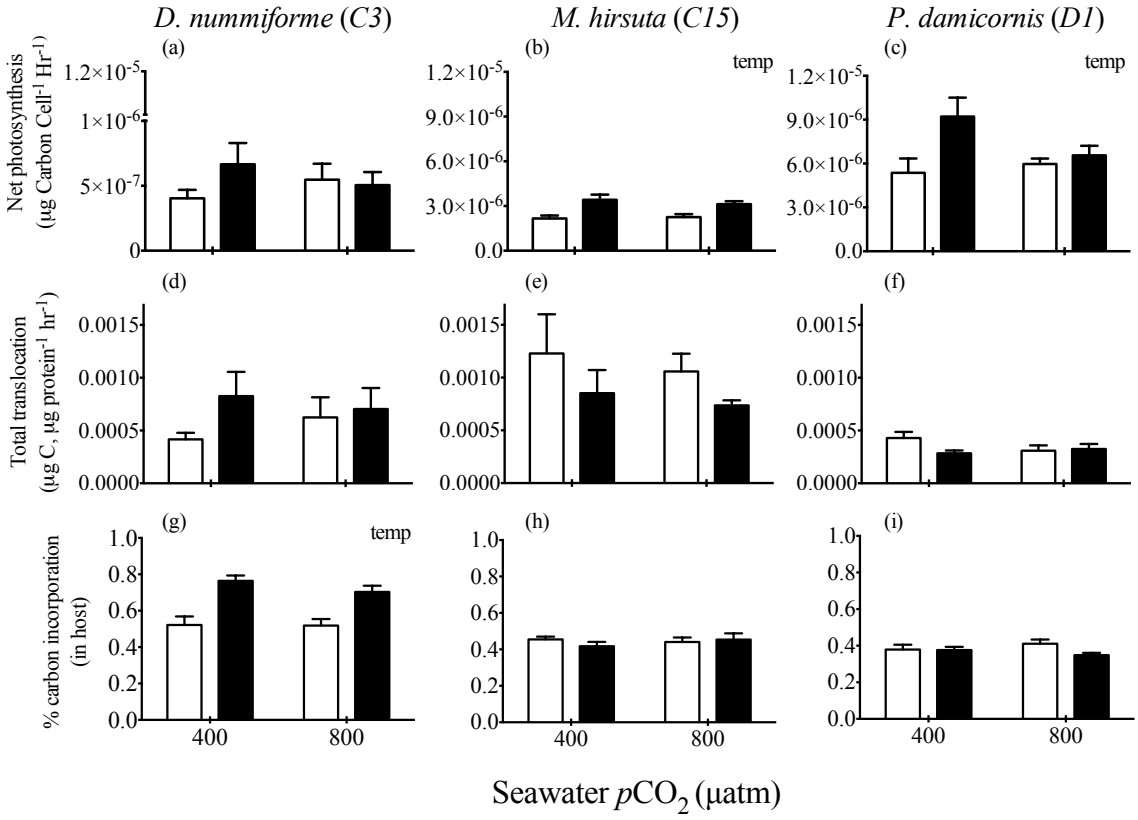

Figure 4.5: Correlations between net photosynthesis and symbiont density (top) and net photosynthesis and total translocation (bottom). Black line on top figure represents nonlinear fit through all data ($R^2 = 0.7996$). Solid lines on bottom figure represent the linear fit for *Discosoma nummiforme* (blue), *Pocillopora damicornis* (green), *Montipora hirsuta* (red) and *Exaiptasia pallida* (black). The grey line represents a P:T ratio of 1, such that the rate of photosynthesis matches the rate of translocated to the host.

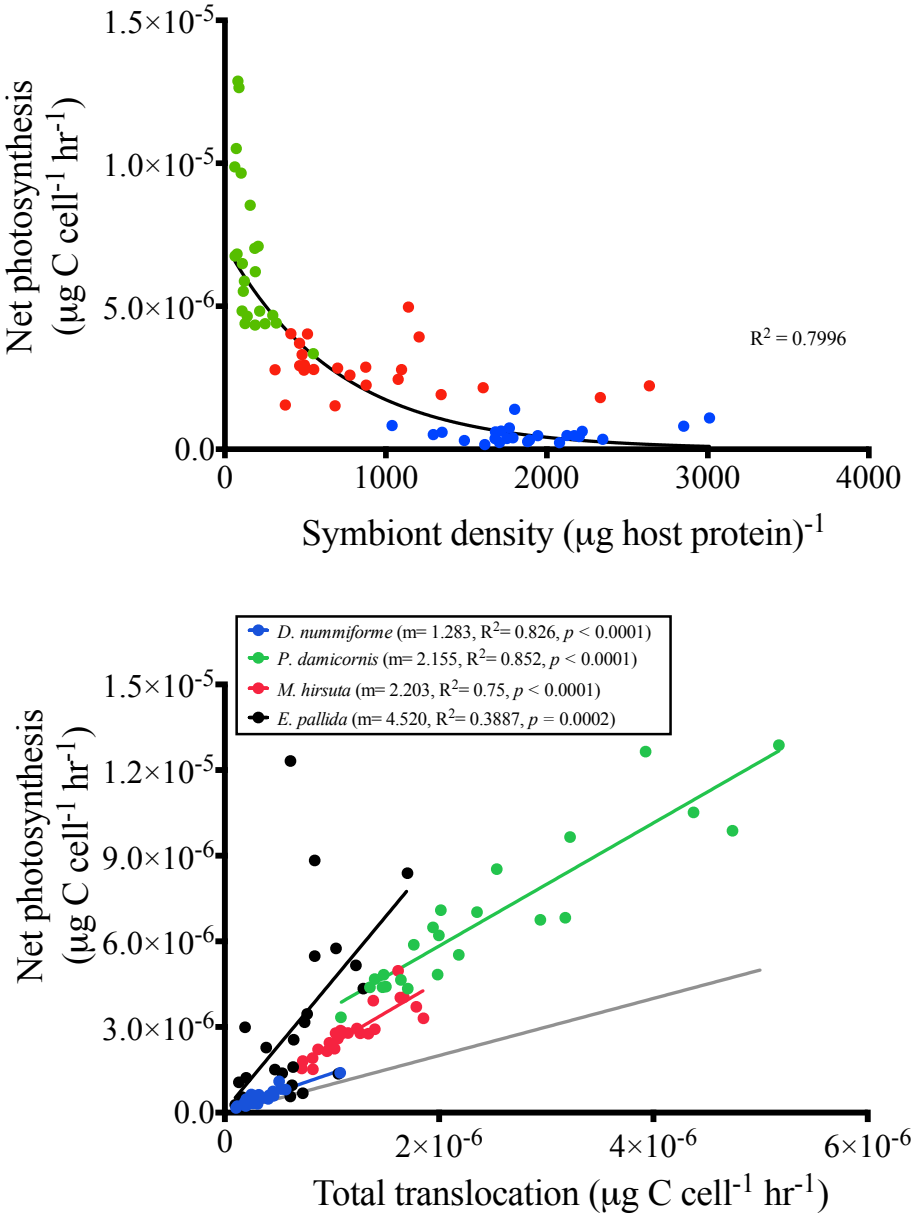

Figure 4.6: Principle Component's Analysis utilizing all eleven physiological variables. Colors indicate species with green = *P. damicornis*, red = *M. hirsuta,* black = *D. nummiforme*. Open circles indicate low temperature and closed circles indicate high temperature treatments. Ellipses represent a 99% confidence bubble around the mean for low (open ellipse) and high (closed ellipse) treatment factors. Only temperature is visualized within the figure as it explained the majority of significant differences among coral fragments.

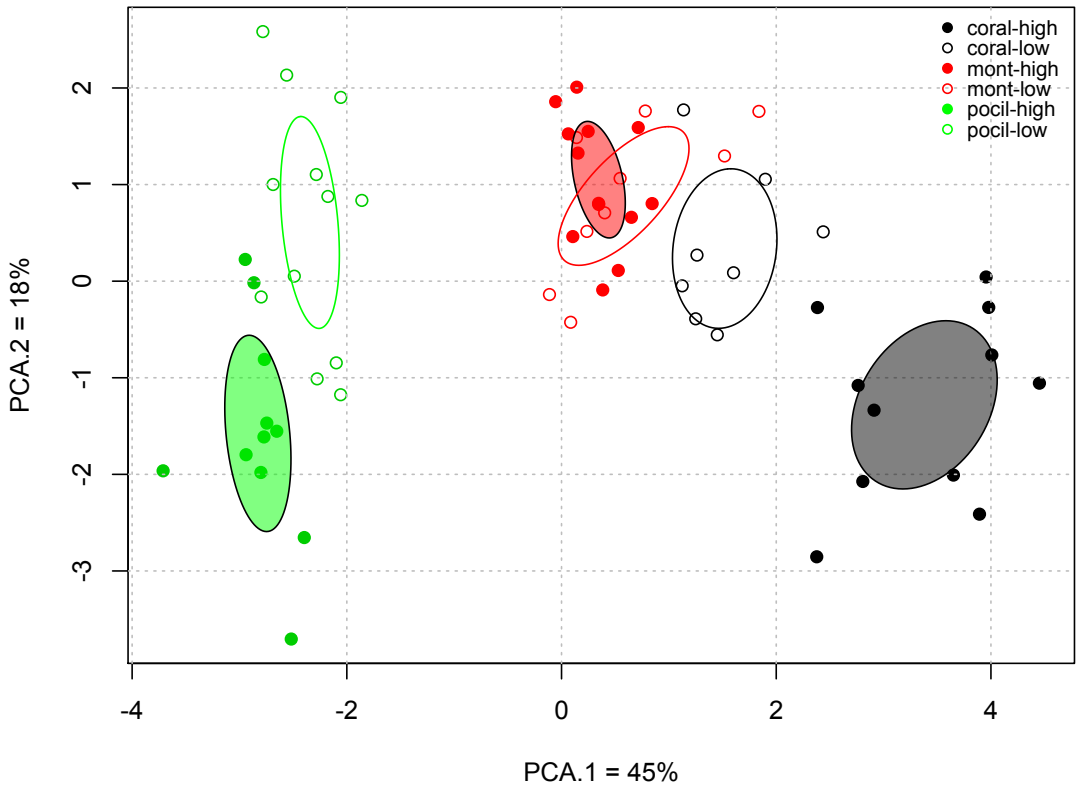

Chapter 5

DIFFERENTIAL CARBON UTILIZATION AND ASEXUAL REPRODUCTION UNDER ELEVATED pCO_2 CONDITIONS IN THE MODEL ANEMONE, *EXAIPTASIA PALLIDA,* HOSTING DIFFERENT SYMBIONTS

5.1 Abstract:

Here we report the effects of elevated pCO_2 on the model symbiotic anemone *Exaiptasia pallida* and how its association with three different strains of the endosymbiotic dinoflagellate *Symbiodinium minutum* (ITS2-type B1) affects its response. Exposure to elevated pCO_2 (70.9 Pa) for 28 days led to an increased effective quantum yield of PSII in actinic light within two of the alga-anemone combinations. Autotrophic carbon fixation, along with the rate of carbon translocated to the animal, were significantly elevated with high pCO_2. Elevated pCO_2 exposure also coincided with significantly greater asexual budding rates in all tested anemones. Further, differences in photochemistry and carbon translocation rates suggest subtle differences in the response to pCO_2 among the three strains of *S. minutum* and their host anemones. This illustrates the potential for physiological diversity at the subspecies level for this ecologically important dinoflagellate. Positive alterations in photosynthesis, carbon utilization, and fitness within this model symbiosis suggest a potential benefit from ocean acidification (OA) not yet observed within corals, which may enable these anthozoans to gain a greater ecological presence under future OA conditions.

5.2 Introduction:

Reductions in oceanic pH, along with changes in seawater carbonate chemistry are two major physical factors resulting from rising atmospheric CO_2 concentrations that pose a threat to marine ecosystems worldwide (Guinotte and Fabry 2008). Present day atmospheric partial CO_2 pressure (pCO_2) is already much higher than the previous 800,000 years (Luthi et al. 2008), and under current CO_2 emission rates, is predicted to double by the end of this century (IPCC 2013). These changes in pH and carbonate chemistry as a result of increasing pCO_2, commonly referred to as ocean acidification (abbreviated as OA hereafter), are especially important for marine organisms reliant on dissolved inorganic carbon (DIC) for photosynthesis and/or calcification (Iglesias-Rodriguez et al. 2008; Hurd et al. 2009; Hofmann et al. 2010). Understanding how such organisms respond to OA is critical towards predicting the future state of marine ecosystems.

For many marine photosynthetic organisms the increase in DIC resulting from rising CO_2 emissions may be beneficial, promoting greater rates of primary productivity due to enhanced carbon availability (Koch et al. 2013). For example, some seagrass species are positively affected by OA, with productivity rates and carbon sequestration increasing significantly (Zimmerman et al. 1997; Alexandre et al. 2012), while increased productivity and growth have also been documented for several phytoplankton species as well (Xia and Gao 2005; Hutchins et al. 2007; Beardall et al. 2009). Conversely, reductions in pH and carbonate ions may pose a significant problem for marine organisms that produce calcium carbonate skeletons or shells. With respect to OA, scleractinian corals are a unique group, as they contain both intracellular symbiotic

dinoflagellates and produce a calcium carbonate skeleton, and hence possibly experience both negative and positive effects of OA. The importance of their carbonate skeleton, in particular to reef accretion, has led many researchers to focus on how calcifying corals respond to OA. Although research is ongoing, recent studies suggest that the response is species specific and for some species, no change or only small reductions in rates could be expected with elevated pCO_2 (Comeau et al. 2013; Edmunds et al. 2013; Schoepf et al. 2013). With respect to photophysiology, reductions in cell density and net photosynthesis due to elevated pCO_2 have been reported for some calcifying coral species (Kaniewska et al. 2012) but not others (Crawley et al, 2009; Wall et al, 2014). Importantly, increases in gross photosynthesis have also been reported (Suggett et al. 2012a) thereby illustrating the broad mix of photophysiological responses to pCO_2 among different scleractinian coral species.

While the impacts of OA have been investigated in many species of reef-building coral, less attention has been given to non-calcifying soft-bodied anthozoans such as sea anemones. In a natural experiment along a CO_2 seep off the coast of Italy, the anemone *Anemonia viridis* significantly increased its growth, size and primary productivity rates near high CO_2 seep locations (Suggett et al. 2012a), while laboratory experiments with *Anthopleura elegantissima* and *Exaiptasia sp*. (temperate and tropical respectively) have noted increased oxygen production with elevated pCO_2 in both anemones (Towanda and Thuesen 2012a). Together these studies suggest that anemones may, in fact, benefit significantly from OA. Disturbance induced community phase-shifts from scleractinian corals towards other symbiotic cnidarians, such as anemones, have been noted (Norstrom et al. 2009; Dudgeon et al. 2010). In contrast, the prevalence of soft-bodied corals

declined with proximity to natural CO_2 seeps off the coast of Papau New Guinea (Fabricius et al. 2011). Whether or not soft-bodied symbiotic anthozoans are better able to acclimatize to climate change will become an increasingly important question as sea surface temperatures and pCO_2 continue to rise.

The sea anemone *Exaiptasia pallida* (formerly *Aiptasia pallida*, see Grajales and Rodríguez (2014)) is rapidly becoming an important model organism for the study of cnidarian-*Symbiodinium* symbioses (Sunagawa et al. 2009b; Lehnert et al. 2012; Voolstra 2013). Associations with the same genera of dinoflagellates as reef corals, ease of culturing, and rapid rate of asexual reproduction make *E. pallida* an ideal system for studying symbiotic anthozoans. In nature, *E. pallida* is globally distributed and maintains natural symbioses with only a select subset of *Symbiodinium* species (Thornhill et al. 2013). However, these anemones are easily maintained in the laboratory without symbionts (i.e. aposymbiotic) and subsequently 'infected' with a genetically diverse set of *Symbiodinium* species (Schoenberg and Trench 1980). The ability to host divergent and specifically chosen symbionts provides a unique opportunity to understand the influence of symbiont identity on the host's response to environmental stress such as OA.

The genus *Symbiodinium* is a highly diverse group of photosynthetic dinoflagellates that form complex associations with a range of host taxa from multiple phyla (Trench 1993; Coffroth and Santos 2005; Sampayo et al. 2009). Although our understanding of the genetic diversity and biogeography of this genus has outpaced that of the comparative physiology, their response to environmental stress can vary greatly among symbiont lineages or groups (Iglesias-Prieto and Trench 1997; Warner and Berry-Lowe 2006; Hennige et al. 2011). Therefore, the dominant symbiont can dramatically

affect the host's response to environmental stress (e.g., (Sampayo et al. 2008; Grottoli et al. 2014). Genetic characterization of *Symbiodinium* by nuclear, chloroplast and mitochondrial markers currently divides this genus into 9 clades (designated by the letters A-I) with each clade containing additional diversity that is resolved using more variable markers such as the ribosomal internal transcribed spacer (ITS) regions (Santos et al. 2003; Coffroth and Santos 2005; Sampayo et al. 2009). While, in some cases, diversity in the ITS regions equates approximately to a species-level designation, the recent use of microsatellite loci provide even finer resolution at the sub-species level, enabling the ability to distinguish different clonal variants or individuals (i.e., multilocus genotypes) within a species (Pettay and Lajeunesse 2007, 2009; Wham et al. 2011). These loci have revealed substantial diversity within individual symbiont species and population patterns that mirror changes in the prevailing environmental conditions (e.g. sea surface temperature), suggesting important physiological differences exist even at the sub-species level (Pettay and LaJeunesse 2013). However, few studies to date have attempted to characterize physiological differences among genetically distinct clonal variants of a *Symbiodinium* species (Leal et al. 2015), or how they interact with the host organism's response to physical stress while *in hospite*.

The aim of this study was to investigate the response of different anthozoan holobionts (used here to define the host + algal symbiont) to OA by utilizing the *Exaiptasia* model system. Throughout its global distribution *E. pallida* associates predominantly with the clade B symbiont, *Symbiodinium minutum* (LaJeunesse et al. 2012; Thornhill et al. 2013). Therefore, three genetically distinct clonal variants of *S. minutum* were chosen to quantify within-species physiological variability and the overall

holobiont response to elevated pCO_2. Subtle differences in photochemistry and physiology were detected and influenced how each host/symbiont combination responded to ocean acidification. This work represents the first characterization of sub-species physiological differences in *Symbiodinium* and their influence on holobiont response to changes in pCO_2.

5.3 Materials and Methods:

5.3.1 Development of Host/Symbiont Combinations:

All anemone/symbiont combinations were maintained in stable symbiosis for approximately one year prior to use in this experiment. Aposymbiotic *E. pallida* (clone CC7, donated by J. Pringle, Stanford University) (Sunagawa et al. 2009a) were held in glass bowls and 'infected' with one of two cultured strains of *S. minutum* (referred to as strains 1 and 2 respectively; Table 2). In addition, a subset of aposymbiotic anemones was maintained under 12:12 hour light:dark (100 μmol quanta m^{-2} s^{-1}) conditions in order to ensure that no remaining symbionts were present and could repopulate the host. After three months, microscopic visualization showed no signs of repopulation for any of the aposymbiotic anemones tested. Algal isolates utilized for infection were originally isolated from *E. pallida* from Florida and from a Caribbean gorgonian (*Plexaura kuna*) (isolates FLAp2 and Pk704 respectively from the BURR culture collection, donated by M.A. Coffroth, University of Buffalo). *S. minutum* belongs to the clade B lineage and is also known as type B1 by characterization of the ITS2 sequence (LaJeunesse 2001). The B1 lineage contains multiple genetic groupings that approximate species-level diversity

and roughly correspond to host associations (Finney et al. 2010; LaJeunesse et al. 2012). For initial infections, anemones were exposed to approximately 1 mL algal culture (10,000-100,000 cells mL^{-1} in log-phase growth) for 48 hrs, followed by a 100% water change with filtered seawater. Anemones were inspected daily under a dissecting microscope, and all anemones appeared to harbor symbionts within their tentacles in the first 24 hours of algal exposure. Once symbiotic, each *Exaiptasia*/alga combination was held in separate 19 L flow through aquaria that received filtered (1μm) and UV-treated seawater and 100 μmol quanta m^{-2} s^{-1} photosynthetically active radiation (PAR) provided by cool-white fluorescent lights on a 12:12 light:dark cycle. All anemones were fed *Artemia* nauplii twice each week. In addition to the CC7 *Exaiptasia* clone, a third, naturally occurring *Exaiptasia/S. minutum* symbiosis (referred to as 'strain 3') was originally collected from Bermuda and also maintained under the same conditions.

5.3.2 Genetic Analysis of Symbionts & Host:

Prior to the experiment and anemone infection, each cultured symbiont was genetically characterized using PCR-DGGE of the partial 5.8S and internal transcribed spacer 2 (ITS2) region of the ribosomal array (LaJeunesse 2002). In addition, the flanker region sequence of the microsatellite locus B7Sym15 was sequenced to verify the placement of these algae within the species *S. minutum* (LaJeunesse et al. 2012), and further genetic analyses using microsatellite loci for clade B *Symbiodinium* were conducted to delineate and verify strain identity in each symbiosis. Five haploid loci were analyzed (Table 2) according to Pettay and LaJeunesse (2007) to create a multilocus genotype (MLG) for each strain. Following the experiment, five replicate anemones for

each symbiont combination from both the treatment and control (n = 10 total combination^{-1}) were analyzed to confirm the stability of the symbioses at both the ITS2 and MLG level of resolution.

In addition to the symbionts, both host anemone populations (CC7 and Bermuda strain) were genetically characterized using newly developed microsatellites for *E. pallida* to verify each line was genetically distinct (Table 3) (Pettay & Grajales in preparation). Briefly, microsatellite loci were developed from EST sequences of *A. pallida* (Sunagawa et al. 2009) that were vectored screened (using VecScreen & the UniVec NCBI vector library) and assembled (CAP3; Huang & Madan, 1999). Contigs and singlet sequences were screened for simple sequence repeats (SSRs) of di, tri, tetra, penta and hexanucleotides with more than 6 repeats (WebSat; Martins et al. 2009). Primers were designed for candidate loci (Primer3; Rozen & Skaletsky, 1999) and the loci screened on *E. pallida* samples from the Florida Keys and Bermuda collected in 2011. The loci were amplified following (Pettay and Lajeunesse 2007) and their descriptions are given in Table 3.

5.3.3 **Experimental Design**:

Small glass bowls (9 cm diameter, 130-mL volume) covered with 300 μm nitex mesh tops were used to hold different anemone/symbiont combinations. Each glass bowl held four anemones, with five glass bowls per host/symbiont combination in each treatment. One glass bowl per host/symbiont combination was placed in each of five replicate aquaria per treatment (described below). To lessen possible tank effects, the position of each bowl within each tank was changed every day, and bowls were moved to

a different aquarium every third day. After an initial 5 days of acclimation to the experimental systems, each treatment ran for 28 days. Anemones were not fed during the 28-day experiment. All bowls and mesh tops were gently cleaned of any fouling debris two times each week.

Each recirculating treatment system consisted of five, 15 L aquaria connected to a central 416 L sump with flow rates in each aquarium of ~567 L hr^{-1}. Anemones were maintained under a 12:12 h light:dark cycle, using a customized uniform LED array (Cree XPG-R5, cool white; 5000–8300 K) that simulated a diel light cycle by ramping light intensity from 10 to 200 μmol photons m^{-2} s^{-1} each day using an Apex Junior AquaController (Neptune Systems). Lights were ramped up from 10-200 μmol photons m^{-2} s^{-1} over a three hour period, maintained at 200 μmol photons m^{-2} s^{-1} for six hours and then ramped back down from 200-10 μmol photons m^{-2} s^{-1} over three hours before turning off for twelve hours. Temperature was maintained at 26.5 °C using titanium heaters housed in each sump and also regulated using an Apex AquaController. Salinity was maintained at 32 psu using a float valve and RO water. Temperature (26.5 °C) and salinity were manually confirmed every other day. In order to minimize variability in seawater chemistry, a 40% water change was performed on each system every other day using filtered and UV sterilized natural seawater collected at the Delaware Indian River inlet during the incoming tide.

CO_2 treatments consisted of ambient (35 Pa) and elevated (70.9 Pa) pCO_2 to represent the current (for the DE water) and predicted conditions expected by the mid to late 21st century (IPCC 2013) and were maintained using a pH stat system for precise control of air and CO_2 gas input (KSgrowstat, University of Essex). To ensure stability of

carbonate chemistry throughout the experiment, pH measurements were taken within each treatment sump every 120 seconds with a glass microelectrode (Thermo Scientific, Orion Ross Ultra pH glass electrode) that was connected to a pH electrode amplifier (PH 02, Technologica Ltd., U.K.). The pH signals were then processed by computer, which then controlled a series of solenoids designed to deliver CO_2, air or CO^2-free air. The microelectrodes were recalibrated each day using NBS calibration buffers and confirmed through independent measurements of pH using a Fischer Scientific A815 Plus pH meter. In addition, pH and total alkalinity (TA) was monitored over several daily cycles and representative data are shown (Table 1). TA was measured using a bromocresol purple based colorimetric assay according to (Yao and Byrne 1998) with a spectrometer set in absorbance mode (Ocean Optics, USB4000-ES) and a titrator (Metrohm 876 Dosimat plus, Switzerland). Parameters for seawater carbonate chemistry based on pH and alkalinity measurements were calculated using the CO2SYS program (Lewis et al. 1998) and are reported in Table 1.

5.3.4 Chlorophyll a Fluorescence:

Dark acclimated maximum quantum yield of photosystem II (F_v:F_m) was measured every three days, one hour after the light period by pulse amplitude modulation fluorometry (Diving PAM, Waltz, Germany). In addition, the effective quantum yield, (Fq':Fm', also known as the operating efficiency of PSII) was also measured on the final day, during midday under the LED lights.

5.3.5 Anemone Preservation & Processing:

Asexual reproduction (budding) rates, were calculated by counting the total number of new recruits within each bowl each week and were then combined to represent the collective reproductive effort of the four original anemones placed within each bowl (number of buds per month). After physiology measurements at the end of the experiment, all anemones were flash frozen in liquid nitrogen and then stored at -80 $^{\circ}$C until further processing. For processing, anemones were ground in 1 mL of seawater using a 1.5 mL Tenbroeck glass tissue grinder, and then centrifuged (5000 × g) for five minutes. Soluble animal protein (mg mL^{-1}) was determined from two replicate 50 μL samples of the animal supernatant, using a BCA Protein kit (Thermo Scientific Pierce), with bovine serum albumin used for standards (Smith et al. 1985). The algal cell pellet was re-suspended in 400 μL of seawater and separated into two 200 μL aliquots, for algal cell density and chlorophyll *a* quantification. Samples for algal cell counting were preserved with 10 μL 1% glyceraldehyde and manually counted by light microscopy, using a hemocytometer (6 independent replicate counts) under 100x magnification. Total protein concentrations for each anemone/symbiont combination were not significantly different between treatments or among host/symbiont combinations (not shown). Therefore any differences observed in algal cell density are not likely influenced by CO_2 induced changes in animal protein concentration. Chlorophyll *a* was extracted by bead beating cells (BioSpec) using 0.5 mm glass beads for 60 s in chilled 90% methanol. Samples were then incubated at -20°C overnight, followed by centrifugation to remove remaining debris. Chlorophyll *a* concentration was then determined spectrophotometrically (Porra et al. 1989).

5.3.6 Carbon Uptake and Translocation:

Individual anemones were placed in separate 7 mL scintillation vials containing 2 mL of seawater spiked with 15 μL of ^{14}C-labeled bicarbonate (specific activity 17 μCi μmol^{-1}). Five anemones were used for each host/symbiont combination and treatment. Vials were placed on a LED light-table (Cool White Cree XPG-R5; 600 μmol photons m^{-2} s^{-1}; 28 °C) for 90 min. Short-term exposure to this light level resulted in no significant change in maximal photosynthesis in control anemones grown at 200 μmol photons m^{-2} s^{-1} (data not shown). An additional two anemones from each treatment and host/symbiont combination were placed in vials with ^{14}C-spiked seawater and held in the dark for 90 minutes to account for carbon uptake in the dark. Three additional vials containing only the spiked seawater were also included for measurement of total activity.

After ^{14}C incubations, the total organic carbon (TOC) released, which is comprised of both particulate and dissolved organic carbon (POC and DOC) released by each holobiont, was calculated by first mixing each vial to ensure a homogenous sample, and then removing 200 μL of seawater for TOC calculations. Each anemone was then removed from the vial and ground in 1mL of seawater in a 1.5 mL glass tenbroeck tissue grinder. A 100 μL sample of the resulting homogenate was removed and fixed with 10 μl 1% glutaraldehyde and used for algal cell counts as described above. The remaining homogenate was centrifuged (5000 × g) for 5 minutes to separate the host and symbiont portions. The supernatant was completely removed, and a 500 μl subsample was utilized for measuring carbon translocated to the host (H_s), while the remaining supernatant was used for calculating host protein content. The remaining algal cell pellet was resuspended

in 500 μl of FSW, vortexed, and then centrifuged again to extract any remaining host supernatant (RH_s) from the algal pellet. The algal pellet (S) was then resuspended a final time in 400μl of FSW. All samples measured for radioactivity were acidified with an equal volume of 0.1 mol L^{-1} HCl, placed in 7 mL scintillation vials for 24 hours and then combined with 5 mL of scintillation cocktail (Ultima Gold, Perkin Elmer) prior to reading with a liquid scintillation counter (Beckman LS-6500). Samples were corrected for background activity and dark incorporation. All sample measurements and calculations follow previously established methods for *E. pallida* (Davy & Cook, 2001). Translocation and photosynthesis rates were determined by the average specific activity (grams C dpm^{-1}) and the duration of the incubation. The fraction of carbon translocated (T_L) was calculated as,

$$T_L = TOC + H_s + RH_s$$

and then normalized algal cell number and to host protein, where TOC is the total organic carbon and H_s and RH_s are the host supernatant and remaining host supernatant respectively.

The fraction of carbon produced from net photosynthesis (P_{net}) was normalized to algal cells $anemone^{-1}$ and calculated as,

$$P_{net} = TOC + H_s + RH_s + S$$

where S is the algal pellet described above.

Using the ratio of the portions described above, the fraction of photosynthate translocated to the host was calculated as,

$$T_L/P_{net} = (TOC + H_s + RH_s)/(TOC + H_s + RH_s + S)$$

5.3.7 Statistical Analysis:

All data sets were tested for assumptions of homogeneity of variance and normality of distribution using the Levene and Shapiro-Wilk tests respectively. If either test invalidated these assumptions, the data was log transformed and retested to ensure normality prior to further analysis. A two-way analysis of variance (ANOVA) was used to test for significant effects of the main variables pCO_2 and symbiont type and the interactive effects between the two (α=0.05). If significant differences in host:symbiont combination was observed, a Tukey post-hoc test was utilized to distinguish significant difference among the three types. If interactive effects were observed, all other main effects were ignored and the analysis was followed up with a pairwise analysis of all six groups. Budding rate data were non-normal after transformation and samples were tested by a Kruskal-Wallis test with multiple comparisons. For maximum quantum yield of PSII (F_v:F_m), separate two-way repeated measures ANOVAs were utilized to test for significant differences among treatments within each symbiont type. A Mauchly's test was also performed to check and correct for violations of sphericity. If significant differences were observed, the analysis was followed up with a paired t-test on each day. All statistical analyses were performed using the open source software R with 'car' and 'pgirmess' packages installed (*http://www.R-project.org/)*.

5.4 Results:

5.4.1 Host/Symbiont Identity and Stability:

All three strains of symbionts were verified as ITS2-type B1 and *S. minutum*, as defined by the ITS2 sequence that dominates their ribosomal array (Genbank#

AF333511) and flanker region sequence of B7Sym15 (Genbank# JX263427), respectively. The clonal lines of *E. pallida* maintained stable associations with each *S. minutum* strain for the duration of culturing and exposure to experimental conditions. The three different strains of *S. minutum* were genetically distinct and differed by as many as five alleles for pairwise comparisons of their microsatellite derived haploid MLGs and were designated as strains 1, 2 or 3 (Table 2). The two *E. pallida* clonal lines were distinct and differed by at least one allele at all six loci except AIPT14 (Table 3). These genetic lineages led to holobiont combinations of the *E. pallida* clone CC7 with *S. minutum* strains 1 & 2, and the Bermuda *A. pallida* clone with *S. minutum* strain 3.

5.4.2 Photosynthesis, Carbon Uptake and Symbiont Physiology:

Elevated CO_2 significantly affected anemone/algal symbioses, with changes occurring at the photochemical, cellular and organismal level. Significant time effects were observed for anemones with strain 1 ($p = 0.003$) and 3 ($p = 0.003$) as maximum quantum yields (F_v:F_m) varied throughout the experiment but no significant treatment effect was observed by the end of the experiment in two of the holobionts (Fig. 1a,c). However there was a significant interactive effect for strain 2 ($p = 0.013$), as maximum quantum yields also varied throughout the experiment, with significant CO_2-induced decreases on day 5 ($p = 0.008$) followed by a significant increase by day 25 ($p = 0.04$)(Fig. 1b). Exposure to elevated CO_2 resulted in a small yet significant increase in the effective quantum yield of PSII in the light (Fq':Fm') ($p = 0.001$) in anemones hosting strains 1 and 2 (Fig. 2a). Additionally, differences among the host:symbiont combinations were also observed as Fq':Fm' levels in anemones hosting strain 3 were significantly

elevated over strain 1 ($p = 0.0001$) and strain 2 ($p < 0.0001$). Although the difference was minimal, strain 1 F_q':F_m' was significantly higher than strain 2 ($p = 0.001$). In addition to these changes in PSII photochemistry, net photosynthesis algal cell^{-1} significantly increased with elevated pCO_2 in all anemones ($p < 0.001$) (Fig. 2b).

While there was no significant main effect of elevated CO_2 exposure on symbiont density, a significant interactive effect ($p = 0.016$) was noted, as patterns in algal cell density differed among the anemone / algal combinations, with symbiont density declining in strains 2 and 3 and rising marginally for strain 1 under the high CO_2 treatment. Symbiont density for the strain 3 holobiont were also significantly higher than strain 1 under ambient but not elevated pCO_2 (Fig. 2c). At ambient CO_2, chlorophyll *a* content also varied significantly with symbiont type ($p < 0.001$), with strain 1 having a greater concentration of chlorophyll *a* algal cell^{-1} than strain 2 ($p < 0.001$) and strain 3 ($p = 0.002$). However, there was no significant change in cellular chlorophyll *a* under elevated CO_2 (Fig. 2d).

5.4.3 Translocation and Host Reproduction:

The percent of carbon translocated to the host differed significantly among holobionts under the ambient CO_2 treatment ($p = 0.002$), with anemones hosting strain 3 receiving a significantly lower portion of photosynthate than animals hosting strain 1 or strain 2 algae ($p = 0.028$, $p = 0.001$, respectively) (Fig. 3a). Meanwhile, the simple means effect of the two way ANOVA found a significant increase with pCO_2 ($p < 0.001$) for translocation rates to the host (expressed as µg carbon µg host protein^{-1} hr^{-1}), driven primarily by increases within strains 1 and 2 (Fig. 3b). The host:symbiont combination

was also a factor, as strain 3 translocation rates were significantly elevated over strains 1 ($p = 0.003$) and 2 ($p = 0.027$) and most notably at ambient pCO_2. A significant ($p = 0.030$) CO_2 induced increase in carbon translocation was also observed when rates were normalized to symbiont cell density (µg carbon released $cell^{-1}$ hr^{-1}) (Fig. 3c). Lastly, elevated pCO_2 exposure led to a significant increase in the rate of asexual reproduction ($p < 0.05$) in all strains.

5.5 Discussion:

Elevated pCO_2 designed to mimic mid to late 21st century conditions over 28 days (70.9 Pa pCO_2) resulted in substantially increased photosynthetic carbon uptake for all three strains of *S. minutum*. Similar increases in photosynthesis (as measured by respirometry) were observed for the temperate symbiotic anemone *Anthopleura elegantissima* during a six-week exposure to pCO_2 of 230.9 Pa (Towanda and Thuesen 2012a) and *Exaiptasia* sp. exposed to *p*CO2 of 69.6 and 147.8 Pa (Gibbin and Davy 2014). In the natural environment, growth and abundance of the symbiotic sea anemone *Anemonia viridis* increased along a natural volcanic CO_2 seep in Italy, suggesting a significant benefit from elevated pCO_2 for this species as well (Suggett et al. 2012a). Together, these studies suggest a beneficial effect of elevated pCO_2 on sea anemones, and further that their photosynthetic symbionts may be carbon limited under ambient pCO_2 conditions.

Elevated dissolved inorganic carbon (DIC) associated with OA is hypothesized to enhance photosynthetic rates for carbon limited endosymbionts (Langdon and Atkinson 2005; Cohen and Holcomb 2009). Similar to early work with free-living phytoplankton

where it was assumed that carbon limitation did not play a role, subsequent studies have observed increases in productivity associated with elevated DIC within a number of free-living phytoplankton, suggesting that carbon limitation may play an important role in productivity rates within the open-ocean as well (Xia and Gao 2005; Hutchins et al. 2007; Beardall et al. 2009). Earlier work with *E. pallida* by (Davy and Cook 2001) observed an increase in net photosynthesis and photosynthate translocation (normalized to algal cell number) after 20-30 days of starvation. During this time, there was a notable decline in symbiont densities in these starved anemones, and the noted increase in net photosynthesis and carbon translocation was thought to result from greater carbon availability per algal cell (Davy and Cook 2001; Wooldridge 2009a). These changes in carbon incorporation point towards DIC limitation within *Symbiodinium* as previously described by (Weis 1993), where net photosynthesis also increased with elevated DIC concentrations within *Aiptasia pulchella*. The substantial rise in net photosynthesis for all three strains of *S. minutum* noted here also supports this hypothesis. Interestingly, *Symbiodinium B1* isolates in culture (presumably closely related to *S. minutum*) (Brading et al. 2011) showed no increase in net photosynthesis in response to elevated pCO_2. This discrepancy among closely related symbionts grown in culture vs. *in hospite* may indicate a greater reliance on host carbon concentrating mechanisms (Leggat et al. 1999) and/or that free-living *Symbiodinium minutum* strains are not DIC limited (Brading et al. 2011).

Along with a major increase in carbon uptake $cell^{-1}$, PSII photosynthetic efficiency remained relatively stable under high pCO_2 conditions within strains 1 and 3, with only a slight increase towards the end of the experiment in strain 2 (Fig. 1). In contrast the effective quantum yield (i.e. operating efficiency of PSII in the light) did

increase significantly (although only slightly in strain 2 and 3) under elevated CO_2 conditions. Photosynthesis in *E. pallida* tends to saturate at light levels near 200 μmol photons m^{-2} s^{-1} (Muller-Parker 1984; Goulet et al. 2005). Therefore, it is likely that anemones used here were light saturated and well poised to take advantage of the greater electron sink provided by elevated carbon availability. As with other marine phytoplankton, the photosynthetic response to elevated pCO_2 may differ significantly under low light conditions where photosynthetic electron flow rather than carbon availability is the rate-limiting step in photosynthesis (Li and Campbell 2013). Reductions in calcification and photosynthesis were greater under low as opposed to high light conditions under elevated pCO_2 for the corals *A. horrida* and *P. cylindrica* and suggest that OA alleviated pCO_2 limitation under high light conditions (Suggett et al. 2012a). It is therefore possible that under lower light levels, the *S. minutum* response to elevated pCO_2 could differ significantly than presented here.

Despite increased photosynthetic productivity and in contrast to the work of Gibbin and Davy (2014) and Suggett et al. (2012b), there was no significant change in the *S. minutum* density in any anemone/algal pairing in response to elevated pCO_2. A drop within strain 3 was apparent, however this was not significant. Towanda and Thuesen (2012) also noted no change in symbiont density for the temperate anemone, *A. elegantissima*, held under two OA scenarios for approximately double the time period used here (Towanda and Thuesen 2012a). This may reflect some decoupling between increased productivity and cell density, as *Symbiodinium* spp. are typically in severe unbalanced growth *in hospite* and release a significant portion of their photosynthetically fixed carbon to the host (Dubinsky and Berman-Frank 2001). Such changes in symbiont

density under excess CO_2 could reflect a change in the balance of carbon and nitrogen supply to the alga and the host, similar to patterns noted for nitrogen limitation in these symbioses. For example, Marubini & Davies (1996) noted a significant increase in algal density after exposure to excess nitrogen. While Gibbin and Davy (2014) did note higher algal density with increased pCO_2, this was at a CO_2 concentration double that utilized here (~147 Pa). Additionally, natural CO_2 levels yielding the largest response in Suggett et al. (2012b) were also considerably higher (144.7 Pa).

An increase in net photosynthesis led to a similar rise in translocation rates (per algal cell) at elevated pCO_2 for all three symbiont strains. From the host perspective, however, greater carbon translocation rates (per host protein) only occurred for anemones hosting algal strains 1 and 2 (Fig. 3b), with a loss in cell density by strain 3 counteracting any potential gain in photosynthate contributed to the host. Higher percent of translocated carbon, but lower photosynthetic rates, were observed under extremely high CO_2 concentrations (394.9 Pa) in the scleractinian coral *Stylophora pistillata* (Tremblay et al. 2013). Unlike our findings for *A. pallida*, the increase in percent translocation to *S. pistillata*, despite a decline in photosynthesis, may indicate an important change in the symbiosis that is not conducive towards sustained growth and health or represent an important difference between calcifying and non-calcifying cnidarians. Alternatively, the differences may be attributed to the large difference in the pCO_2 treatments used in these two studies (70.9 vs. 394.9 *Pa*).

Interestingly, the carbon translocation rate of the anemone hosting the strain 3 alga was significantly higher than the other two host/symbiont combinations despite a smaller percentage of the total photosynthate produced being shared with the host

anemone (Fig. 3a-b). As data presented here were normalized to host protein, it is possible that changes in total protein concentration could influence our understanding of carbon translocation to the host and bias such results. However, no significant differences in total protein per anemone were observed between treatments or among host/symbiont combinations (data not shown). Furthermore, the anemones hosting strains 1 and 2 were from the same clonal line whereas the anemone with strain 3 was a different host genotype, and the differences in photosynthate allocation likely reflect distinct differences in the overall symbioses among the three anemone:symbiont combinations tested here (Leal et al. 2015). These differences in the symbioses may play an even greater role under more severe stressors such as elevated temperature and underscore the need to assess the genetic identity of the alga and animal in such studies. In addition, the use of ^{14}C to measure carbon translocation cannot account for rapidly respired autotrophically derived carbon (Tremblay et al. 2013). It is therefore possible that changes in respiration rates could also underestimate differences in rates of carbon translocation observed here.

While the percentage of photosynthate translocated by the symbionts remained the same, host budding rates increased significantly with elevated pCO_2. Previous work by Clayton, (1985) and Clayton & Lasker (1985) showed that asexual budding rates by *Aiptasia* sp. lead to greater rates of biomass accumulation than host tissue growth, allowing for a clonal population to quickly increase. This is likely due to the relatively cheap reproductive effort required for pedal laceration (asexual budding) whereas sexual reproductive effort can be considerably higher (Hunter 1984). Asexual reproduction can be an advantageous strategy under conditions of frequent environmental disturbance and

or high mortality of small sized colonies (Nakamaru et al. 2007). The small reproductive effort required for asexual budding in anemones, along with environmental disturbances could help explain the shifts from scleractinian species to more soft-bodied cnidarian species noted by Norstrom et al, (2009) and Dudgeon et al. (2010).

The additional energy needed to support increased budding rates for anemones hosting strains 1 and 2 (Fig. 3d) may be explained by the higher translocation rates of these symbionts with increased carbon availability. Interestingly, for the strain 3 holobiont, the rate of photosynthate received by the host did not vary, suggesting that the energetic requirement for the increase in budding rates observed at high pCO_2 may have had a different origin. Host carbonic anhydrases, a central component of the carbon concentrating mechanism (CCM), are important for supplying inorganic carbon to the symbiont for photosynthesis (Weis et al. 1989; Weis and Reynolds 1999). A change in available DIC may reduce the need for actively maintaining energetically costly CCMs within the host and symbiont (Weis et al. 1989; Weis and Reynolds 1999; Leggat et al. 2002) and could represent significant energetic savings with elevated pCO_2, particularly to the host. Such down-regulation of animal derived CCM's may have occurred in the strain 3 holobiont combination used here, with the energetic surplus being reallocated towards greater budding rates as well. Similarly, reallocation of energetic savings may have played a role in the other two host:symbiont combinations. The benefits of energy reallocation have been reported for the alga *Chlorella pyrenoidosa* and *Chlamydomonas reinhardtii*, where reductions in CA activity due to elevated pCO_2 occurred in concert with increases in protein and carbohydrate concentrations, thus boosting energetic reserves within the cell (Xia and Gao 2005). Reductions in host CAs have been observed

for some scleractinian coral species under high CO_2 conditions as well (Moya et al. 2012). In this regard, further studies that incorporate total carbon budgets (*sensu* Tremblay et al. 2013), respiratory demand, and quantify specific biomass from protein, lipids and carbohydrates could contribute substantially to future investigations of how elevated pCO_2 will impact different *Symbiodinium*-based symbioses.

Interestingly, despite the close genetic relationship among the three symbiont strains and two host populations, unique differences were nevertheless observed among the three host/symbiont combinations. Differences in cell density, within the ambient treatments, were segregated between the two host anemone populations as the strain 3-host:symbiont combination (collected from Bermuda) was significantly higher than strains 1 and 2 (in the CC7 clone). As discussed previously, this likely influenced differences in translocation to the host, and may suggest the host as a major driving factor with respect to changes in physiology in response to elevated pCO_2. However, differences in symbiont physiology were also observed both with respect to chlorophyll content and photosynthetic yields, indicating that significant physiological differences can exist even among clonal variants and that these differences may also influence the holobiont response to climate change. How anemones, along with other sessile marine invertebrates, respond to elevated CO_2 and the potential ecological implications of greater asexual budding rates within these clonal organisms will become increasingly important towards understanding future corals reefs under high atmospheric CO_2 conditions. Likewise, whether host vs. symbiont physiological changes can be ranked differently in terms of importance to the overall holobiont response to climate change will become an increasingly important area of *Symbiodinium* symbiosis biology.

Table 5.1: Average conditions for each treatment. Mean ± 1 SE are shown. All seawater carbonate chemistry based on pH and Alkalinity measurements was calculated using the CO2SYS program (Lewis & Wallace, 1998)

	Ambient CO_2	**High CO_2**
Temp. (°C)	26.81 ± 0.1108	26.78 ± 0.1437
pH_T	8.22 ± 0.018	7.95 ± 0.013
***p*CO_2 (Pa)**	35 ± 0.1	70.9 ± 0.15
TA (µmol kg^{-1})	2164 ± 44	2073 ± 3
Ω_{arag}	3.37 ± 0.01	1.97 ± 0.005
Salinity (ppt)	33.36 ± 1.2	33.09 ± 1.3

Table 5.2: Description of the Symbiodinium minutum cultures, including their host of origin, host used and their five-locus genotypes. Strain identify for each anemone host used here is provided in parentheses.

Strain	Culture Name	Original Host	Host Used	Microsatellite Fragment Sizes (bp)				
				B7Sym15	B7Sym34	B7Sym36	CA4.86	CA6.38
1	FLAp2	*Ex. pallida*	*Ex. pallida* (CC7)	263	281	196	182	101
2	PK704	*Plexaura kuna*	*Ex. pallida* (CC7)	263	267	163	199	103
3	N/A	*Ex. pallida*	*Ex. pallida* (Bermuda)	259	271	169	182	101

* Loci B7Sym15, B7Sym34 & B7Sym36 from Pettay and LaJeunesse 2007, while loci CA4.86 & CA6.38 from Santos and Coffroth 2003.

Table 5.3: Description of the six Aiptasia pallida microsatellite loci and MLGs of the two A. pallida clones.

Locus	Primer	Repeat	A_T	Accession #	CC7 Clone	Bermuda Clone
AIP6	F-(HEX)GAATCAGGAATCAACCCAACAT R-TAAGTGCCAGACCAACAACAAC	$(TGA)_7$	59°C	GH577343	302 302	302 318
AIP8	F-(FAM)AAAAGATTCGTGAGCAGAAAGG R-GAGCTGAAATAAGGTGAATACAAGG	$(TA)_6$	59°C	GH574595	293 295	293 293
AIP14	F-(FAM)AAAAGATTGAAGACGAACCAGC R-ATAACTGGGCATTCCACCATAC	$(GCA)_7$	59°C	GH578373	188 191	188 191
AIP15	F-(HEX)TCAGCAGTACGGAGGAATGAAC R-AGGAGGGCACGGTTGTTG	$(CCA)_7$	59°C	GH578373	319 322	319 319
AIP17	F-(HEX)GCTACTTTACCCGAACCCAAG R-TAGACGACTTGCGAGATCAAAA	$(TA)_6$	59°C	GH573936	292 292	294 296
AIP20	F-(FAM)GACTGGCACATTACCATCTATAACA R-AGTTAGTTTGTGTGGTTGCCCT	$(AT)_7$	59°C	GH578509	334 334	339 341

Figure 5.1: Maximum quantum yield of PSII in three different Exaiptasia-Symbiodinium combinations under ambient and elevated CO_2 (a-c). Mean ± 1 SE are shown for ambient and elevated pCO_2 (35 Pa = light symbols, 70.9 Pa = dark symbols). Asterisks represent significant differences (*, $p < 0.05$: **, $p < .01$) between the ambient and high CO_2 treatments on that day.

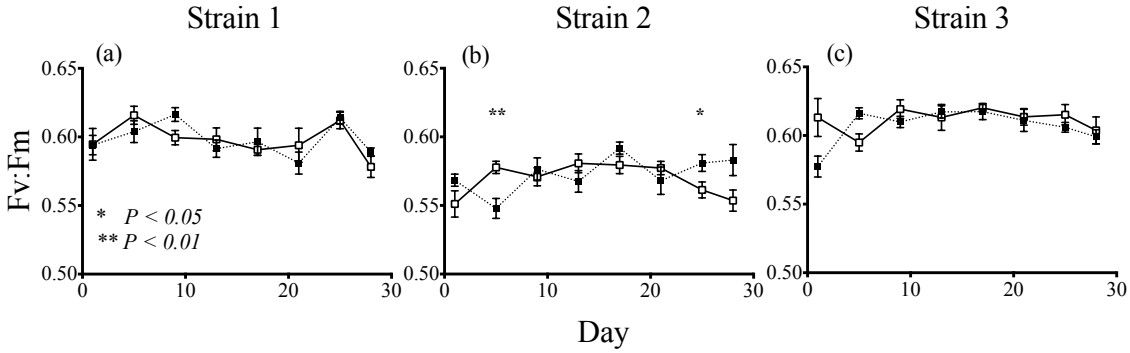

Figure 5.2: Effective quantum yield **(a**) Net photosynthesis **(b)** symbiont cell density and **(c)** chlorophyll a cell^{-1} **(d).** Mean ± 1 SE are shown for ambient and elevated pCO_2 (35 Pa = light bars, 70.9 Pa = dark bars). The abbreviations (sym), (pCO_2) and (Int) in the top right corner of each plot indicate significant differences between symbiont strain, pCO_2 or interactive effects resulting from a two-way ANOVA (n = 5). If a pCO_2 effect was observed, the letters indicate significant differences between pCO_2 groups (n = 5 ± SE). If an interactive effect was observed, the letters above each bar indicate significant differences among the 6 treatments.

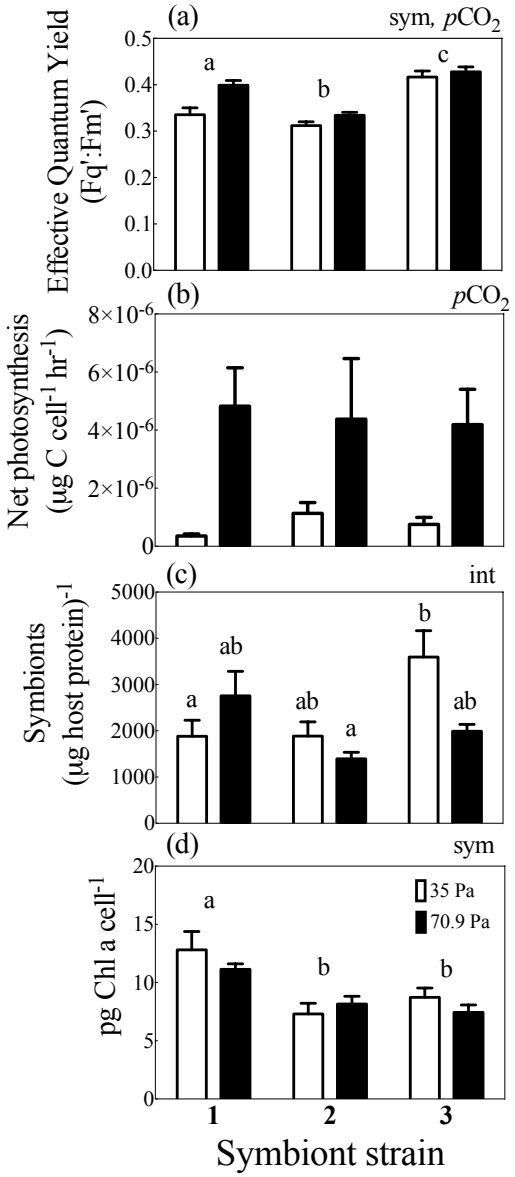

Figure 5.3: Percent of photosynthate translocated to the host **(a),** carbon translocation rate normalized to the host protein **(b),** carbon translocation rate normalized to algal cell number **(c)**, and the number of asexual anemone buds produced month^{-1} **(d)**. Mean ± 1 SE are shown for ambient and elevated pCO_2 (35 Pa = light bars, 70.9 Pa = dark bars). The abbreviations (sym), (pCO_2) and (Int) in the top right of each plot indicate significant differences between symbiont, pCO_2 or interactive effects resulting from a two-way ANOVA (n = 5). Significant differences among strains are denoted by the letters above each treatment group (n = 5 ± SE).

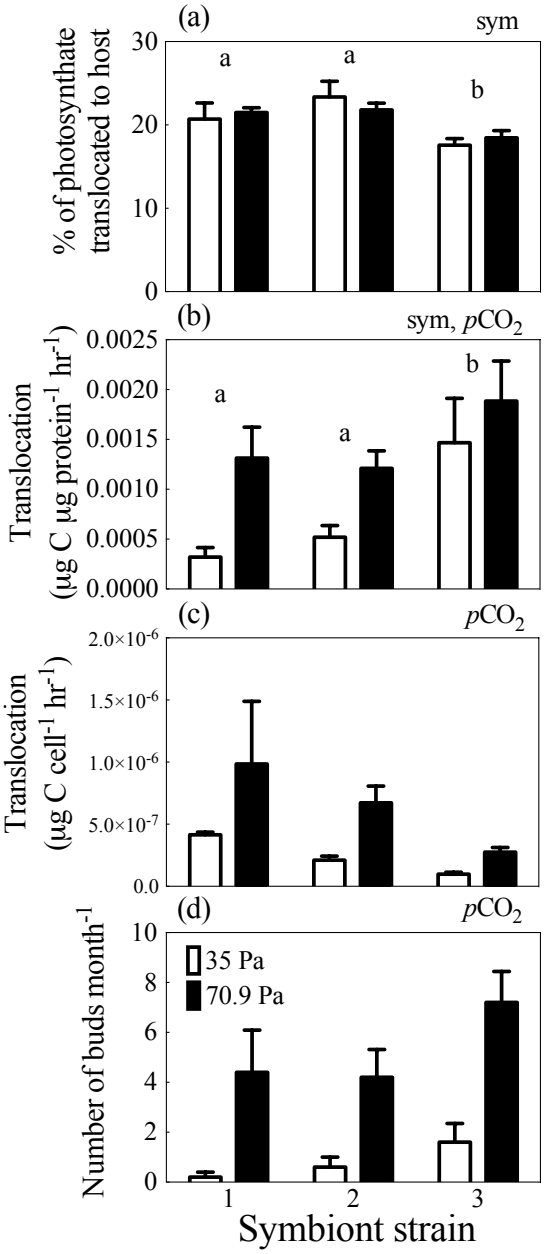

Chapter 6

DIFFERENTIAL THERMAL RESPONSE WITHIN INSHORE VS. OFFSHORE CONGENERIC SCLERACTINIAN SPECIES IN PALAU

6.1 Abstract:

Several reef environments surround the country of Palau, including offshore barrier reefs as well as inshore rock island habitats. The rock island reef habitats of Palau are an ideal location to study climate change effects as corals are exposed to average temperature, nutrient and pCO_2 conditions well above levels experienced offshore. Six coral species *Acropora muricata, Goniastrea aspera, Porities rus, Cyphastrea chalcidicum, Porites cylindrica* and *Pachyseris rugosa*, were collected from these habitats and exposed to high temperature stress (32 Celsius) over 14 days. With the exception of *P. rus* and *P. cylindrica*, which harbored *Symbiodinium C15* at both locations, rock island colonies harbored the thermally tolerant species *D1a* whereas offshore colonies harbored other clade C *Symbiont* types. Significant temperature induced reductions in Fv/Fm and cellular density were greatest for corals collected offshore but were also observed for *A. muricata* and *P. rugosa* corals collected in Nikko bay. For Nikko bay *S. trenchii*, host dependent differences in algal physiology were apparent and likely helped establish the observed differences in thermal response. Differences in physiology across both host species and locations were also observed for *C15* symbionts as temperature induced changes were only observed for symbionts within *P. rus*. However, phylogenetic differences in *C15* genotypes matched species and locational

differences making it difficult to establish whether the observed physiological differences are host or symbiont genotype dependent. For the remaining offshore clade C symbionts, differences in photochemical response to high temperature were also observed as reductions in Fv/Fm for *C40* within *P. rugosa* were likely driven by damage occurring downstream of the PSII reaction center whereas reductions in Fv/Fm for the *C21* symbiont in *G. aspera* were likely in response to changes in connectivity between PSII reaction centers. Overall, prior exposure to warmer temperatures, along with association with more robust symbiont types allowed for rock island coral colonies to exhibit greater thermal tolerance toward high temperature events. However, host dependent differences in symbiont physiology resulted in bleaching within certain coral species despite the presence of thermally tolerant symbionts. Inshore reefs and harbouring thermally tolerant symbiont species may provide temperature refugia to some but not all coral species, and both the host and symbiont need to be taken into account when predicting thermal tolerance.

6.2 Introduction:

The unique rock island habitats found within the inshore waters of Palau are characterized by elevated water temperatures and low pH as compared to the offshore reefs surrounding the island chain (Fabricius et al. 2004; Golbuu et al. 2007b; Woesik et al. 2012). Conditions similar to those found within the rock island habitats are expected for many reef systems world wide under current climate change predictions (IPCC 2013). Therefore, inshore and offshore Palauan reefs make an ideal comparative system for studying climate change effects on coral reefs. Although the overall biological diversity differs across inshore and offshore reef sites (Shamberger et al. 2014; Barkley et al.

2015), many species are found living in both habitats. Habitat specific differences in bleaching response were observed with lower mortality and higher recovery rates within the inshore rock island habitats (Fabricius et al. 2004; Golbuu et al. 2007b; Woesik et al. 2012) following major high temperature events in 1998 and 2010. As current climate change projections suggest a continued increase in seasonal sea surface temperatures and more frequent bleaching events (Hoegh-Guldberg and Bruno 2010; IPCC 2013), characterizing both the environmental and physiological differences across inshore and offshore habitats will be essential to our overall understanding of coral reef resilience.

Previous studies characterizing Palauan reef waters have attributed physical characteristics of the inshore reefs such as higher light attenuation, partial shading and turbid waters as being pivotal in establishing low bleaching susceptibility during high temperature events (Fabricius et al. 2004). High light exposure can exacerbate thermal stress within certain species as excess excitation energy increases susceptibility to thermal damage within the photosynthetic apparatus (Hill et al.; Bhagooli and Hidaka 2004; Fabricius 2006). Similar to low light conditions, which can mitigate thermal stress in some species (Buck et al. 2002; Hoogenboom et al. 2012), the high turbidity and shade available within the rock island habitats may potentially be a powerful advantage during high temperature events, turning the inshore rock islands into bleaching refugia. In addition to the physical properties of the rock island habitat, differences in symbiont populations and previous acclimation to higher water temperatures likely also play a significant role in reducing bleaching susceptibility.

Differences in symbiont species are observed across habitats with greater dominance of the thermally tolerant *S. trenchii* detected within inshore coral colonies

(Fabricius et al. 2004). Similar differences in symbiont species have been documented across environmental gradients for some Pacific coral species and are essential in establishing high and low thermal tolerance within the coral holobiont (Oliver and Palumbi 2011b; Howells et al. 2016). Symbiont shuffling, where an existing background population of symbiotic algae increases in density to become a more dominant population within the host, represents a potential mechanism for establishing these differences in thermal acclimation across colonies. Shuffling from thermally sensitive to thermally tolerant symbiont types during a high temperature event can improve bleaching resistance towards future high temperature events (Grottoli et al. 2014). Conversely, certain coral species are less capable of symbiont shuffling and may be more reliant on differences in host physiology, such as energy reserves and heterotrophy, to establish thermal tolerance vs. sensitivity (Rodrigues and Grottoli 2007; Borell and Bischof 2008; Borell et al. 2008; Grottoli and Rodrigues 2011). The vast amount of genetic variability inherent to both the host and symbiont phenotype is only beginning to be understood and future studies will need to place this within the context of acclimation/adaptive potential to future climate change scenarios.

As mentioned above, *S. trenchii* associates with multiple host species and helps establish a thermally tolerant phenotype (LaJeunesse et al. 2009a; Wham et al. 2011). Specifically, corals hosting *S. trenchii* are less likely to exhibit signs of thermal stress such as loss in symbiont cellular density (Grottoli et al. 2014). However, this is not always the case and cellular loss has been documented for certain corals, despite housing *S. trenchii* (Silverstein et al. 2015). It's possible that differences in host species physiology also influence the symbioses and may alter the thermal response despite

hosting the same *S. trenchii* symbiont species. Thicker host tissue layers can provide extra protection from high light levels to residing symbiont populations (Dimond et al. 2012) and differs across host coral species (Schoepf et al. 2013; Hoadley et al. 2015a). Additionally, differences in the underlying skeletal frame can produce species dependent differences in light scatter, further manipulating internal light fields for residing symbionts (Enriquez et al. 2005; Ulstrup et al. 2006c; Wangpraseurt et al. 2012). Host derived photoprotective pigments may also further change light fields within the colony (Dove 2004; Dove et al. 2006), whereas differences in ROS scavenging mechanisms, along with heat-shock protein expression can further mitigate the thermal response across host species regardless of symbiont type (Fitt et al. 2009). Such potentially major differences within the host environment can influence symbiont physiology along with the alga's response to high temperature stress.

We ran a 14-day high temperature treatment on six congeneric coral species collected from Nikko bay and an offshore reef in order to test if inshore corals displayed a thermal tolerance phenotype without the complication of site specific factors (Shading and rapid light attenuation due to high turbidity within Nikko bay). Overall, Nikko bay corals displayed a greater thermal tolerance than their offshore counterparts and suggest that acclimation to warmer waters and association with thermally tolerant symbiont types likely drives differences observed in bleaching susceptibility across habitats. Site-specific differences in symbiont genotypes provided a total of 13 specific host/symbiont combinations, allowing us to also test for differences in the thermal response across unique host/symbiont combinations as well as host dependent differences in symbiont physiology for *S. trenchii, C15* and *C40* symbionts. Our results display a wide degree of

variability in response to elevated temperature across host/symbiont combinations. At the ecosystem level, Nikko bay corals do appear more thermally tolerant. However, our results show that host dependent differences in symbiont physiology must also be taken into account as bleaching and thermal stress can still occur within some colonies, despite harboring thermally tolerant symbiont types.

6.3 Materials and Methods

6.3.1 Coral Collection:

Offshore corals were collected from Rebotel reef (7°14.93'N, 134°14.149'E) and Inshore corals were collected within Nikko bay (7°32.48'N, 134° 49.34'E). A total of six species were collected for thermal experimentation. Three species were assessed during March of 2014 (*Acropora muricata, Goniastrea aspera* and *Porites rus*). The following March the same experiment was replicated using the coral species *Pachyseris rugosa, Cyphastrea chalcidicum* and *Porites cylindrical*. A total of 8 colonies per species per site were collected between 5-10 meters depth. Colonies of the same species were collected at least 10m apart to ensure genetic variability across all colonies. Colonies were transported back to the Palau International Coral Research Center (PICRC) located on the island of Koror and fragmented into five replicate nubbins then placed into a large (1200L) flow-through aquarium with high water movement. Seawater was collected directly off of the PICRC pier at a depth of 3 m and then passed through a pressurized sand filter and aquarium filter pads prior to use in flow-through and experimental treatment systems. After one day of recovery from fragmentation, Coral nubbins were

attached to 2-inch square PVC tiles using marine epoxy (Splash zone compound A-788). Corals were then allowed to acclimate to ambient conditions for 12-16 days prior to the start of experimentation.

6.3.2 Experimental System:

Each treatment system consisted of between 7 and 12 (56 L) plastic treatment bins connected to a central (~1200 L) sump. Ambient temperature conditions were maintained via a chiller system, whereas titanium heating elements were utilized within the high temperature treatments. Seawater within each sump was conditioned to appropriate temperature conditions prior to being sent to the treatment bins. Treatment bins were setup outdoors, underneath a 60% shade cloth allowing for a peak midday light intensity of 800μmol quanta m^{-2} s^{-1}. For each treatment, three replicate fragments from each colony were placed within separate treatment bins. The temperature was gradually ramped in the heated sump from 27.5°C to 32°C over 4 days, and then maintained at 32°C for an addition 10 days (14 days total). Temperature within the ambient treatment sump was maintained at 27.5°C throughout the full 14 day experiment. Treatment bins and PVC tiles were regularly cleaned to prevent algal fouling throughout the experiment.

At the start of the experiment (time 0), one fragment for each colony and each species was removed from control and treatment tanks and processed for symbiont and biomass metrics (described in detail below). Samples were then collected on days 9 and 14. To remove coral tissue from the skeleton, fragments were held in a plastic container and vigorously airbrushed (100 psi) with filtered (0.22 μm) seawater. The resulting slurry was homogenized with a tissue tearer (Biospec products, Inc), and then centrifuged for 2

minutes (5,000 g) to separate the algal and coral fractions. Pelleted symbionts were resuspended in synthetic seawater and divided into 2mL aliquots. One algal aliquot was preserved with 10 µL of 1% glutaraldehyde for cell enumeration and then stored at 4°C. All other symbiont aliquots were again centrifuged for 2 minutes (5,000 g) and the homogenate poured off prior to storing at -20°C. With the exception of samples containing 1% glutaraldehyde, all samples were shipped back to the United States and then stored at -20°C.

6.3.3 Symbiont Density and Volume:

Cell density and volume was recorded by light and fluorescence microscopy. Four independent replicate counts were performed for each algal sample on a hemocytometer. Samples were photographed using an EVOS digital microscope (4x magnification) and analyzed using the software Image J (NIH) with the Analyze Particles function using methods similar to (Suggett et al. 2015). Colony surface area was determined via the foil method (Marsh 1970) for *G. aspera, P. rugosa,* and *C. chalcidicum* whereas the hot wax method (Stimson and Kinzie 1991) was utilized for the branching coral species *A. muricata, P. rus* and *P. cylindrica*.

6.3.4 Algal Biochemical Composition and Photopigment Concentration:

Algal cells were lysed in 2 mL of filtered seawater in a bead-beater (BioSpec, glass beads) for 2 minutes. A 50 µL subsample of the lysate was utilized to determine protein concentration using the BCA protein method (Thermo Scientific Pierce), with a bovine serum albumin standard (Smith et al. 1985). A 100 µL subsample of the lysate

was utilized for carbohydrate quantification using the sulfuric acid/phenol method and glucose as standard (Dubois et al. 1956). For lipid extraction, a separate pelleted algal aliquot was freeze-dried overnight and then extracted in a chloroform:methanol:sodium chloride mixture (2:1:0.8) (Folch et al. 1957). Lipid quantification was carried out by a sulfo-phospho-vanillin colorimetric assay using corn oil as a standard (Cheng et al. 2011). Absorbance measurements for lipid, carbohydrate and protein assays were made at 540, 485 and 595 nm respectively. For determination of chlorophyll *a*, pelleted symbionts were resuspended in 90% methanol and then homogenized via bead beating for two minutes. Samples were then incubated at -20°C for two hours, and then centrifuged at 2300-g for five minutes. Absorbance of the resulting supernatant was measured at 665, 652 and 750-nm and chlorophyll *a* calculated by published equations (Porra et al. 1989). All absorbance measurements were determined using a FLUOstar Omega plate reader (BMG Labtech, Germany). Protein, lipid, carbohydrate and chlorophyll data were normalized to algal cell number. For each assay, two technical replicates were run per sample.

6.3.5 Symbiont Photophysiology:

Excitation via a single turnover pulse only reduces the primary electron acceptor (Q_A) within the PSII reaction center whereas the longer saturation flash reduces both primary and secondary acceptors within the PSII reaction center and the plastoquinone pool (Suggett et al. 2003). Analysis of the reoxidation rates after both the single and multiturnover flashes allows for a better understanding of what photophysiological properties are responsible for reductions in photochemical yields and Electron Transport

Rates (see table 1 for description of photo-physiological metrics). All photochemical variables ($FvFm^{MT}$, σPSII , τPSII , τPQ , P, NPQ and ETR) were collected with a Fluorescence Induction and Relaxation (FIRe) fluorometer (Satlantic Inc., Halifax) (Gorbunov and Falkowski). Measurements were taken midday on the final day of the experiment, after thirty minutes of dark acclimation. Each measurement consisted of five iterations of a 100-μs single turnover flash followed by a 2000-μs relaxation phase consisting of 1-μs flashes of a light spaced 59-μs apart. This was followed by a 100-*m*s multi-turnover flash and relaxation phase. Each of the five iterations was spaced 5-seconds apart and provided by an external blue (455nm) LED light source (Satlantic Inc, Halifax).

Electron transport rate and Non-photochemical quenching measurements were taken after five minutes incubation under a 500-µmol quanta m^{-2} s^{-1} light source (RG5-cool white CREE LED), and calculated as,

$$ETR^{RCII} = PFD \times F_q'/F_m{}'^{ST} \times \sigma_{PSII} \times 21.683$$

where PFD is the photon flux density, $F_q'/F_m{}'^{ST}$ is the operating efficiency of PSII in the light acclimated state, σ_{PSII} is the functional absorption cross section of PSII in the dark, and 21.683 converts seconds to hours, μmol e^- to mol e^- and $Å^2$ $quanta^{-1}$ to m^2 mol $RCII^{-1}$ (Suggett et al. 2003). NPQ was calculated as,

$$NPQ = (Fm^{MT} - Fm^{MT}{}') / Fm^{MT}{}'$$

Where Fm is the maximum fluorescence under dark acclimated conditions and Fm' is the maximum fluorescence after light acclimation. All photochemical parameters listed above were calculated by fitting each fluorescence transient curve using the *FIREPRO* software (Kolber and Falkowski 1998)

6.3.6 Symbiont Identification:

Symbiont identity was verified through amplification of the internal transcribed spacer 2 region (ITS2) of the ribosomal array, and analysis by previously published protocols for denaturing gradient gel electrophoresis (DGGE) and cycle sequencing (LaJeunesse et al. 2003). A total of 14 microsatellite loci were utilized to determine genetic diversity of our *S. trenchii* population. All microsatellite loci were previously developed for clade D (Pettay and Lajeunesse 2009; Wham et al. 2011) and have also been utilized specifically for *S. trenchii* (Pettay et al. 2015). Samples identified as *C15* were further analyzed by amplifying and then sequencing the non-coding region of the plastid psbA minicircle using previously described primer and protocols (LaJeunesse and Thornhill 2011). Resulting sequences were aligned using ClustalW2 (http://www.ebi.ac.uk/Tools/msa/clustalw2/).

6.3.7 Symbiont Phylogenetic Analyses:

An analysis of molecular variance was preformed for the *S. trenchii* population using the program GenAIEx. Results were also visualized using a Principal Coordinates analysis using the vegan package in R. Phylogenetic reconstructions based on the non-coding region of the psbA gene for *C15* samples were conducted using Maximum parisimony and distance under default setting in PAUP* (Swofford DL).

6.3.8 Statistical Analysis of Symbiont Physiology:

Bleaching response within Nikko bay and Offshore corals was first assessed for separation in algal density and Fv/Fm^{MT} on days 9 and 14 between ambient and heated samples by an ANalyses Of SIMilarities test (ANOSIM) with 9,999 permutations. If significant separation was observed, each variable was compared by Wilcoxon t-test. In order to test for the unique response to elevated temperature within each host/symbiont combination, a total of 14 physiological variables collected on the final day were analyzed. These included Fv/Fm, PSII connectivity, functional absorption cross section, non-photohemical quenching (NPQ), electron transport rate (ETR), PSII electron turnover (tPSII), Plastoquinone electron turnover (tPQ), net photosynthesis, symbiont lipids, symbiont carbohydrates, symbiont protein, symbiont number, symbiont volume and chlorophyll content (mean and standard error for each variable are available for each host symbiont combination in supplementary tables 1-4). ANOSIM analysis across all 14 variables was utilized to test for significant separation across control and high temperature treatments for each host/symbiont combination. If significant separation was observed, a modified differential expression analysis (EdgeR) was utilized to better understand the unique response to high temperature (Robinson et al. 2010; McCarthy et al. 2012). Designed for gene expression data, the EdgeR program models count data using an overdispersed Poisson model to determine which variables are significant across a treatment. We have adapted it for our analysis by first expressing our values as count data. This is achieved by normalizing all samples to the highest value within each variable and then multiplying by 1000. Next, a count matrix was computed and common and tagwise dispersion were estimated and then utilized to calculate pairwise tests for

differential values across control and treatment groups. The resulting p-values were adjusted using a false discover rate correction and only variables with P-values less than 0.05 were included within the final figure. Hierarchical clustering analysis was utilized to create dendrograms across variables and samples.

When the same symbiont type (as identified through the ITS2 region) was found in multiple coral species, ANOSIM and PCA analyses were preformed to compare each host and symbiont combination. Prior to either analysis, variables were standardized to remove potential error from differences in variance across physiological measurements. ANOSIM analysis was preformed across host species and results are provided in table 3. For PCA analysis, only principle components with eigen-values of greater than 1 were retained (Clarke 1993). Significant correlations with each principle component for the 14 variables are provided in supplementary tables 14-16. All statistical analyses were performed using R software with the 'vegan', 'car', 'edgeR', 'gplots' and 'pgirmess' packages installed.

6.4 Results

6.4.1 Overall Bleaching Response:

Although the ANOSIM analysis revealed significant separation between ambient and high temperature treatments on both day 9 (ANOSIM: R = 0.035, P = 0.0417) and day 14 (ANOSIM: R = 0.039, P = 0.0252) for Nikko bay, R-values for both days were less than 0.05 and suggests only minimal change which is unlikely to be biologically relevant (Figure 1, Table 1). In contrast, separation between ambient and elevated

temperature treatments for offshore corals was considerably higher on both day 9 (ANOSIM: R = 0.086, P = 6e-04) and especially on day 14 (ANOSIM: R = 0.299, P = 1e-04) (Figure 1, Table 1). Univariate analyses preformed for offshore corals found a minimal but significant reduction in Fv/Fm^{MT} ($P < 0.001$) for day 9 and significant reductions for cellular density ($P < 0.0001$) and Fv/Fm^{MT} ($P < 0.0001$) on day 14.

6.4.2 Symbiont genotype and population structure:

S. trenchii was the only symbiont identified by DGGE analysis for *A. muricata, G. aspera, C. chalcidicum* and *P. rugosa* collected from Nikko bay. This *S. trenchii* population was further characterized by 14 microsatellite loci to identify specific clonal variants of this species. The resulting principle coordinates analysis indicated a high level of variability across samples, with a potential cluster for *S. trenchii* within the host *C. chalcidicum* (Fig 2a). Analysis of molecular variance also suggested that some variance was attributed to the host coral species (Fig 2 bottom). However, only 9% of the overall variance was attributed to host species and inter individual variance accounting for the remaining 91%. When additional samples collected in 2009 are added to our analysis, they reflect an even greater variance for *S. trenchii* genotypes in *Cyphastrea* than is observed for experimental colonies alone (Appendix D figure 1). For offshore corals, both *A. muricata* and *P. rugosa* harbored *Symbiodinium C40* whereas *G. aspera* harbored *Symbiodinium C21* and *C. chalcidicum* associated with *Symbiodinium C3u.* *Symbiodinium C15* was the dominant symbiont for both *P. cylindrica* and *P. rus* regardless of location (Offshore vs. Nikko Bay). Phylogenetic analysis of the non-coding region of the psbA minicircle for *C15* symbionts revealed 5 separate taxonomic clusters

(Fig 2b). For all host and symbiont combinations, continual specificity was noted throughout the duration of the experiment (day 0, 9 and 14) and between ambient and elevated temperature treatments. However, mixed assemblages of *S. trenchii* and *C40* were observed for 1 colony of offshore *P. rugosa*. A mixed assemblage of *C3u* and *C40* was also found for a single colony of *C. chalcidicum.* These mixed colonies were removed from further analysis.

6.4.3 Day 10 Individual host/symbiont thermal response:

For Nikko bay corals housing *S. trenchii,* the thermal response varied across host/symbiont combinations as significant changes in response to elevated temperature occurred for symbionts within *A. muricata* (ANOSIM: R=0.625, *P*=0.0022), *C. chalcidicum* (ANOSIM: R=0.271, *P*=0.0249) and *P. rugosa* (ANOSIM: R=0.601, *P*=0.0003). No significant separation between ambient and elevated temperature samples was observed for *S. trenchii* in *G. aspera* (ANOSIM: R = 0.149, *P* = 0.0934). For *S. trenchii* in *A. muricata*, symbiont protein and carbohydrate concentration along with net photosynthesis cell^{-1} significantly increased with temperature whereas FvFm, cellular density and volume decreased (Fig 3a, Appendix D table 5). Only chlorophyll a concentrations decreased with elevated temperature for *S. trenchii* in *C. chalcidicum*. In contrast, slight yet significant increases in connectivity, along with the time constant for reoxidation of the plastoquinone pool increased with temperature (Figure 3b, Appendix D table 6). Lastly, NPQ and lipid concentrations increased with temperature for *S. trenchii* within *P. rugosa* whereas ETR, cellular density and Fv/Fm all decreased (Figure 3c, Appendix D table 7).

ANOSIM analyses performed on clade C symbionts within the offshore coral species found significant separation between the ambient and elevated temperature treatments within all four host/symbiont combinations (Figure 4, bottom right). For *S. C40* within *A. muricata,* ETR, cellular density and FvFm decreased with rising temperature whereas carbohydrate content increased (Fig. 4a, Supplemental table 8). Cellular density, FvFm, ETR and cellular density decreased with temperature for *C40* symbionts within *P. rugosa.* However, cellular volume along with τPQ increased with rising temperature (Fig. 4d, Appendix D table 11). For *C3u* symbionts within offshore *C. chalcidicum*, high temperature induced significant increases in protein, carbohydrate and lipid contents. In contrast, significant reductions are observed for cellular density, FvFm and ETR (Fig. 4c, Appendix D table 10). Similarly, cellular density, ETR and FvFm also decreased with temperature for *C21* symbionts in the offshore coral *G. aspera.* We again see a high temperature induced an increase in lipid and protein content, along with greater connectivity across PSII reaction centers (Fig. 4b, Appendix D table 9).

Overall physiological stability in response to elevated temperature was greatest for our *S. C15* symbionts in *P. cylindrica* as no significant separation was observed for inshore or offshore host/symbiont combinations. Only *S. C15* within *P. rus* showed any significant physiological separation between ambient and elevated temperature treatments, both for Nikko bay (ANOSIM: R=0.328, *P*=0.0025) and Offshore (ANOSIM: R=0.341, *P*=0.0101) corals (Fig 5a-b). For *C15* symbionts within offshore *P. rus*, Fv/Fm, cellular density and the time constant for reoxidation of the plastoquinone pool all decreased with rising temperature. In contrast, cellular volume along with τPSII both significantly increased with temperature for offshore *C15* in *P. rus* (Fig 5a, Supplemental

table 12). For Nikko bay *C15* symbionts in *P. rus,* cellular volume and carbohydrates both increased with temperature whereas reductions in the time constant for reoxidation of the plastoquinole pool were observed (Fig 5b, Appendix D table 13).

6.4.4 Host dependent differences in symbiont physiology:

Differences in symbiont physiology are observed within all three symbiont types found across multiple host species. For *S. trenchii* the top four principle components within our analysis had eigen-values greater than 1. PC1 (eigenvalue = 2.283), PC2 (eigenvalue = 1.49), PC3 (eigenvalue = 1.35) and PC4 (eigenvalue = 1.07) explained 37.1%, 15.9%, 13.1% and 8.2% of the variance respectively (Appendix D table 14). Focusing on just the largest two principle components (Fig. 6a), variables with their highest loadings on PC1 included the functional cross section of PSII, cellular density and τPQ, which correlated positively with PC1 whereas protein, lipids, Net photosynthesis, and connectivity correlated negatively. Electron transport rates and FvFm correlated positively with and had their highest loadings on PC2. The highest loading for NPQ was also on PC2 and correlated negatively with the axis.

ANOSIM analysis incorporating all 14 symbiont specific physiological variables across all hosts harboring *S. trenchii* revealed strong separation across most species (Table 3, Fig. 6a). Although significant, only minimal separation between *S. trenchii* physiology within *P. rugosa* and *C. chalcidicum* was observed as the R-value fell below 0.2 (ANOSIM: R=0.177, *P*=0.003). However, all other host comparisons across *S. trenchii* were significant and with R values above 0.4 (Table 3).

For *C15* symbionts, the top four principle components also had eigen-values greater than 1. PC1 (eigenvalue = 2.28), PC2 (eigenvalue = 1.56), PC3 (eigenvalue = 1.41) and PC4 (eigenvalue = 1.09) explained 37.2%, 17.4%, 14.1% and 8.6% of the variance respectively (Appendix D table 15). For two largest principle components (PC1 and PC2), the highest loadings for cellular density, Fv/Fm and NPQ correlated positively with PC1 whereas Chla and Net photosynthesis were negatively correlated. Variables with their highest loadings on PC2 were all negatively correlated and include protein, carbohydrate, lipids and the functional absorption cross-section of PSII (Fig. 6b). Physiological separation was greatest across host species, (ANOSIM: $R > 0.8$, $P < 0.0003$) (Table 3). Significant separation was also observed between inshore and offshore *C15* symbionts in *P. rus,* however the R-value was less than 2.5 and therefore not considered to be biologically relevant. For *C15* symbionts in *P. cylindrica,* differences in symbiont physiology were significant between Nikko bay and both offshore variants (ANOSIM: $R < 0.28$, $P < 0.0002$).

Physiological differences are also observed for *S. C40* within the offshore coral species, *A. muricata* and *P. rugosa* (ANOSIM: R=0.677, *P*=1e-04) (Table 3). From our *S. C40* analysis, only three principle components had eigen-values greater than 1 as PC1 (eigenvalue = 2.35), PC2 (eigenvalue = 1.94) and PC3 (eigenvalue = 1.27) explained 39.5%, 26.9% and 11.5% of the variance respectively (Appendix D table 16). Symbiont carbohydrate and lipid content, along with chla, net photosynthesis, and the functional absorption cross section all correlated positively with PC1 where as cellular density, τPSII and NPQ correlated negatively with it. Variables with their highest loadings on

PC2 included cellular volume and τPQ which both correlated negatively whereas both ETR and FvFm correlated positively with PC2 (Fig 6c).

6.5 Discussion:

At the habitat level, our results show greater resilience to high temperature induced bleaching for corals from Nikko bay as compared to their Offshore counterparts (Fig 1). This is consistent with previous field observations documenting habitat dependent differences in coral bleaching susceptibility and recovery across the Palauan coral reef system following high temperature bleaching events in 1998 and 2010 (Golbuu et al. 2007a; Woesik et al. 2012). Differences in symbiont associations, along with prolonged exposure to higher temperature for Nikko bay corals are thought to play an important role in bleaching resistance and recovery for inshore reefs (Fabricius et al. 2004). Additionally, the relatively high turbidity, and partial shading within Nikko bay may also benefit corals during high temperature events by attenuating the light field (Woesik et al. 2012). However, light fields were consistent for all corals within our experimental heating design, suggesting that differences in symbiotic associations and/or previous high temperature acclimatization likely play a greater role in the high thermal tolerance of Nikko bay corals than reduced photon dose.

There are several examples of thermal tolerance in corals with a history of exposure to high temperature has been previously documented within other reef systems (Oliver and Palumbi 2011a; Grottoli et al. 2014; Howells et al. 2016). Coral species collected from highly variable reef pools on Ofu island displayed greater thermal resistance than conspecifics collected nearby from moderately variable pools (Oliver and

Palumbi 2011a). Similarly, colonies of *Platygra daedalea* living in warm waters in the Persian Gulf are able to maintain photosynthetic efficiency and ROS scavenging activity during a high temperature event than their counterparts collected from cooler waters in the Sea of Oman (Howells et al. 2016). For both studies, differences in symbiont type were noted across conspecific corals and likely played a critical role in establishing heat sensitive vs. tolerant phenotypes. Changes in the dominant symbiont type after an initial experimental bleaching in some Caribbean coral species allowed for greater thermal tolerance during a second experimental heating the following year (Grottoli et al. 2014). Similarly, differences in symbiont species play an important role in the contrasted bleaching response between inshore and offshore corals in this study (Figure 1). *A. muricata, G. aspera, C. chalcidicum* and *P. rugosa* coral colonies collected offshore harbored various clade C symbionts, while the host generalist symbiont *S. trenchii* dominated these four coral species in Nikko bay. For Nikko bay corals, symbiont physiology differed across host species and illustrates the large host influence and physiological plasticity inherent to the *S. trenchii* symbiont strain.

As determined through ITS2-DGGE methods, *S. trenchi* sampled from corals throughout the globe are phylogenetically indistinguishable (LaJeunesse et al. 2014). However, markers with greater taxonomic resolution (e.g. microsatellite loci) reveal high rates of interindividual genotypic diversity across the Pacific (Pettay et al. 2015). Analysis of *S. trenchii* within our four generalist coral species is consistent with previous studies showing high rates of unique *S. trenchii* genotypes within Nikko bay and suggests a high rate of sexual recombination for the species (Pettay et al. 2015). Although some *S. trenchii* genotypic structure is evident across host species as symbionts within *C.*

chalcidicum cluster separately than the rest (Fig. 2), less than 10% of the overall variance can be attributed to host level differences and analyses of inshore corals from more locations surrounding Palau indicate high homogeneity of *S. trenchi* genotypes across these coral taxa (Suppl. Fig 1). This suggests a rather ubiquitous population within Nikko bay, with little evidence to support host influence on the genetic variation of *S. trenchii* genotypes. In contrast, physiological differences in *S. trenchii* are apparent across coral hosts, indicating a strong host influence on symbiont response. Differences in host tissue thickness and pigmentation, along with skeletal structure are known to substantially influence the internal light fields of endosymbiotic alga (Dimond et al. 2012; Wangpraseurt et al. 2012). This may potentially allow for high and low light algal phenotypes dependent on the physiology of the host in which they reside.

Despite hosting the thermally tolerant *S. trenchii,* algal loss was still observed for *A. muricata* and *P. rugosa* from Nikko bay. At least one other study has documented the loss of *S. trenchii* due to elevated temperature(Silverstein et al. 2015). However, reductions in cellular density and Fv/Fm^{MT} for the *S. trenchii* living within *P. rugosa*, were accompanied by reductions in ETR along with an increase in NPQ and are typical of the bleaching phenotype observed in many thermally sensitive coral species (Warner et al. 1996; Fitt et al. 2001; Hennige et al. 2011). In contrast, reductions in bleaching and Fv/Fm^{MT} were less pronounced for *S. trenchii* in *A. muricata* and were accompanied by increases in protein, carbohydrates and net photosynthesis $cell^{-1}$, along with a reduction in cellular volume. Similar temperature induced increases in symbiont protein and carbohydrates were also observed for *S. trenchii* in *Turbinaria reniformis* and the *C15* symbiont in *Montipora monastreata* (Hoadley et al. 2015a) and may be more indicative

of thermal acclimation than thermal stress. This is further supported by the significant increase in net photosynthesis cell^{-1} that accompanied the reduction in algal number within *A. muricata*. This paradoxical rise in photosynthesis with a loss in total symbionts may be driven by an alleviation of carbon limitation while *in hospite* (Hoadley et al. 2016). Greater DIC availability, along with the relatively small reduction in FvFm, suggests that *S. trenchii* within *A. muricata* were not subjected to the same degree of thermal damage as symbionts within *P. rugosa*. Although small changes in PSII reaction center connectivity, reoxidation rates (τPQ) and chlorophyll a concentration were evident in *S. trenchii* within *G. aspera,* there was no significant loss in algal number for this coral. Similarly, there was no change in *S. trenchii* physiology within *C. chalcidicum.* In summary, this study provides four distinct physiological responses to elevated temperature within a single symbiont population of *S. trenchii.* Because the *S. trenchii* genotypes observed in *C. chalcidicum* cluster separately from the other genotypes, it is possible that the greater thermal stability observed may be at least partially driven by genotypic differences in the alga. However, physiological differences in thermal response are still present within the other three species and are likely driven by host dependent factors.

For *A. muricata, P. rugosa, G. aspera* and *C. chalcidicum* collected offshore, elevated temperature led to significant reductions in Fv/Fm, ETR, and cellular density for their respective clade C symbionts. These reductions are indicative of the classic bleaching phenotype (Warner et al. 1996; Fitt et al. 2001; Weis 2008; Hennige et al. 2011). However, for *C21* (in *G. aspera*) and *C40* (in *P. rugosa*) symbionts, loss in Fv/Fm and ETR appear to be rooted in differences in their photochemical response. The primary

site of photodamage varies across different *Symbiodinium* (Buxton et al. 2012), with thermal damage occurring at or near the PSII reaction center for some (Warner et al. 1999; Hill et al. 2004, 2011) and downstream of the plastoquinone pool for others (Buxton et al. 2012; Roberty et al. 2014). Significant declines in plastoquinone pool reoxidation rates (as indicated through an increase in τPQ) suggest that changes in the photosynthetic electron transport chain beyond the PSII reaction center are likely responsible for the reduction in maximum quantum yield and electron transport rates observed for *Symbiodinium C40* within *P. rugosa*. Significant changes in τPQ were not observed for *Symbiodinium C21* in *G. aspera.* However, high temperature stress increased connectivity between PSII reaction centers and likely dissipated excess excitation energy. The reduction in excess excitation energy during high temperature stress may have alleviated partial pressure over the PSII reaction center, thereby reducing the potential for further downstream degradation for *C21* symbionts. Interestingly, changes in τPQ were also not observed for the *C40* symbionts in *A. muricata.* As visualized through the PCA plot, slower electron transport rates through the PSII reaction cycle (i.e. τPSII), along with higher levels of NPQ were observed for *C40* symbionts in *P. rugosa*, whereas lipid and carbohydrate concentrations tended to be higher for *C40* symbionts within *A. muricata.* Although bleaching was noted in both corals harboring *C40* symbionts, the differences in photochemistry, along with greater reserves of lipid and carbohydrates in the *C40* symbionts in *A. muricata* likely influenced the observed photophysiological differences in response to increased temperature.

Only *C15* symbionts were found both inshore and offshore for the corals *P. cylindrica* and *P. rus*. *Symbiodinium C15* is also considered thermally tolerant as only

minimal changes in photophysiology are observed for C15 in *Montipora hirsuta* in response to elevated temperature (Hoadley et al. 2016). However, unlike *S. trenchii,* the *C15* symbionts are considered host specialists and typically associate with just one coral species (LaJeunesse et al. 2003). Phylogenetic differences based on analysis of the non-coding region of the psbA minicircle place the C15 assemblage into 5 distinct clusters. Interestingly, differences in C15 physiology across *P. rus* and *P. cylindrica* corals are driven by a different set of variables than those responsible for the differences observed for *C15* symbionts within *P. cylindrica*. Cellular density, Fv/Fm and NPQ all tended to be higher for algae within *P. cylindrica* whereas net photosynthesis and chlorophyll *a* concentration were higher for symbionts in *P. rus.* Large physiological differences were also observed across the three distinct *C15* genotypes found within *P. cylindrica.* However, differences here are driven by greater cellular protein, carbohydrate and lipid concentrations within offshore symbionts as compared to those found in Nikko bay. Despite the major physiological differences for *C15* symbionts within *P. cylindrica,* there was no significant response to high temperature. Both *C15* genotypes in *P. rus* did respond to elevated temperatures, however, which resulted in a decline in Fv/Fm as well as algal density in offshore colonies. Because of the observed phylogenetic differences in *C15,* it is unclear if the differences in thermal response noted here were a result of host-based or algal-based heat tolerance.

Surprisingly, major changes in the reoxidation rate of PSII (τ_{QA}) were not observed, indicating that degradation to the PSII reaction center is not a significant contributor to reduced photosynthetic efficiency for any of the symbiont types in this study. This differs from other bleaching studies where degradation of the D1 protein

within the PSII reaction center is thought to be the primary site of thermal degradation (Warner et al. 1999; Hill et al. 2004, 2011). It is possible that our thermal treatment was not sufficient to induce D1 degradation within our thermally sensitive symbiont types and a longer incubation time, or higher temperature would have induced greater damage. Alternatively, high temperature increases in D1 degradation may have still occurred within the symbionts, however protein turnover and repair rates were sufficient to maintain stable reoxidation rates (Ragni et al. 2010). Nevertheless, symbiont cellular loss was still noted across most offshore coral species, along with inshore *A. muricata* and *P. rugosa*. Although high temperature induced damage to the D1 protein within the PSII reaction center and subsequent increases in ROS production by the symbiont do play an important role in inducing coral bleaching within certain species (Lesser 2006; Weis 2008; Lesser 2011), our data clearly show that other pathways can also lead to coral bleaching and photoreduction.

For open ocean phytoplankton, increases in cellular volume are typically associated with a stronger package effect, as greater chlorophyll *a* concentrations within larger cells increase shading and thereby attenuate the light intensity within the cell (Thompson et al. 1991; Key et al. 2010). However, the correlation between package effect and cellular volume assumes a similar density of chlorophyll within the cell. Changes in chlorophyll density could also affect light attenuation as reductions in chlorophyll concentration cell^{-1} could reduce shading and increase light absorption per unit of remaining chlorophyll a. For *S. trenchii* within *A. muricata,* no change in chlorophyll a cell^{-1} was detected. However a reduction in cellular volume with high temperature did occur and may have attenuated the overall light intensity by increasing

the overall package effect relative to ambient temperature conditions. This strategy could prove extremely important during high temperature stress by reducing the effective light field and therefore the potential for photo-stress. In contrast, the increase in cellular volume and no change in chlorophyll a cell^{-1} observed for *C40* in *P. rugosa* and both *C15* variants in *P. rus* would have decreased the overall package effect (relative to ambient conditions), thereby enhancing light intensity within the cell. Increased cellular volume after exposure to high temperature has been observed within other symbionts, including *S. trenchii* within *T. reniformis* (Hoadley et al. 2015a, 2016). Lowered cellular density increases light scattering and coral skeletal reflectance, thereby increasing the internal light field for remaining symbionts (Enriquez et al. 2005; Wangpraseurt et al. 2012). The combined impact of a lower package effect due to increased cellular volume, along with greater light scattering due to algal loss can markedly alter internal light fields, exposing thermally stressed chloroplasts to greater amounts of excess excitation energy. It is therefore difficult to fully understand what role increased cellular volume plays in the high temperature/light stress mitigation and future studies are needed to investigate this response.

Overall, corals collected from Nikko bay were more resilient to high temperature stress as fewer reductions in cellular density and photochemical efficiency were observed. Importantly, these differences were noted despite the advantage of site-specific parameters such as increased shading and high light attenuation within Nikko bay as opposed to Offshore. Similar to previous studies, phenotypic differences in symbiont types observed for Offshore vs. Inshore corals are likely a major component of the thermal tolerance phenotype within Nikko bay. However, host dependent differences in

symbiont physiology suggest that the host coral species must also be taken into consideration when predicting bleaching susceptibility as reductions in cellular density are still observed within some coral species despite hosting the thermally tolerant symbiont type *S. trenchii*. Similarly, host dependent differences may also influence thermal tolerance for *C15* as only symbionts within the coral *P. rus* displayed any change in response to elevated temperature. However, the phyletic distances between types within this group of *C15* symbionts complicate the story, as it is unclear if thermal tolerance is dictated by the host or symbiont genotype. With respect to the symbiont response to high temperature, reductions in the rate of reoxidation of the Q_a site did not accompany reductions in Fv/Fm for any symbiont type within the study. Rather, changes further downstream, appear to drive the observed changes in Fv/Fm and/or ETR. Nevertheless, reductions in cellular density are still observed, suggesting that multiple cellular pathways may lead to bleaching after exposure to elevated temperatures. Additionally, high temperature induced changes in cellular volume, along with increases in symbiont protein, carbohydrate and/or lipid content are observed within both thermally sensitive and tolerant symbiont types. Changes in cellular volume with little change in chlorophyll a can influence the incident irradiance experienced by the cell. Differences in the light field can alter the overall physiological response to elevated temperature, making differences in cellular volume highly influential to the overall thermal response. These potentially important, albeit variable thermal acclimation strategies are as of now poorly understood and further studies are needed. Inshore reef habitats such as Nikko bay may be considered bleaching refugia for Palauan coral reefs due to the dominance of thermally tolerant symbiont types and acclimation to higher seasonal water temperatures.

However, host dependent differences in symbiont physiology indicate that such refugia may be more species specific and not all species currently found within their waters will withstand end of century climate predictions for temperature rise.

Table 6.1: Table of terms, definitions and units.

Term	Definition	Units
Fv/Fm	Dark acclimated maximum quantum yield of PSII (multiturnover)	
σPSII	Dark acclimated effective absorption cross section of PSII	$Å^2 q^{-1}$
τPSII	Rate constant for reoxidation of the Q^a site of the D1 protein within the PSII RC	μ-seconds
τPQ	Rate constant for reoxidation of the plastoquinole pool.	μ-seconds
ETR	RCII-specific electron transport rate	mol e^- mol $RCII^{-1} h^{-1}$
NPQ	Non-photochemical quenching	
Photosynthesis	Net photosynthesis	$cell^{-1}$
P	Connectivity between PSII reaction centers	
Carbohydrates	Carbohydrate concentration $cell^{-1}$	μg carbohydrate $cell^{-1}$
Protein	Protein concentration $cell^{-1}$	μg protein $cell^{-1}$
Lipids	Lipid concentration $cell^{-1}$	μg lipids $cell^{-1}$
Chlorophyll	Chlorophyll concentration $cell^{-1}$	pg chlorophyll a $cell^{-1}$
Cell Volume	Symbiont cellular volume	$μm^{-3}$
Cell Density	Symbiont cellular density	Cells cm^{-2}

Table 6.2: Overall bleaching response per habitat. ANalysis Of SIMilarity (ANOSIM with 9,999 permutations), for day 9 and day 14 for Offshore and Nikko bay corals. Wilcox test for each variable follow multivariate analysis with R > 0.05.

Location	Source of variation	Time	ANOSIM		Univariate Wilcox Test (P-value)	
			R	*P* value	Density	FvFm
Offshore	Temperature	Day 9	**0.086**	**6e-04**	0.2769	**7.8e-10**
	Temperature	**Day 14**	**0.299**	**1e-04**	**8.7e-06**	**1.1e-14**
Nikko Bay	Temperature	Day 9	0.035	0.0417		
	Temperature	Day 14	0.039	0.0252		

Table 6.3: Comparison of symbiont physiology across hosts. ANalysis Of SIMilarity (ANOSIM with 9,999 permutations), for day 14. Comparison of symbiont physiology within hosts found to contain the same symbiont type. OP_r = Offshore *Porites rus*. NP_r = Nikko bay *Porites rus,* OP_{c1} = Offshore *Porites cylindrica type1,* OP_{c2} = Offshore *Porites cylindrica type2,* NP_c = Nikko bay *Porites cylindrica.*

	Source of variation	Host Coral	R	*p* value
S. trenchii	Host species	*A. muricata – G. aspera*	0.425	1e-04
		A. muricata – C. chalcidicum	0.737	1e-04
		A. muricata – P. rugosa	0.785	1e-04
		G. aspera – C. chalcidicum	0.825	1e-04
		G. aspera – P. rugosa	0.856	1e-04
		C. chalcidicum – P. rugosa	0.177	0.003
S. C40	Host species	*A. muricata – P. rugosa*	0.677	1e-04
S. C15	Host			
	OPr vs. *NPr*	$C15_{OPr} – C15_{NPr}$	0.245	1e-04
	OPr vs. *NPc*	$C15_{OPr} – C15_{NPc}$	0.934	1e-04
	OPr vs. *OPc1*	$C15_{OPr} – C15_{OPc1}$	0.900	1e-04
	OPr vs. *OPc2*	$C15_{OPr} – C15_{OPc2}$	0.863	2e-04
	NPr vs. *NPc*	$C15_{NPr} – C15_{NPc}$	0.970	1e-04
	NPr vs. *OPc1*	$C15_{NPr} – C15_{OPc1}$	0.953	1e-04
	NPr vs. *OPc2*	$C15_{NPr} – C15_{OPc2}$	0.952	2e-04
	NPc vs. OPc1	$C15_{NPc} – C15_{OPc1}$	0.287	0.005
	NPc vs. OPc2	$C15_{NPc} – C15_{OPc2}$	0.449	2e-04
	OPc1 vs. OPc2	$C15_{OPc1} – C15_{OPc2}$	0.234	0.030

Figure 6.1: Temporal response to elevated temperature. 2-dimensional plots of cellular density ($1x10^6$ cells cm^{-2}) and maximum quantum yield of PSII (Fv/Fm) throughout the 14-day experiment. **Top:** initial time point for Nikko bay (a) and offshore (b) corals. **Middle:** day nine of the experiment (four days of ramping followed by 5 days at 32°C) for Nikko bay (c) and Offshore (d) corals. **Bottom:** final day of the experiment (four days of ramping followed by ten days at 32°C) for Nikko bay (e) and Offshore (f) corals. Black circles are (28°C) and red circles indicate (32°C).

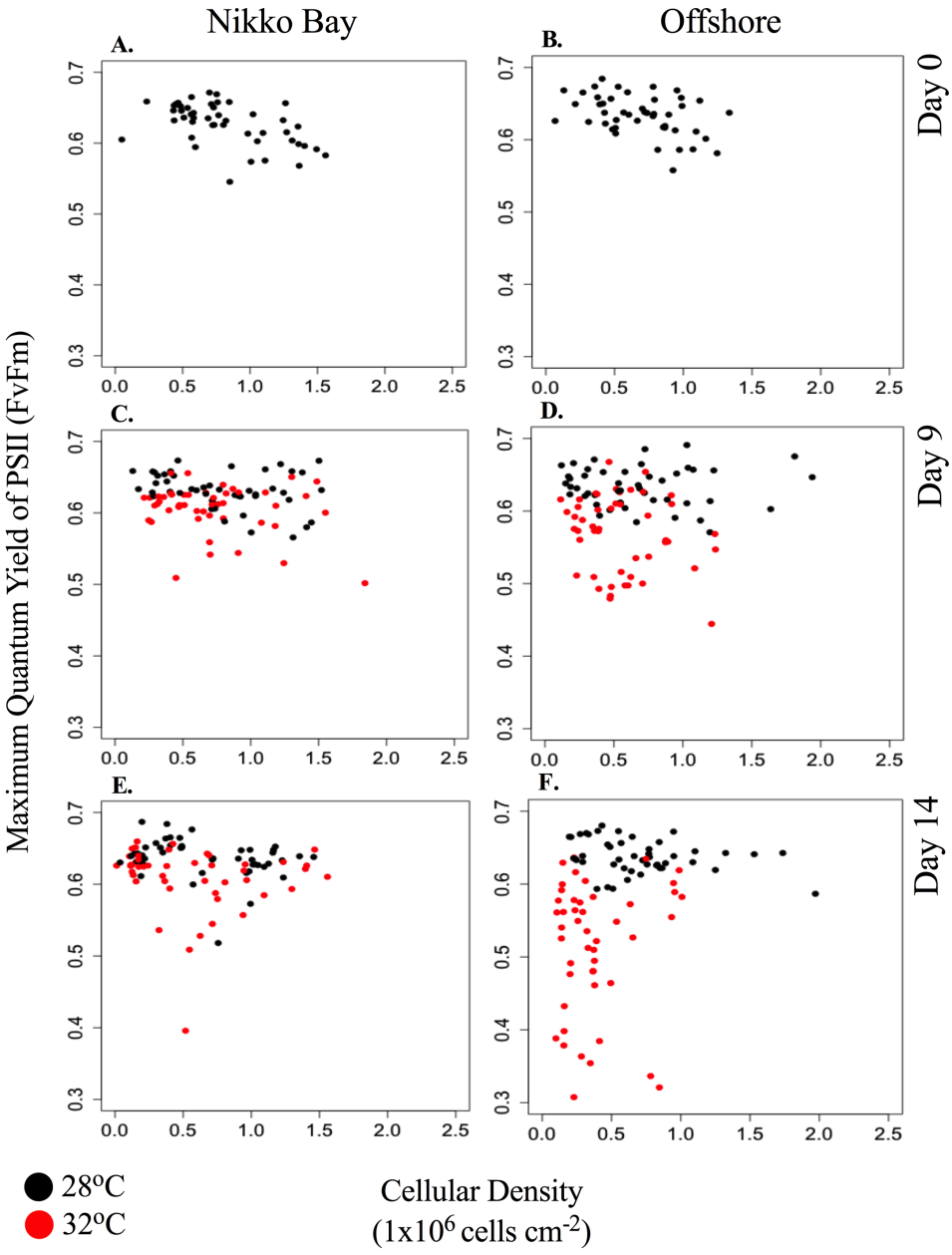

Figure 6.2: Genotypic analysis for *S. trenchii* and *C15* symbionts. The **left** panel (**A)** is a principle coordinates plot utilizing 14 microsatellite markers to visualize variance across *S. trenchii* symbionts for all four coral species in Nikko bay. The **bottom left** panel reflects the AMOVA results for variance across *S. trenchii* samples. The tree on the **Right (B)** reflects a consensus of 1000 bootstrap replicates using the Maximum parsimony and distance method based on analysis of the psbA minicircle. The map on the top right reflects the site across Palau where *Porites sp.* colonies were collected.

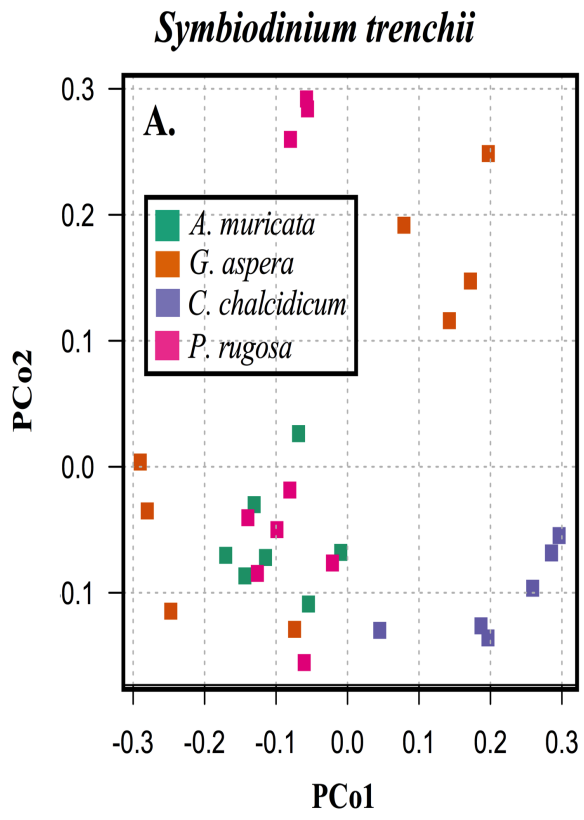

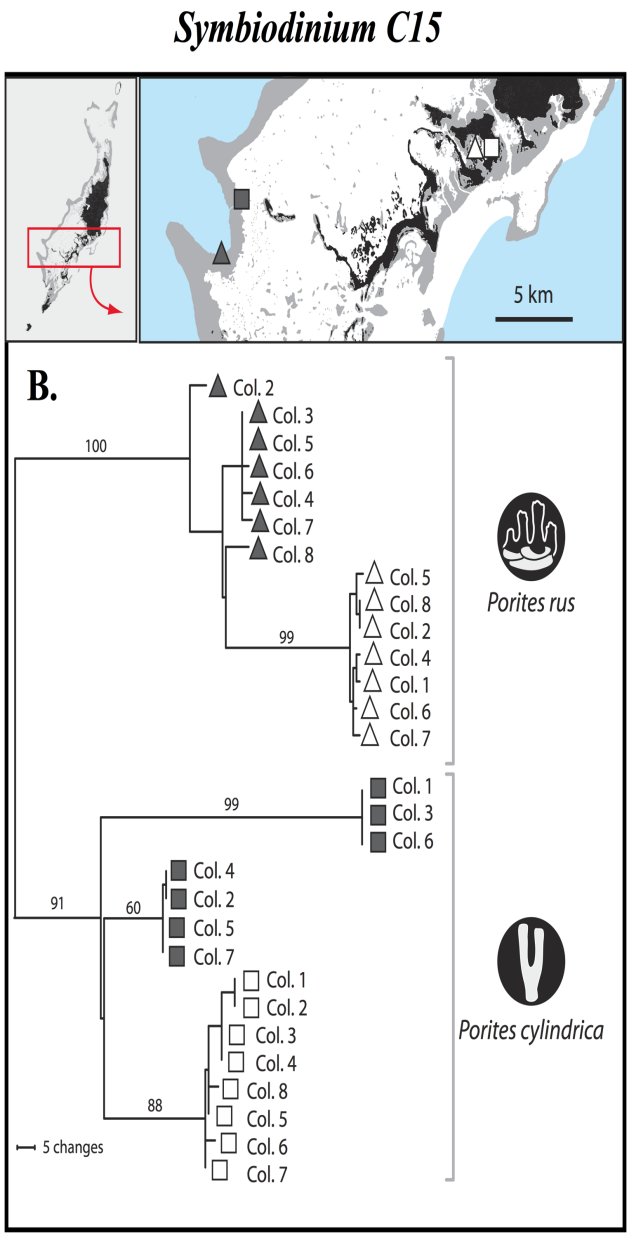

AMOVA Summary

Source	df	SS	MS	Est. Var.	%
Among Hosts	3	366	122	6.3	9%
Among Indiv	26	730	28.1	0.0	0%
Within Indiv	30	1844	61.4	61.5	91%
Total	59	2940		67.7	100%

Figure 6.3: Differential analysis for *S. trenchii* symbioses in Nikko Bay. **(Bottom right)** are results as detected through ANOSIM analysis of all 14 variables. Heat maps were only generated for symbioses found to have significant separation between ambient (28°C) and elevated (32°C) temperature treatments. (**A.**) *S. trenchii* in *A. muricata*, (**B.**) *S. trenchii* in *C. chalcidicum* and (**C.**) *S. trenchii* in *P. rugosa*. Each heat map only contains physiological variables that were significantly differentiated between ambient and elevated temperature treatments. Dendrograms depict resulting hierarchical clustering analysis based on variable values. Individual sample ID numbers and treatment groups (C = 28°C, T = 32°C) can be found directly below each heat-map and is accompanied by a color-coded bar **(black** = 28°C, **red** = 32°C**).** The color key reflects the value for each sample variable after a scaling normalization has been applied. Scaling for each variable consists of dividing each sample by the highest value within the variable and then multiplying by 1000.

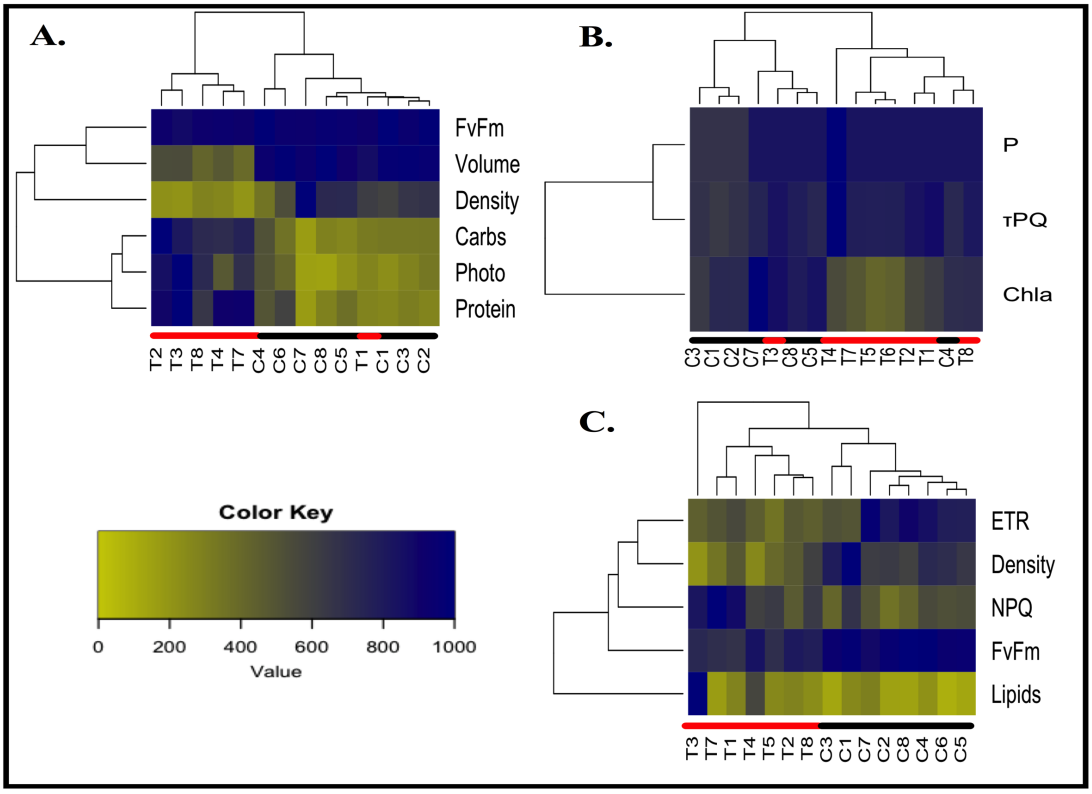

ANOSIM

Fig. Panel		R	P-val
A.	*A. muricata*	**0.625**	**0.0022**
B.	*C. chalcidicum*	**0.271**	**0.0249**
C.	*P. rugosa*	**0.601**	**3e-04**
	G. aspera	0.149	0.0934

Symbiodinium trenchii

Figure 6.4: Differential analysis for Offshore Clade C symbioses. **(Bottom right)** are results as detected through ANOSIM analysis of all 14 variables. Heat maps were only generated for symbioses found to have significant separation between ambient (28°C) and elevated (32°C) temperature treatments. **(A.)** *C40* in *A. muricata*, **(B.)** *C21* in *G. aspera*, **(C.)** *C3u* in *C. chalcidicum* and **(D.)** *C40* in *P. rugosa.* Each heat-map only contains physiological variables that were significantly differentiated between ambient and elevated temperature treatments. Dendrograms depict resulting hierarchical clustering analysis based on variable values. Individual sample ID numbers and treatment groups (C = 28°C, T = 32°C) can be found directly below each heat-map and is accompanied by a color-coded bar **(black** = 28°C, **red** = 32°C**).** The color key (**Bottom left**) reflects the value for each sample variable after a scaling normalization has been applied. Scaling for each variable consists of dividing each sample by the highest value within the variable and then multiplying by 1000. A and D are boxed to reflect a similar symbiont type within each host species.

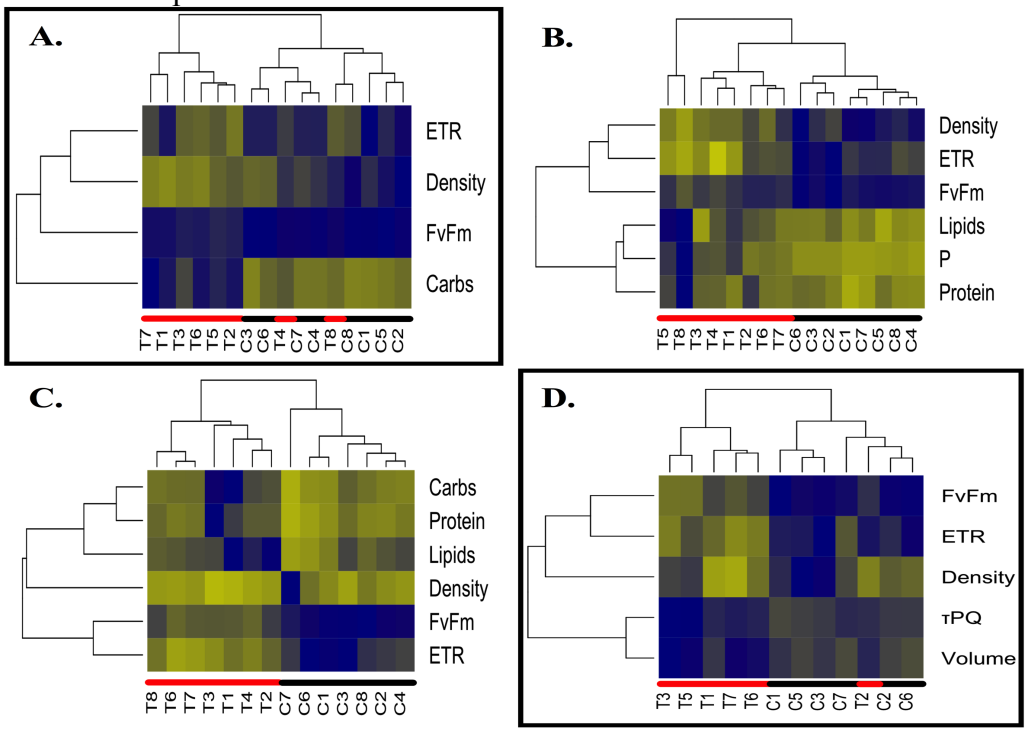

Fig. Panel		R	P-val
ANOSIM	**A.** *A. muricata* (*C40*)	**0.596**	**7e-04**
	D. *P. rugosa* (*C40*)	**0.517**	**0.003**
	B. *G. aspera* (*C21*)	**0.699**	**2e-04**
	C. *C. chalcidicum* (*C3u*)	**0.716**	**6e-04**

Figure 6.5: Differential analysis for *C15* symbionts. **(Bottom)** are results as detected through ANOSIM analysis of all 14 variables. Heat maps were only generated for symbioses found to have significant separation between ambient (28°C) and elevated (32°C) temperature treatments. **(A.)** $C15_{OPr}$ in Offshore *P. rus* and **(B.)** $C15_{NPr}$ in Nikko bay *P. rus*. Each heat map only contains physiological variables that were significantly differentiated between ambient and elevated temperature treatments. Dendrograms depict resulting hierarchical clustering analysis based on variable values. Individual sample ID numbers and treatment groups (C = 28°C, T = 32°C) can be found directly below each heat-map and is accompanied by a color-coded bar **(black** = 28°C, **red** = 32°C**).** The color key (**Bottom left**) reflects the value for each sample variable after a scaling normalization has been applied. Scaling for each variable consists of dividing each sample by the highest value within the variable and then multiplying by 1000.

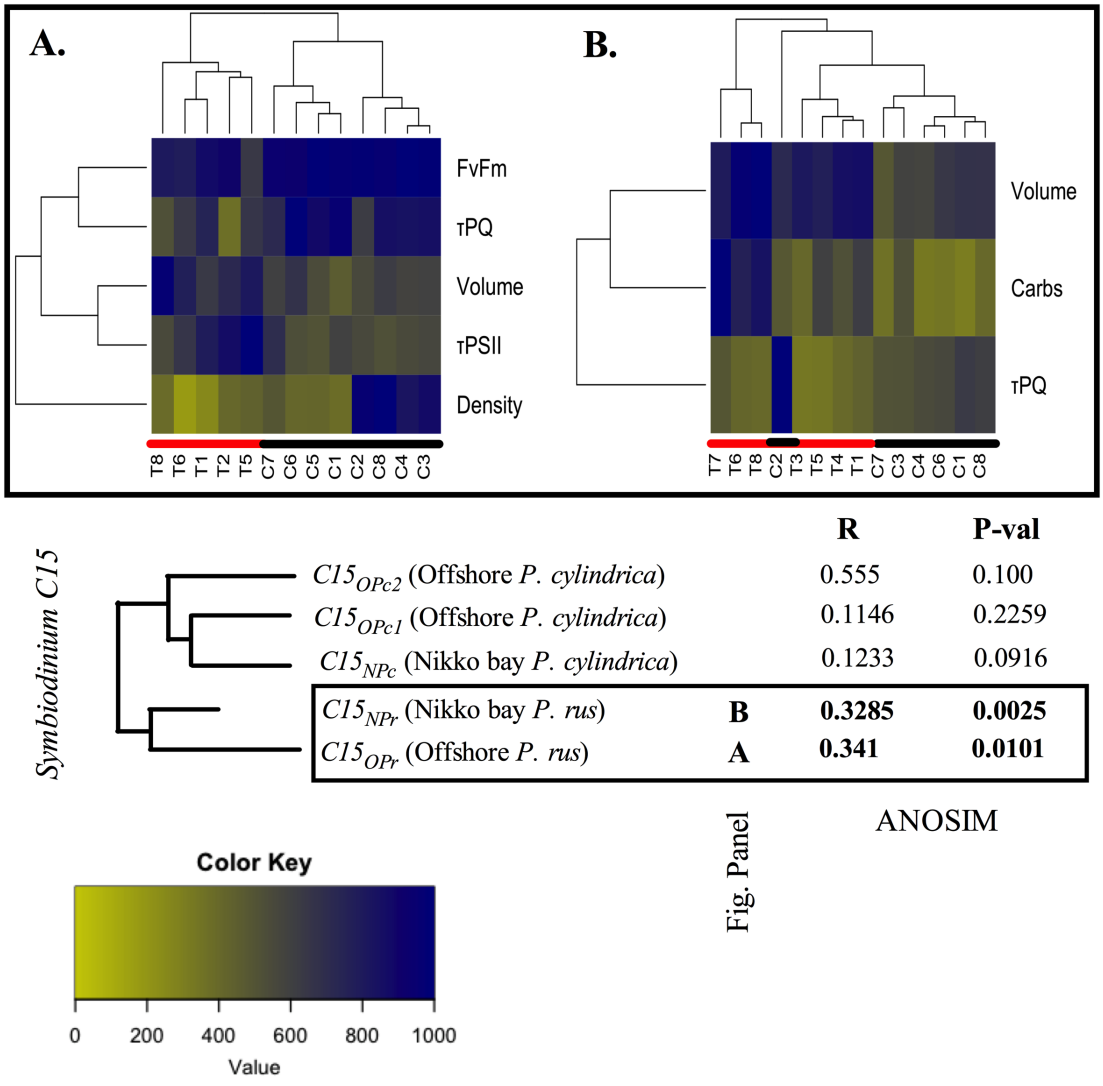

Figure 6.6: Principle Components Analysis for host dependent differences in symbiont physiology. The resulting PCA for *S. trenchii* is plotted within the **top** panel and color-coded according to host coral. The **middle** panel represents the resulting PCA plot for *C15* symbionts, color-coded to represent each *C15* symbiont genotype. The **bottom** panel represents the resulting PCA plot for *C40* symbionts and color-coded according to host coral. Treatments are depicted by open (28°C) and closed (32°C) symbols. Square symbols represent Nikko bay samples whereas circular symbols are from the offshore site. Ellipses are color-coded the same as their respective host or symbiont and reflect a 95% confidence interval around the group average. Figure legends, along with the ANOSIM results are to the right of their respective plots. OP_r = Offshore *Porites rus*. NP_r = Nikko bay *Porites rus,* OP_{c1} = Offshore *Porites cylindrica type1,* OP_{c2} = Offshore *Porites cylindrica type2,* NP_c = Nikko bay *Porites cylindrica.*

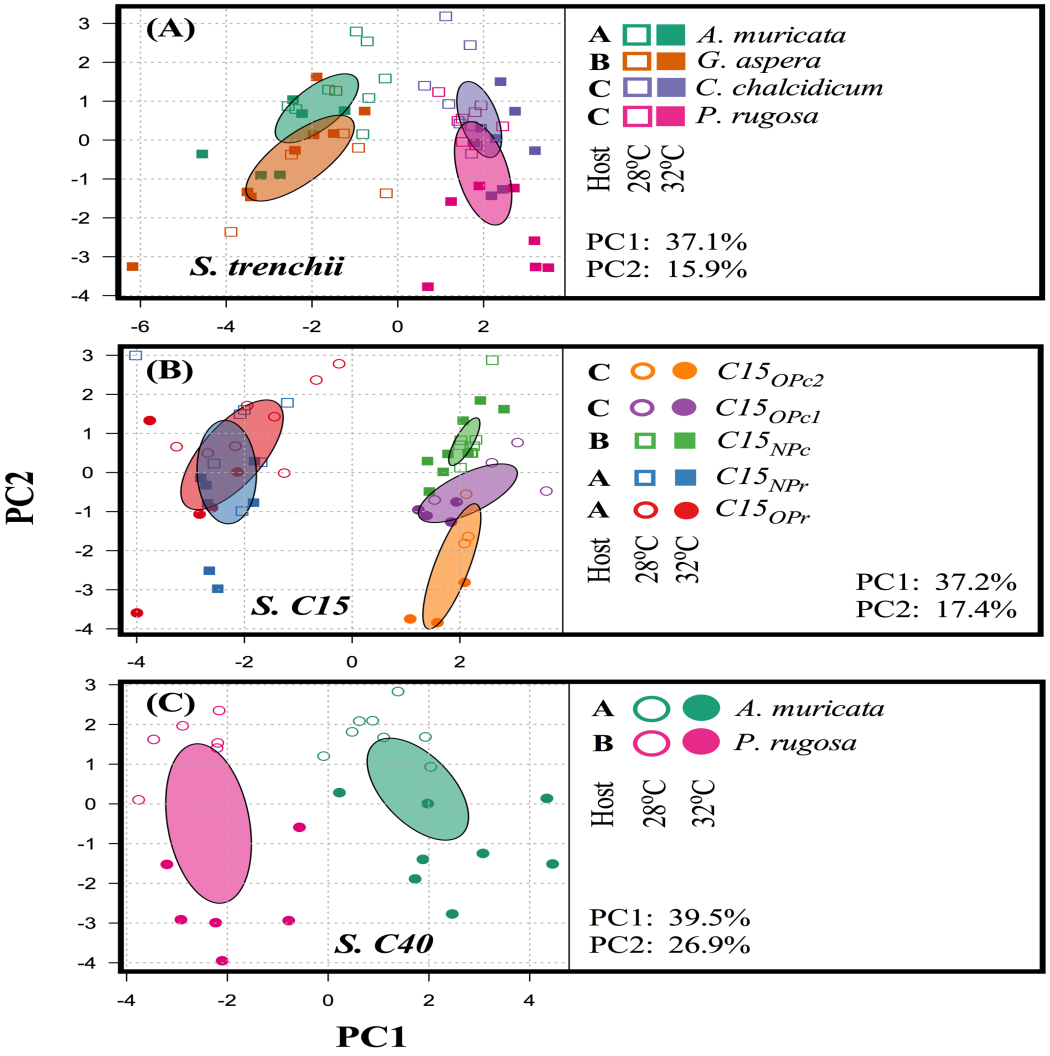

Chapter 7

EPIGENETIC MODIFICATION OF AN ANEMONE GENOME THROUGH CYTOSINE METHYLATION REVEALS PLASTICITY IN RESPONSE TO TEMPERATURE STRESS AND SYMBIONT TYPE

7.1 Abstract:

Epigenetic DNA modification through cytosine methylation provides an important mechanism for modifying gene expression patterns in response to environmental cues. Here we characterize the underlying CpG frequency across the promoter and gene body regions for the anemone *Exaiptasia pallida* and then utilize a next generation sequencing (NGS) technique to describe the overall methylome and specific changes in methylation under ambient (26^{o}C) and elevated (32^{o}C) temperature conditions and between anemones hosting *Symbiodinium* B1 and D4-5. The underlying CpG frequency within the promoter and gene bodies showed similar functional structure across KEGG class categories, along with a gradual increase in CpG frequency with greater proximity to the transcriptional start site. A highly bimodal distribution of methylation scores was found across the genome with a majority of scored sites under low methylation, consistent with patterns observed within other invertebrate species. In response to temperature and symbiont type, less than 70% of queried CpG sites showed a change in methylation status greater than 10%. Overall methylation increased with temperature and was greater in *A. pallida* hosting D4-5 as compared to B1 symbionts. Interestingly, the largest average net change occurred within the promoter regions as

opposed to introns or exons. CpG sites located within genes categorized under the environmental information processing KEGG class attributed the greatest to overall change in response to temperature (34%) and symbiont type (44%). The work provides an initial assessment of the potential for change in a cnidarian methylome in response to temperature and symbiont type. Understanding the degree of flexibility in DNA methylation across the genome may serve as a proxy of phenotypic plasticity within the organism, providing clues to the overall ability to acclimate under future climate change scenarios

7.2 Introduction:

With sea surface temperatures predicted to continue to rise over the next century (IPCC 2013), understanding coral acclimation and adaptive potential towards climate change has been a key point of interest within the coral reef research community. For symbiotic corals, the species of dinoflagellate algae living within the coral's tissue can play a major role in establishing the corals bleaching susceptibility, mortality and recovery rates (Fabricius et al. 2004; LaJeunesse et al. 2009b; Grottoli et al. 2014). However, host specific physiology is also important in establishing the coral response to high temperature stress (Grottoli et al. 2006; Fitt et al. 2009). With recent gains in the availability of genomic tools, differences in host genetics and expression profiles have begun to be discussed within the context of global climate change (Kenkel et al. 2013; Bay and Palumbi 2014; Parkinson et al. 2015).

Although adaptation through natural selection is the major source of change over long periods of time, acclimation by the individual coral colony may also play an

important role over short periods of time. *Acropora hycinathus* corals collected from moderately variable tidal pools and acclimated to warmer tidal pools displayed an equal amount of resistance towards a high temperature stress event than coral colonies originating from the warmer tidal pools (Oliver and Palumbi 2011a; Palumbi et al. 2014). This suggests that for some species, acclimation can be an important factor to consider in the context of reef resilience to future climate scenarios. Regardless of whether thermal tolerance is driven through acclimation or adaptation, variance in gene expression profiles does appear to play a role. For *A. hyacinthus*, differences in transcript abundance prior to the onset of a high temperature stress have been observed between colonies previously acclimated to warm water conditions and their cool water counterparts (Barshis et al. 2013). Understanding what cellular mechanisms are involved in establishing these differences is likely an important step in predicting what role phenotypic plasticity may play in the coral response to future climate change scenarios.

In humans, epigenetic modification of the genome through cytosine methylation is an important regulatory method for gene expression (Majewski and Ott 2002). Changes in DNA methylation may provide the mechanism on which phenotypic plasticity functions and the epigenetic potential of a genome may provide insights into the species ability to adapt to changes in the environment (Kucharski et al. 2008; Roberts and Gavery 2012). For metazoan species, DNA methylation typically occurs on the cytosine residue of a CpG motif (Mandrioli 2007). Within vertebrate systems, changes in the methylation status of CpG motifs within the promoter regions can influence transcription rates of the downstream gene body (Elango and Soojin 2008b). However, large amounts of variance in genome methylation status exists across metazoan species and methylation rates within

invertebrates tend to be lower than those observed for vertebrate species (Gavery and Roberts 2014). In addition, most methylation within invertebrates occurs within the gene body (Gavery and Roberts 2014). For some invertebrate species, including *N. vectensis,* CpG density, along with methylation status have a bimodal distribution and are negatively correlated, as lower CpG frequency regions tend to be more methylated (Sarda et al. 2012).

For the mollusk, *C. gigas,* high rates of gene expression correlated positively with higher methylation scores for CpG sites within both promoter and gene body regions, thereby differing from trends reported in mammalian systems (Olson and Roberts 2014). It is unclear if similar positive correlation exists between methylation and gene expression within cnidarian systems. Gene expression profiles for several coral species were compared to CpG frequency within the underlying gene bodies (Dixon et al. 2014; Dimond and Roberts 2015) and greater change in gene expression occurred within gene bodies that had low CpG frequencies. The two studies suggest a strong link between potential for change in gene expression and the underlying methylation potential of the genome. However, few studies have looked at methylation patterns within cnidarian organisms. Within the promoter region of the anemone *Nematostella vectensis* and the scleractinian coral *Acropora digitifera,* CpG frequency differed across functional gene categories (Marsh et al. 2016) and suggests that CpG patterns within this basal group of metazoans may play an important role in transcriptional regulation. Analysis of cnidarian methylomes and their underlying CpG density patterns may provide a potentially useful metric for assessing phenotypic plasticity within a coral population.

This study provides an initial look at methylation patterning as well as the underlying CpG frequency within the genome of the model cnidarian anemone, *Exaiptasia pallida.* Using a methyl sensitive restriction endonuclease technique to differentiate methylated and non-methylated CpG sites across the genome, we test for plasticity in the methylation status of the *E. pallida* genome through comparison of anemones hosting different symbiont types and exposed to ambient and elevated temperature conditions. Scored CpG sites display a strong bimodal distribution in low and high methylation status. Patterns mimic the underlying CpG frequency as methylation status increased in proximity to the transcriptional start site. Changes in methylation are observed in response to temperature and symbiont type, with the greatest amount of change in methylation occurring within the promoter regions. Overall, changes in methylation appear to be most dynamic within the environmental information processing KEGG class and may suggest this as a particularly plastic group of genes.

7.3 Materials and Methods:

7.3.1 Development of Host/Symbiont Combinations:

Techniques utilized here are based on methods outlined in (Hoadley et al. 2015b). Briefly, aposymbiontic *Exaiptasia pallida* anemones (clone CC7, donated by J. Pringle, Stanford University)(Sunagawa et al. 2009a) were infected with either a naturally occurring B1 symbiont type (*S. minutum*) or with *Symbiodinium D4-5*. The *B1* symbiont was originally isolated from *Cassiopeia xamachana* collected in Jamaica and the *D4-5* symbiont was isolated from an anemone in Okinawa Japan. Initial infections were

performed by injecting 1 mL of cultured symbiondium (in log-phase growth) into glass bowls with aposymbiontic anemones and incubating at room temperature for 48hrs prior to a water change. After infection, symbiotic anemones were grown in 19L grow out aquariums and fed *Artemia nauplii* twice per week. Host/symbiont combinations were stable for at least 6-months prior to start of the experimental treatment.

7.3.2 Experimental treatment:

Using the same experimental system as described in (Hoadley et al. 2015b), each anemone/symbiont combination was held in separate glass bowls, each covered with a 300-μm nitex mesh top. Each bowl contained three individual anemones with a total of three bowls per anemone/symbiont combination. Bowls were held in separate 19L aquaria connected to a central 416-L sump. All anemones were maintained within the experimental system at ambient temperature (27°C) for an initial 30 days prior to thermal ramping. After an initial 30-days, temperature was slowly ramped up from 27°C by 0.5°C each day until 32°C was reached. Temperature was then held at 32°C for an additional 20-days. A 40% water change was preformed every three days using filtered seawater collected at the Delaware Indian River inlet during the incoming tide. Salinity was maintained at 32 ppt and anemones were not fed during the experiment.

After the initial 30-day incubation under ambient (27°C) temperature, a single anemone per bowl was sampled for a total of three anemones per host/symbiont combination. Sampled anemones were immediately flash frozen in liquid nitrogen and then stored at -80°C for downstream processing. The sampling process was repeated after the remaining anemones had been exposed to 32°C temperatures for 20-days.

7.3.3 DNA extraction and sequencing:

Frozen anemones from each host/symbiont combination and treatment were combined prior to DNA extraction, so that each of the four DNA extractions were comprised of three anemones each. The combined anemones were homogenized in lysis buffer using 0.5 um glass beads and then DNA was extracted utilizing Qiagen's DNeasy Blood and Tissue Kit according to standard protocols. A small 10 ul aliquot of DNA was preserved for symbiont identification. Samples were treated with a methyl-sensitive restriction endonuclease *Hpa*II using techniques described in Marsh and Pasqualone (2014). Briefly, this process cleaves at 'CCGG' motifs unless methylation on the secondary nucleotide is present (Jelinek et al. 2012). After digestion, DNA samples were again washed using the Quiagen QIAquick PCR Purification kit prior to shearing to an average size of 300 bp (Covaris AFA technology). The resulting DNA samples were prepared for sequencing using Illumina's Genomic DNA sample preparation kit. Sequenced was preformed at the Delaware Biotechnology Institute (University of Delaware) using a HiSeq 2500 (1 lane per DNA sample).

7.3.4 Annotation and Methylation analysis:

For mapping our resulting sequence read libraries, a customized gene sequence library was constructed utilizing the publicly available *A. pallida* genome (Baumgarten et al. 2015). The custom library only contained KEGG annotated gene bodies, and included up to 2000bp of sequence upstream of the transcriptional start site. Transcript models for each gene were KEGG annotated via the Zoophyte database (bioserv7.bioinfo.pbf.hr), which lists 19,000 KEGG annotated genes for the closely related cnidarian *Acropora*

digitifera (Dunlap et al. 2013). The resulting alignments (BLAST: $e < 10^{-8}$) resulted in 19,648 KEGG annotated *A. pallida* gene models. Designation of methylation sites as located within the intron, exon or promoter region are based on the current genome annotation of *A. pallida* (Baumgarten et al. 2015).

Methylation probability scores were calculated using a proprietary MSRE technique (Marsh and Pasqualone 2013). This pipeline performs all tasks from initial quality control on raw sequence reads, isolation of target sequence reads, sequence compression, assembly of contigs (based on custom gene sequence library), quantification and comparison of methyl sites between treatment groups. Net change in methylation per site for each treatment comparison is calculated as:

Temperature: (H - L) samples

Symbiont type: (D – B) samples

For temperature comparison, the H stands for *A. pallida* samples from the high temperature treatment where as L stands for *A. pallida* samples from the low temperature treatment. For symbiont type comparison, only ambient temperature samples are compared. The D stands for *A. pallida* samples housing the D4-5 symbiont and B stands for *A. pallida* samples housing the B1 symbiont.

7.3.5 CpG density analysis:

For each annotated sequence within the custom gene library, a running average of CpG density was calculated utilizing scripts and protocols obtained form (Marsh et al.

2016). For each gene, CpG frequency normalized to GC content was calculated in 50-bp increments starting 2000-bp upstream of the transcriptional start site.

7.3.6 Resources:

Genomic gene sequence data for *A. pallida* was sourced from: (http://aiptasia.reefgenomics.org). PERL scripts and custom genome libraries utilized in the analysis are available from K.D.H at (http://github.com/khoadley).

7.3.7 Symbiont Identification:

Symbiont identification was confirmed through amplification of the internal transcribed spacer 2 region (ITS2) of the ribosomal array, and subsequent analysis by previously published protocols for denaturing gradient gel electrophoresis (DGGE) fingerprinting (LaJeunesse et al. 2003).

7.3.8 Statistical Analysis:

To test for significant differences across KEGG categories within the promoter region and gene body, CpG frequency for a 1000-bp section within each region was also measured and only genes that were not cross listed in multiple KEGG categories were utilized in our analysis (Fig 1 and Table 1). Within each section (promoter or Gene-body), significance across all six KEGG class categories was determined using a Kruskal-Wallace test with Bonferonni correction. If significant differences were observed, a Dunn's test was utilized to compare rank sums between categories. Differences in methylation status between high and low temperature treatments and

between *A. pallida* hosting B1 vs. D4-5 symbionts were calculated as the net change from high to low temperature or from D4-5 to B1 symbiont types. Increases in methylation of more than 10% were classified as hypermethylation, whereas decreases in methylation of more than 10% were classified as hypomethylation. Differences in methylation amounting to a less than 10% net change were classified as stable or 'no change' (Figure 3). For examination of the overall net difference in methylation across gene regions, CpG sites with a net change in methylation less than 10% were filtered out of our analysis. A Kruskal-Wallace test with Bonferonni correction was then utilized to determine differences in methylation across gene regions in response to elevated temperature or symbiont type, (Fig 4).

7.4 Results:

7.4.1 Symbiont Identification:

For *A. pallida* hosting the B1 symbiont *S. minutum*, continual specificity was observed through out the experiment. However, for *A. pallida* originally infected with the D4-5 symbiont, identification was stable at ambient temperaute but switched to a B1 symbiont at elevated temperature. As a result, the high temperature *A. pallida* samples originally infected with D4-5 were removed from further analysis.

7.4.2 CpG Frequency Across KEGG Class Categories:

Significant structure across KEGG class categories was observed within both the promoter and gene body regions (Fig 1). CpG frequency appears to increase with closer

proximity to the transcriptional start site for both promoter and gene body regions and within all KEGG class categories. With respect to functional category, the most striking difference in CpG frequency exists between the environmental information processing (EIP) KEGG category, which has a significantly higher mean CpG frequency than the genetic information-processing (GIP) group. This is apparent for both the promoter and gene-body regions. All other categories are intermediary with smaller, yet still significant differences observed in between categories (Fig 1).

7.4.3 DNA methylation:

Of the 113,630 'CCGG' motifs present within our *A. pallida* gene library, the MSRE analysis was able to calculate methylation scores for 96,091 sites for a recovery rate of 84%. The histogram plots reveal strong bimodal distribution in methylation status across individual CpG sites and few major differences in distribution patterns across treatment groups (Fig 2). This is likely due to the fact that most CpG sites remained stable in response to increased temperature (72%) or between symbiont types (70%). Interestingly, symbiont type induced a greater number of CpG sites to change methylation status (28,441) than did elevated temperature (26,661) (Table 2). With respect to symbiont type, 16.7% of CpG sites were hypermethylated in *A. pallida* hosting D4-5 symbionts as compared to B1 symbionts (Figure 3). An additional 13.5% were hypomethylated, resulting in a small net increase in methylation for *E. pallida* hosting D4-5 as opposed to anemones hosting the B1 symbiont. In response to elevated temperature, 16% of CpG sites were hypermethylated and 12.3% hypomethylated as compared to anemones maintained at ambient temperature (Figure 3). We again have a

net increase in methylation resulting from elevated temperature. The cumulative difference for sites showing hyper or hypomethylation is plotted by gene region at the bottom of figure 3. For both treatment groups, the cumulative difference in methylation (for hyper and hypomethylated sites) increases as they approach the transcriptional start site. Although our analysis suggests that the area of greatest methylation surrounds the TSS, we are also interested in which areas display the greatest change in methylation state in response to an environmental or physiological state. Focusing on CpG sites where methylation status changed by more than 10%, we compared the average absolute change per site across gene regions. In response to elevated temperature, the average change in methylation (either increase or decrease) was significantly higher for sites located within the promoter region as compared with sites located within introns ($P = 0.038$) or exons ($P = 0.0013$) (Fig 4). Differences in methylation status attributed to symbiont type were also significantly larger for sites within the promoter region as compared to sites located within introns ($P = 0.0483$) or exons ($P = 0.007$) (Fig 4).

7.4.4 Pathway-specific net change in methylation:

In response to elevated temperature, 34% of the net change in methylation was attributed to CpG sites located within genes involved with Environmental Information Processing (Fig. 5). Both Metabolism and Organismal Processes contributed the next highest with 22% each. Cellular processes contributed 11% and Diseases 9% to the overall net change in response to elevated temperature. Genetic Information Processing contributed the least with 2% of the overall net change.

Similar to that observed for temperature, the net difference in methylation between *E. pallida* hosting B1 vs. D4-5 symbionts was mostly attributed to genes involved with Environmental Information Processing which contributed 44% of the observed net change in methylation. Both Diseases and Organismal Processes contributed the next highest with 18% each. Cellular processes contributed 14% and Metabolism 5% to the overall net change in response to elevated temperature. Genetic Information Processing again contributed the least with 2% of the overall net change.

7.5 Discussion:

This study takes an initial look at the potential for change in DNA methylation as a metric for plasticity within the *E. pallida* genome. As environmentally induced stress increases for many marine invertebrates, the potential for acclimation and adaptation is becoming an increasingly important subject within the field of marine research and in particular, coral reef science. Changes in gene expression have been documented which show the potential for acclimation to environmental stressors such as high temperature (Barshis et al. 2013; Palumbi et al. 2014), however little is known about the underlying mechanism that allows for this plasticity. Because cytosine methylation likely plays an important epigenetic role in regulating expression patterns within the cnidarian phyla, assessing flexibility in the overall methylation pattern may provide insight into the phenotypic plasticity of a species and its ability to acclimate to future climate change scenarios.

Differences in the underlying CpG frequency are present within the promoter regions of *A. pallida,* mimicking results found within the cnidarians *A. digitifera* and *N. vectensis* (Marsh et al. 2016). However, our current study extends this analysis into the

gene body, confirming similar functional structure exists within the gene body as well. Dixon et al. (2014) and Dimond and Roberts (2015) also confirm differences in CpG frequency across functional categories within the mRNA transcripts of several other cnidarian species. They further link underlying CpG frequency with the mean expression levels and find a distinct correlation between expression and underlying CpG frequency. Whether or not similar correlations between gene expression and CpG frequency are also found in the promoter region is unclear. However, similar distribution and skew is observed for overall CpG frequency within the promoter and mRNA transcripts for *E. pallida* genes (data not show). This suggests a similar selective pressure towards reducing CpG frequency is active within both regions. Within both the promoter and gene body of *C. gigas,* positive correlations between DNA methylation and gene expression are observed (Olson and Roberts 2014) and may suggest some overlap in DNA methylation function between promoter and gene body regions. However, invertebrate methylation profiles characterized thus far display considerable variability across species (Head 2014) and care must be taken when comparing patterns.

Plasticity in *E. pallida* DNA methylation was assessed through comparison of low and high temperature treatments and between anemones hosting different symbiont strains. Between 25% and 30% of scored methylation sites responded with a change in methylation greater than 10%. As is illustrated in figure 3, considerable hyper and hypomethylation occurred in response to temperature and symbiont type, with most change occurring in close proximity to the transcriptional start site. Similar to other invertebrate species, the underlying CpG density within the *E. pallida* genome increases with closer proximity to the transcriptional start site (Fig 1) and it is therefore perhaps not

surprising that the highest methylation rates occur here as well (Keller et al. 2015). The overall response to both temperature and symbiont was a net increase in DNA methylation, consistent with thermal experiments on the Antarctic polychaete, *Spiophanes tcherniai* (Marsh and Pasqualone 2013). For *S. tcherniai*, increases in seawater temperature from -1.5 C to 3.5 C over a 4-week period resulted in a net increase in genomic methylation. Future studies are needed to understand whether increased methylation allows for greater flexibility, or is a sign of down regulation in response to environmental stress.

Interestingly, the overall change and the resulting net increase in methylation were significantly higher within the promoter region as compared to either introns or exons (Figure 3 + 4). Methylation of cytosine residues within the promoter region of mammalian systems are well documented as regulatory mechanisms, down-regulating transcriptional expression (Law and Jacobsen 2010). Whether or not epigenetic changes in cytosine methylation are equally important within the promoter regions of invertebrates remains poorly understood. However, mammalian genomes are between 60-90% methylated (Glastad et al. 2011), whereas invertebrate genomes are typically less than 10% methylated (Head 2014). Despite differences in overall methylation status, gene bodies tend to be more methylated than promoter regions in both invertebrates (Roberts and Gavery 2012; Gavery and Roberts 2014) and mammalian systems (Bird 1985). The larger changes in methylation observed in the promoter region of the *E. pallida* may suggest that, similar to mammalian systems, the promoter regions plays an important role in epigenetic regulation of gene expression. Temperature, along with changes in symbiont type are known to induce transcriptional changes in corals (Desalvo

et al. 2008, 2010; Barshis et al. 2013) and the changes in methylation patterns observed here likely also correspond to changes in the downstream gene expression. Future studies will need to correlate changes in cytosine methylation with differential gene expression patterns.

Differences in symbiont genotype induced change within a greater number of CpG sites than did elevated temperature. For the Caribbean coral *Montastrea faveolata* (now known as *Orbicella faveolata*), symbiont type also induced a greater difference in gene expression profiles than temperature (DeSalvo et al. 2010). Many cellular processes are involved in formation of the host/symbiont symbioses (Oakley et al. 2015) and large genetic distances separate the Clade B and Clade D symbionts utilized within this study (Coffroth and Santos 2005). It is likely that such diversity necessitates a difference within the underlying symbioses, thus accounting for the degree of change observed in gene expression within *O faveolata* and methylation observed within *E. pallida*.

If we separate differences in methylation according to functional categories, Environmental Information Processing contributes the greatest amount to overall net change for both temperature and symbiont comparisons (Fig 5). Interestingly, other categories are less shared as diseases attributes much more to change across symbiont type whereas differences in metabolism appear more important in response to elevated temperature. Changes in metabolism can occur during high temperature stress and differential expression of metabolic genes has been recorded within *A. aspera* (Rosic et al. 2014) and *A. millepora* (Kaniewska et al. 2015). The KEGG class category of Disease mainly contains genes involved with cell recognition, which is thought to play a major role in establishing different symbioses across host/symbiont combinations (Oakley et al.

2015). The net changes observed here are therefore consistent with what has been previously reported through transcriptomic studies suggesting a strong role of DNA methylation in regulating gene expression within the cnidarian phyla.

Estimating the degree of physiological plasticity within an organism can provide insight into its potential to acclimate to a changing environment. Epigenetic changes can provide a potential metric of physiological plasticity and our study provides a first look at these differences in DNA methylation within the model species *E. pallida.* Our work suggests a similar selective force has shaped the underlying CpG frequency within promoter and gene body regions and that similar differences across functional categories also exist between the gene regions. Despite these similarities, greater net change occurs within the promoter regions as compared to exons and introns/gene bodies. Changes in methylation status occurred mostly within CpG sites associated with environmental information processing and may suggest greater plasticity for these genes. Differences in methylation patterns across species may help us better understand which corals are more or less capable of quickly acclimating to changes in the environment and future studies should focus on comparison of methylation patterns across multiple coral species and across different environmental conditions.

Table 7.1: KEGG class information was obtained using the Zoophyte database (Dunlap et al. 2013). Class categories are filtered to only include genes with a single class grouping.

KEGG CLASS	Unique Genes	Unique CCGG Sites
Metabolism	2,902	14,710
Environmental Information Processing	2,680	16,656
Genetic Information Processing	2,436	11,156
Cellular Processes	1,147	5,906
Organismal Processes	1,480	8,151
Disease	581	2,893

Table 7.2: CpG methylation differences for temperature and symbiont comparisons.

CpG Comparison	Temp	Symbiont Type
Matched CpG sites	96,091	96,091
Unchanged CpG sites	69,430	67,650
Changed CpG sites	26,661	28,441

Figure 7.1: CpG frequency across functional KEGG categories. CpG motif frequencies starting 2000-bp upstream of the transcritptional start site and running through 4000-bp of the gene body. Each line plot represents a separate KEGG functional class. The top line graph contains the classes, Environmental Information Processing, Genetic Information Processing and Metabolism. The bottom line graph contains the classes, Organismal Systems, Cellular Processing and Diseases. The top bar graph on the right depicts the average CpG density within a 1000bp region in the gene body as outlined in grey. The bottom bar graph on the right depicts the average CpG density within a 1000bp region in the promoter region as outlined in grey. Significantly different groups resulting from a Dunn's test are reflected through letters above each bar. Color codes for each KEGG class are depicted on the left hand side.

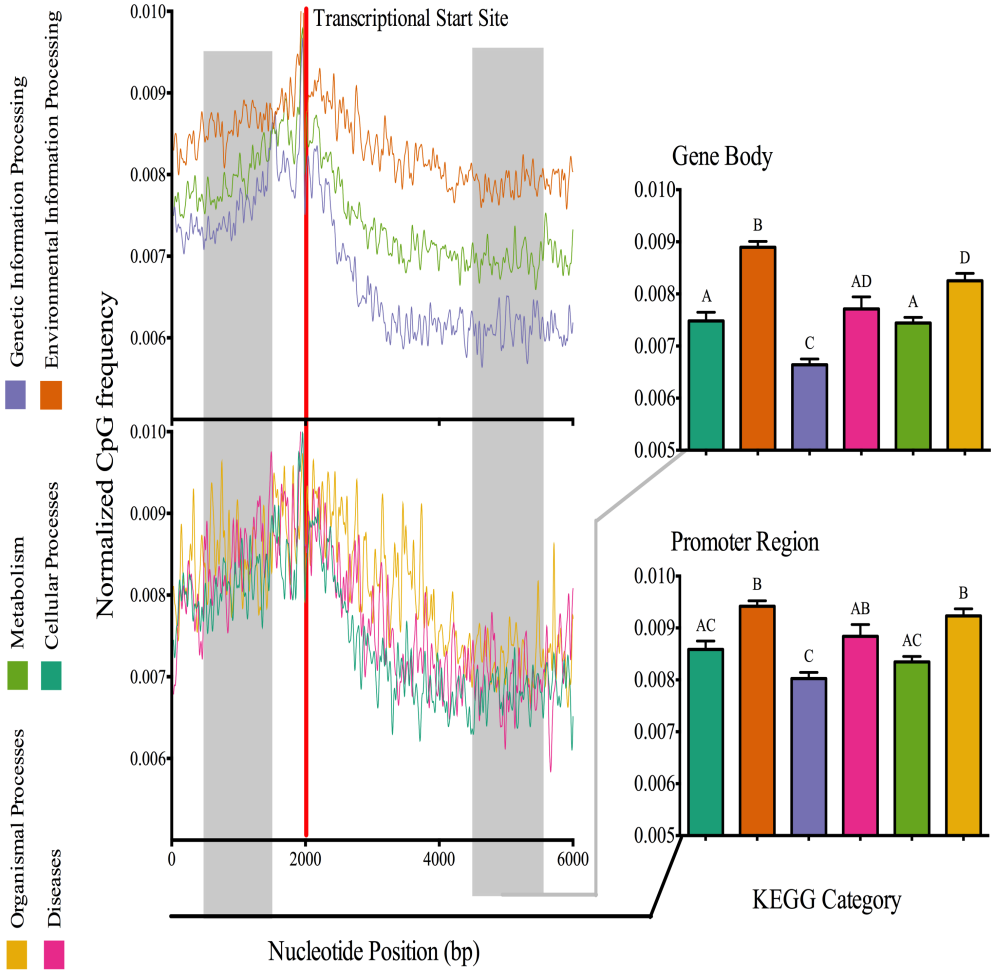

Figure 7.2: Methylation histograms for all three treatments. **(Top)** *E. pallida* hosting *B1* symbionts under ambient temperature. **(Middle)** *E. pallida* hosting *B1* symbionts within the high temperature treatments. **(Bottom)** *E. pallida* hosting *D4-5* symbionts within the low temperature treatments. Histograms are overlaid by a density curve to better showcase trends.

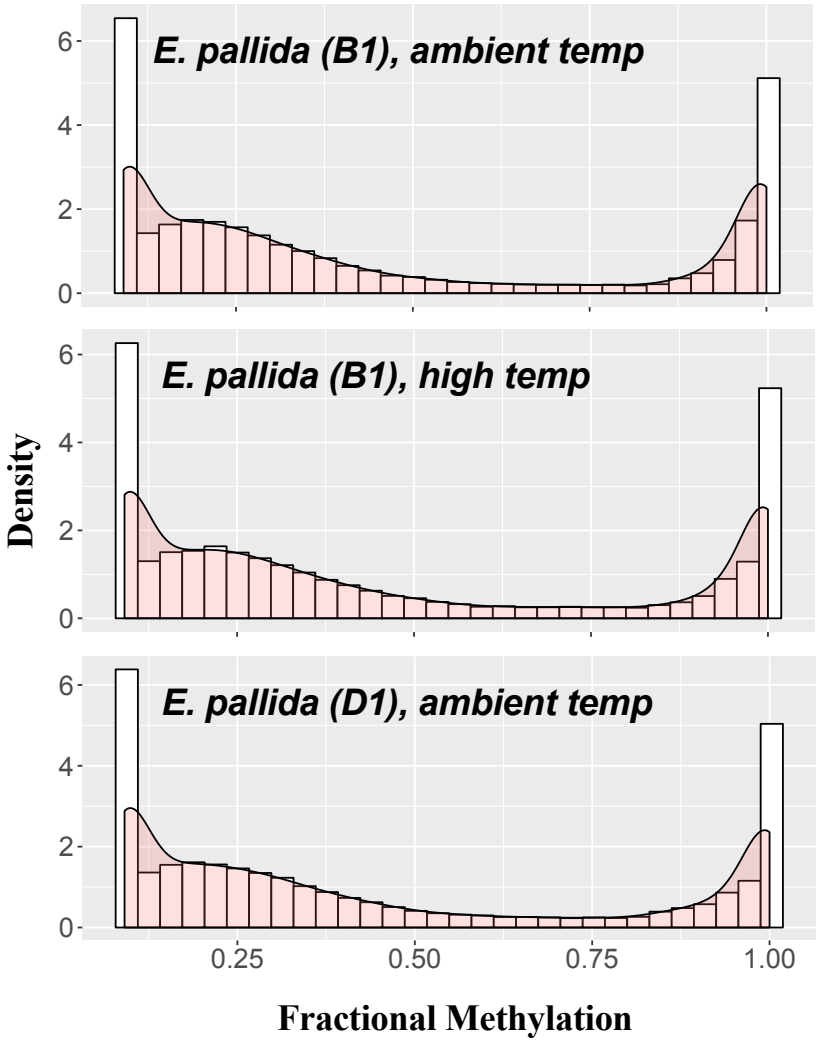

Figure 7.3: Changes in methylation. Net difference in methylation: Hypermethylation includes sites with a net increase in methylation of greater than 10%, where as hypomethylation includes sites with a net decrease in methylation of greater than 10%. Stable 'CCGG' sites include those where the net change in methylation was observed to be less than 10% and are considered to be no change. The **top** two fractional bar charts reflect the relative proportion of 'CCGG' sites showing hypermethylation (**green**), hypomethylation (**orange**) or no change (**grey**) in methylation in response to temperature (top) and symbiont type (bottom). The **Bottom** two cumulative histograms (400bp bin width) reflect the sum of difference (cumulative net change) in methylation across a representative gene body. The sum difference for hypermethylated 'CCGG' sites is depicted in green; where as the sum difference for hypomethylated sites is depicted in orange and then net change is in blue.

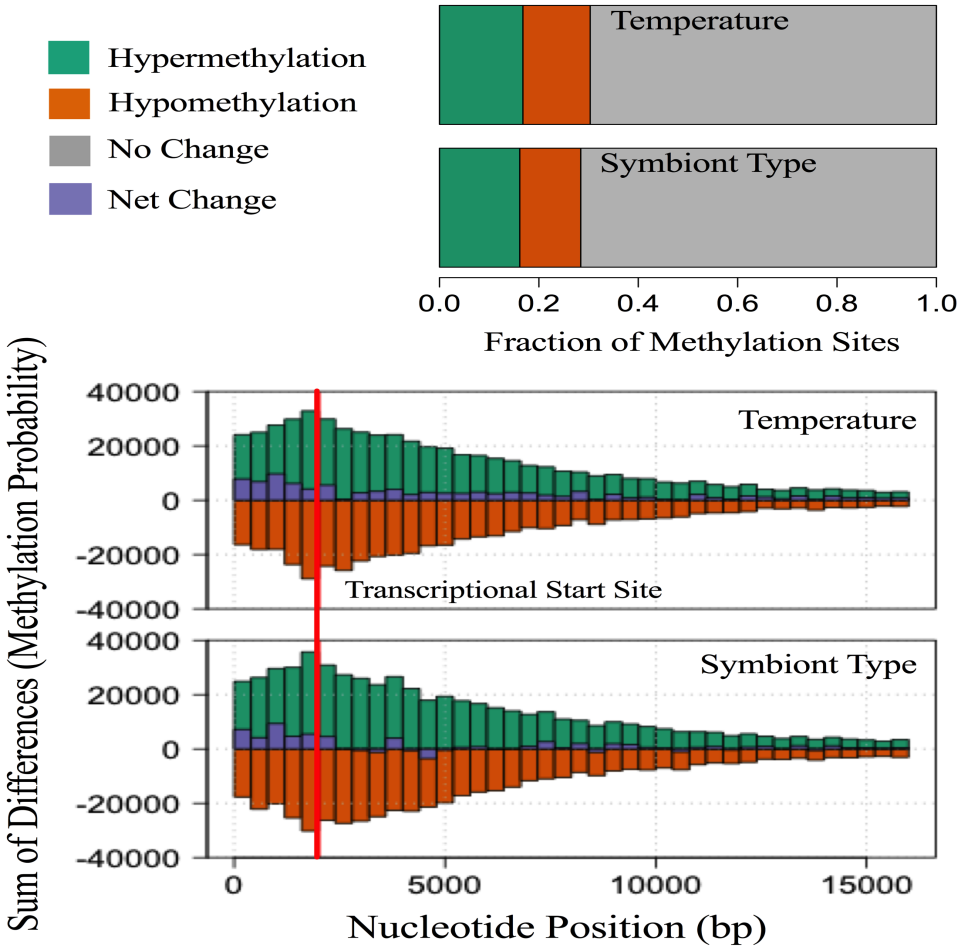

Figure 7.4: Absolute change in methylation across gene structures. Average absolute change in methylation per site: Changes in response to temperature (**Top**) and symbiont type (**Bottom**) are separated by gene regions. Only sites showing a greater than 10% change in methylation are included in the analysis. The letters on top of each bar reflect significant differences in net change in methylation across gene sections.

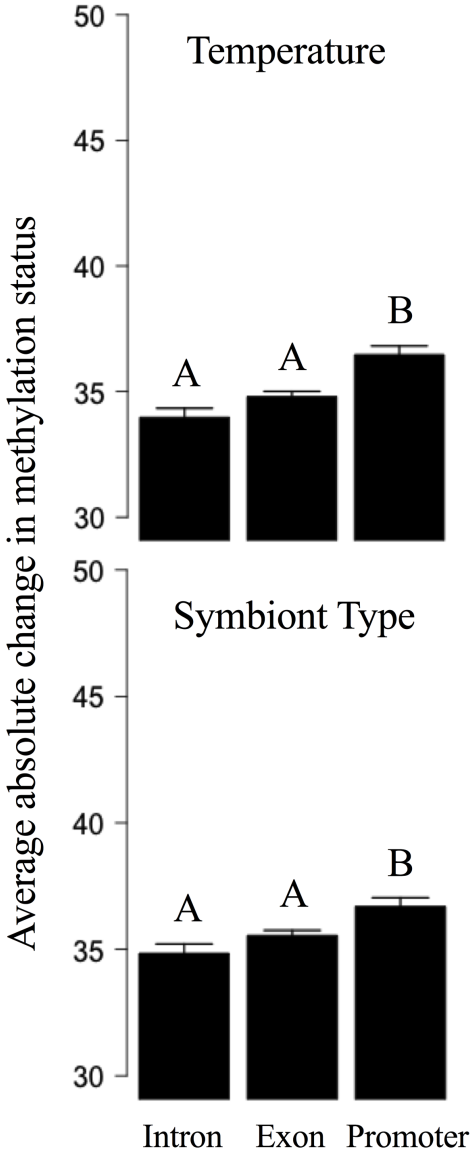

Figure 7.5: Pathway-specific change in methylation. KEGG pathway-specific contribution to the total net change in methylation. The **top** pie chart reflects net change in response to elevated temperature. The **bottom** pie chart reflects differences in methylation between anemones hosting the D5b symbiont as compared with anemones hosting the B1 symbiont.

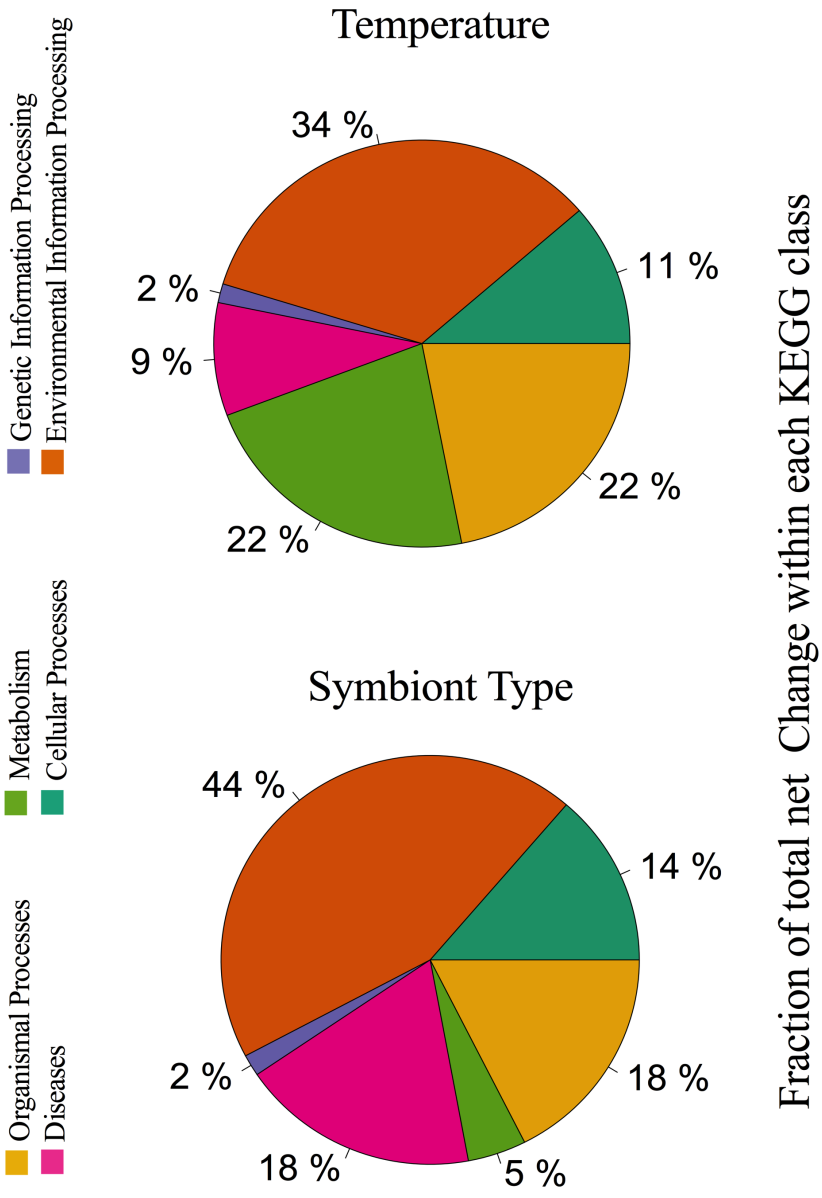

Chapter 8

CONCLUSIONS

Much of what we understand about the effects of temperature and ocean acidification on coral reefs was gleaned through the study of a relatively small set of model cnidarian species. The use of model species to study the effects of climate change can be highly beneficial as they provide the field with a well-characterized system on which to study coral physiology. However, high biological diversity exists within the host coral species, as well as the symbiotic algae. The use of model systems must therefore be balanced so as to account for the high degree of physiological diversity. Through comparative studies of several coral species and morphologies, my dissertation has focused on merging physiological variability with genetic diversity within the coral symbioses in an effort to better understand how climate change will affect future coral reefs.

In Chapter 2, I compared the physiological response to temperature and CO_2 across four Pacific coral species and noted not only differences across species, but also varying trends within each symbiosis itself, as the host response in terms of biochemical composition often differed from that of the symbiont. Our work suggests that many of the nuanced responses to temperature and pCO_2 that have been well documented in the literature may only be appropriate for the species and algal types in question and are less applicable over a wide range of coral algal symbioses. Furthermore, reliance on measurement of only a few physiological variables may not fully characterize differences

across species and their responses to environmental change. Importantly, this chapter also clearly showed that within each species, temperature induced a greater degree of physiological response than did pCO_2. Similar findings were also observed in Chapter 3 where I also examined the role of increased nutrient concentrations. Here temperature remained the most influential factor for inducing a physiological response. However the longer time frame of the study enabled me to also detect important interactive effects between temperature, pCO_2 and nutrients in the coral *T. reniformis* and its symbiont *S. trenchii*. Although Chapter 3 only looked at a single coral species, thereby limiting its implications, the presence of this interactive effect between global (temperature and ocean acidification) along with regional factors (nutrient concentration) is nevertheless important. Experiments that only focus on an individual environmental factor may be less informative in terms of predicting a species response to climate change if other cofactors are not taken into account.

Chapters 4 and 5 are similar to Chapter 2 as they also focus on physiological variability across species (host or symbiont type). However, whereas chapter 2 focused on separating the host from symbiont response within each of the four coral species, Chapters 4 and 5 centered on physiological metrics that speak to the symbioses itself. By tracing the flow of carbon from symbiont to host, clear differences across species were noted with respect to the ratio of carbon uptake and translocation. The B1 symbionts within the anemone *E. pallida* translocated the least amount of photosynthate $cell^{-1}$ whereas the corallimorph *D. nummiforme* translocated the most, despite having much lower rates of overall photosynthesis $cell^{-1}$ than the two scleractinian corals, *P. damicornis* and *M. hirsuta.* Importantly, the inverse relationship between cell density and

net photosynthesis observed across species corroborates previous work on carbon limitation. Because reductions in cell density are common in response to elevated temperature conditions, increases in net photosynthesis observed for *A. muricata* in Chapter 6 are likely also explained by this relationship. Changes in the carbon supply may play a major role during thermal stress or during other events where changes in cell density occur. Additionally, Chapter 5 utilized three different B1 symbiont types to study the response to elevated pCO_2 conditions. Despite the close genetic distance between the B1 symbiont types utilized, significant differences in the ratio of carbon uptake to translocation were still found.

Chapter 6 continues our investigation of physiological variability across host and symbiont combinations by focusing on 6 coral species found within offshore and inshore reef habitats. Greater reductions in cell density and photosynthetic efficiency occurred for offshore corals as opposed to their inshore counterparts, and indicated greater bleaching resilience for inshore coral colonies. Inshore reef habitats are characterized by higher light attenuation and shading as compared to the offshore sites and this difference in light levels is thought to play a role in the higher bleaching resistance. However, because both inshore and offshore coral colonies were tested within the same experimental system, differences in the observed bleaching response are more likely related to physiological differences between inshore and offshore coral colonies, than physical differences in the habitats themselves. Our results indicate that prior exposure to warmer temperatures, along with association with more robust symbiont types allowed for rock island coral colonies to exhibit greater thermal tolerance toward high temperature events. Analysis of 14 different physiological variables within each host + symbiont combination revealed

different responses to elevated temperature, similar to findings observed in Chapter 2. In addition, host dependent differences in symbiont physiology resulted in bleaching within certain coral species despite the presence of thermally tolerant symbionts. Acclimation to warmer waters and harboring thermally tolerant symbiont species may provide temperature refugia to some but not all coral species, and both the host and symbiont should be taken into account when predicting thermal tolerance.

With respect to individual physiological variables, increases in algal volume due to elevated temperature were noted within several symbiont types across four separate studies and likely plays a major role in mediating the internal light fields for individual chloroplasts within the symbiont cell. Because increases in cellular volume are typically associated with greater functional absorption cross sections in open ocean phytoplankton, this unique response in *in hospite Symbiodinium* represents a new mechanism by which symbionts respond to elevated temperature. Future studies will need to investigate why this increase occurs and if it represents a strategy during, or a consequence of, high thermal stress.

Lastly, I used available genomic resources along with an NGS technique to assess the epigenetic potential within the anemone *E. pallida.* First, by surveying the underlying CpG frequency within the genome, I found significant differences in CpG frequency across functional KEGG categories both within the promoter and gene-body regions. Interestingly, changes in methylation profiles in response to temperature were less than those observed across anemones hosting different symbiont strains and speak to the differences in overall symbioses that are established in *E. pallida* hosting one symbiont species vs. another. Our work also indicates that high temperature stress increases

methylation status across the genome and that changes in methylation appear to be more significant within the promoter region as compared to the gene-body. Measuring changes in DNA methylation may provide a metric for calculating phenotypic plasticity within a species and provide clues to its potential to acclimate to future environmental conditions. Future research focusing on epigenetic profiling across coral species may provide additional information of the overall physiological plasticity within a species.

Starting from the individual colony perspective, we show that epigenetic changes in the genome can occur in response to environmental stress and that quantification of this differential methylation may provide us with a potentially useful metric for assessing phenotypic plasticity within an organism in the future. With respect to within species comparisons, I have shown that physiological differences can occur even across clonal variants of the same symbiont type (B1) and that these differences can potentially influence the overall response of the symbioses to environmental stress. This is particularly important as differences in physiology at this genetic level are necessary in order for selective forces to drive adaptation to a changing climate through survival of the more tolerant symbioses. Lastly, by comparing the physiological response to environmental stress between model and non-model cnidarian species, my dissertation has provided additional biological diversity to the study of the effects of climate change on coral reefs. I have shown that the physiological response to elevated temperature and pCO_2 can differ significantly between coral species and is a function of the unique physiology inherent to each host and symbiont combination. The diversity of physiological responses to environmental stress that have been documented here is an

important factor towards our understanding of coral reef system-wide effects from climate change.

REFERENCES

Alexandre A, Silva J, Buapet P, Björk M, Santos R (2012) Effects of CO_2 enrichment on photosynthesis, growth, and nitrogen metabolism of the seagrass *Zostera noltii*. Ecol Evol 2: 2625-2635

Anthony KRN, Maynard JA, Diaz-Pulido G, Mumby PJ, Marshall PA, Cao L, Hoegh-Guldberg O (2011) Ocean acidification and warming will lower coral reef resilience. Glob Chang Biol 17: 1798-1808

Anthony KRN, Hoogenboom MO, Maynard JA, Grottoli AG, Middlebrook R (2009) Energetics approach to predicting mortality risk from environmental stress: a case study of coral bleaching. Funct Ecol 23: 539-550

Anthony KRN, Kline DI, Diaz-Pulido G, Dove S, Hoegh-Guldberg O (2008) Ocean acidification causes bleaching and productivity loss in coral reef builders. Proc Natl Acad USA 105: 17442-17446

Aronson RB, Precht WF (2000) Herbivory and algal dynamics on the coral reef at Discovery Bay, Jamaica. Limnol Oceanogr 45: 251-255

Bachvaroff TR, Place AR (2008) From stop to start: tandem gene arrangement, copy number and trans-splicing sites in the dinoflagellate *Amphidinium carterae*. PLoS One 3: DOI: 10.1371/journal.pone.0002929

Baird AH, Bhagooli R, Ralph PJ, Takahashi S (2009) Coral bleaching: the role of the host. Trends Ecol Evol 24: 16-20

Baker AC (2003) Flexibility and specificity in coral-algal symbiosis: diversity, ecology, and biogeography of *Symbiodinium*. Annual Review of Ecology, Evolution, and Systematics 34: 661-689

Barkley HC, Cohen AL, Golbuu Y, Starczak VR, DeCarlo TM, Shamberger KEF (2015) Changes in coral reef communities across a natural gradient in seawater pH. Science advances 1: e1500328

Barshis DJ, Ladner JT, Oliver TA, Seneca FO, Traylor-Knowles N, Palumbi SR (2013) Genomic basis for coral resilience to climate change. Proceedings of the National Academy of Sciences 110: 1387-1392

Baumgarten S, Simakov O, Esherick LY, Liew YJ, Lehnert EM, Michell CT, Li Y, Hambleton EA, Guse A, Oates ME (2015) The genome of Aiptasia, a sea anemone model for coral symbiosis. Proceedings of the National Academy of Sciences 112: 11893-11898

Bay RA, Palumbi SR (2014) Multilocus adaptation associated with heat resistance in reef-building corals. Current Biology 24: 2952-2956

Beardall J, Stojkovica S, Larsena S (2009) Living in a high CO_2 world: impacts of global climate change on marine phytoplankton. Plant Ecol Divers 2: 191-205

Ben-Zvi O, Eyal G, Loya Y (2014) Light-dependent fluorescence in the coral Galaxea fascicularis. Hydrobiologia 1-12

Béraud E, Gevaert F, Rottier C, Ferrier-Pagès C (2013) The response of the scleractinian coral *Turbinaria reniformis* to thermal stress depends on the nitrogen status of the

coral holobiont. J Exp Biol 216: 2665-2674
Berges JA, Varela DE, Harrison PJ (2002) Effects of temperature on growth rate, cell composition and nitrogen metabolism in the marine diatom *Thalassiosira pseudonana* (Bacillariophyceae). Mar Ecol Prog Ser 225: 139-146
Bertucci A, Tambutte S, Supuran CT, Allemand D, Zoccola D (2011) A new coral carbonic anhydrase in *Stylophora pistillata*. Mar Biotechnol 13: 992-1002
Bhagooli R, Hidaka M (2004) Photoinhibition, bleaching susceptibility and mortality in two scleractinian corals, *Platygyra ryukyuensis* and *Stylophora pistillata*, in response to thermal and light stresses. Comparative Biochemistry and Physiology 137: 547-555
Bird AP (1985) CpG-rich islands and the function of DNA methylation. Nature 321: 209-213
Black NA, Voellmy R, Szmant AM (1995) Heat-Shock Protein Induction in Montastraea-Faveolata and Aiptasia-Pallida Exposed to Elevated-Temperatures. Biol Bull (Woods Hole) 188: 234-240
Boldt L, Yellowlees D, Leggat W (2009) Measuring *Symbiodinium* sp. gene expression patterns with quantitative real-time PCR. (eds), 118-122
Borell EM, Yuliantri AR, Bischof K, Richter C (2008) The effect of heterotrophy on photosynthesis and tissue composition of two scleractinian corals under elevated temperature. J Exp Mar Biol Ecol 364: 116-123
Borell EM, Bischof K (2008) Feeding sustains photosynthetic quantum yield of a scleractinian coral during thermal stress. Oecologia 157: 593-601
Brading P, Warner ME, Smith DJ, Suggett DJ (2013) Contrasting modes of inorganic carbon acquisition amongst *Symbiodinium* (Dinophyceae) phylotypes. New Phytol 200: 432-442
Brading P, Warner ME, Davey P, Smith DJ, Achterberg EP, Suggett DJ (2011) Differential effects of ocean acidification on growth and photosynthesis among phylotypes of *Symbiodinium* (Dinophyceae). Limnol Oceangr 56: 927-938
Brown B (1997) Coral bleaching: causes and consequences. Coral Reefs 16: 129-138
Brown BE, Sya'Rani L, Le Tissier M (1985) Skeletal form and growth in Acropora aspera (Dana) from the Pulau Seribu, Indonesia. J Exp Mar Biol Ecol 86: 139-150
Buck BH, Rosenthal H, Saint-Paul U (2002) Effect of increased irradiance and thermal stress on the symbiosis of< i> Symbiodinium microadriaticum and< i> Tridacna gigas. Aquat Living Resour 15: 107-117
Buxton L, Takahashi S, Hill R, Ralph PJ (2012) Variability in the primary site of photosynthetic damage in *Symbiodinium sp.* (dinophyceae) exposed to thermal stress1. J Phycol 48: 117-126
Cai WJ, Hu X, Huang WJ, Jiang LQ, Wang Y, Peng TH, Zhang X (2010) Alkalinity distribution in the western North Atlantic Ocean margins. J Geophys Res 115: DOI: 10.1029/2009JC005482
Carninci P, Sandelin A, Lenhard B, Katayama S, Shimokawa K, Ponjavic J, Semple CAM, Taylor MS, Engström PG, Frith MC (2006) Genome-wide analysis of mammalian promoter architecture and evolution. Nature genetics 38: 626-635
Carvalho AP, Monteiro CM, Malcata FX (2009) Simultaneous effect of irradiance and temperature on biochemical composition of the microalga *Pavlova lutheri*. J Appl Phycol 21: 543-552

Cheng Y-S, Zheng Y, VanderGheynst J (2011) Rapid quantitative analysis of lipids using a colorimetric method in a microplate format. Lipids 46: 95-103
Clarke KR (1993) Non parametric multivariate analyses of changes in community structure. Aust J Ecol 18: 117-143
Coffroth MA, Santos SR (2005) Genetic diversity of symbiotic dinoflagellates in the genus *Symbiodinium*. Protist 156: 19-34
Cohen AL, Holcomb M (2009) Why corals care about ocean acidification: uncovering the mechanism. Oceanogr 22: 118-127
Comeau S, Gorsky G, Jeffree R, Teyssie JL, Gattuso JP (2009) Impact of ocean acidification on a key Arctic pelagic mollusc (Limacina helicina). Biogeosciences 6: 1877-1882
Cook CB, Mullerparker G, Orlandini CD (1994) Ammonium enhancement of dark carbon fixation and nitrogen limitation in zooxanthellae symbiotic with the reef corals *Madracis mirabilis* and *Montastrea annularis*. Mar Biol 118: 157-165
Cooper TF, Ulstrup KE, Dandan SS, Heyward AJ, Kühl M, Muirhead A, O'Leary RA, Ziersen BEF, Van Oppen MJH (2011) Niche specialization of reef-building corals in the mesophotic zone: metabolic trade-offs between divergent Symbiodinium types. Proc R Soc B 278: 1840-1850
Cornwall CE, Hurd CL (2015) Experimental design in ocean acidification research: problems and solutions. ICES J Mar Sci doi:10.1093/icesjms/fsv118
Cunning R, Vaughan N, Gillette P, Capo TR, Maté JL, Baker AC (2015) Dynamic regulation of partner abundance mediates response of reef coral symbioses to environmental change. Ecology 96: 1411-1420
Cunning R, Baker AC (2013) Excess algal symbionts increase the susceptibility of reef corals to bleaching. Nature Clim Change 3: 259-262
D'Angelo C, Wiedenmann J (2014) Impacts of nutrient enrichment on coral reefs: new perspectives and implications for coastal management and reef survival. Current Opinion in Environmental Sustainability 7: 82-93
Davy SK, Cook C (2001) The relationship between nutritional status and carbon flux in the zooxanthellate sea anemone, *Aiptasia pallida*. Mar Biol 139: 999-1005
Davy SK, Lucas IAN, Turner JR (1996) Carbon budgets in temperate anthozoan-dinoflagellate symbioses. Mar Biol 126: 773-783
Desalvo MK, Rvoolstra C, Sunagawa S, Schwarz JA, Stillman JH, Coffroth MA, Szmant AM, Medina M (2008) Differential gene expression during thermal stress and bleaching in the Caribbean coral *Montastraea faveolata*. Mol Ecol 17: 3952-3971
DeSalvo MK, Sunagawa S, Fisher PL, Voolstra CR, Iglesias-Prieto R, Medina M (2010) Coral host transcriptomic states are correlated with Symbiodinium genotypes. Mol Ecol 19: 1174-1186
Dimond JL, Holzman BJ, Bingham BL (2012) Thicker host tissues moderate light stress in a cnidarian endosymbiont. J Exp Biol 215: 2247-2254
Dimond JL, Roberts SB (2015) Germline DNA methylation in reef corals: patterns and potential roles in response to environmental change. Mol Ecol
Dixon GB, Bay LK, Matz MV (2014) Bimodal signatures of germline methylation are linked with gene expression plasticity in the coral Acropora millepora. BMC genomics 15: 1
Dove S, Ortiz JC, Enriquez S, Fine M, Fisher P, Iglesias-Prieto R, Thornhill D, Hoegh-

Guldberg O (2006) Response of holosymbiont pigments from the scleractinian coral Montipora monasteriata to short-term heat stress. Limnol Oceanogr 51: 1149-1158
Dove S (2004) Scleractinian corals with photoprotective host pigments are hypersensitive to thermal bleaching. Mar Ecol Prog Ser 272: 99-116
Dubois M, Giles KA, Hamilton JK, Pevers PA, Smith F (1956) Colorimetric method for determination of sugar and related substances. Anal Chem 28: 350-356
Dudgeon SR, Aronson RB, Bruno JF, Precht WF (2010) Phase shifts and stable states on coral reefs. Mar Ecol Prog Ser 413: 201-216
Dunlap WC, Starcevic A, Baranasic D, Diminic J, Zucko J, Gacesa R, Van Oppen MJH, Hranueli D, Cullum J, Long PF (2013) KEGG orthology-based annotation of the predicted proteome of Acropora digitifera: ZoophyteBase-an open access and searchable database of a coral genome. BMC genomics 14: 509
Edge SE, Morgan MB, Gleason DF, Snell TW (2005) Development of a coral cDNA array to examine gene expression profiles in *Montastraea faveolata* exposed to environmental stress. Mar Pollut Bull 51: 507-523
Edmunds PJ (2011) Zooplanktivory ameliorates the effects of ocean acidification on the reef coral *Porites spp*. Limnol Oceanogr 56: 2402-2410
Edmunds PJ, Carpenter RC, Comeau S (2013) Understanding the threats of ocean acidification to coral reefs. Oceanogr 26: 149-152
Elango N, Soojin VY (2008a) DNA methylation and structural and functional bimodality of vertebrate promoters. Mol Biol Evol 25: 1602-1608
Elango N, Soojin VY (2008b) DNA methylation and structural and functional bimodality of vertebrate promoters. Mol Biol Evol 25: 1602-1608
Engebretson HP, Muller-Parker G (1999) Translocation of photosynthetic carbon from two algal symbionts to the sea anemone *Anthopleura elegantissima*. Biol Bull (Woods Hole) 197: 72-81
Enriquez S, Mendez ER, Iglesias-Prieto R (2005) Multiple scattering on corals enhances light absorption by symbiotic algae. Limnol Oceanogr 50: 1025-1032
Enríquez S, Méndez ER, Iglesias-Prieto R (2005) Multiple scattering on coral skeletons enhances light absorption by symbiotic algae. Limnol Oceanogr 50: 1025-1032
Fabricius KE (2006) Effects of irradiance, flow, and colony pigmentation on the temperature microenvironment around corals: Implications for coral bleaching? Limnol Oceanogr 51: 30-37
Fabricius KE, Mieog JC, Colin PL, Idip D, Van Oppen MJH (2004) Identity and diversity of coral endosymbionts (zooxanthellae) from three Palauan reefs with contrasting bleaching, temperature and shading histories. Mol Ecol 13: 2445-2458
Fabricius KE (2005) Effects of terrestrial runoff on the ecology of corals and coral reefs: review and synthesis. Mar Pollut Bull 50: 125-146
Falkowski P, Dubinsky Z, Muscatine L, McCloskey LR (1993) Population control in symbiotic corals. Biological Science 43: 606-611
Ferrier-Pages C, Gattuso JP, Dallot S, Jaubert J (2000) Effect of nutrient enrichment on growth and photosynthesis of the zooxanthellate coral Stylophora pistillata. Coral Reefs 19: 103-113
Ferrier-Pagès C, Rottier C, Beraud E, Levy O (2010) Experimental assessment of the feeding effort of three scleractinian coral species during a thermal stress: Effect on the rates of photosynthesis. J Exp Mar Biol Ecol 390: 118-124

Finkel ZV (2001) Light absorption and size scaling of light-limited metabolism in marine diatoms. Limnol Oceanogr 46: 86-94
Finney JC, Pettay DT, Sampayo EM, Warner ME, Oxenford HA, LaJeunesse TC (2010) The relative significance of host-habitat, depth, and geography on the ecology, endemism, and speciation of coral endosymbionts in the genus *Symbiodinium.* Microb Ecol 60: 250-263
Fitt W (1985) Effect of different strains of the zooxanthella *Symbiodinium microadriaticum* on growth and survival of their coelenterate and molluscan hosts. Proc Fith Intl Coral Reef Symp 6: 131-136
Fitt W, Brown BE, Warner M, Dunne R (2001) Coral bleaching: interpretation of thermal tolerance limits and thermal thresholds in tropical corals. Coral Reefs 20: 51-65
Fitt WK, McFarland FK, Warner ME, Chilcoat GC (2000) Seasonal patterns of tissue biomass and densities of symbiotic dinoflagellates in reef corals and relation to coral bleaching. Limnol Oceanogr 45: 677-685
Fitt WK, Gates RD, Hoegh-Guldberg O, Bythell JC, Jatkar A, Grottoli AG, Gomez M, Fisher P, Lajuenesse TC, Pantos O (2009) Response of two species of Indo-Pacific corals, *Porites cylindrica* and *Stylophora pistillata*, to short-term thermal stress: The host does matter in determining the tolerance of corals to bleaching. J Exp Mar Biol Ecol 373: 102-110
Folch J, Lees M, Sloane-Stanley GH (1957) A simple method for the isolation and purification of total lipids from animal tissues. J Biol Chem 226: 497-509
Furman BT, Heck KL (2008) Effects of nutrient enrichment and grazers on coral reefs: an experimental assessment. Mar Ecol Prog Ser 363: 89-101
Gao K, Helbling EW, Hader D-P, Hutchins DA (2012) Responses of marine primary producers to interactions between ocean acidification, solar radiation, and warming. Mar Ecol Prog Ser 470: 167-189
Gavery MR, Roberts SB (2014) A context dependent role for DNA methylation in bivalves. Briefings in functional genomics elt054
Gibbin EM, Davy SK (2014) The Photo-physiological response of a model cnidarian-dinoflagellate symbiosis to CO_2-induced acidification at the cellular level. J Exp Mar Biol Ecol 457: 1-7
Gigova L, Ivanova N, Gacheva G, Andreeva R, Furnadzhieva S (2012) Response of *Trachydiscus minutus* (Xanthophyceae) to temperature and light. J Phycol 48: 85-93
Glastad KM, Hunt BG, Yi SV, Goodisman MAD (2011) DNA methylation in insects: on the brink of the epigenomic era. Insect Mol Biol 20: 553-565
Golbuu Y, Victor S, Penland L, Idip Jr D, Emaurois C, Okaji K, Yukihira H, Iwase A, Van Woesik R (2007a) Palau's coral reefs show differential habitat recovery following the 1998-bleaching event. Coral Reefs 26: 319-332
Golbuu Y, Victor S, Penland L, Idip D, Emaurois C, Okaji K, Yukihira H, Iwase A, Woesik R (2007b) Palau's coral reefs show differential habitat recovery following the 1998-bleaching event. Coral Reefs 26: 319-332
Gorbunov MY, Falkowski PG Fluorescence induction and relaxation (FIRe) technique and instrumentation for monitoring photosynthetic processes and primary production in aquatic ecosystems. (eds), Allen Press Lawrence, KS, USA. pp 1029-1031, pp 1029-1031
Goreau T (1959) The physiology of skeletal formation in corals. I. A method for

measuring the rate of calcium deposition by corals under different conditions. Biol Bull 116: 59-75
Goulet TL, Cook CB, Goulet D (2005) Effect of short-term exposure to elevated temperatures and light levels on photosynthesis of different host-symbiont combinations in the *Aiptasia pallida/Symbiodinium* symbiosis. Limnol Oceanogr 50: 1490-1498
Grottoli AG, Rodrigues LJ, Palardy JE (2006) Heterotrophic plasticity and resilience in bleached corals. Nature 440: 1186-1189
Grottoli AG, Rodrigues LJ, Juarez C (2004) Lipids and stable carbon isotopes in two species of Hawaiian corals, *Porites compressa* and *Montipora verrucosa*, following a bleaching event. Mar Biol 145: 621-631
Grottoli AG, Warner ME, Levas SJ, Aschaffenburg MD, Schoepf V, McGinley M, Baumann J, Matsui Y (2014) The cumulative impact of annual coral bleaching can turn some coral species winners into losers. Glob Chang Biol DOI: 10.1111/gcb.12658
Grottoli AG, Rodrigues LJ (2011) Bleached *Porites compressa* and *Montipora capitata* corals catabolize δ13C-enriched lipids. Coral Reefs 30: 687-692
Grover R, Maguer JF, Allemand D, Ferrier-Pages C (2003) Nitrate uptake in the scleractinian coral Stylophora pistillata. Limnol Oceanogr 48: 2266-2274
Guinotte JM, Fabry VJ (2008) Ocean acidification and its potential effects on marine ecosystems. Ann N Y Acad Sci 1134: 320-342
Halsey KH, O'Malley RT, Graff JR, Milligan AJ, Behrenfeld MJ (2013) A common partitioning strategy for photosynthetic products in evolutionarily distinct phytoplankton species. New Phytol 198: 1030-1038
Hawkins TD, Krueger T, Wilkinson SP, Fisher PL, Davy SK (2015) Antioxidant responses to heat and light stress differ with habitat in a common reef coral. Coral Reefs DOI 10.1007//s00338-015
Hawkins TD, Hagemeyer JCG, Hoadley KD, Marsh AG, Warner ME (2016) Partitioning of Respiration in an Animal-Algal Symbiosis: Implications for Different Aerobic Capacity Between< i> Symbiodinium spp. Frontiers in Physiology 7: 128
Head JA (2014) Patterns of DNA methylation in animals: an ecotoxicological perspective. Integrative and comparative biology icu025
Helbling EW, Buma AGJ, Boelen P, Van der Strate HJ, Giordanino M, Villafane VE (2011) Increase in Rubisco activity and gene expression due to elevated temperature partially counteracts ultraviolet radiation-–induced photoinhibition in the marine diatom *Thalassiosira weissflogii*. Limnol Oceanogr 56: 1330-1342
Helmuth BST, Timmerman BEH, Sebens KP (1997) Interplay of host morphology and symbiont microhabitat in coral aggregations. Mar Biol 130: 1-10
Hennige SJ, Suggett DJ, Warner ME, McDougall KE, Smith DJ (2009) Photobiology of *Symbiodinium* revisited: bio-physical and bio-optical signatures. Coral Reefs 28: 179-195
Hennige SJ, McGinley MP, Grottoli AG, Warner ME (2011) Photoinhibition of *Symbiodinium* spp. within the reef corals *Montastraea faveolata* and *Porites astreoides*: implications for coral bleaching. Mar Biol 158: 2515-2526
Hill R, Larkum AWD, Frankart C, Kuhl M, Ralph PJ (2004) Loss of functional Photosystem II reaction centres in zooxanthellae of corals exposed to bleaching

conditions: using fluorescence rise kinetics. Photosynthesis Research 82: 59-72
Hill R, Larkum AWD, Prášil O, Kramer DM, Szabó M, Kumar V, Ralph PJ Light-induced dissociation of antenna complexes in the symbionts of scleractinian corals correlates with sensitivity to coral bleaching. Coral Reefs 1-13
Hill R, Brown CM, DeZeeuw K, Campbell DA, Ralph PJ (2011) Increased rate of D1 repair in coral symbionts during bleaching is insufficient to counter accelerated photo-inactivation. Limnol Oceangr 56: 139-146
Hoadley KD, Pettay DT, Grottoli A, Cai WJ, Melman TF, Schoepf V, Hu X, Li Q, Xu H, Wang Y, Matsui Y, Baumann J, Warner ME (2015a) Physiological response to elevated temperature and pCO2 varies across four Pacific coral species: Understanding the unique host+ symbiont response. Sci Rep 5, 18371; doi: 10.1038/srep18371:
Hoadley KD, Pettay DT, Dodge D, Warner ME (2016) Contrasting physiological plasticity in response to environmental stress within different cnidarians and their respective symbionts. Coral Reefs 1-14
Hoadley KD, Rollison D, Pettay DT, Warner ME (2015b) Differential carbon utilization and asexual reproduction under elevated pCO2 conditions in the model anemone, *Exaiptasia pallida*, hosting different symbionts. Limnol Oceanogr 60: 2108-2120
Hoadley KD, Szmant AM, Pyott SJ (2011) Circadian clock gene expression in the coral *Favia fragum* over diel and lunar reproductive cycles. PloS one 6: DOI: 10.1371/journal.pone.0019755
Hoegh-Guldberg O, Bruno JF (2010) The impact of climate change on the world's marine ecosystems. Science 328: 1523-1528
Hoegh-Guldberg O (1999) Climate change, coral bleaching and the future of the world's coral reefs. Marine Freshwater Research 50: 839-866
Hoegh-Guldberg O, Mumby PJ, Hooten AJ, Steneck RS, Greenfield P, Gomez E, Harvell CD, Sale PF, Edwards AJ, Caldeira K, Knowlton N, Eakin CM, Iglesias-Prieto R, Muthiga N, Bradbury RH, Dubi A, Hatziolos ME (2007) Coral reefs under rapid climate change and ocean acidification. Science 318: 1737-1742
Hoegh-Guldberg O, Williamson J (1999) Availability of two forms of dissolved nitrogen to the coral *Pocillopora damicornis* and its symbiotic zooxanthellae. Mar Biol 133: 561-570
Hofmann GE, Barry JP, Edmunds PJ, Gates RD, Hutchins DA, Klinger T, Sewell MA (2010) The effect of ocean acidification on calcifying organisms in marine ecosystems: an organism-to-ecosystem perspective. Annu Rev Ecol Evol Syst 41: 127-147
Holcomb M, McCorkle DC, Cohen AL (2010) Long-term effects of nutrient and CO_2 enrichment on the temperate coral *Astrangia poculata* (Ellis and Solander, 1786). J Exp Mar Biol Ecol 386: 27-33
Hoogenboom MO, Campbell DA, Beraud E, DeZeeuw K, Ferrier-Pagès C (2012) Effects of light, food availability and temperature stress on the function of photosystem II and photosystem I of coral symbionts. PLoS one 7: e30167-e30167
Howells EJ, Abrego D, Meyer E, Kirk NL, Burt JA (2016) Host adaptation and unexpected symbiont partners enable reef building corals to tolerate extreme temperatures. Global change biology
Hughes TP, Baird AH, Bellwood DR, Card M, Connolly SR, Folke C, Grosberg R,

Hoegh-Guldberg O, Jackson JBC, Kleypas J, Lough JM, Marshall P, Nystrom M, Palumbi SR, Pandolfi JM, Rosen B, Roughgarden J (2003) Climate change, human impacts, and the resilience of coral reefs. Science 301: 929-933

Hughes TP, Connell JH (1999) Multiple stressors on coral reefs: A long-term perspective. Limnol Oceanogr 44: 932-940

Hurd CL, Hepburn CD, Currie KI, Raven JA, Hunter KA (2009) Testing the effects of ocean acidification on algal metabolism: considerations for experimental design. J Phycol 45: 1236-1251

Hutchins DA, Fu FX, Zhang Y, Warner ME, Feng Y, Portune K, Bernhardt PW, Mulholland MR (2007) CO_2 control of *Trichodesmium* N_2 fixation, photosynthesis, growth rates, and elemental ratios: Implications for past, present, and future ocean biogeochemistry. Limnol Oceanogr 52: 1293-1304

Iglesias-Prieto R, Trench RK (1997) Acclimation and adaptation to irradiance in symbiotic dinoflagellates. II. Response of chlorophyll-protein complexes to different photon-flux densities. Mar Biol 130: 23-33

Iglesias-Rodriguez MD, Halloran PR, Rickaby REM, Hall IR, Colmenero-Hidalgo E, Gittins JR, Green DRH, Tyrrell T, Gibbs SJ, von D, P, Rehm E, Armbrust EV, Boessenkool KP (2008) Phytoplankton calcification in a high-CO_2 world. Science 320: 336-340

IPCC (2013) Summary for Policymakers. In: *C*limate Change 2013: The Physical Science Basis. Contribution of Working Group I to the Fifth Assessment Report of the Intergovernmental Panel on Climate Change. Cambridge University Press, Cambridge, United Kingdom and New York, NY, USA. (ed), Groupe d'experts intergouvernemental sur l'evolution du climat/Intergovernmental Panel on Climate Change-IPCC, C/O World Meteorological Organization, 7bis Avenue de la Paix, CP 2300 CH-1211 Geneva 2 (Switzerland),

Iwase A, Sakai K, Suzuki A, van Woesik R (2008) Phototropic adjustment of the foliaceous coral< i> Echinopora lamellosa in Palau. Est Coast Shelf Sci 77: 672-678

Jelinek J, Liang S, Lu Y, He R, Ramagli LS, Shpall EJ, Estecio MRH, Issa J-PJ (2012) Conserved DNA methylation patterns in healthy blood cells and extensive changes in leukemia measured by a new quantitative technique. Epigenetics 7: 1368-1378

Jin P, Gao K, Villafae VE, Campbell DA, Helbling EW (2013) Ocean acidification alters the photosynthetic responses of a coccolithophorid to fluctuating ultraviolet and visible radiation. Plant Physiol 162: 2084-2094

Johannes RE, Wiebe WJ (1970) Method for determination of coral tissue biomass and composition. Limnol Oceanogr 15:822-824

Jokiel PL, Margos JW, Franzisket L (1978) Coral growth buoyant weight technique. UNESCO, Paris, pp 529-542

Jones A, Berkelmans R (2010a) Potential Costs of Acclimatization to a Warmer Climate: Growth of a Reef Coral with Heat Tolerant vs. Sensitive Symbiont Types. Plos One 5: ARTN e10437

Jones A, Berkelmans R (2010b) Potential costs of acclimatization to a warmer climate: growth of a reef coral with heat tolerant vs. sensitive symbiont types. PLoS One 5: e10437

Kaniewska P, Campbell PR, Kline DI, Rodriguez-Lanetty M, Miller DJ, Dove S, Hoegh-

Guldberg O (2012) Major cellular and physiological impacts of ocean acidification on a reef building coral. PLoS one 7 [DOI: 10.1371/journal.pone.0034659]
Kaniewska P, Anthony KRN, Hoegh-Guldberg O (2008) Variation in colony geometry modulates internal light levels in branching corals, Acropora humilis and Stylophora pistillata. Mar Biol 155: 649-660
Kaniewska P, Chan C-KK, Kline D, Ling EYS, Rosic N, Edwards D, Hoegh-Guldberg O, Dove S (2015) Transcriptomic changes in coral holobionts provide insights into physiological challenges of future climate and ocean change. PloS one 10: e0139223
Kaniewska P, Magnusson SH, Anthony KRN, Reef R, Kühl M, Hoegh-Guldberg O (2011) Importance of macro- versus microstructure in modulating light levels inside coral colonies. J Phycol 47: 846-860
Keller TE, Han P, Soojin VY (2015) Evolutionary Transition of Promoter and Gene Body DNA Methylation across Invertebrate-Vertebrate Boundary. Mol Biol Evol msv345
Kemp DW, Cook CB, LaJeunesse TC, Brooks WR (2006) A comparison of the thermal bleaching responses of the zoanthid Palythoa caribaeorum from three geographically different regions in south Florida. J Exp Mar Biol Ecol 335: 266-276
Kenkel CD, Goodbody Gringley G, Caillaud D, Davies SW, Bartels E, Matz MV (2013) Evidence for a host role in thermotolerance divergence between populations of the mustard hill coral (Porites astreoides) from different reef environments. Mol Ecol 22: 4335-4348
Key T, McCarthy A, Campbell DA, Six C, Roy S, Finkel ZV (2010) Cell size trade-offs govern light exploitation strategies in marine phytoplankton. Environ Microbiol 12: 95-104
Kirk JTO (1994) Light and photosynthesis in aquatic ecosystems. Cambridge University Press, Cambridge
Kitahara MV, Lin M-F, Forêt S, Huttley G, Miller DJ, Chen CA (2014) The "Naked Coral" Hypothesis Revisited–Evidence for and Against Scleractinian Monophyly. PloS one 9 [DOI: 10.1371/journal.pone.0094774]
Koch M, Bowes G, Ross C, Zhang X (2013) Climate change and ocean acidification effects on seagrasses and marine macroalgae. Glob Change Biol 19: 103-132
Kolber Z, Falkowski P (1998) Measurements of variable chlorophyll fluorescence using fast repetition rate techniques: defining methodology and experimental protocols. Biochim Biophys 1367: 88-107
Krueger T, Hawkins TD, Becker S, Pontasch S, Dove S, Hoegh-Guldberg O, Leggat W, Fisher PL, Davy SK (2015) Differential coral bleaching—-Contrasting the activity and response of enzymatic antioxidants in symbiotic partners under thermal stress. Comparative Biochemistry and Physiology Part A: Molecular & Integrative Physiology 190: 15-25
Kucharski R, Maleszka J, Foret S, Maleszka R (2008) Nutritional control of reproductive status in honeybees via DNA methylation. Science 319: 1827-1830
Kuguru B, Achituv Y, Gruber DF, Tchernov D (2010) Photoacclimation mechanisms of corallimorpharians on coral reefs: photosynthetic parameters of zooxanthellae and host cellular responses to variation in irradiance. J Exp Mar Biol Ecol 394: 53-62
Kwiatkowski L, Cox P, Halloran PR, Mumby PJ, Wiltshire AJ (2015) Coral bleaching

under unconventional scenarios of climate warming and ocean acidification. Nature Clim Change 5: 771-781
LaJeunesse TC, Loh WKW, van Woesik R, Hoegh-Guldberg O, Schmidt GW, Fitt WK (2003) Low symbiont diversity in southern Great Barrier Reef corals, relative to those of the Caribbean. Limnol Oceanogr 48: 2046-2054
LaJeunesse TC, Reyes-Bonilla H, Warner ME (2007a) Spring bleaching among *Pocillopora* in the Sea of Cortez, eastern Pacific. Coral Reefs 26: 265-270
LaJeunesse TC (2001) Investigating the biodiversity, ecology, and phylogeny of endosymbiotic dinoflagellates in the genus *Symbiodinium* using the ITS region: In search of a "species" level marker. J Phycol 37: 866-880
LaJeunesse TC, Reyes-Bonilla H, Warner ME (2007b) Spring "bleaching" among Pocillopora in the Sea of Cortez, eastern Pacific. Coral Reefs 26: 265-270
Lajeunesse TC, Smith R, Walther M, Pinzon J, Pettay DT, McGinley M, Aschaffenburg M, Medina-Rosas P, Cupul-Magana AL, Perez AL, Reyes-Bonilla H, Warner ME (2010) Host-symbiont recombination versus natural selection in the response of coral-dinoflagellate symbioses to environmental disturbance. Proc Biol Sci
LaJeunesse TC, Smith RT, Finney J, Oxenford H (2009a) Outbreak and persistence of opportunistic symbiotic dinoflagellates during the 2005 Caribbean mass coral 'bleaching' event. Proc Biol Sci 276: 4139-4148
LaJeunesse TC, Smith RT, Finney J, Oxenford H (2009b) Outbreak and persistence of opportunistic symbiotic dinoflagellates during the 2005 Caribbean mass coral 'bleaching' event. Proc R Soc B 276: 4139-4148
LaJeunesse TC, Parkinson JE, Reimer JD (2012) A genetics‐based description of *Symbiodinium minutum* sp. nov. and *S. psygmophilum* sp. nov.(Dinophyceae), two dinoflagellates symbiotic with cnidaria. J Phycol 48: 1380-1391
LaJeunesse TC, Thornhill DJ (2011) Improved resolution of reef-coral endosymbiont (Symbiodinium) species diversity, ecology, and evolution through psbA non-coding region genotyping. PLoS One 6: e29013
LaJeunesse TC, Wham DC, Pettay DT, Parkinson JE, Keshavmurthy S, Chen CA (2014) Ecologically differentiated stress-tolerant endosymbionts in the dinoflagellate genus *Symbiodinium (Dinophyceae)* Clade D are different species. Phycologia 53: 305-319
Langdon C, Atkinson MJ (2005) Effect of elevated pCO_2 on photosynthesis and calcification of corals and interactions with seasonal change in temperature/irradiance and nutrient enrichment. J Geophys Res 110: DOI: 10.1029/2004JC002576
Law JA, Jacobsen SE (2010) Establishing, maintaining and modifying DNA methylation patterns in plants and animals. Nature Reviews Genetics 11: 204-220
Leal MC, Hoadley K, Pettay DT, Grajales A, Calado R, Warner ME (2015) Symbiont type influences trophic plasticity of a model cnidarian?dinoflagellate symbiosis. J Exp Biol 218: 858-863
Leggat W, Marendy EM, Baillie B, Whitney SM, Ludwig M, Badger MR, Yellowlees D (2002) Dinoflagellate symbioses: strategies and adaptations for the acquisition and fixation of inorganic carbon. Funct Plant Biol 29: 309-322
Leggat W, Seneca F, Wasmund K, Ukani L, Yellowlees D, Ainsworth TD (2011) Differential responses of the coral host and their algal symbiont to thermal stress.

PloS one 6: DOI: 10.1371/journal.pone.0026687
Lehnert EM, Burriesci MS, Pringle JR (2012) Developing the anemone *Aiptasia* as a tractable model for cnidarian-dinoflagellate symbiosis: the transcriptome of aposymbiotic *A. pallida*. BMC genomics 13: DOI: 10.1186/1471-2164
Lesser M (1997) Oxidative stress causes coral bleaching during exposure to elevated temperatures. Coral Reefs 16: 187-192
Lesser MP (2006) Oxidative stress in marine environments: biochemistry and physiological ecology. Annu Rev Physiol 68: 253-278
Lesser MP (2011) Coral bleaching: causes and mechanismsCoral reefs: an ecosystem in transition. Springer, 405-419
Levas S, Grottoli AG, Warner ME, Cai W-J, Bauer J, Schoepf V, Baumann JH, Matsui Y, Gearing C, Melman TF (2015) Organic carbon fluxes mediated by corals at elevated pCO_2 and temperature. Mar Ecol Prog Ser 519: 153-164
Levas SJ, Grottoli AG, Hughes A, Osburn CL, Matsui Y (2013) Physiological and biogeochemical traits of bleaching and recovery in the mounding species of coral *Porites lobata*: Implications for resilience in mounding corals. PloS one 8: DOI: 10.1371/journal.pone.0063267
Levy O, Appelbaum L, Leggat W, Gothlif Y, Hayward DC, Miller DJ, Hoegh-Guldberg O (2007) Light-responsive cryptochromes from a simple multicellular animal, the coral *Acropora millepora*. Sci Signal 318: 467-472
Lewis E, Wallace D, Allison LJ (1998) Program developed for CO_2 system calculations. Carbon Dioxide Information Analysis Center, managed by Lockheed Martin Energy Research Corporation for the US Department of Energy,
Li G, Campbell DA (2013) Rising CO_2 interacts with growth light and growth rate to alter photosystem II photoinactivation of the coastal diatom *Thalassiosira pseudonana*. PLoS one 8: DOI: 10.1371/journal.pone.0055562
Lomas MW, Glibert PM (1999) Temperature regulation of nitrate uptake: a novel hypothesis about nitrate uptake and reduction in cool-water diatoms. Limnol Oceanogr 44: 556-572
Loya Y, Sakai K, Yamazato K, Nakano Y, Sambali H, van Woesik R (2001) Coral bleaching: the winners and the losers. Ecol Lett 4: 122-131
Luthi D, Le Floch M, Bereiter B, Blunier T, Barnola JM, Siegenthaler U, Raynaud D, Jouzel J, Fischer H, Kawamura K, Stocker TF (2008) High-resolution carbon dioxide concentration record 650,000-800,000 years before present. Nature 453: 379-382
Majewski J, Ott J (2002) Distribution and characterization of regulatory elements in the human genome. Genome research 12: 1827-1836
Mandrioli M (2007) A new synthesis in epigenetics: towards a unified function of DNA methylation from invertebrates to vertebrates. Cellular and molecular life sciences 64: 2522-2524
Manzello DP (2015) Rapid recent warming of coral reefs in the Florida Keys. Sci Rep 5: doi:10.1038/srep16762
Marsh AG, Hoadley KD, Warner ME (2016) Distribution of CpG Motifs in Upstream Gene Domains in a Reef Coral and Sea Anemone: Implications for Epigenetics in Cnidarians. PloS one 11: e0150840
Marsh AG, Pasqualone AA (2013) DNA methylation and temperature stress in an

Antarctic polychaete, Spiophanes tcherniai. Frontiers in physiology 5: 173-173
Marsh J (1970) Primary productivity of reef-building calcareous and red algae. Ecology 55: 255-263
Marubini F, Atkinson MJ (1999) Effects of lowered pH and elevated nitrate on coral calcification. Mar Ecol Prog Ser 188: 117-121
Marubini F, Davies PS (1996) Nitrate increases zooxanthellae population density and reduces skeletogenesis in corals. Mar Biol 127: 319-328
McCarthy DJ, Chen Y, Smyth GK (2012) Differential expression analysis of multifactor RNA-Seq experiments with respect to biological variation. Nucleic Acids Res gks042
Medina M, Collins AG, Takaoka TL, Kuehl JV, Boore JL (2006) Naked corals: skeleton loss in Scleractinia. Proceedings of the National Academy of Sciences 103: 9096-9100
Middlebrook R, Anthony KR, Hoegh-Guldberg O, Dove S (2010) Heating rate and symbiont productivity are key factors determining thermal stress in the reef-building coral *Acropora formosa.* J Exp Biol 213: 1026-1034
Miller DJ, Ball EE, Forêt S, Satoh N (2011) Coral genomics and transcriptomics—ushering in a new era in coral biology. J Exp Mar Biol Ecol 408: 114-119
Moya A, Tambutte S, Bertucci A, Tambutte E, Lotto S, Vullo D, Supuran CT, Allemand D, Zoccola D (2008) Carbonic anhydrase in the scleractinian coral *Stylophora pistillata*: characterization, localization, and role in biomineralization. J Biol Chem 283: 25475-25484
Moya A, Huisman L, Ball EE, Hayward DC, Grasso LC, Chua CM, Woo HN, Gattuso JP, Forêt S, Miller DJ (2012) Whole transcriptome analysis of the coral *Acropora millepora* reveals complex responses to CO_2-driven acidification during the initiation of calcification. Mol Ecol 21: 2440-2454
Muller-Parker G (1984) Photosynthesis-irradiance responses and photosynthetic periodicity in the sea-anemone *Aiptasia-pulchella* and its zooxanthellae. Mar Biol 82: 225-232
Muller-Parker G, McCloskey LR, Hoegh-Guldberg O, McAuley PJ (1994) The effect of ammonium enrichment on animal and algal biomass of the coral *Pocillopora damicornis*. Pac Sci 48: 273-283
Mumby PJ, Chisholm JRM, Edwards AJ, Andrefouet S, Jaubert J (2001) Cloudy weather may have saved Society Island reef corals during the 1998 ENSO event. Marine Ecology-Progress Series 222: 209-216
Nishiyama Y, Yamamoto H, Allakhverdiev SI, Inaba M, Yokota A, Murata N (2001) Oxidative stress inhibits the repair of photodamage to the photosynthetic machinery. EMBO J 20: 5587-5594
Norström AV, Nyström M, Lokrantz J, Folke C (2009) Alternative states on coral reefs: beyond coral-macroalgal phase shifts. Mar Ecol Prog Ser 376: 295-306
Norstrom AV, Nystrom M, Lokrantz J, Folke C (2009) Alternative states on coral reefs: beyond coral-macroalgal phase shifts. Mar Ecol Prog Ser 376: 295-306
Oakley CA, Hopkinson BM, Schmidt GW (2014a) Mitochondrial terminal alternative oxidase and its enhancement by thermal stress in the coral symbiont *Symbiodinium.* Coral Reefs 33: 543-552
Oakley CA, Ameismeier MF, Peng L, Weis VM, Grossman AR, Davy SK (2015)

Symbiosis induces widespread changes in the proteome of the model cnidarian Aiptasia. Cellular microbiology
Oakley CA, Schmidt GW, Hopkinson BM (2014b) Thermal responses of Symbiodinium photosynthetic carbon assimilation. Coral Reefs 33: 501-512
Ogawa D, Bobeszko T, Ainsworth T, Leggat W (2013) The combined effects of temperature and CO_2 lead to altered gene expression in *Acropora aspera*. Coral Reefs 32: 895-907
Okamoto OK, Robertson DL, Fagan TF, Hastings JW, Colepicolo P (2001) Different regulatory mechanisms modulate the expression of a dinoflagellate iron-superoxide dismutase. J Biol Chem 276: 19989-19993
Oliver TA, Palumbi SR (2011a) Do fluctuating temperature environments elevate coral thermal tolerance. Coral Reefs 30: 429-440
Oliver TA, Palumbi SR (2011b) Many corals host thermally resistant symbionts in high-temperature habitat. Coral Reefs 30: 241-250
Olson CE, Roberts SB (2014) Genome-wide profiling of DNA methylation and gene expression in Crassostrea gigas male gametes. Front Physiol 5: 224
Osovitz CJ, Hofmann GE (2005) Thermal history-dependent expression of the HSP70 gene in purple sea urchins: Biogeographic patterns and the effect of temperature acclimation. J Exp Mar Biol Ecol 327: 134-143
Palumbi SR, Barshis DJ, Traylor-Knowles N, Bay RA (2014) Mechanisms of reef coral resistance to future climate change. Science 344: 895-898
Parker MS, Armbrust E (2005) Synergistic effects of light, temperature, and nitrogen source on transcription of genes for carbon and nitrogen metabolism in the centric diatom *Thalassiosira pseudonana* (Baccillariophyceae). J Phycol 41: 1142-1153
Parkinson JE, Banaszak AT, Altman NS, LaJeunesse TC, Baums IB (2015) Intraspecific diversity among partners drives functional variation in coral symbioses. Sci Rep 5:
Pettay DT, LaJeunesse TC (2013) Long-range dispersal and high-latitude environments influence the population structure of a "stress-tolerant" dinoflagellate endosymbiont. PLOS ONE 8: DOI: 10.1371/journal.pone.0079208
Pettay DT, Wham DC, Smith RT, Iglesias-Prieto R, LaJeunesse TC (2015) Microbial invasion of the Caribbean by an Indo-Pacific coral zooxanthella. Proceedings of the National Academy of Sciences 112: 7513-7518
Pettay DT (2011) Diversity, Stability and Connectivity of Symbiodinium Populations at Various Spatial Scales. pp
Pettay DT, Lajeunesse TC (2007) Microsatellites from clade B *Symbiodinium spp*. specialized for Caribbean corals in the genus *Madracis*. Mol Ecol Notes 7: 1271-1274
Pettay DT, Lajeunesse TC (2009) Microsatellite loci for assessing genetic diversity, dispersal and clonality of coral symbionts in 'stress-tolerant' clade D *Symbiodinium*. Mol Ecol Resour 9: 1022-1025
Porra RJ, Thompson WA, Kriedemann PE (1989) Determination of accurate extinction coefficients and simultaneous equations for assaying chlorophylls *a* and *b* extracted with four different solvents: verification of the concentration of chlorophyll standards by atomic absorption spectroscopy. Biochim Biophys Acta 975: 384-394
Ragni M, Airs RL, Hennige SJ, Suggett DJ, Warner ME, Geider RJ (2010) PSII photoinhibition and photorepair in *Symbiodinium* (Pyrrhophyta) differs between

thermally tolerant and sensitive phylotypes. Mar Ecol Prog Ser 406: 57-70
Rands ML, Loughman BC, Douglas AE (1993) The symbiotic interface in an alga invertebrate symbiosis. P Roy Soc Lond B Bio 253: 161-165
Renaud SM, Zhou HC, Parry DL, Thinh L-V, Woo KC (1995) Effect of temperature on the growth, total lipid content and fatty acid composition of recently isolated tropical microalgae *Isochrysis sp., Nitzschia closterium, Nitzschia paleacea,* and commercial species *Isochrysis sp.*(clone T. ISO). J Appl Phycol 7: 595-602
Reynaud S, Leclercq N, Romaine-Lioud S, Ferrier-Pages C, Jaubert J, Gattuso JP (2003) Interacting effects of CO_2 partial pressure and temperature on photosynthesis and calcification in a scleractinian coral. Glob Chang Biol 9: 1660-1668
Roberts SB, Gavery MR (2012) Is there a relationship between DNA methylation and phenotypic plasticity in invertebrates. Front Physiol 2: 116
Roberty S, Berne N, Bailleul B, Cardol P (2014) PSI Mehler reaction is the main alternative photosynthetic electron pathway in *Symbiodinium sp.,* symbiotic dinoflagellates of cnidarians. New Phytol 204: 81-91
Robinson MD, McCarthy DJ, Smyth GK (2010) edgeR: a Bioconductor package for differential expression analysis of digital gene expression data. Bioinformatics 26: 139-140
Roche RC, Abel RL, Johnson KG, Perry CT (2011) Spatial variation in porosity and skeletal element characteristics in apical tips of the branching coral *Acropora pulchra* (Brook 1891). Coral Reefs 30: 195-201
Rodolfo-Metalpa R, Martin S, Ferrier-Pagès C, Gattuso J-P (2010) Response of the temperate coral *Cladocora caespitosa* to mid-and long-term exposure to pCO_2 and temperature levels projected for the year 2100 AD. Biogeosciences 7: 289-300
Rodrigues LJ, Grottoli AG (2007) Energy reserves and metabolism as indicators of coral recovery from bleaching. Limnol Oceanogr 52: 1874-1882
Rodríguez-Román, Iglesias-Prieto R (2005) Regulation of photochemical activity in cultured symbiotic dinoflagellates under nitrate limitation and deprivation. Mar Biol 146: 1063-1073
Rodriguez-Román A, Hernández-Pech X, Thomé PE, Enriquez S, Iglesias-Prieto R (2006) Photosynthesis and light utilization in the Caribbean coral *Montastraea faveolata* recovering from a bleaching event. Limnol Oceanogr 51: 2702-2710
Rosic N, Kaniewska P, Chan C-KK, Ling EYS, Edwards D, Dove S, Hoegh-Guldberg O (2014) Early transcriptional changes in the reef-building coral Acropora aspera in response to thermal and nutrient stress. BMC genomics 15: 1052
Rosic NN, Pernice M, Rodriguez-Lanetty M, Hoegh-Guldberg O (2011a) Validation of housekeeping genes for gene expression studies in *Symbiodinium* exposed to thermal and light stress. Mar Biotechnol 13: 355-365
Rosic NN, Pernice M, Dove S, Dunn S, Hoegh-Guldberg O (2011b) Gene expression profiles of cytosolic heat shock proteins Hsp70 and Hsp90 from symbiotic dinoflagellates in response to thermal stress: possible implications for coral bleaching. Cell Stress Chaperon 16: 69-80
Comeau S, Edmunds PJ, Spindel NB, Carpenter RC (2013) The responses of eight coral reef calcifiers to increasing partial pressure of CO_2 do not exhibit a tipping point. Limnol Oceanogr 589: 388-398
Sampayo EM, Ridgeway T, Bongaerts P, Hoegh-Gulberg O (2008) Bleaching

susceptibility and mortality of corals are determined by fine-scale differences in symbiont type. Proc Natl Acad Sci USA 105: 10444-10449
Sampayo EM, Dove S, Lajeunesse TC (2009) Cohesive molecular genetic data delineate species diversity in the dinoflagellate genus *Symbiodinium*. Mol Ecol 18: 500-519
Santos SR, Gutierrez-Rodriguez C, Coffroth MA (2003) Phylogenetic identification of symbiotic dinoflagellates via length heteroplasmy in domain V of chloroplast large subunit (cp23S)-ribosomal DNA sequences. Mar Biotechnol 5: 130-140
Santos SR, Taylor DJ, Kinzie RA, Sakai K, Coffroth MA (2002) Evolution of length variation and heteroplasmy in the chloroplast rDNA of symbiotic dinoflagellates (Symbiodinium, Dinophyta) and a novel insertion in the universal core region of the large subunit rDNA. Phycologia 41: 311-318
Sarda S, Zeng J, Hunt BG, Soojin VY (2012) The evolution of invertebrate gene body methylation. Mol Biol Evol mss062
Saxonov S, Berg P, Brutlag DL (2006) A genome-wide analysis of CpG dinucleotides in the human genome distinguishes two distinct classes of promoters. Proceedings of the National Academy of Sciences 103: 1412-1417
Schoenberg D, Trench R (1980) Genetic variation in *Symbiodinium* (=*Gymnodinium*) *microadriaticum* Freudenthal, and specificity in its symbioses with marine invertebrates. I. Isoenzyme and soluble protein patterns of axenic cultures of *Symbiodinium microadriaticum*. Proc R Soc A 207: 405-427
Schoepf V, Grottoli AG, Warner ME, Cai WJ, Melman TF, Hoadley KD, Pettay DT, HU X, Li Q, Xu H, Wang Y, Matsui Y, Baumann JH (2013) Coral energy reserves and calcification in a high-CO_2 world at two temperatures. PLoS one 8 [DOI: 10.1371/journal.pone.0075049]
Schoepf V, Stat M, Falter JL, McCulloch MT (2015) Limits to the thermal tolerance of corals adapted to a highly fluctuating, naturally extreme temperature environment. Sci Rep 5:
Seneca FO, Foret S, Ball EE, Smith-Keune C, Miller DJ, van Oppen MJ (2010) Patterns of gene expression in a scleractinian coral undergoing natural bleaching. Mar Biotechnol 12: 594-604
Seveso D, Montano S, Strona G, Orlandi I, Galli P, Vai M (2013) Exploring the effect of salinity changes on the levels of Hsp60 in the tropical coral *Seriatopora caliendrum*. Mar Environ Res 90: 96-103
Shamberger KEF, Cohen AL, Golbuu Y, McCorkle DC, Lentz SJ, Barkley HC (2014) Diverse coral communities in naturally acidified waters of a Western Pacific reef. Geophys Res Lett 41: 499-504
Shick JM, Iglic K, Wells ML, Trick CG, Doyle J, Dunlap WC (2011) Responses to iron limitation in two colonies of Stylophora pistillata exposed to high temperature: Implications for coral bleaching. Limnol Oceangr 56: 813-828
Shick JM, Dowse HB (1985) Genetic basis of physiological variation in natural populations of sea anemones: Intra-and interclonal analyses of variance.
Silverstein RN, Cunning R, Baker AC (2015) Change in algal symbiont communities after bleaching, not prior heat exposure, increases heat tolerance of reef corals. Glob Chang Biol 21: 236-249
Smith DJ, Suggett DJ, Baker NR (2005) Is photoinhibition of zooxanthellae photosynthesis the primary cause of thermal bleaching in corals? Global Change

Biology 11: 1-11
Smith JE, Hunter CL, Smith CM (2010) The effects of top-down versus bottom-up control on benthic coral reef community structure. 163(2). Univ Calif San Diego, Scripps Inst Oceanog, La Jolla, CA 92093 USA
Smith LW, Barshis D, Birkeland C (2007) Phenotypic plasticity for skeletal growth, density and calcification of Porites lobata in response to habitat type. Coral Reefs 26: 559-567
Smith PK, Krohn RI, Hermanson GT, Mallia AK, Gartner FH, Provenzano MD, Fujimoto EK, Goeke NM, Olson BJ, Klenk DC (1985) Determination of protein concentration by the bicinchoninic acid method. Anal Biochem 150: 76-85
Steglich C, Behrenfeld M, Koblizek M, Claustre H, Penno S, Prasil O, Partensky F, Hess WR (2001) Nitrogen deprivation strongly affects Photosystem II but not phycoerythrin level in the divinyl-chlorophyll *b*-containing cyanobacterium *Prochlorococcus marinus*. Biochimica Et Biophysica Acta-Bioenergetics 1503: 341-349
Stimson J, Kinzie RA (1991) The temporal pattern and rate of release of zooxanthellae from the reef coral *Pocillopora damicornis* (Linnaeus) under nitrogen-enrichment and control conditions. J Exp Mar Biol Ecol 153: 63-74
Stimson JS (1987) Location, Quantity and Rate of Change in Quantity of Lipis in Tissue of Hawaiian Hermatypic Corals. Bull Mar Sci 41: 889-904
Suggett DJ, Hall‐Spencer JM, Rodolfo‐Metalpa R, Boatman TG, Payton R, Tye Pettay D, Johnson VR, Warner ME, Lawson T (2012a) Sea anemones may thrive in a high CO_2 world. Glob Chang Biol 18: 3015-3025
Suggett DJ, Warner ME, Smith DJ, Davey P, Hennige S, Baker NR (2008) Photosynthesis and production of hydrogen peroxide by *Symbiodinium* (Pyrrhophyta) phylotypes with different thermal tolerances. J Phycol 44: 948-956
Suggett DJ, Goyen S, Evenhuis C, Szabó M, Pettay DT, Warner ME, Ralph PJ (2015) Functional diversity of photobiological traits within the genus Symbiodinium appears to be governed by the interaction of cell size with cladal designation. New Phytol
Suggett DJ, MacIntyre HL, Kana TM, Geider RJ (2009) Comparing electron transport with gas exchange: parameterising exchange rates between alternative photosynthetic currencies for eukaryotic phytoplankton. Aquat Microb Ecol 56: 147-162
Suggett DJ, Dong LF, Lawson T, Lawrenz E, Torres L, Smith DJ (2012b) Light availability determines susceptibility of reef building corals to ocean acidification. Coral Reefs 32: 327-337
Suggett DJ, Oxborough K, Baker NR, MacIntyre HL, Kana TM, Geider RJ (2003) Fast repetition rate and pulse amplitude modulation chlorophyll a fluorescence measurements for assessment of photosynthetic electron transport in marine phytoplankton. Eur J Phycol 38: 371-384
Sunagawa S, Wilson EC, Thaler M, Smith ML, Caruso C, Pringle JR, Weis VM, Medina M, Schwarz JA (2009a) Generation and analysis of transcriptomic resources for a model system on the rise: the sea anemone *Aiptasia pallida* and its dinoflagellate endosymbiont. BMC Genomics 10: 258
Sunagawa S, Wilson E, Thaler M, Smith M, Caruso C, Pringle J, Weis V, Medina M,

Schwarz J (2009b) Generation and analysis of transcriptomic resources for a model system on the rise: the sea anemone Aiptasia pallida and its dinoflagellate endosymbiont. BMC genomics 10: 258
Swofford DL PAUP*, Phylogenetic analysis using parsimony (*and other methods). version 4.0b10, Sinauer, Sunderland, MA,
Takahashi S, Murata N (2008) How do environmental stresses accelerate photoinhibition? Trends Plant Sci 13: 178-182
Takahashi S, Nakamura T, Sakamizu M, van Woesik R, Yamasaki H (2004) Repair machinery of symbiotic photosynthesis as the primary target of heat stress for reef-building corals. Plant Cell Physiol *45*: 251-255
Takahashi S, Whitney S, Badger M (2009) Different thermal sensitivity of the repair of photodamaged photosynthetic machinery in cultured *Symbiodinium* species. Proc Natl Acad Sci USA 106: 3237-3242
Takahashi S, Yoshioka-Nishimura M, Nanba D, Badger MR (2013) Thermal acclimation of the symbiotic alga *Symbiodinium* spp. alleviates photobleaching under heat stress. Plant Physiol 161: 477-485
Thompson PA, Harrison PJ, Parslow JS (1991) Influence of irradiance on cell volume and carbon quota for ten species of marine phytoplankton. J Phycol 27: 351-360
Thornhill DJ, LaJeunesse TC, Kemp DW, Fitt WK, Schmidt GW (2006) Multi-year seasonal genotypic surveys of coral-algal symbioses reveal prevalent stability or post-bleaching reversion. Mar Biol 148: 711-722
Thornhill DJ, Xiang Y, Pettay DT, Zhong M, Santos SR (2013) Population genetic data of a model symbiotic cnidarian system reveal remarkable symbiotic specificity and vectored introductions across ocean basins. Mol Ecol 22: 4499-4515
Tkachenko KS, Wu B-J, Fang L-S, Fan T-Y (2007) Dynamics of a coral reef community after mass mortality of branching Acropora corals and an outbreak of anemones. Mar Biol 151: 185-194
Tolosa I, Treignier C, Grover R, Ferrier-Pages C (2011) Impact of feeding and short-term temperature stress on the content and isotopic signature of fatty acids, sterols, and alcohols in the scleractinian coral *Turbinaria reniformis*. Coral Reefs 30: 763-774
Tomascik T, Sander F (1987) Effects of eutrophication on reef-building corals. Mar Biol 94: 53-75
Toseland ADSJ, Daines SJ, Clark JR, Kirkham A, Strauss J, Uhlig C, Lenton TM, Valentin K, Pearson GA, Moulton V (2013) The impact of temperature on marine phytoplankton resource allocation and metabolism. Nat Clim Change 3: 979-984
Towanda T, Thuesen EV (2012a) Prolonged exposure to elevated CO_2 promotes growth of the algal symbiont *Symbiodinium muscatinei* in the intertidal sea anemone *Anthopleura elegantissima*. Open Biol 1: 615-621
Towanda T, Thuesen EV (2012b) Prolonged exposure to elevated CO_2 promotes growth of the algal symbiont *Symbiodinium muscatinei* in the intertidal sea anemone *Anthopleura elegantissima*. Open Biol 1: 615-621
Tremblay P, Fine M, Maguer JF, Grover R (2013) Ocean acidification increases photosynthate translocation in a coral–-dinoflagellates symbiosis. Biogeosciences 10: 83-109
Tremblay P, Grover R, Maguer JF, Legendre L, Ferrier-Pagès C (2012) Autotrophic carbon budget in coral tissue: a new 13C-based model of photosynthate

translocation. J Exp Biol 215: 1384-1393
Trench R (1993) Microalgal-invertebrate symbioses: a review. Endocytobiosis & Cell Resources 9: 135-175
Trimborn S, Thoms S, Petrou K, Kranz SA, Rost B (2014) Photophysiological responses of Southern Ocean phytoplankton to changes in CO_2 concentrations: Short-term versus acclimation effects. J Exp Mar Biol Ecol 451: 44-54
Ulstrup KE, Berkelmans R, Ralph PJ, van Oppen MJH (2006a) Variation in bleaching sensitivity of two coral species across a latitudinal gradient on the Great Barrier Reef: the role of zooxanthellae. Mar Ecol Prog Ser 314: 135-148
Ulstrup KE, Ralph PJ, Larkum AWD, Kühl M (2006b) Intra-colonial variability in light acclimation of zooxanthellae in coral tissues of Pocillopora damicornis. Mar Biol 149: 1325-1335
Ulstrup KE, Ralph PJ, Larkum AWD, Kuhl M (2006c) Intra-colonial variability in light acclimation of zooxanthellae in coral tissues of Pocillopora damicornis. Mar Biol 149: 1325-1335
Vega Thurber RL, Burkepile DE, Fuchs C, Shantz AA, McMinds R, Zaneveld JR (2014) Chronic nutrient enrichment increases prevalence and severity of coral disease and bleaching. Glob Chang Biol 20: 544-554
Vidal-Dupiol J, Zoccola D, Tambutté E, Grunau C, Cosseau C, Smith KM, Freitag M, Dheilly NM, Allemand D, Tambutté S (2013) Genes related to ion-transport and energy production are upregulated in response to CO_2-driven pH decrease in corals: new insights from transcriptome analysis. PloS one 8: DOI: 10.1371/journal.pone.0058652
Voolstra CR (2013) A journey into the wild of the cnidarian model system *Aiptasia* and its symbionts. Mol Ecol 22: 4366-4368
Wall CB, Fan TY, Edmunds PJ (2014) Ocean acidification has no effect on thermal bleaching in the coral *Seriatopora caliendrum*. Coral Reefs 33:119-130:
Wangpraseurt D, Larkum AWD, Ralph PJ, Kuhl M (2012) Light gradients and optical microniches in coral tissues. Frontiers in microbiology 3 [doi: 10.3389/fmicb.2012.00316]
Warner M, Fitt W, Schmidt G (1996) The effects of elevated temperature on the photosynthetic efficiency of zooxanthellae *in hospite* from four different species of reef coral: a novel approach. Plant Cell and Environment 19: 291-299
Warner M, Fitt W, Schmidt G (1999) Damage to photosystem II in symbiotic dinoflagellates: a determinant of coral bleaching. Proc Natl Acad Sci U S A 96: 8007-8012
Warner ME, Berry-Lowe S (2006) Differential xanthophyll cycling and photochemical activity in symbiotic dinoflagellates in multiple locations of three species of Caribbean coral. J Exp Mar Biol Ecol 339: 86-95
Weis VM, Reynolds WS (1999) Carbonic anhydrase expression and synthesis in the sea anemone *Anthopleura elegantissima* are enhanced by the presence of dinoflagellate symbionts. Physiol Biochem Zool 72: 307-316
Weis VM, Smith GJ, Muscatine L (1989) A CO_2 supply mechanism in zooxanthellate cnidarians - role of carbonic-anhydrase. Mar Biol 100: 195-202
Weis VM (1993) Effect of dissolved inorganic carbon concentration on the photosynthesis of the symbiotic sea anemone *Aiptasia pulchella* Carlgren: Role of

carbonic anhydrase. J Exp Mar Biol Ecol 174: 209-225
Weis VM (2008) Cellular mechanisms of Cnidarian bleaching: stress causes the collapse of symbiosis. J Exp Biol 211: 3059-3066
Weisz JB, Massaro AJ, Ramsby BD, Hill MS (2010) Zooxanthellar symbionts shape host sponge trophic status through translocation of carbon. Biol Bull-us 219: 189-197
Wham DC, Pettay DT, LaJeunesse TC (2011) Microsatellite loci for the host-generalist "zooxanthella" *Symbiodinium trenchi* and other Clade D *Symbiodinium*. Conserv Genet Resour 3: 541-544
Wiedenmann J, D''Angelo C, Smith EG, Hunt AN, Legiret F-E, Postle AD, Achterberg EP (2013) Nutrient enrichment can increase the susceptibility of reef corals to bleaching. Nature Clim Change 3: 160-164
Woesik R, Houk P, Isechal AL, Idechong JW, Victor S, Golbuu Y (2012) Climate change refugia in the sheltered bays of Palau: analogs of future reefs. Ecology and evolution 2: 2474-2484
Wooldridge SA (2009a) A new conceptual model for the warm-water breakdown of the coral-algae endosymbiosis. Mar Freshwater Res 60: 483-496
Wooldridge SA (2009b) A new conceptual model for the enhanced release of mucus in symbiotic reef corals during 'bleaching'conditions. Mar Ecol Prog Ser 396: 145-152
Xia JR, Gao KS (2005) Impacts of elevated CO_2 concentration on biochemical composition, carbonic anhydrase, and nitrate reductase activity of freshwater green algae. J Integr Plant Biol 47: 668-675
Yao W, Byrne RH (1998) Simplified seawater alkalinity analysis: Use of linear array spectrometers. Deep-Sea Res PT I 45: 1383-1392
Yellowlees D, Rees TA, Leggat W (2008) Metabolic interactions between algal symbionts and invertebrate hosts. Plant Cell Environ 31: 679-694
Ziegler M, Roder CM, B?chel C, Voolstra CR (2014) Limits to physiological plasticity of the coral Pocillopora verrucosa from the central Red Sea. Coral Reefs 33: 1115-1129
Zimmerman RC, Kohrs DG, Steller DL, Alberte RS (1997) Impacts of CO_2 enrichment on productivity and light requirements of Eelgrass. Plant Physiol 115: 599-607
Zoccola D, Tambutté E, Kulhanek E, Puverel S, Scimeca J-C, Allemand D, Tambutté S (2004) Molecular cloning and localization of a PMCA P-type calcium ATPase from the coral *Stylophora pistillata*. Biochim Biophys Acta (BBA) 1663: 117-126

Appendix A

CHAPTER 2: PHYSIOLOGICAL RESPONSE TO ELEVATED TEMPERATURE AND pCO_2 VARIES ACROSS FOUR PACIFIC CORAL SPECIES, UNDERSTANDING THE UNIQUE HOST+SYMBIONT RESPONSE

Figure A.1. Thermal profiles for each experimental system. **LTLC:** Low Temperature, Low CO_2; **HTLC:** High Temperature, Low pCO_2; **LTMC:** Low Temperature, Medium pCO_2; **HTMC:** High Temperature, Medium pCO_2; **LTHC:** Low Temperature, High pCO_2; **HTHC:** High Temperature, High pCO_2.

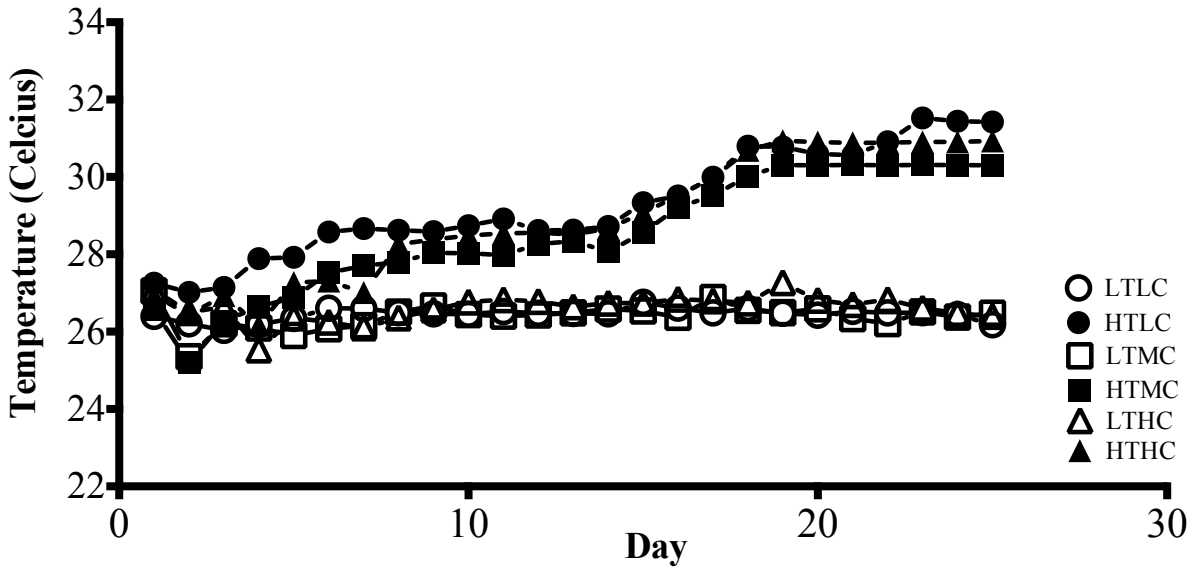

Table A.1. Mean (± 1 SE) carbonate chemistry parameters for 6 treatments representing three pCO_2 levels at two temperatures. From Schoepf et al (2013).

	Ambient pCO_2		**Medium pCO_2**		**High pCO_2**	
Temp. (°C)	Ambient	Elevated	Ambient	Elevated	Ambient	Elevated
pH_T	8.07 ± 0.009	8.04 ± 0.013	7.90 ± 0.011	7.89 ± 0.010	7.83 ± 0.012	7.81 ± 0.014
***p*CO_2 (µatm)**	364.31± 9.69	400.62 ± 16.83	598.37 ± 18.50	616.08 ± 24.24	732.04 ± 22.37	749.63 ± 26.21
TA (µmol kg^{-1})	2269.4 ± 10.84	2270.1 ± 11.15	2303.8 ± 9.34	2288.3 ± 10.43	2306.3 ± 10.64	2304.5 ± 9.08
Ω_{arag}	3.69 ± 0.07	3.79 ± 0.09	2.75 ± 0.05	2.91 ± 0.05	2.40 ± 0.06	2.52 ± 0.06

Table A.2. Quantitative real-time PCR primer sets and efficiencies. All *P. damicornis* contig ID numbers are from PocilloporaBase (Cnidarians.Bu.edu).

Gene ID	Forward (5'-3')	Reverse (5'-3')	Efficiency	Accession number, citation or contig ID number
A. millepora				
GAPDH	ACCATCCATGCTTACACTGCGACA	AGGAATCACCTTTCCCACAGCCTT	100.5	EZ026309.1
HSP90	ACTCCGCGAGCAACCATAAACTCT	AGCCTGCGCTCTTTCTTTGACTCT	104.9	EZ012996
Ca-ATPase	TTGCTCCAGAAGAGTGCGAAGGTT	TACTTTGCAGGCCACGAAACTGCT	102.3	EZ002337.1
CA-IN	GGCAAAGAAATACAAGTTCGAGC	TGTGTCTCGCAATCCCAATG	106.2	EU863783.1
CA-EX	TCGGTGAAGATTGGAGTTACAG	AGTTGGTCAAGGTGAAGCTC	103.5	EU863782.1
RP-s7	AGCAAAGGAGGTTGATGTGG	GACGGGTCTGGATCTTTTGA	107.7	Seneca 2010
EF1-a	TGGCTTTTGTACCTATCTCTGG	TTGTCCAGTGCGTCGATAAG	107.7	GO003400
P. damicornis				
GAPDH	TTGGAAGACCGGCAGCCTTGTTAT	ACAGATTTGCCTGGCGCTAACACT	101.3	bu_91849.1_c2778
HSP90	AAACATGCCCTGATGGAGCGAGTT	TAGTGGCTGGTGGACTGGCATCTAAT	97.6	bu_91849.1_c7242
Ca-ATPase	TCAAGGGCATCATTGACAGCAAGC	TCTGTTCCAGCAATACCCATGGCA	103	bu_91849.1_c48148
CA-IN	ACTGCACGCTCATGTAAGGGACAA	CTCTGGCTGAATGCGTCAAATGGA	98.4	bu_91849.1_cl6633
CA-EX	ACATCAGAGCGACGCGGAAAGTTA	ACCAGTTGCTGGTGCAGGCATTAT	96.8	bu_91849.1_lrc17419
RP-s7	TCAGGAACAGGCGAGCCAAATGAA	AAGCTGCGACTTGAGATCGGTAGA	99.6	bu_91849.1_c20236
EF1-a	TTGGTTGTTGCTGCTGGTACTGGT	ATACTTGGGCTCAGTGGTGTCCAT	99.6	AB245432.2
Symbiodinium				
GLUS	GAGGAAACCGAGGCCCGTCAGGAAGTGA	AGCAGGCAAGAAGCCGGTCTCGGTCATC	103	Leggat 2011
KETO	ATCAAGATGCGAAAGGAATACAAG	GCATAAGCACTGGCCAGAAAGAAC	101.3-105	Leggat 2011
McOA	TTTCCAAAGGGCTTCTCGTGTGC	ACCCTTCTTCTCAGCCAGCTCCTTCAG	101.3-102	Leggat 2011
SAM	GCCTACATTTGCCGACAGATG	AATGGCTTGGCAACACCAAT	94.6-102	Leggat 2011
PCNA	GAGTTTCAGAAGATTTGCCGAGAT	ACATTGCCACTGCCGAGGTC	99.6-102	Leggat 2011

Table A.3. Statistical tables for all univariate analysis**. LTLC:** low temperature, low CO_2; **HTLC:** high temperature, low CO_2; **LTMC:** low temperature, medium CO_2; **HTMC:** high temperature, medium CO_2; **LTHC:** low temperature, high CO_2; **HTHC:** high temperature, high CO_2; **HT:** high temperature treatments**; LT:** low temperature treatments; **LC:** low CO_2 treatments; **MC:** medium CO_2 treatments; **LC:** low CO_2 treatments. **Temp = temperature**

Kruskal Wallace	**Effect**	**p-value**	**pair-wise**	**HTHC**	**HTLC**	**HTMC**	**LTHC**	**LTLC**
C21a (A. millepora)	Temperature	**8.20E-06**	HTLC	0.8719	-	-	-	-
Fv/Fm	CO2	non sig	HTMC	0.8066	1	-	-	-
			LTHC	**0.0093**	0.2105	0.275	-	-
			LTLC	**0.0148**	0.275	0.35	1	-
			LTMC	**0.0067**	0.1719	0.2287	1	0.9999

Kruskal Wallace	**Effect**	**p-value**	**pair-wise**	HTHC	HTLC	HTMC	LTHC	LTLC
C1c-d-t (P. damicornis)	Temperature	**3.50E-07**	HTLC	0.9989	-	-	-	-
Fv/Fm	CO2	non sig	HTMC	1	0.9973	-	-	-
			LTHC	**0.0129**	**0.0033**	**0.017**	-	-
			LTLC	0.0754	**0.0251**	0.0932	0.9918	-
			LTMC	0.1142	**0.0411**	0.1386	0.975	1

Two-Way ANOVA	**Effect**	**Df**	**SS**	**Mean Sq**	**F-statistic**	**p-value**
C15 (M. monasteriata)	Temperature	1	0.013754086	0.013754086	14.813643	0.000577484
Fv/Fm	CO2	2	0.001033265	0.000516632	0.5564315	0.579054114
	Temp*CO2	2	0.013465859	0.00673293	7.2516061	**0.002697419**

Two-Way ANOVA	**Effect**	**Df**	**SS**	**Mean Sq**	**F-statistic**	**p-value**
S. trenchii	Temperature	1	0.000233411	0.000233411	0.1963175	0.6608886
Fv/Fm	CO2	2	0.005149653	0.002574826	2.1656348	0.1322729
	Temp*CO2	2	0.001597135	0.000798567	0.6716589	0.5183753

Table A.4: Photosynthesis:Respiration and Light Enhanced Dark Respiration

Two-Way ANOVA	Effect	Df	SS	Mean Sq	F-statistic	p-value
A. millepora	Temperature	1	0.01161436	0.01161436	0.08406219	0.7740025
PR	CO2	2	0.11041134	0.05520567	0.39956642	0.6743738
	Temp*CO2	2	0.06470174	0.03235087	0.23414843	0.7927781

Two-Way ANOVA	Effect	Df	SS	Mean Sq	F-statistic	p-value
A. millepora	Temperature	1	0.001611096	0.001611096	4.48637	0.04317498
LEDR	CO2	2	0.002544945	0.001272472	3.543415	0.04248097
	Temp*CO2	2	0.002637175	0.001318588	3.671831	**0.03835754**

Two-Way ANOVA	Effect	Df	SS	Mean Sq	F-statistic	p-value
P. damicornis	Temperature	1	0.03119582	0.031195823	1.7619512	0.1943948
PR	CO2	2	0.05016106	0.025080532	1.4165574	0.2583078
	Temp*CO2	2	0.01022753	0.005113764	0.2888272	0.7512012

Two-Way ANOVA	Effect	Df	SS	Mean Sq	F-statistic	p-value
P. damicornis	Temperature	1	0.049345424	0.049345424	23.766759	3.31E-05
LEDR	CO2	2	0.007069672	0.003534836	1.702521	1.99E-01
	Temp*CO2	2	0.018384301	0.009192151	4.427313	**2.07E-02**

Table A.4: Continued

Two-Way ANOVA	Effect	Df	SS	Mean Sq	F-statistic	p-value
M. monasteriata	Temperature	1	1.600893	1.600893	4.133195	0.05098114
PR	CO2	2	0.3945851	0.1972926	0.509371	0.60597695
	Temp*CO2	2	1.9949465	0.9974733	2.575282	0.09286121
Two-Way ANOVA	**Effect**	**Df**	**SS**	**Mean Sq**	**F-statistic**	**p-value**
M. monasteriata	Temperature	1	0.074260104	0.074260104	21.3928375	**6.70E-05**
LEDR	CO2	2	0.003188824	0.001594412	0.4593179	6.36E-01
	Temp*CO2	2	0.002684055	0.001342028	0.3866111	6.83E-01
Two-Way ANOVA	**Effect**	**Df**	**SS**	**Mean Sq**	**F-statistic**	**p-value**
T. reniformis	Temperature	1	0.7713854	0.7713854	0.5261016	0.4738708
PR	CO2	2	0.4065798	0.2032899	0.1386481	0.8710889
	Temp*CO2	2	0.9256682	0.4628341	0.3156629	0.7316981
Two-Way ANOVA	**Effect**	**Df**	**SS**	**Mean Sq**	**F-statistic**	**p-value**
T. reniformis	Temperature	1	0.022615564	0.022615564	9.2055349	**0.004946435**
LEDR	CO2	2	0.001244397	0.000622198	0.2532623	0.777907262
	Temp*CO2	2	0.003013143	0.001506571	0.6132412	0.548242709

Table A.5: Symbiont protein, carbohydrate, lipid and cellular volume

Two-Way ANOVA	Effect	Df	SS	Mean Sq	F-statistic	p-value	Tukey
C21a (A. millepora)	Temperature	1	0.06425421	0.06425421	0.8275925	0.37022096	LC=HC MC>HC MC=LC
Symbiont Protein	CO2	2	0.6209829	0.31049145	3.9991213	**0.02886464**	
	Temp*CO2	2	0.23093761	0.1154688	1.487235	0.24218735	
Two-Way ANOVA	**Effect**	**Df**	**SS**	**Mean Sq**	**F-statistic**	**p-value**	
C21a (A. millepora)	Temperature	1	8.89E-15	8.89E-15	0.02420762	0.877400001	
Symbiont Carboh	CO2	2	5.18E-12	2.59E-12	7.0509905	0.003089921	
	Temp*CO2	2	4.82E-12	2.41E-12	6.56843629	**0.004306148**	
Two-Way ANOVA	**Effect**	**Df**	**SS**	**Mean Sq**	**F-statistic**	**p-value**	
C21a (A. millepora)	Temperature	1	2.95E-10	2.95E-10	0.01201786	0.91343603	
Symbiont Lipid	CO2	2	1.59E-07	7.93E-08	3.2295768	0.05366858	
	Temp*CO2	2	2.77E-08	1.38E-08	0.56331289	0.57522553	
Two-Way ANOVA	**Effect**	**Df**	**SS**	**Mean Sq**	**F-statistic**	**p-value**	**Tukey**
C21a (A. millepora)	Temperature	1	4626.516	4626.516	0.7112414	4.06E-01	LC=HC LC<MC MC>HC
Cell Volume	CO2	2	277391.555	138695.778	21.3219129	**1.73E-06**	
	Temp*CO2	2	9814.963	4907.481	0.7544346	4.79E-01	
Two-Way ANOVA	**Effect**	**Df**	**SS**	**Mean Sq**	**F-statistic**	**p-value**	
C1c-d-t (P. damicornis)	Temperature	1	3.03E-06	3.03E-06	0.4242534	0.51995086	
Symbiont Protein	CO2	2	7.14E-05	3.57E-05	4.9993833	0.01363118	
	Temp*CO2	2	6.39E-05	3.19E-05	4.4735648	**0.02026173**	

Table A.5: Continued

Two-Way ANOVA	Effect	Df	SS	Mean Sq	F-statistic	p-value	
C1c-d-t (P. damicornis)	Temperature	1	6.16E-12	6.16E-12	2.1261698	0.1551926	
Symbiont Carboh	CO2	2	2.25E-12	1.12E-12	0.3876247	0.6820169	
	Temp*CO2	2	1.05E-11	5.23E-12	1.8031908	0.1821766	
Two-Way ANOVA	**Effect**	**Df**	**SS**	**Mean Sq**	**F-statistic**	**p-value**	
C1c-d-t (P. damicornis)	Temperature	1	1.42E-04	0.000141877	0.000368309	0.9848296	
Symbiont Lipid	CO2	2	3.76E-01	0.187816429	0.48756739	0.6194215	
	Temp*CO2	2	9.36E-01	0.468015399	1.214957865	0.3124346	
Two-Way ANOVA	**Effect**	**Df**	**SS**	**Mean Sq**	**F-statistic**	**p-value**	
C1c-d-t (P. damicornis)	Temperature	1	7.54E+00	7.535757	0.00055118	0.9814251	
Cell Volume	CO2	2	3.87E+04	19362.45907	1.416207927	0.2583903	
	Temp*CO2	2	4.45E+04	22260.8887	1.628204708	0.2131515	
Two-Way ANOVA	**Effect**	**Df**	**SS**	**Mean Sq**	**F-statistic**	**p-value**	**Tukey**
C15 (M. monasteriata)	Temperature	1	0.52382161	0.52382161	7.2954821	**0.01125692**	LC<MC
Symbiont Protein	CO2	2	0.53504901	0.2675245	3.7259254	**0.03586902**	MC=HC
	Temp*CO2	2	0.04103308	0.02051654	0.2857424	0.75347846	LC=HC
Two-Way ANOVA	**Effect**	**Df**	**SS**	**Mean Sq**	**F-statistic**	**p-value**	
C15 (M. monasteriata)	Temperature	1	1.83E-07	1.83E-07	0.8703756	0.35829966	
Symbiont Carboh	CO2	2	1.08E-06	5.38E-07	2.5608217	0.09401484	
	Temp*CO2	2	3.83E-07	1.92E-07	0.9121471	0.41251251	

Table A.5: Continued

Two-Way ANOVA	Effect	Df	SS	Mean Sq	F-statistic	p-value	
C15 (M. monasteriata)	Temperature	1	9.24E-07	9.24E-07	26.471077	1.70E-05	
Symbiont Lipid	CO2	2	1.10E-07	5.52E-08	1.581878	2.23E-01	
	Temp*CO2	2	2.38E-07	1.19E-07	3.403997	**4.70E-02**	
Two-Way ANOVA	**Effect**	**Df**	**SS**	**Mean Sq**	**F-statistic**	**p-value**	
C15 (M. monasteriata)	Temperature	1	83087.23	83087.23	5.325177	**0.02809773**	
Cell Volume	CO2	2	49103.64	24551.82	1.573561	0.22393991	
	Temp*CO2	2	49569.74	24784.87	1.588497	0.22093434	
Two-Way ANOVA	**Effect**	**Df**	**SS**	**Mean Sq**	**F-statistic**	**p-value**	
S. trenchi	Temperature	1	8.93483601	8.93483601	14.16275096	**0.00072852**	
Symbiont Protein	CO2	2	1.31446666	0.65723333	1.04179103	0.365238093	
	Temp*CO2	2	0.04482602	0.02241301	0.03552722	0.965137008	
Two-Way ANOVA	**Effect**	**Df**	**SS**	**Mean Sq**	**F-statistic**	**p-value**	
S. trenchi	Temperature	1	1.37E-06	1.37E-06	5.1088584	**0.03122135**	
Symbiont Carboh	CO2	2	5.04E-07	2.52E-07	0.9407707	0.40154033	
	Temp*CO2	2	7.68E-07	3.84E-07	1.4324963	0.25457499	
Two-Way ANOVA	**Effect**	**Df**	**SS**	**Mean Sq**	**F-statistic**	**p-value**	**Tukey**
S. trenchi	Temperature	1	6.62E-13	6.62E-13	17.539846	**0.000253298**	LC=MC
Symbiont Lipid	CO2	2	5.02E-13	2.51E-13	6.649796	**0.004334828**	MC>HC
	Temp*CO2	2	2.03E-13	1.02E-13	2.68976	0.085406567	LC=HC
Two-Way ANOVA	**Effect**	**Df**	**SS**	**Mean Sq**	**F-statistic**	**p-value**	**Tukey**
S. trenchi	Temperature	1	168144.174	168144.174	19.9607248	**0.000104195**	LC>MC
Cell Volume	CO2	2	211103.567	105551.784	12.5302594	**0.000110717**	MC<HC
	Temp*CO2	2	4151.868	2075.934	0.2464382	0.783146329	LC=HC

Table A.6: Figure 5-Univariate analysis of host protein, carbohydrate and lipids

Two-Way ANOVA	**Effect**	**Df**	**SS**	**Mean Sq**	**F-statistic**	**p-value**	**Tukey**		
A. millepora	Temperature	1	1.077	1.0779601	12.069	**0.0016**	LC>MC MC<HC LC=HC		
Host Protein	CO2	2	1.201	0.6007703	6.726	**0.0039**			
	Temp*CO2	2	0.0291	0.01459761	0.163	0.8499			
Kruskal Wallace	**Effect**	**Df**	**p-value**	**Pair-wise**	HTHC	HTLC	HTMC	LTHC	LTLC
A. millepora	Temperature	non sig	0.3569	HTLC	1	-	-	-	-
Host Carboh	CO2	non sig		HTMC	0.9	0.96	-	-	-
				LTHC	0.95	0.89	0.39	-	-
				LTLC	0.94	0.87	0.39	1	-
				LTMC	1	1	0.97	0.86	0.84
2-Way ANOVA	**Effect**	**Df**	**SS**	**Mean Sq**	**F-statistic**	**p-value**	**Tukey**		
A. millepora	Temperature	1	246.839	246.839269	17.409	**0.00024**	LC=MC MC<HC LC<HC		
Host Lipid	CO2	2	215.881	107.940551	7.613	**0.0022**			
	Temp*CO2	2	19.4704	9.735236	0.686	0.5112			
2-Way ANOVA	**Effect**	**Df**	**SS**	**Mean Sq**	**F-statistic**	**p-value**	**Tukey**		
P. damicornis	Temperature	1	50.237	50.23762	0.0051	0.943	LC>MC MC=HC LC>HC		
Host Protein	CO2	2	109790.38	54895.19377	5.6231	**0.008**			
	Temp*CO2	2	59415.23	29707.61913	3.0430	0.062			
2-Way ANOVA	**Effect**	**Df**	**SS**	**Mean Sq**	**F-statistic**	**p-value**	**Tukey**		
P. damicornis	Temperature	1	0.4076846	0.4076846	3.566584	0.0686568 2	LC=MC MC=HC LC>HC		
Host Carboh	CO2	2	1.003146	0.501573	4.387957	**0.0213004 2**			
	Temp*CO2	2	0.5341872	0.2670936	2.336639	0.1139974 5			

Table A.6: Continued

Two-Way ANOVA	Effect	Df	SS	Mean Sq	F-statistic	p-value	
P. damicornis	Temperature	1	2152.1836	2152.184	0.2179618	0.6442098	
Host Lipid	CO2	2	977.2959	488.648	0.04948769	0.9517999	
	Temp*CO2	2	4214.602	2107.301	0.21341633	0.8091216	
Two-Way ANOVA	**Effect**	**Df**	**SS**	**Mean Sq**	**F-statistic**	**p-value**	
M. monsateriata	Temperature	1	463267.11	463267.11	7.0900639	**0.01234073**	
Host Protein	CO2	2	21328.58	10664.29	0.1632115	0.85016068	
	Temp*CO2	2	59633.23	29816.61	0.4563279	0.63793152	
Two-Way ANOVA	**Effect**	**Df**	**SS**	**Mean Sq**	**F-statistic**	**p-value**	
M. monsateriata	Temperature	1	2.088318	2.088318	9.0806056	**0.005211103**	
Host Carboh	CO2	2	0.900713	0.4503565	1.9582792	0.15872384	
	Temp*CO2	2	0.1154596	0.0577298	0.2510257	0.779620208	
Two-Way ANOVA	**Effect**	**Df**	**SS**	**Mean Sq**	**F-statistic**	**p-value**	
M. monsateriata	Temperature	1	262.1559	262.15585	11.606965	0.002006491	
Host Lipid	CO2	2	168.2153	84.10767	3.723872	0.036810539	
	Temp*CO2	2	272.1934	136.09669	6.025688	**0.00666144**	
Two-Way ANOVA	**Effect**	**Df**	**SS**	**Mean Sq**	**F-statistic**	**p-value**	
T. reniformis	Temperature	1	0.5877775	0.58777752	5.2269059	**0.02947197**	
Host Protein	CO2	2	0.0568307	0.02841535	0.2526881	0.77834665	
	Temp*CO2	2	0.6450141	0.32250704	2.8679456	0.07248524	

Table A.6: Continued

Two-Way ANOVA	Effect	Df	SS	Mean Sq	F-statistic	p-value	
T. reniformis	Temperature	1	0.6396687	0.6396687	1.371227	0.25081861	
Host Carboh	CO2	2	1.1589829	0.5794914	1.242228	0.30316905	
	Temp*CO2	2	4.4289894	2.2144947	4.747106	**0.01617399**	
Two-Way ANOVA	**Effect**	**Df**	**SS**	**Mean Sq**	**F-statistic**	**p-value**	**Tukey**
T. reniformis	Temperature	1	0.08404074	0.08404074	0.08418799	0.77383825	LC=MC
Host Lipid	CO2	2	9.43285477	4.71642738	4.72469141	**0.01706032**	MC<HC
	Temp*CO2	2	0.0263496	0.0131748	0.01319788	0.98689496	LC<HC

Table A.7: Figure 6-Univariate analyses of host gene expression

Two-Way ANOVA	**Effect**	**Df**	**SS**	**Mean Sq**	**F-statistic**	**p-value**
A. millepora	Temperature	1	0.72112297	0.72112297	48.642954	**1.15E-07**
Intercellular CA	CO2	2	0.02881448	0.014407242	0.9718326	3.90E-01
	Temp*CO2	2	0.01338252	0.006691261	0.4513554	6.41E-01
Two-Way ANOVA	**Effect**	**Df**	**SS**	**Mean Sq**	**F-statistic**	**p-value**
A. millepora	Temperature	1	0.01131596	0.01131596	0.01436702	0.9054186
Extracellular CA	CO2	2	1.02830797	0.51415398	0.65278234	0.528076
	Temp*CO2	2	0.20685355	0.10342678	0.13131314	0.8774616
Two-Way ANOVA	**Effect**	**Df**	**SS**	**Mean Sq**	**F-statistic**	**p-value**
A. millepora	Temperature	1	0.006332565	0.006332565	0.5978577	0.44565374
CA ATPase	CO2	2	0.053055872	0.026527936	2.5045034	0.09923359
	Temp*CO2	2	0.01844037	0.009220185	0.870478	0.42940699
Two-Way ANOVA	**Effect**	**Df**	**SS**	**Mean Sq**	**F-statistic**	**p-value**
A. millepora	Temperature	1	0.03153086	0.03153086	2.599704	0.11809982
HSP90	CO2	2	0.04527893	0.02263947	1.866613	0.17338571
	Temp*CO2	2	0.08226181	0.04113091	3.391223	**0.04799221**
Two-Way ANOVA	**Effect**	**Df**	**SS**	**Mean Sq**	**F-statistic**	**p-value**
A. millepora	Temperature	1	0.06001288	0.06001288	1.414271	0.24399508
GAPDH	CO2	2	0.25454003	0.12727002	2.999262	0.06547115
	Temp*CO2	2	0.35853608	0.17926804	4.224654	**0.02453782**
Two-Way ANOVA	**Effect**	**Df**	**SS**	**Mean Sq**	**F-statistic**	**p-value**
P. damicornis	Temperature	1	0.4118403	0.41184033	1.0153888	0.3216741
Intercellular CA	CO2	2	0.1155619	0.05778093	0.1424584	0.8678068
	Temp*CO2	2	0.1834858	0.09174291	0.2261914	0.7989133

Table A.7: Continued

Two-Way ANOVA	Effect	Df	SS	Mean Sq	F-statistic	p-value
P. damicornis	Temperature	1	0.06385155	0.063851554	2.3530601	0.135517
Extracellular CA	CO2	2	0.03881364	0.019406819	0.7151809	0.4972538
	Temp*CO2	2	0.01084885	0.005424423	0.1999011	0.8198936
Two-Way ANOVA	**Effect**	**Df**	**SS**	**Mean Sq**	**F-statistic**	**p-value**
P. damicornis	Temperature	1	0.01843521	0.018435213	1.7717456	0.1931941
CA ATPase	CO2	2	0.03628078	0.018140392	1.7434114	0.1921806
	Temp*CO2	2	0.01880771	0.009403854	0.9037724	0.4157829
Two-Way ANOVA	**Effect**	**Df**	**SS**	**Mean Sq**	**F-statistic**	**p-value**
P. damicornis	Temperature	1	0.076421	0.076421001	11.7017899	**0.001821118**
HSP90	CO2	2	0.01357568	0.006787838	1.039372	0.366065225
	Temp*CO2	2	0.01243095	0.006215476	0.9517305	0.397421927
Two-Way ANOVA	**Effect**	**Df**	**SS**	**Mean Sq**	**F-statistic**	**p-value**
P. damicornis	Temperature	1	0.05465948	0.054659479	1.378668	0.24956517
GAPDH	CO2	2	0.26228275	0.131141373	3.307759	0.05033163
	Temp*CO2	2	0.01917611	0.009588053	0.241838	0.78669929

Table A.8: Figure 7- Univariate analysis of symbiont gene expression

Two-Way ANOVA	Effect	Df	SS	Mean Sq	F-statistic	p-value		
C21a (A. millepora)	Temperature	1	0.0445	0.0445	0.282	0.599		
GLUS	CO2	2	0.7170	0.3585	2.268	0.122		
	Temp*CO2	2	0.3987	0.1993	1.261	0.298		
Two-Way ANOVA	**Effect**	**Df**	**SS**	**Mean Sq**	**F-statistic**	**p-value**	**Tukey**	
C21a (A. millepora)	Temperature	1	0.6622	0.6622	8.950	**0.0056**	LC=MC	
KETO	CO2	2	0.5889	0.2944	3.980	**0.0296**	MC=HC	
	Temp*CO2	2	0.2581	0.1290	1.744	0.1925	LC<HC	
Two-Way ANOVA	**Effect**	**Df**	**SS**	**Mean Sq**	**F-statistic**	**p-value**	**Tukey**	
C21a (A. millepora)	Temperature	1	0.6136	0.6136	4.511	**0.0423**	LC<MC	
McOA	CO2	2	1.4700	0.7350	5.404	**0.0101**	MC=HC	
	Temp*CO2	2	0.3206	0.1603	1.178	0.3219	LC<HC	
Two-Way ANOVA	**Effect**	**Df**	**SS**	**Mean Sq**	**F-statistic**	**p-value**		
C1c-d-t (P. damicornis)	Temperature	1	0.4049	0.4049	21.101	**7.3E-05**		
GLUS	CO2	2	0.0147	0.0073	0.384	0.6838		
	Temp*CO2	2	0.0223	0.0118	0.582	0.5649		
Two-Way ANOVA	**Effect**	**Df**	**SS**	**Mean Sq**	**F-statistic**	**p-value**		
C1c-d-t (P. damicornis)	Temperature	1	0.0538	0.0538	6.327	0.0174		
KETO	CO2	2	0.2053	0.1026	12.061	0.0001		
	Temp*CO2	2	0.0978	0.0489	5.745	**0.0077**		
Kruskal-Wallace	**Effect**	**p-value**	**pair-wise**	HTHC	HTLC	HTMC	LTHC	LTLC
C1c-d-t (P. damicornis)	Temperature	non sig	HTLC	1	-	-	-	-
McOA	CO2	non sig	HTMC	0.98	1	-	-	-
			LTHC	1	1	1	-	-
			LTLC	0.97	0.91	0.68	0.92	-
			LTMC	1	1	0.97	1	0.98

Table A.9: SIMPER analysis: Temperature. hlipid = host lipid, hprotein = host protein, hcarbo = host carbohydrates, slipid = symbiont lipids, sprotein = symbiont protein, scarbo = symbiont carbohydrates, LEDRr = light enhanced dark respiration, PR = photosynthesis:respiration.

	Variables	Average Dissimilarity	Standard deviation	ratio	% contribution
A. millepora	hlipid	0.02117	0.016766	1.263	13.22
	hprotein	0.01902	0.017032	1.117	11.87
	LEDRr	0.01814	0.013373	1.357	11.33
	hcarbo	0.01739	0.016907	1.029	10.85
	FvFm	0.0162	0.007785	2.082	10.12
	slipid	0.01597	0.014834	1.077	9.97
	sprotein	0.01531	0.013281	1.153	9.56
	scarbo	0.01525	0.011836	1.289	9.52
	PR	0.01111	0.007983	1.391	6.93
	volume	0.01062	0.008425	1.261	6.63
P. damicornis	LEDRr	0.019431	0.012869	1.51	13.59
	hlipid	0.018664	0.014081	1.325	13.06
	slipid	0.018622	0.017224	1.081	13.03
	scarbo	0.017283	0.012975	1.332	12.09
	hcarbo	0.015662	0.013333	1.175	10.96
	sprotein	0.01317	0.011131	1.183	9.21
	hprotein	0.012723	0.009209	1.382	8.9
	PR	0.011775	0.009695	1.215	8.24
	volume	0.008777	0.006336	1.385	6.14
	FvFm	0.006835	0.003311	2.064	4.78

Table A.9: SIMPER analysis: Temperature continued

M. monasteriata	slipid	0.030115	0.02437	1.236	16.64
	LEDRr	0.025096	0.016328	1.537	13.87
	hcarbo	0.020284	0.01667	1.217	11.21
	hprotein	0.019484	0.013287	1.466	10.77
	hlipid	0.018015	0.018001	1.001	9.96
	scarbo	0.015297	0.013114	1.166	8.45
	volume	0.015076	0.010452	1.442	8.33
	PR	0.015075	0.011736	1.285	8.33
	sprotein	0.014846	0.012803	1.16	8.21
	FvFm	0.007659	0.005412	1.415	4.23
T. reniformis	sprotein	0.032555	0.023252	1.4001	15.67
	slipid	0.032457	0.022394	1.4493	15.63
	LEDRr	0.026393	0.018766	1.4064	12.71
	hcarbo	0.022442	0.018231	1.231	10.81
	scarbo	0.021306	0.017366	1.2269	10.25
	hlipid	0.020377	0.02279	0.8941	9.82
	hprotein	0.018	0.014965	1.2028	8.66
	volume	0.015385	0.009836	1.5642	7.41
	PR	0.012941	0.016865	0.7674	6.23
	FvFm	0.005834	0.004211	1.3855	2.81

Appendix B

CHAPTER 3: HIGH TEMPERATURE ACCLIMATION STRATEGIES WITHIN THE THERMALLY TOLERANT ENDOSYMBIONT *SYMBIODINIUM TRENCHII* AND ITS CORAL HOST, *TURBINARIA RENIFORMIS,* DIFFERS WITH CHANGING pCO_2 AND NUTRIENTS

Table B.1: (Figure 2) Results from three factor ANOVA for each variable in figure 2. For results from the tukey posthoc, LCLT = low pCO_2 and low temperature, LCHT = low pCO2 and high temperature.

Three-factor ANOVA	**Effect**	**Df**	**Mean Sq**	**F-statistic**	**p-value**	**Tukey**
S. trenchii (T. reniformis)	pCO2	1	0.1095	0.4332	0.5145	
Net photosynthesis cell^{-1}	Nutrients	1	0.2312	0.9147	0.3452	
	Temp	1	1.1592	4.5860	0.0390	LCLT
	pCO2:Nutrients	1	0.7185	2.8427	0.1004	<
	pCO2:Temp	**1**	**1.1678**	**4.6200**	**0.0383**	LCHT
	Nutrients:Temp	1	0.0179	0.0710	0.7912	
	pCO2:Nutrients:Temp	1	0.1336	0.5288	0.4718	
Three-factor ANOVA	**Effect**	**Df**	**Mean Sq**	**F-statistic**	**p-value**	
S. trenchii (T. reniformis)	**pCO2**	**1**	**117327.529**	**6.7066**	**0.0138**	
Cellular Volume	Nutrients	1	5882.575	0.3362	0.566	
	Temp	**1**	**422743.224**	**24.1648**	**1.94E-05**	
	pCO2:Nutrients	1	159.263	0.0091	0.9250	
	pCO2:Temp	1	53365.53	3.0504	0.0892	
	Nutrients:Temp	1	27938.360	1.5970	0.2140	
	pCO2:Nutrients:Temp	1	554.322	0.0316	0.8600	
Three-factor ANOVA	**Effect**	**Df**	**Mean Sq**	**F-statistic**	**p-value**	**Tukey**
S. trenchii (T. reniformis)	pCO2	1	0.0245	0.2532	0.6179	
Chlorophyll a	Nutrients	1	0.1289	1.3314	0.2563	
	Temp	1	0.4755	4.9119	0.0332	LCLT
	pCO2:Nutrients	1	0.1217	1.2579	0.2696	<
	pCO2:Temp	**1**	**0.6987**	**7.2171**	**0.0109**	LCHT
	Nutrients:Temp	1	0.0052	0.0540	0.8174	
	pCO2:Nutrients:Temp	1	0.1304	1.3469	0.2536	
Three-factor ANOVA	**Effect**	**Df**	**Mean Sq**	**F-statistic**	**p-value**	
S. trenchii (T. reniformis)	pCO2	1	4.47E-07	0.1171	0.7341	
Cellular Protein	Nutrients	1	8.66E-06	2.2731	0.1403	
	Temp	**1**	**2.93E-05**	**7.6915**	**0.0087**	
	pCO2:Nutrients	1	1.13E-06	0.2972	0.5889	
	pCO2:Temp	1	1.25E-06	0.3284	0.5701	
	Nutrients:Temp	1	3.66E-07	0.0959	0.7585	
	pCO2:Nutrients:Temp	1	6.29E-07	0.1649	0.6870	

Table B.2: (figure 3) Results from three factor ANOVA for each variable in figure 3. For results from the tukey posthoc, HT = high temperature, LT = low temperature, HC = high pCO_2, LC = low pCO_2, HN = high nutrients and LN = low nutrients.

Three-factor ANOVA	**Effect**	**Df**	**Mean Sq**	**F-statistic**	**p-value**	
T. reniformis	pCO2	1	0.302	1.3640	0.2505	
Cell Density	Nutrients	1	0.055	0.2520	0.6184	
	Temp	**1**	**1.713**	**7.7340**	**0.0085**	
	pCO2:Nutrients	1	0.002	0.0130	0.9093	
	pCO2:Temp	1	0.191	0.8650	0.3582	
	Nutrients:Temp	1	0.302	1.3650	0.2503	
	pCO2:Nutrients:Temp	1	0.405	1.8280	0.1847	
Three-factor ANOVA	**Effect**	**Df**	**Mean Sq**	**F-statistic**	**p-value**	
T. reniformis	**pCO2**	**1**	**0.1852**	**6.239**	**0.018**	
Calcification day^{-1}	Nutrients	1	0.0192	1.104	0.302	
	Temp	1	0.0115	0.666	0.421	
	pCO2:Nutrients	1	0.0115	0.303	0.586	
	pCO2:Temp	1	0.0052	0.339	0.565	
	Nutrients:Temp	1	0.0009	0.057	0.813	
	pCO2:Nutrients:Temp	1	0.0009	0.054	0.817	
Three-factor ANOVA	**Effect**	**Df**	**Mean Sq**	**F-statistic**	**p-value**	
T. reniformis	pCO2	**1**	**3.42E-04**	**6.1183**	**0.0182**	
LEDR	Nutrients	1	6.34E-05	1.1344	0.2939	
	Temp	1	5.20E-06	0.0930	0.7621	
	pCO2:Nutrients	1	1.90E-05	0.3404	0.5632	
	pCO2:Temp	1	1.23E-05	0.2193	0.6423	
	Nutrients:Temp	1	4.82E-05	0.8624	0.3592	
	pCO2:Nutrients:Temp	1	1.22E-05	0.2191	0.6424	
Three-factor ANOVA	**Effect**	**Df**	**Mean Sq**	**F-statistic**	**p-value**	**Tukey**
T. reniformis	pCO2	1	0.3907	3.7802	0.0597	LCLN < HCLN
Photosynthesis:Respiration	Nutrients	1	0.0659	0.6380	0.4296	
	Temp	1	0.1014	0.9814	0.3284	
	pCO2:Nutrients	**1**	**0.6024**	**5.8277**	**0.0209**	
	pCO2:Temp	1	0.0008	0.0081	0.9287	
	Nutrients:Temp	1	0.2629	2.5440	0.1194	
	pCO2:Nutrients:Temp	1	0.0684	0.6619	0.4212	

Table B.3: (Figure 5) Results from generalized linear mixed model analyses to test for effects of time, temperature (Temp), nutrients (Nutrients) and pCO_2 (Carbon).

Effect	Num df	Den df	*F*-statistic	*P*-value
Fv/Fm				
Time	14	480	30.101	< 0.0001
Carbon	1	70	35.412	< 0.0001
Temp	1	480	74.646	< 0.0001
Nutrient	1	480	5.630	0.0180
Time X Carbon	14	480	1.326	0.1875
Time X Nutrient	14	480	0.442	0.9603
Time X Temp	14	480	5.255	< 0.0001
Carbon X Temp	1	480	5.147	0.0237
Temp X Nutrient	1	480	0.242	0.6277
Carbon X Nutrient	1	480	6.840	0.0092
Time X Temp X Nutrient	14	480	1.213	0.2621
Time X Carbon X Temp	14	480	1.608	0.0732
Time X Carbon X Nutrient	14	480	1.092	0.3622
Carbon X Temp X Nutrient	**1**	**480**	**36.729**	**< 0.0001**
Time X Carbon X Temp X Nutrient	14	480	1.328	0.1861

Table B.4: (Figure 4) Results from three factor ANOVA for each variable in figure 5. For results from the tukey posthoc, HT = high temperature, LT = low temperature, HC = high pCO_2, LC = low pCO_2, HN = high nutrients and LN = low nutrients. Bold values reflect significant three-way interactive effect.

Three-factor ANOVA	**Effect**	**Df**	**Mean Sq**	**F-statistic**	**p-value**	**Pairwise**
S. trenchii (T. reniformis)	pCO2	1	0.0301	3.9263	0.0550	HCLNLT > HCLNHT, HCHNLT, HCHNHT
Fv.Fm	Nutrients	1	0.0153	1.9969	0.1660	
	Temp	1	0.0748	9.7673	0.0034	
	pCO2:Nutrients	1	0.0162	2.1085	0.1549	
	pCO2:Temp	1	0.0139	1.8166	0.1859	
	Nutrients:Temp	1	0.0130	1.7004	0.2003	
	pCO2:Nutrients:Temp	**1**	**0.0491**	**6.4062**	**0.0158**	
Three-factor ANOVA	**Effect**	**Df**	**Mean Sq**	**F-statistic**	**p-value**	**Pairwise**
S. trenchii (T. reniformis)	pCO2	1	23699.6074	18.6870	0.0001	LCLNLT < HCLNLT, HCLNHT, HCHNHT LCLNHT < HCLNLT
Sigma	Nutrients	1	96.6494	0.0762	0.7840	
	Temp	1	396.1957	0.3124	0.5795	
	pCO2:Nutrients	1	9479.3143	7.4744	0.0095	
	pCO2:Temp	1	1868.1528	1.4730	0.2324	
	Nutrients:Temp	1	14.9610	0.0118	0.9141	
	pCO2:Nutrients:Temp	**1**	**8642.8571**	**6.8149**	**0.0129**	

Appendix C

CHAPTER 4: CONTRASTING PHYSIOLOGICAL PLASTICITY IN RESPONSE TO ENVIRONMENTAL STRESS WITHIN DIFFERENT CNIDARIANS AND THEIR RESPECTIVE SYMBIONT

Figure C.1: Temperature profiles for each system during the experimental treatment. Open circles are ambient pCO_2 and closed circles are elevated pCO_2 treatments. The dotted lines are the ambient temperature treatments and the black lines are the high temperature treatments.

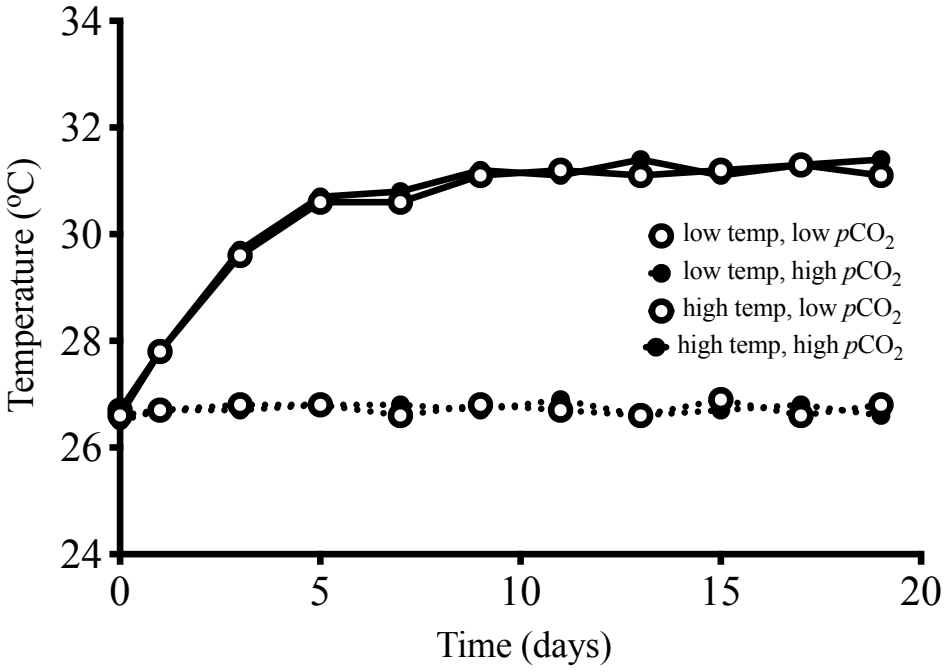

Table C.1: Electron Transport Rates. Results from the Two-Way ANOVA preformed for each species. Temperature and pCO_2 reflect the main effects whereas temp*pCO_2 reflects interactive effects between temperature and pCO_2. Significant effects are in bold.

Species	Effect	Df	SS	MS	F-statistic	p-value
***C3* (*D. nummiforme*)**	**Temperature**	**1**	**2.34E+10**	**2.34E+10**	**5.522**	**0.0297**
	pCO_2	1	7.57E+09	7.57E+09	1.79	0.1967
	Temp*pCO_2	1	7.97E+08	7.97E+08	0.189	0.6691
***C15* (M. *hirsuta*)**	Temperature	1	1.02E+09	1.02E+09	0.1	7.54E-01
	pCO_2	1	6.95E+09	6.95E+09	0.686	4.17E-01
	Temp*pCO_2	1	4.79E+09	4.79E+09	0.473	5.00E-01
***D1* (P. *damicornis*)**	**Temperature**	**1**	**1.92E+10**	**1.92E+10**	**5.636**	**0.0277**
	pCO_2	1	2.53E+08	2.53E+08	0.074	0.788
	Temp*pCO_2	1	4.83E+09	4.83E+09	1.422	0.2471

Table C.2: Absorbance at 675nm. Results from Kruskal-Wallis or Two-Way ANOVA preformed for each species. For Kruskal-Wallis test: HTHC = high temperature and high pCO_2 treatment, HTLC = High temperature and low pCO_2 treatment, LTHC = low temperature and high pCO_2 treatment and LTLC = low temperature and low pCO_2 treatment. For the Two Way ANOVA: Temperature and pCO_2 reflect the main effects whereas temp*pCO_2 reflects interactive effects between temperature and pCO_2. Significant effects are in bold.

***C3* (*Discosoma nummiforme*)**						
Kruskal–Wallis test	**Effect**	**p-value**	**pair-wise**	HTHC	HTLC	LTHC
	group	0.6048	HTLC	0.64	-	-
			LTHC	0.99	0.78	-
			LTLC	1	0.66	1
***C15* (M. *hirsuta*)**						
Two-way ANOVA	**Effect**	**df**	**SS**	**MS**	**F-statistic**	**p-value**
	Temp	**1**	**0.2251**	**0.2251**	**20.5816**	**0.0002**
	pCO_2	1	0.0372	0.0372	3.4044	0.0798
	Temp*pCO_2	1	0.0029	0.0029	0.2670	0.6110
***D1* (P. *damicornis*)**						
Two-way ANOVA	**Effect**	**df**	**SS**	**MS**	**F-statistic**	**p-value**
	Temp	1	0.1830	0.1830	75.7020	3.11E-08
	pCO_2	1	0.0093	0.0093	3.8820	6.28E-02
	Temp*pCO_2	**1**	**0.1242**	**0.1242**	**51.3733**	**6.09E-07**

Table C.3: Physiology**.** Results from the Two-Way ANOVA preformed for each species and physiological variable. Temperature and pCO_2 reflect the main effects whereas temp*pCO_2 reflects interactive effects between temperature and pCO_2. Significant effects are in bold.

	Effect	Df	SS	MS	F-statistic	p-value
***C3* (*Discosoma nummiforme*)**						
Chlorophyll a	**Temperature**	**1**	**32.5258**	**32.5258**	**35.8314**	**1.16E-05**
	pCO_2	1	0.0763	0.0763	0.0841	7.75E-01
	Temp*pCO_2	1	0.9829	0.9829	1.0828	3.12E-01
Cell density	Temperature	1	230794.997	230794.997	1.2053	0.2852
	pCO_2	1	516729.357	516729.357	2.6987	0.1160
	Temp*pCO_2	1	4023.798	4023.798	0.0210	0.8861
Cell volume	Temperature	1	2425.338	2425.338	0.4703	0.5010
	pCO_2	1	6641.441	6641.441	1.2881	0.2705
	Temp*pCO_2	1	1929.328	1929.328	0.3741	0.5479
Chlorophyll density	**Temperature**	**1**	**4.08E-05**	**4.08E-05**	**33.9210**	**2.03E-05**
	pCO_2	1	6.82E-08	6.82E-08	0.0566	8.15E-01
	Temp*pCO_2	1	1.67E-06	1.67E-06	1.3867	2.55E-01
***C15* (*Montipora hirsuta*)**						
Chlorophyll a	**Temperature**	**1**	**1.9063**	**1.9063**	**7.1543**	**0.0149**
	pCO_2	1	0.0784	0.0784	0.2943	0.5937
	Temp*pCO_2	1	0.0195	0.0195	0.0732	0.7895
Cell density	**Temperature**	**1**	**1.8383**	**1.8383**	**6.3034**	**0.0212**
	pCO_2	1	0.0007	0.0007	0.0026	0.9597
	Temp*pCO_2	1	0.0023	0.0023	0.0079	0.9300
Cell volume	**Temperature**	**1**	**18359.1394**	**18359.1394**	**10.5867**	**0.0041**
	pCO_2	1	4935.0198	4935.0198	2.8457	0.1079
	Temp*pCO_2	1	692.5433	692.5433	0.3993	0.5349
Chlorophyll density	Temperature	1	2.11E-07	2.11E-07	0.1382	0.7141
	pCO_2	1	1.23E-07	1.23E-07	0.0806	0.7795
	Temp*pCO_2	1	6.74E-08	6.74E-08	0.0442	0.8356
***D1* (*Pocillopora damicornis*)**						
Chlorophyll a	**Temperature**	**1**	**7.5237**	**7.5237**	**7.3172**	**0.0140**
	pCO_2	1	2.0713	2.0713	2.0145	0.1719
	Temp*pCO_2	1	1.4793	1.4793	1.4387	0.2450
Cell density	Temperature	1	0.5626	0.5626	2.2307	0.1517
	pCO_2	1	0.0312	0.0312	0.1239	0.7286

	Temp*pCO_2	**1**	**1.6326**	**1.6326**	**6.4729**	**0.0198**
Cell volume	Temperature	1	74148.2281	74148.2281	22.1853	0.0001
	pCO_2	1	214.8565	214.8565	0.0642	0.8025
	Temp*pCO_2	**1**	**30732.1381**	**30732.1381**	**9.1951**	**0.0068**
Chlorophyll density	Temperature	1	1.56E-04	1.56E-04	25.6089	6.94E-05
	pCO_2	1	2.27E-05	2.27E-05	3.7171	0.0689
	Temp*pCO_2	**1**	**5.11E-05**	**5.11E-05**	**8.3832**	**0.0092**

Table C.4: Carbon uptake and Translocation. Results from Kruskal-Wallis or Two-Way ANOVA preformed for each species. For Kruskal-Wallis test: HTHC = high temperature and high pCO_2 treatment, HTLC = High temperature and low pCO_2 treatment, LTHC = low temperature and high pCO_2 treatment and LTLC = low temperature and low pCO_2 treatment. For the Two Way ANOVA: Temperature and pCO_2 reflect the main effects whereas temp*pCO_2 reflects interactive effects between temperature and pCO_2. Significant effects are in bold.

	Effect	Df	SS	MS	F-statistic	p-value
***C3* (*Discosoma nummiforme*)**						
Photosynthesis	Temperature	1	2.12E-01	2.12E-01	0.7883	0.3851
	pCO_2	1	8.45E-05	8.45E-05	0.0003	0.9860
	Temp*pCO_2	1	4.13E-01	4.13E-01	1.5399	0.2289
Translocation	Temperature	1	0.8590	0.8590	2.7792	0.1110
	pCO_2	1	0.0176	0.0176	0.0571	0.8135
	Temp*pCO_2	1	0.3490	0.3490	1.1293	0.3005
Carbon incorporation	**Temperature**	**1**	**0.2622**	**0.2622**	**34.8040**	**1.11E-05**
	pCO_2	1	0.0064	0.0064	0.8510	3.68E-01
	Temp*pCO_2	1	0.0048	0.0048	0.6370	4.35E-01
***C15* (*Montipora hirsuta*)**						
Photosynthesis	**Temperature**	**1**	**8.93E-12**	**8.93E-12**	**24.0241**	**9.91E-05**
	pCO_2	1	8.85E-14	8.85E-14	0.2382	6.31E-01
	Temp*pCO_2	1	2.95E-13	2.95E-13	0.7950	3.84E-01
Translocation	Temperature	1	0.1246	0.1246	0.4396	0.5152
	pCO_2	1	0.0004	0.0004	0.0014	0.9695
	Temp*pCO_2	1	0.0071	0.0071	0.0252	0.8754
Carbon incorporation	Temperature	1	0.0010	0.0010	0.2988	0.5909
	pCO_2	1	0.0004	0.0004	0.1396	0.7127
	Temp*pCO_2	1	0.0020	0.0026	0.7575	0.3949
***D1* (*Pocillopora damicornis*)**						
Photosynthesis	**Temperature**	**1**	**0.7975**	**0.7975**	**8.0737**	**0.0104**
	pCO_2	1	0.0276	0.0276	0.2798	0.6029
	Temp*pCO_2	1	0.3422	0.3422	3.4645	0.0782
Translocation	Temperature	1	1.95E-09	1.95E-09	0.1816	0.6747
	pCO_2	1	1.24E-08	1.24E-08	1.1587	0.2952
	Temp*pCO_2	1	2.56E-08	2.56E-08	2.3883	0.1387
	Effect	**p-value**	**pair-wise**	HTHC	HTLC	LTHC
Carbon incorporation	group	0.2041	HTLC	0.45	-	-
			LTHC	0.16	0.92	-
			LTLC	0.45	1	0.92

Appendix D

CHAPTER 6: DIFFERENTIAL THERMAL RESPONSE WITHIN INSHORE VS. OFFSHORE CONGENERIC SCLERACTINIAN SPECIES IN PALAU

Figure D.1: A principle coordinates plot utilizing 14 microsatellite markers to visualize variance across *S. trenchii* symbionts for all four coral species in Nikko bay. Coral species are separated by color. Triangles reflect samples from the experiment (2013) whereas circles reflect additional rock island coral colonies sampled in 2009. The additional samples reflect a greater variance for *S. trenchii* genotypes in *Cyphastrea* than is observed for experimental colonies (2013) alone.

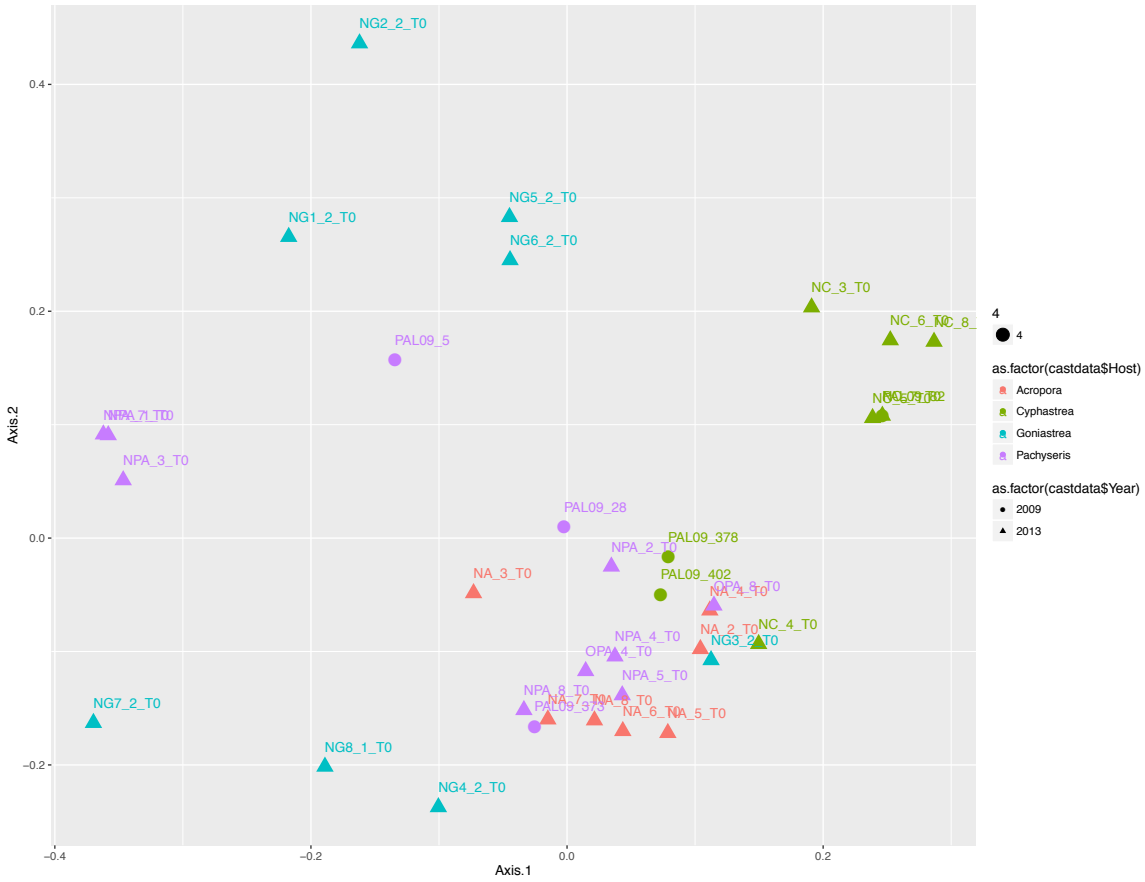

Table D.1: Mean +/- standard deviation for each variable at ambient and elevated temperatures for *S. trenchii.* C = ambient temperature, T = elevated temperature.

	Treatment	C	T	C	T	C	T	C	T
	Host	Acropora	Acropora	Cyphastrea	Cyphastrea	Goniastrea	Goniastrea	Pachyseris	Pachyseris
Protein	mean	4.38E-04	9.78E-04	3.32E-04	2.87E-04	5.01E-04	9.22E-04	4.32E-04	6.03E-04
	se	6.09E-05	1.38E-04	2.35E-05	2.88E-05	1.25E-04	1.98E-04	2.16E-05	9.99E-05
Carbohydrate	mean	5.07E-03	1.12E-02	1.47E-03	1.23E-03	1.18E-03	1.85E-03	1.54E-03	2.54E-03
	se	5.40E-04	1.42E-03	1.71E-04	1.13E-04	1.40E-04	2.73E-04	1.23E-04	8.66E-04
Lipid	mean	6.88E-04	1.01E-03	5.75E-04	3.78E-04	2.69E-03	2.13E-03	1.96E-04	4.63E-04
	se	1.65E-04	3.26E-04	7.47E-05	8.07E-05	5.67E-04	6.40E-04	4.72E-05	1.18E-04
Volume	mean	532.6	301.4	559.8	626.7	547.6	645.6	479.3	562.4
	se	6.1	39.0	21.7	27.3	44.0	25.6	16.7	16.9
Chlorophyll	mean	6.7	3.9	4.2	3.1	3.8	5.7	2.8	3.5
	se	0.658	2.694	0.246	0.286	0.439	0.785	0.230	0.554
Photosynthesis	mean	3.53E-09	8.28E-09	2.14E-09	1.54E-09	7.72E-09	1.15E-08	1.52E-09	1.61E-09
	se	5.57E-10	1.31E-09	1.80E-10	2.06E-10	2.51E-09	2.67E-09	1.51E-10	2.67E-10
Sigma	mean	177.2	181.3	216.1	212	170.1	171.1	191	214.7
	se	3.6	4.1	5.8	4.8	4.3	2.4	5.7	10.7
Connectivity	mean	0.136	0.14	0.045	0.051	0.113	0.128	0.055	0.055
	se	0.026	0.014	0.002	0.001	0.013	0.013	0.002	0.002
ETR	mean	358078.4	318917.1	456600.6	319356.7	267183.3	317773.8	275679.8	166633.8
	se	39539.0	41361.2	49737.2	32655.9	28764.6	24035.6	19376.3	7306.7
Density	mean	369829.6	169403.4	820014.3	984558.0	386259.1	314722.4	1056538.0	545490.3
	se	36949.0	36811.5	67449.9	103966.7	58531.1	53419.4	68286.3	78450.9
tPSII	mean	1458.8	1604.6	1696.2	1589.1	2082.8	1815	1741.8	1707.6
	se	74.5	29.5	66.6	60.1	84.2	71.1	58.3	91.0
tPQ	mean	19832.3	19555.6	23646.5	27722.2	18725	13648.6	26327.5	31496.1
	se	855.2	943.2	650.3	881.5	2256.7	894.1	838.4	1021.7
$FvFm^{MT}$	mean	0.542	0.514	0.544	0.507	0.535	0.511	0.542	0.433
	se	0.005	0.003	0.008	0.010	0.004	0.008	0.005	0.013
NPQ	mean	0.212	0.210	0.546	0.801	0.313	0.223	0.617	0.894
	se	0.048	0.058	0.094	0.113	0.058	0.032	0.049	0.067

Table D.2: Mean +/- standard deviation for each variable at ambient and elevated temperatures for clade C symbionts offshore. C = ambient temperature, T = elevated temperature.

	Treatment	C	T	C	T	C	T	C	T
	Host	Acropora (C40)	Acropora (C40)	Pachyseris (C40)	Pachyseris (C40)	Cyphastrea (C3u)	Cyphastrea (C3u)	Goniastrea (C21)	Goniastrea (C21)
Protein	mean	4.63E-04	7.90E-04	4.75E-04	9.37E-04	5.05E-04	1.08E-03	3.93E-04	7.23E-04
	se	7.69E-05	1.38E-04	4.73E-05	1.92E-04	7.81E-05	1.79E-04	5.08E-05	1.15E-04
Carbohydrate	mean	3.37E-03	7.17E-03	1.73E-03	2.19E-03	1.98E-03	4.14E-03	1.86E-03	2.86E-03
	se	1.75E-04	7.42E-04	3.59E-04	4.05E-04	2.95E-04	6.95E-04	1.12E-04	4.95E-04
Lipid	mean	9.68E-04	1.95E-03	3.69E-04	8.51E-04	7.05E-04	1.23E-03	9.47E-04	1.96E-03
	se	1.52E-04	5.14E-04	8.35E-05	3.14E-04	1.16E-04	1.52E-04	1.05E-04	3.45E-04
Volume	mean	718.6	909.4	656.1	929.8	802.9	1210.9	590.9	731.8
	se	26.1	35.5	25.1	56.6	57.9	83.1	20.1	40.6
Chlorophyll	mean	6.8	7.8	3.3	3.6	5.5	5.0	6.7	5.4
	se	0.324	0.848	0.327	0.657	0.893	0.197	0.637	0.897
Photosynthesis	mean	2.83E-09	5.48E-09	1.48E-09	1.84E-09	3.33E-09	3.05E-09	1.43E-09	3.98E-09
	se	7.59E-10	1.04E-09	2.54E-10	5.77E-10	6.87E-10	3.17E-10	3.71E-10	6.12E-10
Sigma	mean	194.2	216.7	171	190.8	241.2	270.7	187	197.8
	se	1.8	4.0	2.8	3.8	8.9	9.9	4.9	3.99
Connectivity	mean	0.193	0.208	0.063	0.105	0.041	0.052	0.095	0.262
	se	0.015	0.026	0.004	0.022	0.001	0.003	0.005	0.038
ETR	mean	452750.5	301376.0	292308.5	165016.6	458978	168424.2	385712.1	151821.6
	se	27067.3	31117.3	26268.2	32861.8	40631.1	22518.4	30851.7	37849.9
Cell Density	mean	328661.8	207639.5	907664.7	479197.8	716127.5	289704.5	778319.4	386863.9
	se	35865.0	32884.3	132357.8	117133.3	216385.7	44952.8	46523.9	53240.1
tPSII	mean	1136.6	1241.6	1600.3	1724	1606.8	1957.4	1789	1989.1
	se	82.3	63.8	152.3	53.8	70.0	114.1	126.5	107.9
tPQ	mean	22128.3	25599.7	24242.5	31842.3	20593.2	26626.8	18972.8	16811.1
	se	742.5	1449.2	772.4	2024.8	556.7	1006.7	834.8	1476.3
$FvFm^{MT}$	mean	0.533	0.457	0.572	0.314	0.530	0.287	0.505	0.372
	se	0.005	0.011	0.011	0.033	0.013	0.017	0.012	0.018
NPQ	mean	0.239	0.370	0.724	0.754	0.780	1.119	0.335	0.583
	se	0.026	0.042	0.066	0.173	0.137	0.078	0.046	0.085

Table D.3: Mean +/- standard deviation for each variable at ambient and elevated temperatures for C15 symbionts in *Porites rus*. C = ambient temperature, T = elevated temperature.

	Treatment	C	T	C	T
	symbiont	$C15_{OPr}$	$C15_{OPr}$	$C15_{NPr}$	$C15_{NPr}$
Protein	mean	6.08E-04	9.75E-04	9.74E-04	1.05E-03
	se	7.80E-05	2.79E-04	1.16E-04	1.17E-04
Carbohydrate	mean	2.87E-03	3.67E-03	1.93E-03	3.34E-03
	se	3.32E-04	7.02E-04	1.55E-04	3.77E-04
Lipid	mean	4.49E-04	7.79E-04	4.48E-04	4.85E-04
	se	8.49E-05	2.25E-04	6.14E-05	1.06E-04
Volume	mean	362.8	489.3	349.8	487.5
	se	13.5	34.4	16.3	18.3
Chlorophyll	mean	6.2	5.8	8.8	7.7
	se	0.720	0.644	0.460	0.668
Photosynthesis	mean	2.31E-09	3.08E-09	3.32E-09	4.92E-09
	se	5.12E-10	3.89E-10	3.92E-10	7.11E-10
Sigma	mean	163.6	181	174	185.5
	se	2.9	7.2	4.9	4.3
Connectivity	mean	0.163	0.248	0.152	0.105
	se	0.019	0.076	0.077	0.006
ETR	mean	384885.4	367778.3	464474.6	465060.0
	se	45782.0	57489.8	62338.7	48389.0
Cell Density	mean	396391.3	196904.3	186836.7	151113.4
	se	56133.0	29083.1	9558.8	9849.2
tPSII	mean	1954.5	2668.6	1825.7	1663.7
	se	73.1	271.5	128.4	59.2
tPQ	mean	18592.8	12990.4	25298.1	16344.1
	se	966.2	1429.3	2619.2	838.0
$FvFm^{MT}$	mean	0.505	0.419	0.482	0.491
	se	0.005	0.023	0.032	0.004
NPQ	mean	0.157	0.168	0.030	0.043
	se	0.091	0.131	0.036	0.042

Table D.4: Mean +/- standard deviation for each variable at ambient and elevated temperatures for C15 symbionts in *Porites cylindrica.* C = ambient temperature, T = elevated temperature.

	Treatment	C	T	C	T	C	T
	symbiont	$C15_{NPc}$	$C15_{NPc}$	$C15_{OPc1}$	$C15_{OPc1}$	$C15_{OPc2}$	$C15_{OPc2}$
Protein	mean	9.27E-04	9.53E-04	1.20E-03	1.19E-03	1.25E-03	2.08E-03
	se	5.40E-05	1.15E-04	1.09E-04	7.24E-05	1.50E-04	2.63E-04
Carbohydrate	mean	1.46E-03	1.05E-03	2.50E-03	3.06E-03	2.58E-03	3.40E-03
	se	1.52E-04	9.07E-05	2.25E-04	2.09E-04	1.75E-04	2.90E-04
Lipid	mean	3.32E-04	2.76E-04	6.68E-04	8.33E-04	7.42E-04	8.70E-04
	se	2.27E-05	3.97E-05	7.92E-05	1.18E-04	1.43E-04	4.18E-05
Volume	mean	484.8	476.7	435.2	479.8	461.2	497.1
	se	20.9	30.8	36.0	19.4	21.0	29.4
Chlorophyll	mean	1.2	2.1	1.8	2.3	2.6	2.6
	se	0.288	0.487	0.780	0.420	0.917	0.538
Photosynthesis	mean	8.74E-10	1.19E-09	9.62E-10	1.27E-09	1.01E-09	9.12E-10
	se	9.54E-11	1.72E-10	1.81E-10	1.66E-10	1.22E-10	1.39E-10
Sigma	mean	170.2	183.2	170.7	181.7	196.3	212.6
	se	4.6	3.7	7.3	5.9	6.2	6.3
Connectivity	mean	0.055	0.047	0.052	0.057	0.043	0.05
	se	0.005	0.003	0.009	0.004	0.003	0
ETR	mean	336403.6	366738.1	247988.4	351223.9	229774.7	348893.9
	se	39841.8	34918.4	30175.2	25934.5	13687.1	14205.1
Cell Density	mean	1151544.9	1031672.0	1280247.6	961106.3	905534.7	790411.7
	se	82393.7	108355.8	217792.1	16381.0	100667.8	104063.0
tPSII	mean	1296.8	1119	1132.5	1009.5	1185.3	1229.6
	se	90.7	87.5	124.3	80.7	54.1	43.2
tPQ	mean	20546.7	21330	23128.2	23493.7	20307.3	18792.6
	se	568.8	333.2	964.7	835.8	627.0	477.9
$FvFm^{MT}$	mean	0.603	0.574	0.599	0.572	0.656	0.600
	se	0.005	0.008	0.008	0.002	0.006	0.020
NPQ	mean	0.676	0.669	1.245	0.710	0.665	0.689
	se	0.096	0.102	0.253	0.132	0.128	0.047

Table D.5: *Acropora muricata* with *S. trenchii.* Results from differential analysis. Variables with adjusted pValues for Tgw (tagwise dispersion) (5th column) less than $P < 0.05$ **(boldface)** are visualized in the heatmaps.

	logMet	logFC	pVal.Tgw	**adj.pVal.Tgw**	Tgw.Disp
Volume	-0.910	16.490	8.1E-08	**1.1E-06**	0.0438
Density	-1.196	15.877	1.5E-04	**1.1E-03**	0.1506
Protein	1.055	15.889	3.5E-04	**1.6E-03**	0.1436
Carbs	1.031	15.786	4.7E-04	**1.6E-03**	0.1430
Photosynthesis	1.118	15.647	7.9E-03	**2.2E-02**	0.2931
FvFm	-0.168	16.746	1.2E-02	**2.8E-02**	0.0062
Chla	-1.007	15.214	1.8E-01	3.5E-01	0.8089
tPQ	-0.116	16.562	2.2E-01	3.9E-01	0.0136
ETR	-0.245	16.231	3.5E-01	5.4E-01	0.1062
Lipids	0.428	15.187	4.1E-01	5.8E-01	0.4602
Sigma	-0.059	16.686	4.7E-01	6.0E-01	0.0096
tPSII	0.053	16.620	5.4E-01	6.3E-01	0.0114
NPQ	-0.130	15.647	7.9E-01	8.5E-01	0.3429
Connectivity	-0.048	16.023	8.8E-01	8.8E-01	0.1508

Table D.6: *Cyphastrea chalcidicum* with *S. trenchii.* Results from differential analysis. Variables with adjusted pValues for Tgw (tagwise dispersion) (5th column) less than $P < 0.05$ **(boldface)** are visualized in the heatmaps.

	logMet	logFC	pVal.Tgw	**adj.pVal.Tgw**	Tgw.Disp
tPQ	0.253	16.248	0.001	**0.021**	0.010
Chla	-0.406	16.027	0.005	**0.027**	0.036
Connectivity	0.191	16.305	0.006	**0.027**	0.007
Volume	0.187	16.305	0.019	0.054	0.010
Photosynthesis	-0.456	15.952	0.019	0.054	0.067
ETR	-0.493	15.867	0.039	0.092	0.101
Lipids	-0.578	15.807	0.077	0.154	0.190
NPQ	0.572	15.749	0.092	0.162	0.199
Density	0.282	15.996	0.178	0.229	0.076
FvFm	-0.082	16.457	0.180	0.229	0.006
Protein	-0.189	16.188	0.180	0.229	0.034
Carbs	-0.230	15.872	0.242	0.274	0.068
tPSII	-0.073	16.359	0.255	0.274	0.006
Sigma	-0.005	16.407	0.944	0.944	0.007

Table D.7: *Pachyseris rugosa* with *S. trenchii.* Results from differential analysis. Variables with adjusted pValues for Tgw (tagwise dispersion) (5th column) less than P <0.05 **(boldface)** are visualized in the heatmaps.

	logMet	logFC	pVal.Tgw	**adj.pVal.Tgw**	Tgw.Disp
FvFm	-0.436	16.606	4.4E-10	**6.2E-09**	0.007
ETR	-0.804	16.154	3.9E-07	**2.7E-06**	0.042
Density	-0.907	16.021	6.1E-05	**2.9E-04**	0.087
Lipids	1.004	14.938	0.004	**0.013**	0.209
NPQ	0.441	16.083	0.017	**0.047**	0.059
tPQ	0.184	16.484	0.030	0.070	0.012
Volume	0.136	16.570	0.052	0.105	0.008
Photosynthesis	-0.317	16.131	0.098	0.172	0.064
Carbs	0.593	14.660	0.139	0.217	0.283
tPSII	-0.112	16.521	0.226	0.316	0.014
Sigma	0.127	16.451	0.260	0.331	0.022
Protein	0.128	15.680	0.533	0.621	0.073
Connectivity	-0.062	16.450	0.584	0.629	0.021
Chla	0.108	15.648	0.654	0.654	0.102

Table D.8: *Acropora muricata* with *S. C40.* Results from differential analysis. Variables with adjusted pValues for Tgw (tagwise dispersion) (5th column) less than P <0.05 **(boldface)** are visualized in the heatmaps.

	logMet	logFC	pVal.Tgw	**adj.pVal.Tgw**	Tgw.Disp
FvFm	-0.444	16.679	1.7E-10	**2.3E-09**	0.008
ETR	-0.812	16.231	3.0E-06	**2.1E-05**	0.056
Carbs	0.863	15.843	3.8E-05	**1.8E-04**	0.081
Density	-0.891	16.050	0.001	**0.005**	0.145
Lipids	0.807	14.947	0.052	0.146	0.320
NPQ	0.418	15.955	0.082	0.186	0.109
Protein	0.558	15.520	0.093	0.186	0.207
Photosynthesis	0.777	15.341	0.145	0.253	0.527
Volume	0.110	16.456	0.236	0.368	0.015
Sigma	-0.065	16.605	0.329	0.461	0.008
tPSII	-0.089	16.505	0.378	0.481	0.018
Connectivity	-0.121	16.091	0.558	0.651	0.079
Chla	-0.044	16.240	0.776	0.836	0.045
tPQ	-0.012	16.321	0.911	0.911	0.020

Table D.9: *Goniastrea aspera* with *S. C21.* Results from differential analysis. Variables with adjusted pValues for Tgw (tagwise dispersion) (5th column) less than $P < 0.05$ **(boldface)** are visualized in the heatmaps.

	logMet	logFC	pVal.Tgw	**adj.pVal.Tgw**	Tgw.Disp
FvFm	-0.590	16.536	1.3E-07	**1.8E-06**	0.022
Connectivity	1.297	15.427	6.2E-05	**4.3E-04**	0.191
Density	-1.139	16.219	1.5E-04	**7.2E-04**	0.167
ETR	-1.488	16.030	0.003	**0.011**	0.461
Lipids	0.864	15.627	0.007	**0.018**	0.187
Protein	0.702	15.526	0.013	**0.030**	0.148
tPQ	-0.334	16.421	0.042	0.084	0.050
NPQ	0.634	15.934	0.054	0.088	0.203
Photosynthesis	1.382	15.415	0.056	0.088	0.943
Volume	0.151	16.425	0.117	0.163	0.016
Carbs	0.440	15.765	0.156	0.198	0.180
Chla	-0.481	16.369	0.175	0.204	0.237
Sigma	-0.064	16.749	0.441	0.475	0.012
tPSII	0.007	16.499	0.959	0.959	0.029

Table D.10: *Cyphastrea chalcidicum* with *S. C3u.* Results from differential analysis. Variables with adjusted pValues for Tgw (tagwise dispersion) (5th column) less than $P < 0.05$ **(boldface)** are visualized in the heatmaps.

	logMet	logFC	pVal.Tgw	**adj.pVal.Tgw**	Tgw.Disp
FvFm	-1.096	16.420	5.2E-16	**7.3E-15**	0.029
ETR	-1.677	16.043	1.3E-11	**9.4E-11**	0.096
Density	-1.546	14.997	4.5E-04	**2.1E-03**	0.304
Carbs	0.862	15.629	0.004	**0.014**	0.145
Protein	0.890	15.446	0.006	**0.017**	0.171
Lipids	0.620	15.941	0.017	**0.040**	0.111
Volume	0.399	16.168	0.028	0.056	0.054
tPQ	0.156	16.555	0.135	0.222	0.017
NPQ	0.330	16.339	0.143	0.222	0.083
Chla	-0.317	16.174	0.230	0.322	0.115
Photosynthesis	-0.302	15.805	0.319	0.406	0.151
Connectivity	0.139	16.303	0.435	0.508	0.051
tPSII	0.068	16.493	0.533	0.574	0.018
Sigma	-0.044	16.615	0.625	0.625	0.012

Table D.11: *Pachyseris rugosa* with *S. C40.* Results from differential analysis. Variables with adjusted pValues for Tgw (tagwise dispersion) (5th column) less than $P < 0.05$ **(boldface)** are visualized in the heatmaps.

	logMet	logFC	pVal.Tgw	**adj.pVal.Tgw**	Tgw.Disp
FvFm	-0.953	16.466	6.7E-11	**9.4E-10**	0.029
ETR	-0.935	16.242	0.002	**0.011**	0.121
Volume	0.433	16.466	0.004	**0.021**	0.032
tPQ	0.328	16.472	0.008	**0.027**	0.020
Density	-0.986	16.024	0.013	**0.038**	0.221
Protein	0.880	15.662	0.023	0.054	0.208
Lipids	1.071	14.906	0.060	0.114	0.443
Connectivity	0.675	15.831	0.065	0.114	0.188
Sigma	0.077	16.768	0.363	0.564	0.009
Carbs	0.249	15.938	0.471	0.659	0.169
Photosynthesis	0.181	15.679	0.689	0.878	0.286
tPSII	0.043	16.452	0.786	0.917	0.034
Chla	0.054	16.021	0.868	0.931	0.148
NPQ	-0.032	16.004	0.931	0.931	0.194

Table D.12: *Porites rus* with *S. C15$_{OPr}$.* Results from differential analysis. Variables with adjusted pValues for Tgw (tagwise dispersion) (5th column) less than $P < 0.05$ **(boldface)** are visualized in the heatmaps.

	logMet	logFC	pVal.Tgw	**adj.pVal.Tgw**	Tgw.Disp
tPQ	-0.500	16.525	7.9E-05	**0.001**	0.022
Volume	0.465	16.369	0.001	**0.007**	0.029
tPSII	0.464	16.337	0.007	**0.028**	0.043
Density	-0.982	16.102	0.008	**0.028**	0.184
FvFm	-0.251	16.819	0.013	**0.035**	0.014
Protein	0.676	15.501	0.041	0.097	0.166
Connectivity	0.617	15.498	0.094	0.189	0.206
Sigma	0.169	16.675	0.116	0.204	0.016
Lipids	0.793	15.423	0.174	0.270	0.529
Carbs	0.368	15.727	0.209	0.292	0.129
Photosynthesis	0.446	15.975	0.242	0.308	0.223
Chla	-0.062	16.303	0.803	0.937	0.081
ETR	-0.040	16.332	0.893	0.961	0.104
NPQ	-0.037	15.042	0.977	0.977	1.887

Table D.13: *Porites rus* with *S. C15*$_{NPr}$**.** Results from differential analysis. Variables with adjusted pValues for Tgw (tagwise dispersion) (5th column) less than P <0.05 **(boldface)** are visualized in the heatmaps.

	logMet	logFC	pVal.Tgw	**adj.pVal.Tgw**	Tgw.Disp
Volume	0.448	16.363	2.1E-05	**2.9E-04**	0.017
Carbs	0.747	15.885	1.3E-04	**0.001**	0.061
tPQ	-0.660	15.845	0.002	**0.009**	0.073
Photosynthesis	0.532	16.072	0.041	0.128	0.111
Density	-0.313	16.406	0.046	0.128	0.040
Chla	-0.218	16.536	0.122	0.284	0.032
Connectivity	-0.583	14.560	0.275	0.488	0.463
tPSII	-0.169	16.346	0.279	0.488	0.039
Sigma	0.066	16.633	0.447	0.695	0.012
NPQ	0.209	15.313	0.711	0.960	0.518
Protein	0.059	16.073	0.768	0.960	0.064
Lipids	0.059	15.627	0.871	0.960	0.218
FvFm	0.006	16.654	0.959	0.960	0.019
ETR	0.012	16.229	0.960	0.960	0.088

Table D.14: Factor loadings for each variable within the principle components (PC) analysis for *S. Trenchii.* Eigen-values and % variance for each PC are indicated at the top of the table. Only significant ($P < 0.05$) correlations are included. For each variable, values in bold face indicate the axis of strongest loading.

		PC1	PC2	PC3	PC4
	Eigen-value	2.283	1.4926	1.3549	1.0766
	% variance	37.2	15.9	13.1	8.2
	Variable				
	Protein	**-0.327**	-0.289	-0.121	-0.127
	Carbohydrate	-0.231		**-0.572**	
	Lipids	**-0.315**	-0.232	0.296	-0.123
	Volume		-0.100	0.569	0.437
	Chla	-0.180			**0.698**
	Photosynthesis	**-0.360**	-0.210	0.143	
	Sigma	**0.327**	-0.133	-0.108	
	Connectivity	**-0.325**			0.178
	ETR		**0.515**		-0.113
	Density	**0.352**	0.168	0.148	-0.125
	tPSII		-0.265	0.328	**-0.440**
	tPQ	**0.329**	-0.200	-0.211	
	FvFm	-0.113	**0.512**	0.158	-0.151
	NPQ	0.320	**-0.350**		

Table D.15: Factor loadings for each variable within the principle components (PC) analysis for *S. C15*. Eigen-values and % variance for each PC are indicated at the top of the table. Only significant ($P < 0.05$) correlations are included. For each variable, values in bold face indicate the axis of strongest loading.

		PC1	PC2	PC3	PC4
	Eigen-val	**2.2827**	**1.5618**	**1.4073**	**1.0992**
	% variance	**37.2**	**17.4**	**14.14**	**8.6**
	Variable				
	Protein		**-0.496**	0.206	0.297
	Carbohydrate	-0.216	**-0.390**	0.298	
	Lipids		**-0.443**	0.357	
	Volume	0.133	-0.248		**-0.391**
	Chla	**-0.381**			0.289
	Photosynthesis	**-0.342**	-0.114	-0.115	0.217
	Sigma		**-0.476**	-0.302	
	Connectivity	-0.267	0.160	**0.402**	-0.109
	ETR	-0.198			**-0.521**
	Density	**0.404**			
	tPSII	-0.323		0.115	**-0.404**
	tPQ	0.120	0.213	0.306	**0.631**
	FvFm	**0.377**	-0.115	-0.165	0.113
	NPQ	**0.360**		0.247	

Table D.16: Factor loadings for each variable within the principle components (PC) analysis for *S. C40.* Eigen-values and % variance for each PC are indicated at the top of the table. Only significant ($P < 0.05$) correlations are included. For each variable, values in bold face indicate the axis of strongest loading.

		PC1	PC2	PC3
	Eigen-val	**2.3524**	**1.9437**	**1.2673**
	% variance	**39.5**	**26.9**	**11.5**
	Variable			
	Protein	0.104	-0.336	**-0.468**
	Carbohydrate	**0.361**	-0.160	-0.106
	Lipids	**0.296**	-0.156	-0.286
	Volume		**-0.379**	0.320
	Chla	**0.370**		
	Photosynthesis	**0.313**		-0.272
	Sigma	**0.329**	-0.205	
	Connectivity	0.284		**0.460**
	ETR	0.212	**0.401**	
	Density	**-0.327**	0.149	
	tPSII	**-0.276**	-0.247	-0.243
	tPQ	-0.163	**-0.392**	0.290
	FvFm		**0.449**	-0.242
	NPQ	**-0.290**	-0.208	-0.286

Appendix E

PERMISSIONS

Chapter 1 is published in the journal Scientific Reports and is permitted for use here through the license and copyright agreements as stated on the Nature publishing group website, http://www.nature.com/reprints/permission-requests.html

Chapter 2 and 3 are published in the journals Marine Biology and Coral Reefs respectively. Both of these journals are part of the Springer publishing group and are permitted for publication here as well. http://www.springer.com/gp/open-access/authors-rights

Chapter 4 is published in the Wiley Journal: Limnology and Oceanography. No permission is needed for republication by the author. http://aslopubs.onlinelibrary.wiley.com/hub/permissions.html